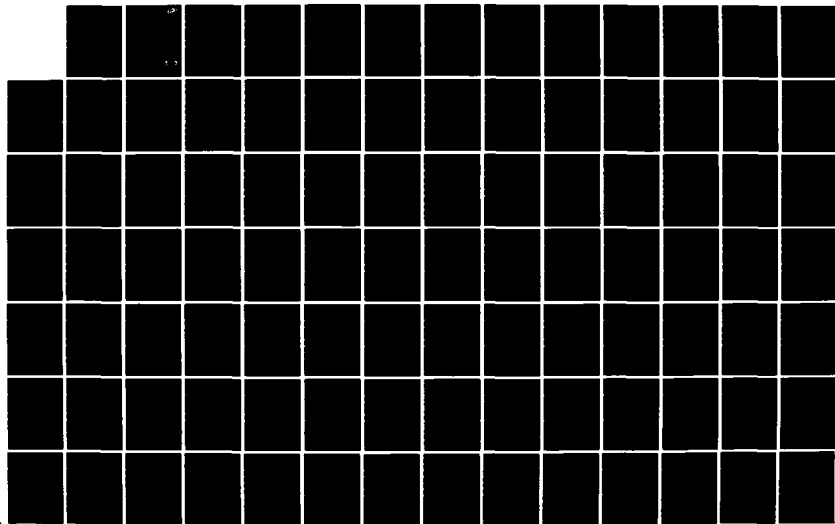AD-A130 539   AIRBORNE SYSTEMS COURSE TEXTBOOK ELECTRO-OPTICAL   1/4
               SYSTEMS TEST AND EVALUATION(U) NAVAL TEST PILOT SCHOOL
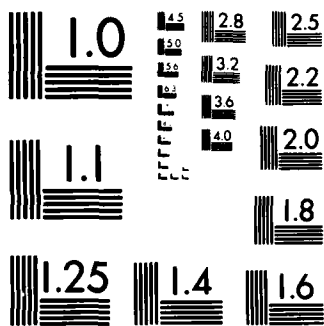   PATUXENT RIVER MD G W MASTERS 01 JUN 81

UNCLASSIFIED   F/G 5/9   NL

MICROCOPY RESOLUTION TEST CHART

NATIONAL BUREAU OF STANDARDS-1963-A

UNITED STATES NAVAL
TEST PILOT SCHOOL

AIRBORNE SYSTEMS COURSE
TEXTBOOK

By

George W. Masters
1 June, 1981

DTIC
ELECTE
JUL 22 1983

D

83 07 21 087

REPORT DOCUMENTATION PAGE		READ INSTRUCTIONS BEFORE COMPLETING FORM
1. REPORT NUMBER -	2. GOVT ACCESSION NO. AD - ?\'?? ???	3. RECIPIENT'S CATALOG NUMBER -
4. TITLE *(and Subtitle)* Electro-Optical Systems Test & Evaluation		5. TYPE OF REPORT & PERIOD COVERED -
		6. PERFORMING ORG. REPORT NUMBER -
7. AUTHOR(*s*) George W. Masters		8. CONTRACT OR GRANT NUMBER(*s*) -
9. PERFORMING ORGANIZATION NAME AND ADDRESS U. S. Naval Test Pilot School Naval Air Test Center Patuxent River, Maryland 20670		10. PROGRAM ELEMENT, PROJECT, TASK AREA & WORK UNIT NUMBERS -
11. CONTROLLING OFFICE NAME AND ADDRESS Academics Branch U. S. Naval Test Pilot School		12. REPORT DATE 1 June 1981
		13. NUMBER OF PAGES 318
14. MONITORING AGENCY NAME & ADDRESS(*if different from Controlling Office*) -		15. SECURITY CLASS. *(of this report)* UNCLASSIFIED
		15a. DECLASSIFICATION/DOWNGRADING SCHEDULE -

16. DISTRIBUTION STATEMENT *(of this Report)*
    Approved for public release; distribution unlimited

17. DISTRIBUTION STATEMENT *(of the abstract entered in Block 20, if different from Report)*
    -

18. SUPPLEMENTARY NOTES
    -

19. KEY WORDS *(Continue on reverse side if necessary and identify by block number)*
    Electro-Optics, Infrared Sensors, Low-Light-Level Sensors, Laser Systems,
    Imaging Sensors, Avionics, Airborne Systems, Weapon Systems, Test and
    Evaluation, Flight Testing

20. ABSTRACT *(Continue on reverse side if necessary and identify by block number)*
    Textbook for teaching test and evaluation of electro-optical sensor systems,
    including theory of operation, operating characteristics, and test
    methodology. Topics include radiation physics, optics, physical optics,
    fourier optics, radiation detectors, infrared detectors, low-light-level
    television detectors, lasers, point-source detectors, imaging sensors,
    electro-optical system hardware and test equipment, and test methods.

ELECTRO-OPTICAL SYSTEMS

TEST AND EVALUATION

TABLE OF CONTENTS

Angular Resolution
Bandwidth
Beamwidth
Bearing Accuracy
Blind Ranges
Boresight Accuracy
Field-of-View (FOV)
Image Definition
Instantaneous Field-of-View (IFOV)
Line-of-Sight Limits
Line-of-Sight Slew Rate, Max.
Line-of-Sight Stability
Maximum Range
Minimum Resolvable Differential Temperature (MRΔT)
Misfire Rate
Modulation Transfer Function (MTF)
Noise-Equivalent Differential Temperature (NEΔT)
Pointing Accuracy
Power Output
Pulse Amplitude
Pulse Amplitude Stability
Pulse Energy
Pulse Width
Pulse Repetition Frequency (PRF)
PRF Accuracy
PRF Stability
Range Accuracy
Range Resolution
Spatial Frequency Response
Spectrum
Temporal Frequency Response
Thermal Resolution
Time Response

ELECTRO-OPTICAL SYSTEMS

1.0 Introduction

Electro-optical systems are systems that utilize optical-frequency electro-magnetic radiation to convey information (or energy) from one point to another. The principal airborne applications are those listed below.

    Target Detection, Identification, and Tracking
    Threat Detection and Warning
    Surveillance and Ground Mapping
    Navigation (Celestial and Terrestrial)
    Communication
    Weapon Delivery (Control)
    Direct Radiation (Laser) Weapons

Electro-optical systems offer certain advantages in comparison with RF systems. Perhaps the greatest advantage is the ability of an infrared (I/R) sensor to passively detect a target utilizing the radiation emitted by any object above absolute zero in temperature. Passive detection not only allows covert operation, but also manifests no blind ranges. It should be noted that currently operational airborne E/O sensors do not have passive ranging capability, although passive optical range finders have long been employed in other fields. In addition, it is difficult to conceal targets from an infrared sensor since almost all militarily significant targets dissipate energy in the form of heat. Another important advantage is the improved accuracy in position determination resulting from the narrow beamwidths possible with E/O sensors. A third advantage is the much greater information bandwidth afforded by the extremely high E/O carrier frequencies. The narrow beamwidth and narrow bandwidth also make it very difficult to intercept and/or jam the emissions from an E/O system.

The principal disadvantage of E/O systems, in comparison with RF systems, is the much greater atmospheric absorption at E/O frequencies. This absorption greatly reduces the effective range of terrestrial E/O systems. Range is also limited by

line-of-sight propagation. Another important disadvantage of E/O systems is the prevalence of natural clutter and noise in the infrared region. (Just as all targets above zero degrees absolute temperature omit infrared radiation, so also do all non-targets above absolute zero. In comparison, very few natural objects spontaneously emit RF radiation.)

A common feature of all electro-optical systems, (except direct-radiation laser weapons), is the generalized radiation sensor depicted in Figure 1.0.0.1. The target, which can be self-radiating or illuminated by an active sensor, emits radiation in the optical frequency range. Surrounding objects (clutter) also emit or reflect such radiation. The radiation passes through a propagating medium, (atmosphere in the case of most terrestrial sensors), thereby suffering (relatively large) absorption and scattering losses. The radiation typically is collected by an objective lens or mirror, passed through a reticle, and directed onto a radiation detector by a field lens or mirror. The reticle is a multi-purpose optical element designed to improve the signal-to-noise ratio by discriminating between target and clutter or noise on the basis of position (image scanning), size and shape (spatial filtering), radiation frequency (chromatic filtering), or time (optical modulation or chopping). The radiation detector is an energy transducer that converts electromagnetic wave energy to a more easily processed form such as electrical voltage or current. The output signal from the detector is processed (filtered, amplified, or otherwise modified in amplitude or spectrum) and output to a display or other device.

Since an electro-optical system utilizes electromagnetic radiation to convey information from one point to another, it satisfies the broad definition of a "communications" system employed in the text on communications systems. The

(Cold Stop for I/R Shield)

Disp

Display

Elec

Electronics

Detector

Det

Field Lens

Reticle

Objective Lens

Scattering and Absorbing Medium

Target Radiation

Background Clutter

Target
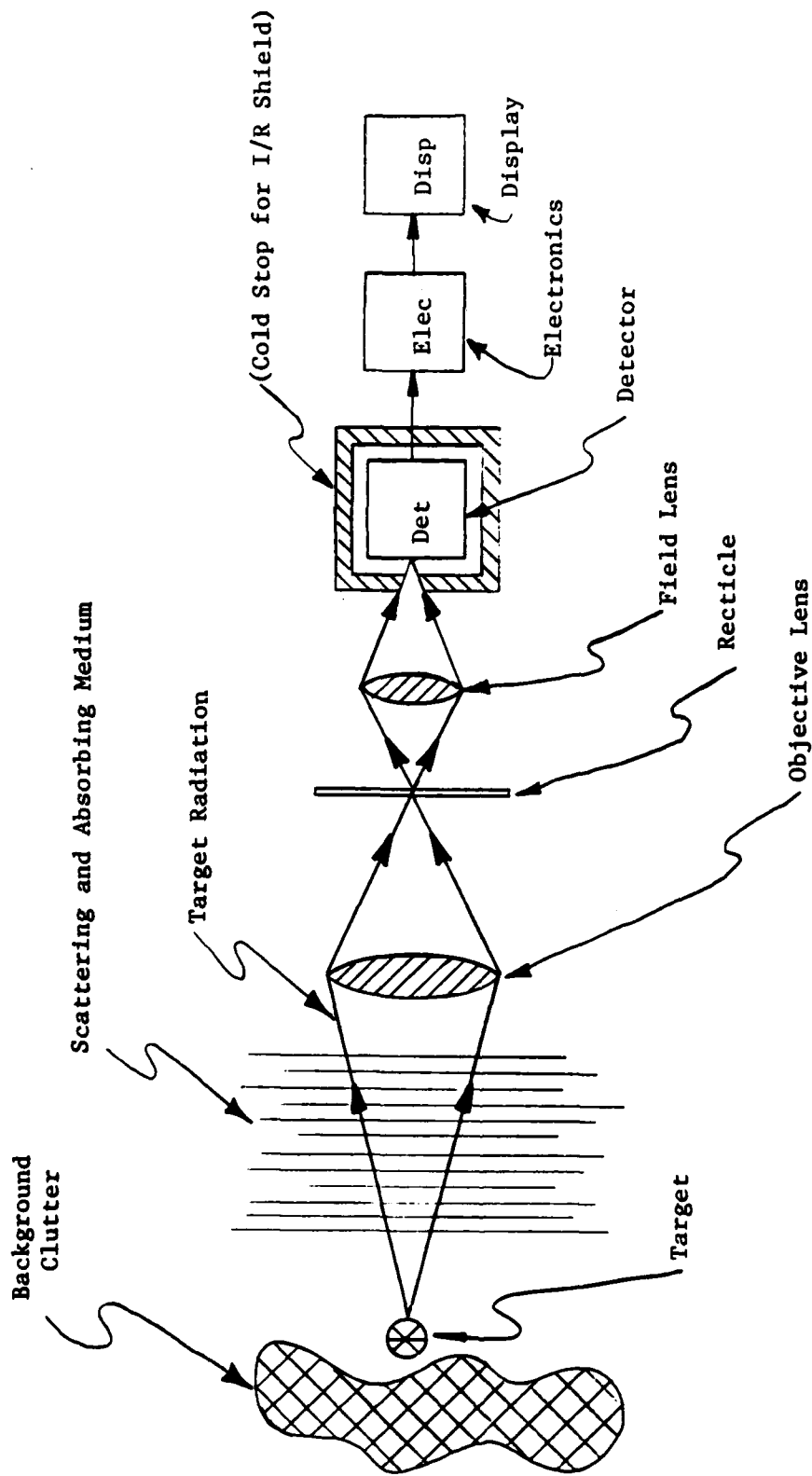
Figure 1.0.0.1 -- Generalized Electro-Optical Sensor

reader is referred, therefore, to the text on communications systems, especially Section 2.4 on electromagnetic waves, for a general discussion of "communications" theory and "communications" systems. The discussions in this text are primarily concerned with those aspects of "communications" systems peculiar to the field of electro-optics. These "peculiarities" are a result of the extremely high frequencies employed in E/O systems, in comparison with those employed in RF systems, and to the fact, previously indicated, that all objects at temperatures above absolute zero radiate infrared radiation. The reader is referred to the text on radar systems for discussions of target sensors, detection theory, and target tracking. In addition, the reader is referred to the text on electronic warfare for discussion of EW principles applicable to E/O systems.

The principles of operation, operating characteristics, and test and evaluation of electro-optical systems are the subject of this text. The necessary information will be provided to allow the reader to design experiments (tests) which will reveal the significant characteristics of the E/O system being evaluated. Sufficient theoretic background will be provided to allow him to analyze the design of the system under test and thereby anticipate its likely performance characteristics (strengths and weaknesses). Only in this manner can an adequate test plan be devised. The difficulties in designing an adequate test are due, in large part, to the ever-present funding and time limitations. The tester virtually never has enough time or funding to perform exhaustive testing. For that reason, he must concentrate on those tests which reveal the likely performance weaknesses of the subject system. Only by understanding the system design and its implications can he identify the appropriate areas of concentration.

Section 2.0 of this text will present the necessary background theory (in addition to that presented in the texts referenced above). Section 3.0 will discuss the pertinent characteristics of various E/O systems. Section 4.0 will present the E/O system performance characteristics to be experimentally determined and the methods for their measurement. In a separate text will be presented the non-performance (environmental, electromagnetic compatibility, hardware viability, maintainability, reliability, and crew safety) characteristics to be determined, the general methods for their determination, and the applicable specifications and references.

2.0 Electro-Optical Theory

2.1 Radiation Physics

2.1.1 The electromagnetic spectrum -- In Figure 2.1.1.1 is shown a chart of the portion of the electromagnetic spectrum containing the optical frequencies. As indicated by the chart, the optical frequencies, (infrared, visible, and ultraviolet radiation), are bordered below by extremely high frequency RF, and above by x-rays· As previously indicated, the major differences between RF and electro-optical system characteristics are a result of the tremendous difference in frequency or wavelength. Both types of systems utilize electromagnetic radiation.

2.1.2 The Emission and Absorption of Radiation by Bodies and Surfaces -- As previously indicated, all bodies at temperatures above zero degrees absolute emit electromagnetic radiation. Such bodies also absorb radiation. The radiant energy emitted and/or absorbed depends upon the physical characteristics of both the body and the transmitting medium. In order to describe radiation emission and absorption phenomena, the following terms are defined. [1] (When the dimensions of a radiant source are very small compared to the distance from the source to the point of observation, the source can be said to be a point source. When the dimensions of the source are not negligible, the source can be said to be an extended source.)

----

(1) It should be noted that symbols and terms for physical quantities other than those used in this text are sometimes encountered in the field of electro-optics (especially photometry). The terms defined herein are those most commonly employed in the field of infrared radiation and are, therefore, most appropriate for the purpose of discussing the systems of principal interest here.
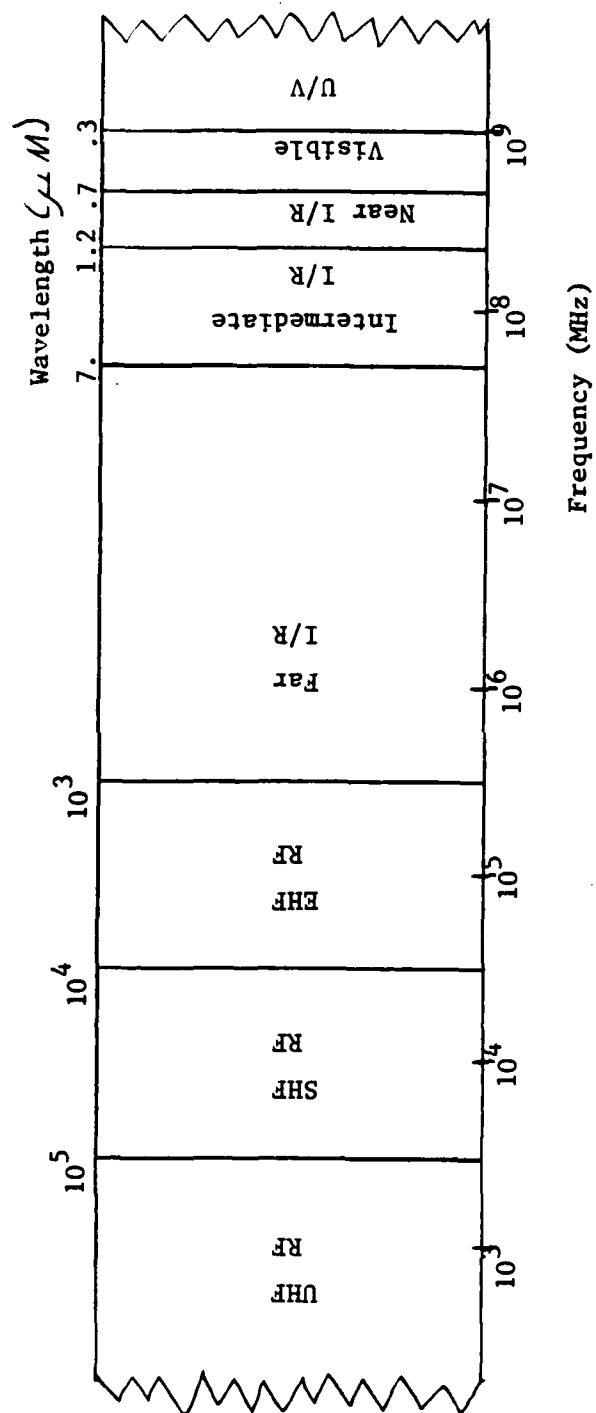
Figure 2.1.1.1 --   The Electromagnetic Spectrum

Radiant Flux: P (Watts) -- The radiant energy per unit time (power) emitted by a source or transmitted through a medium or interface.

Radiant Emittance: W (Watts/cm^2) -- The radiant flux per unit area emitted by an extended source (surface). Thus:

$$W = P/A_s; \quad A_s = \text{Area of Source } (cm^2)$$

Radiant Intensity: J (Watts/Stearadian) -- The radiant flux per unit solid angle emitted from a point source. Thus:

$$J = P/\Omega; \quad \Omega = \text{Solid Angle (Stearadians)}$$

(The stearadian is a measure of a two-dimensional angle such that a central solid angle of one stearadian subtends a unit area on the surface of a sphere of unit radius. The central solid angle, in stearadians, is equal to the subtended spherical surface divided by the square of the radius of the sphere. The total solid central angle of a sphere is, thus, 4π stearadians.)

Radiance: N (Watts/cm^2 - Stearadian) -- The radiant emittance per stearadian emitted from an extended source (surface). Thus:

$$N = W/\Omega; \quad \Omega = \text{Solid Angle (Stearadians)}$$

Radiant Photon Emittance: Q (Photons/Sec-cm^2) -- The number of photons per second emitted from an extended source per unit source area. Thus:

$$Q = (\text{No. of Photons per Second})/A_s$$

$$A_s = \text{Area of Source } (cm^2)$$

Irradiance: H (Watts/cm^2) -- The radiant flux per unit area incident upon a surface. Thus:

$$H = J/R^2$$

J = Radiant Intensity of Point Source (W/S$_r$)

R = Range from point source to irradiated surface (cm)

Spectral Radiant Flux: P$_\lambda$ (Watts/Micrometer) -- The radiant flux per unit wavelength interval at a given wavelength. "Spectral" (frequency dependent) parameters are necessary when the parameter values vary with frequency or wavelength. That is:

$$P_\lambda(\lambda) = \frac{\Delta P}{\Delta \lambda} = \frac{dP(\lambda)}{d\lambda}; \quad P = \int P_\lambda(\lambda) \, d\lambda$$

λ = Wavelength (Micrometers)

$\Delta\lambda$ = Wavelength Interval (Micrometer)

Spectral Radiant Emittance: W$_\lambda$ (Watts/cm^2 - Micrometer) -- The radiant emittance per unit wavelength interval at a given wavelength. That is:

$$W_\lambda(\lambda) = \frac{\Delta W}{\Delta \lambda} = \frac{dW(\lambda)}{d\lambda}; \quad W = \int W_\lambda(\lambda) \, d\lambda$$

Spectral Radiant Intensity: J$_\lambda$ (Watts/Stearadian - Micrometer)-- The radiant intensity per unit wavelength interval at a given wavelength. That is:

$$J_\lambda(\lambda) = \frac{\Delta J}{\Delta \lambda} = \frac{dJ(\lambda)}{d\lambda}; \quad J = \int J_\lambda(\lambda) \, d\lambda$$

Spectral Radiant Photon Emittance: Q$_\lambda$ (Photons/Sec - cm^2 - Micrometer) -- The radiant photon emittance per unit wavelength interval at a given wavelength. That is:

$$Q_\lambda(\lambda) = \frac{\Delta Q}{\Delta \lambda} = \frac{dQ(\lambda)}{d\lambda}; \quad Q = \int Q_\lambda(\lambda) \, d\lambda$$

Spectral Irradiance: H_λ (Watts/cm^2 - Micrometer) -- The irradiance at a surface per unit wavelength interval at a given wavelength. That is:

$$H_\lambda (\lambda) = \frac{\Delta H}{\Delta \lambda} = \frac{dH(\lambda)}{d\lambda} \; ; \; H = \int H_\lambda (\lambda) d\lambda$$

Radiant Emissivity: ε (Non-Dimensional) -- The ratio of the radiant emittance of a source to that of a blackbody at the same temperature. That is:

$$\varepsilon = W_S / W_{BB} \qquad (T_S = T_{BB})$$

$$\varepsilon = 1 \quad \text{for a blackbody.}$$

Radiant Absorptance: α (Non-Dimensional) -- The ratio of radiant flux absorbed by a body to the radiant flux incident upon its surface. That is:

$$\alpha = P_{Absorbed} / P_{Incident}$$

$$\alpha = 1 \quad \text{for a blackbody}$$

The following physical properties and relationships describe the emission and absorption of radiant flux by bodies and surfaces.

Kirchoff's Law -- Kirchoff's law states that the radiant emissivity and radiant absorptance of a body are equal. That is:

$$\varepsilon = \alpha \qquad (N.D.)$$

This equality is a consequence of the Principle of Reciprocity discussed in the texts on communications.

Blackbody -- A blackbody is an object that radiates (and absorbs) radiant
energy of all wavelengths perfectly. That is:

$$\epsilon_{BB}(\lambda) = \epsilon_{BB} = \alpha_{BB}(\lambda) = \alpha_{BB} = 1 \qquad (N.D.)$$

Graybody -- A graybody is an object that radiates (and absorbs) radiant energy
of all wavelengths equally but less than perfectly. That is:

$$\epsilon_{GB}(\lambda) = \epsilon_{GB} = \alpha_{GB}(\lambda) = \alpha_{GB} < 1 \qquad (N.D.)$$

Stefan-Boltzmann Law -- The Stefan-Boltzmann Law states that the radiant emittance of a blackbody is proportional to the fourth power of its absolute temperature. That is:

$$W_{BB} = \left(\frac{2 \pi^5 k^4}{15 h^3 c^2} \right) T^4 \quad (Watts/cm^2)$$

or:

$$W_{BB} = \sigma T^4 \quad (Watts/cm^2)$$

C = Velocity of Propagation = 3×10^{10} (cm/sec)

h = Planck's Constant = 6.63×10^{-34} (Watts-Sec^2)

k = Boltzmann's Constant = 1.38×10^{-23} (Watts-Sec/Deg)

σ = Stefan-Boltzmann Constant = 5.67×10^{-12} (Watts/cm^2-Deg^4)

T = Absolute Temperature (Degrees, Kelvin)

Planck's Law -- Planck's Law expresses the spectral radiant emittance of a blackbody as a function of wavelength and temperature. That is:

$$W_\lambda = \frac{2 \pi h c^2 \times 10^{16}}{\lambda^5 \left(e^{b_\lambda / kT} - 1\right)} \quad (Watts/cm^2 - Micrometer)$$

where:

$\quad E_\lambda$ = Photon Energy = $\frac{hc}{\lambda}$ (Joules)

$\quad h$ = Planck's Constant = 6.63×10^{-34} (Watts-Sec^2)

$\quad k$ = Boltzmann's Constant = 1.38×10^{-23} (Watts-Sec/Deg)

$\quad c$ = Velocity of Propagation = 3×10^{10} (cm/sec)

$\quad T$ = Absolute Temperature (Degrees, Kelvin)

$\quad \lambda$ = Radiation Wavelength (Micrometers)

Typical curves of spectral radiant emittance versus radiation wavelength are shown, for various temperatures, in Figure 2.1.2.1.

Wien's Displacement Law -- Wein's Displacement Law states that the wavelength for which the spectral radiant emittance is a maximum for a blackbody at a given temperature is inversely proportional to the absolute temperature. That is:

$$\lambda_{(max \, W_\lambda)} = a / T \quad (Micrometers)$$

where:

$$a = 2898 \quad (Micrometer-Degrees)$$

The locus of W_λ maxima is indicated in Figure 2.1.2.2. A corollary to Wien's Law states that the W_λ maxima are proportional to the fifth power of absolute temperature. That is:
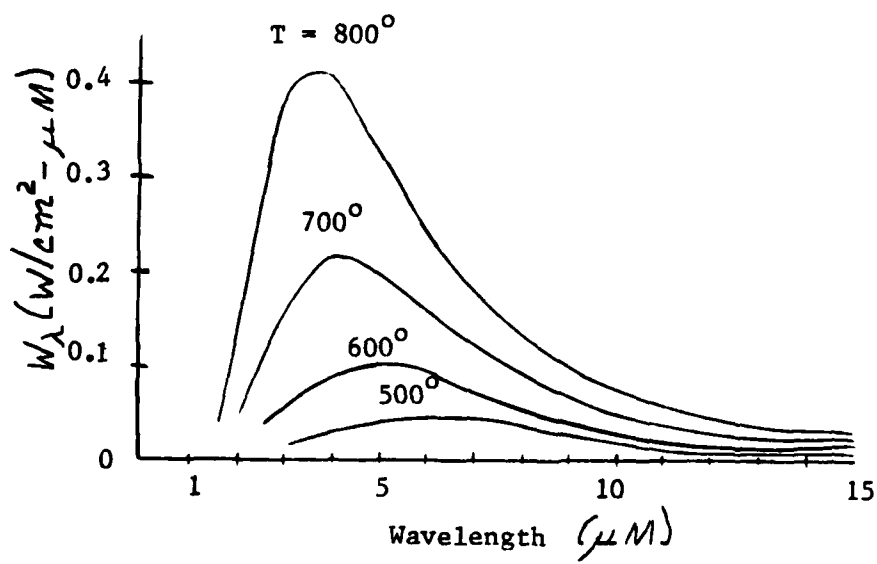
Figure 2.1.2.1 -- Spectral Radiant Emittance Versus
Wavelength for a Blackbody
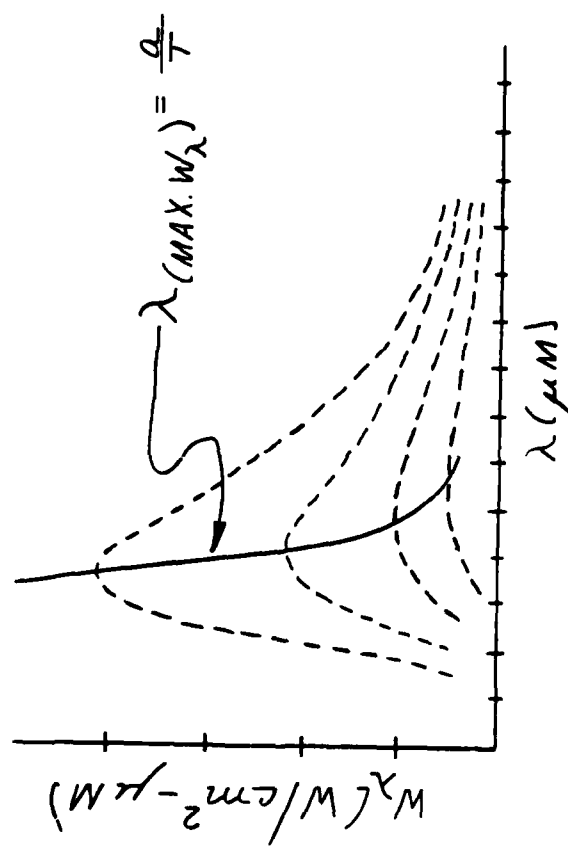
Figure 2.1.2.2 -- Wien's Displacement Law

2.7b

$$W_\lambda (Max) = b\,T^5 \quad (Watts/cm^2\text{-}Micrometer)$$

where:
$$b = 1.3 \times 10^{-15} \quad (Watts/cm^2\text{-}Micrometer\text{-}Deg^5)$$

Lambert's Cosine Law -- A Lambertian (point) source is a radiating, perfectly diffuse, flat surface radiating into a hemisphere, so that the radiant intensity varies with angle from the normal according to the equation:

$$J(\theta) = J_0 \cos(\theta) = \left(\frac{P}{\pi}\right) \cos(\theta) \quad (Watts/stearadian)$$

The radiant intensity pattern of a Lambertian source is shown in Figure 2.1.2.3.

2.1.3 The Transmission of Radiation Through a Body or Medium -- In the process of transmission through a body or medium, electromagnetic waves undergo changes in amplitude and direction of propagation produced by the transmitting, re-flecting, absorbing, and scattering properties of the body or medium. These processes are described by the following terms and relationships.

Transmittance: (τ) (Non-Dimensional) -- The ratio of the radiant flux trans-mitted through a body to the radiant flux incident upon its surface. That is:

$$\tau = P_{Transmitted} / P_{Incident}$$

Reflectance: (ρ) (Non-Dimensional) -- The ratio of the radiant flux reflected by a body to the radiant flux incident upon its surface. That is:

$$\rho = P_{Reflected} / P_{Incident}$$

$$J = J_0 \cos(\alpha) = \frac{P}{\pi} \cos(\alpha) \quad (Watts/S_r)$$
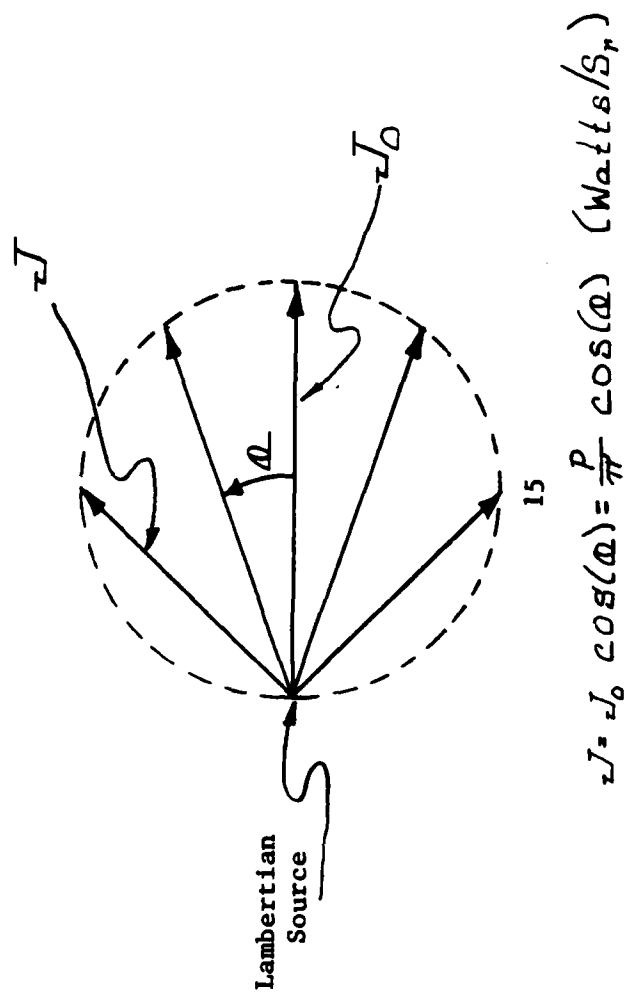
Figure 2.1.2.3 -- Lambertian Source

Absorption Coefficient: a (cm^{-1}) -- The coefficient of decay of radiant flux (or irradiance) due to absorption in passing through an absorbing medium. That is:

$$P(R) = P_{(R=0)}\, e^{-aR} \qquad (Watts)$$

or:

$$H(R) = H_{(R=0)}\, e^{-aR} \qquad (Watts/cm^2)$$

where:

$$R = Distance\ from\ source\ (cm)$$

Scattering Coefficient: (γ) (cm^{-1}) -- The coefficient of decay of radiant flux (or irradiance) due to scattering in passing through a scattering medium. That is:

$$P(R) = P_{(R=0)}\, e^{-\gamma R} \qquad (Watts)$$

or:

$$H(R) = H_{(R=0)}\, e^{-\gamma R} \qquad (Watts/cm^2)$$

where:

$$R = Distance\ from\ source\ (cm)$$

Extinction Coefficient: (σ) (cm^{-1}) -- The coefficient of exponential decay of radiant flux (or irradiance) due to all losses (but not free-space attenuation) in passing through a medium. That is:

$$P(R) = P_{(R=0)}\, e^{-\sigma R} \qquad (Watts)$$

or:

$$H(R) = H_{(R=0)}\, e^{-\sigma R} \qquad (Watts/cm^2)$$

where:

$$R = Distance\ from\ source\ (cm)$$

and:

$$\sigma = a + \gamma$$

2.9

The transmittance of an optical path in an absorbing or scattering medium can be expressed in terms of the extinction coefficient. That is:

$$\tau = e^{-\sigma R} = e^{-(a + \gamma)R} \qquad (N.D.)$$

where:

R = Path Length in Medium (cm)

The Conservation of Radiant Energy -- The sum of the radiant flux reflected, transmitted, and absorbed by a body must be equal to the radiant flux incident upon its surface. That is:

$$P_{Reflected} + P_{Transmitted} + P_{Absorbed} = P_{Incident} \qquad \text{(Watts)}$$

or:

$$\rho + \alpha + \tau = 1$$

For an opaque body ($\tau = 0$):

$$\rho + \alpha = 1$$

For an non-absorbing or scattering body ($\alpha = 0$):

$$\rho + \tau = 1$$

The transmittance of the Atmosphere -- Due to selective (frequency dependent) absorption by resonant molecules, (principally water and carbon dioxide), the transmittance of the atmosphere is rather poor for electromagnetic waves at most optical frequencies. Typical curves of atmospheric transmittance versus wavelength are shown in Figure 2.1.3.1 for altitudes of zero and thirty thousand feet. At thirty thousand feet altitude, the transmittance is much greater than at sea level due to the rarefied atmosphere. For use within the atmosphere, especially for low altitude applications, infrared systems must be designed to

2.10
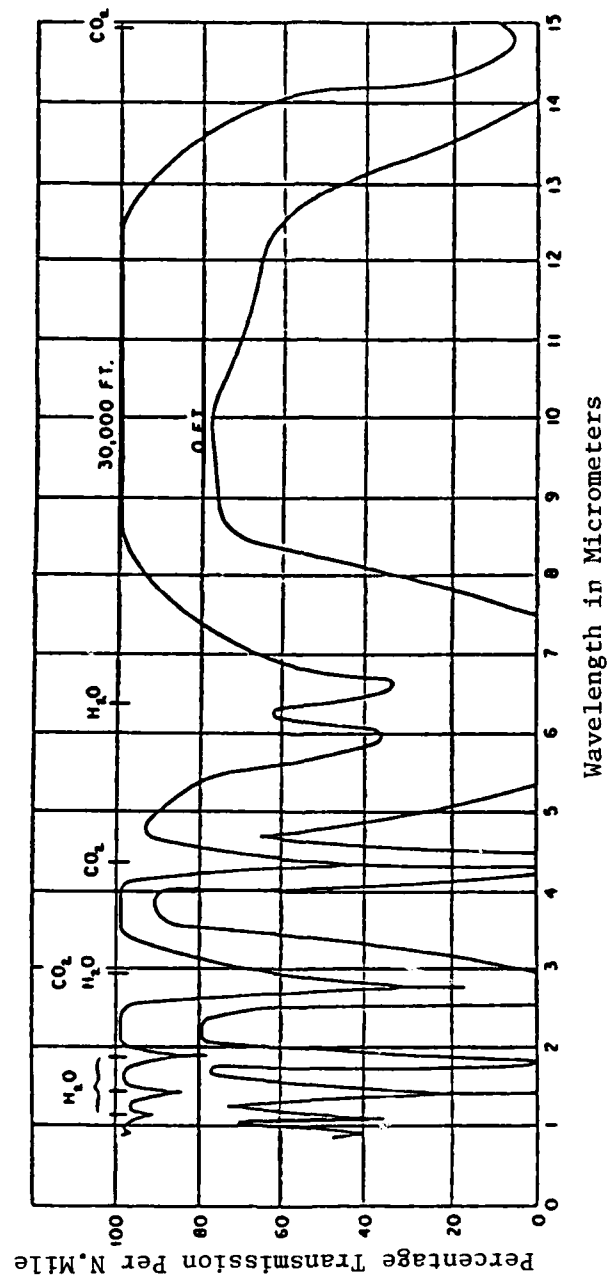
Figure 2.1.3.1--Transmittance of the Atmosphere

2.10a

operate in the atmospheric "windows" or regions of relatively high trans-
mittance. Space applications have no such problem and allow the system
designer greater opportunity to utilize the inherently superior imaging and
information-carrying capabilities of optical-frequency systems (as opposed to
radio-frequency systems).

Free-Space Attenuation (Geometric Spreading) -- In free space (no absorption
or scattering), the irradiance due to a point (or distant) source is still
attenuated by the geometric spreading of the waves. That is:

$$H(R) = J_{source} / R^2 \qquad \text{(Watts/cm}^2\text{)}$$

where:

J_{Source} = Intensity of Source   (Watts/Stearadian)

R = Distrance from Source to Irradiated Surface (cm)

Index of Refraction: (n) (Non-Dimensional) -- The velocity of propagation of
an electromagnetic wave in a given medium depends upon the electric permittivity
(ε) and magnetic permeability (μ) of that medium. In terms of the index of
refraction (n), the velocity of propagation is given by:

$$v = c / n \qquad \text{(cm/sec)}$$

where:

C = Velocity of electromagnetic wave in free space = 3×10^{10} cm/sec.

and:

$$n = \left[\left(\frac{\varepsilon}{\varepsilon_o} \right) \left(\frac{\mu}{\mu_o} \right) \right]^{1/2}$$

where:

ε_o and μ_o are the values in vacuum.

The index of refraction is a nonlinear function of frequency.

2.1.4 The Refraction of Electromagnetic Radiation at the Interface Between
Two Media -- The direction of propagation (ray path) of electromagnetic
radiation is, in general, altered in passing through the interface between
two media of different index of refraction. The relationship between the
angles of the ray path, from the normal to the interface, before and after
refraction, is shown in Figure 2.1.4.1. The angles θ_1 and θ_2 are related
by Snell's Law, given by:

$$\frac{Sin(\theta_2)}{Sin(\theta_1)} = \frac{n_1}{n_2}$$

where n_1 and n_2 are the indices of refraction.

For purposes of optical system design, the trigonometric function, sin (θ), is
generally approximated by the first few terms in the power series expansion,
given by:

$$Sin(\theta) = \theta - \frac{\theta^3}{3!} + \frac{\theta^5}{5!} - \frac{\theta^7}{7!} + \cdots$$

First-order optical design includes only the first term.
That is:

$$Sin(\theta) = \theta \quad (Rad.)$$

Snell's Law then becomes:

$$\frac{\theta_2}{\theta_1} = \frac{n_1}{n_2}$$

Third-order and fifth-order optical design include the second and third term,
respectively. The above approximations can produce significant effects in
electro-optical system performance.
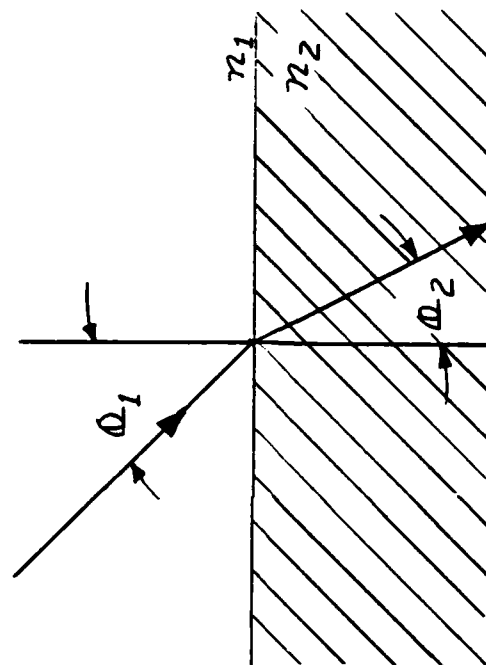
$$\frac{Sin(\alpha_2)}{Sin(\alpha_1)} = \frac{n_1}{n_2}$$

Figure 2.1.4.1 -- The Refraction of Electromagnetic Radiation at the Interface Between Two Media

2.1.5 The Reflection of Electromagnetic Radiation at the Interface Between Two Media -- At the interface between two media of different index of refraction, a portion of the incident electromagnetic flux is reflected back into the first medium and a portion passes into the second medium. The direction of propagation (ray path) of the reflected portion obeys the Law of Reflection, (Angle of Reflection equals Angle of Incidence), as illustrated in Figure 2.1.5.1.

The radiant flux of (or irradiance produced by) the reflected and transmitted waves are given by the relationships defined in Section 2.1.3 of this text. That is:

$$P_{Reflected} = \rho \; P_{Incident} \qquad \text{(Watts)}$$

$$P_{Transmitted} = \tau \; P_{Incident} \qquad \text{(Watts)}$$

where:

$$\rho + \tau = 1$$

The reflectance of the interface, for a normally-incident ray, is a function only of the indices of refraction and is given by:

$$\rho = \left(\frac{n_2 - n_1}{n_2 + n_1} \right)^2 \qquad (N.D.)$$

Thus, for a normally incident ray, the transmittance of the interface between two media is given by:

$$\tau = \frac{4 \, n_1 \, n_2}{(n_1 + n_2)^2} \qquad (N.D.)$$

In general, the reflectance and transmittance for non-normal rays are nonlinear functions of the angle of incidence. (See Section 2.4.2 of the text on Communications Systems for a discussion of reflection phenomena.)

2.13

$\alpha_3 = \alpha_1$

n_1

n_2

α_1 α_3

$n_1, n_2 =$ Indices of Refraction
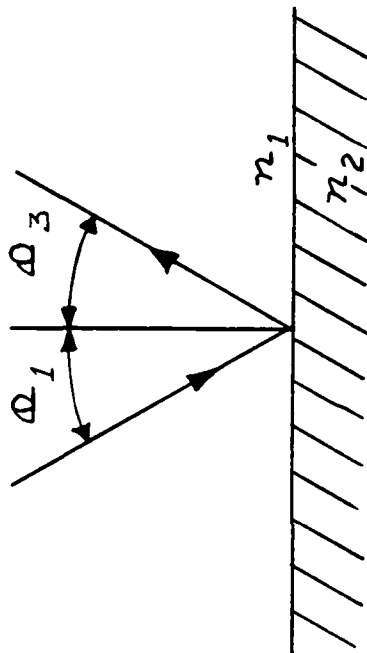
$\alpha_1 =$ Angle of Incidence

$\alpha_3 =$ Angle of Reflection

Figure 2.1.5.1 -- The Reflection of Electromagnetic Radiation at the Interface Between Two Media

Critical Angle (Total Internal Reflection) -- When the incident ray is in the medium of greater index of refraction ($n_1 > n_2$ in Figure 2.1.5.2), all of the incident radiant flux is reflected, by the interface between two media, when the angle of incidence (θ_1) is greater than the Critical Angle given by:

$$\theta_c = Sin^{-1} \left[n_2 / n_1 \right] \qquad \text{(Radians)}$$

Total internal reflection can be achieved by utilizing reflection from the inner surface of a silvered prism face as shown in the Figure. (The reflections at the unsilvered faces are small due to normal incidence.)

Brewster's Angle -- At the interface between two media, the component of an incident ray with polarization in the plane of incidence, ($\overrightarrow{\mathcal{E}_V}$ in Figure 2.1.5.3), is entirely transmitted through the interface, for a specific angle of incidence known as Brewster's Angle (θ_B). Thus the reflected ray is plane polarized in the direction parallel to the reflecting surface ($\overrightarrow{\mathcal{E}_H}$ in Figure 2.1.5.3). Brewster's Angle is given by:

$$\theta_B = Tan^{-1} \left[n_1 / n_2 \right] \qquad (Rad) \qquad \text{(Radians)}$$

where n_1 and n_2 are the indices of refraction of the media.

2.1.5 The Diffraction of Electromagnetic Radiation -- Any constriction or obstruction in the propagation path of electromagnetic radiation produces non-reflective, non-refractive alterations in the radiation pattern that are functions of the physical dimensions of the obstruction and the wavelength of the radiation. These effects, termed diffraction effects, are due to wave interference between waves from various portions of the radiative field. (For a more detailed dis-cussion of diffraction effects and wave interference phenomena, see Section 2.4.2 of the text on Communications Systems.) For example, if the radiant flux from

2.14
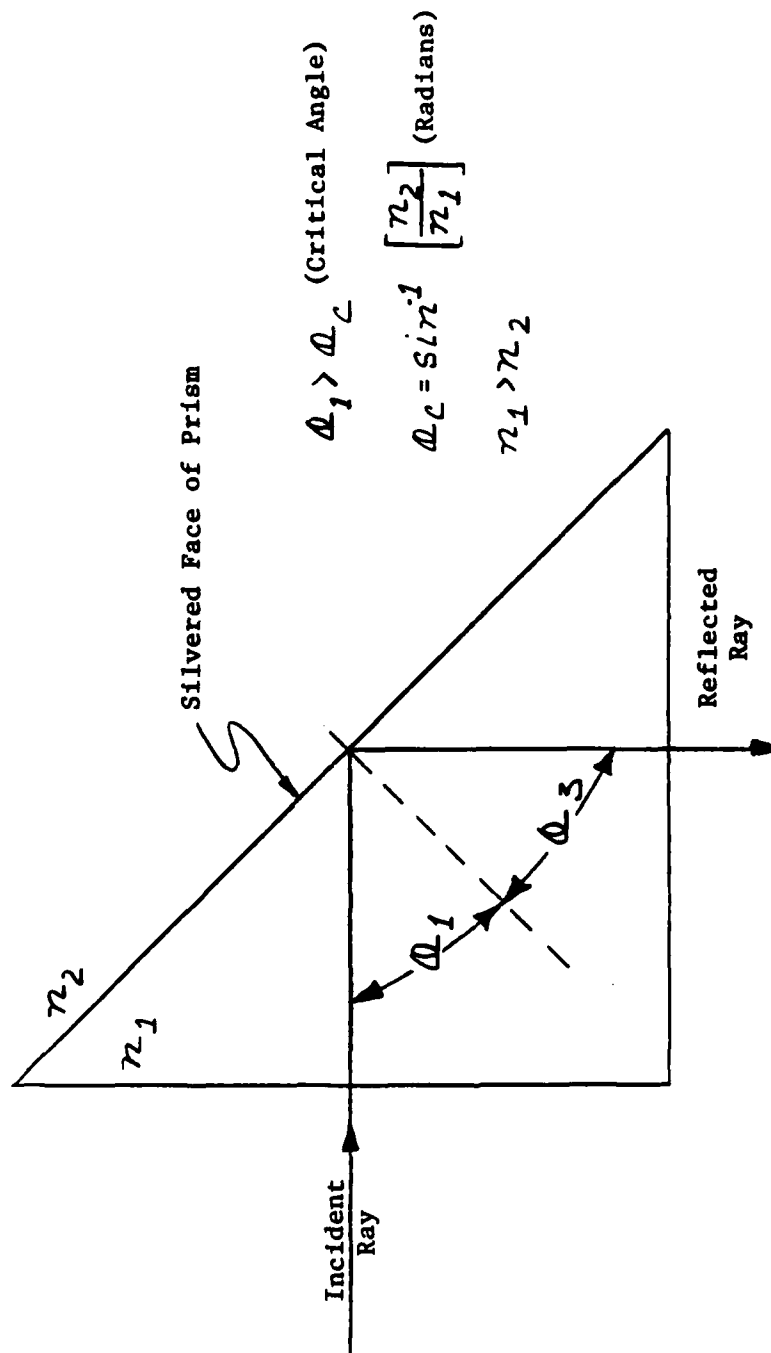
Figure 2.1.5.2 -- Total Internal Reflection (Critical Angle)

Horizontally
Polarized Ray

Unpolarized Ray

$\vec{E}_V$
$\vec{E}_H$

θ_B

n_1

n_2

$\vec{E}_H$

$\vec{E}_V$

Vertically
Polarized Ray
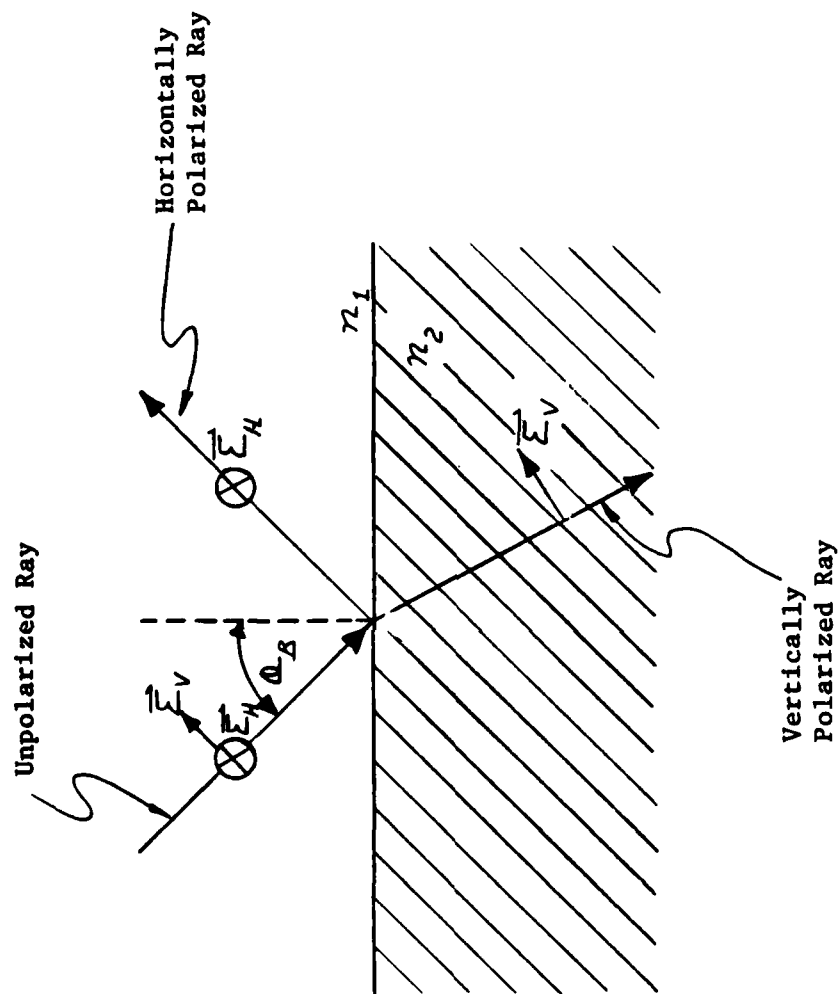
$$\theta_B = Tan^{-1}\left[\frac{n_1}{n_2}\right] \text{(radians)}$$

Figure 2.1.5.3 -- Brewster's Angle

2.14b

a point source is focused upon a screen by a diffraction limited optical system, (one in which the ability to focus a point source perfectly as a point is limited only by diffraction effects), the image of the point source will be not a point but a "spot" of finite diameter surrounded by increasingly faint concentric rings. The distribution of radiant flux, as a function of radius from the center of the pattern, is plotted in Figure 2.1.6.1. The "spot" in the center is called the Airy Disk and, if assumed to extend out to the first minima, contains 84% of the total flux in the pattern. The angular subterse of the Airy Disk (out to the first minima) is given by the equation:

$$\theta_{ad} = \frac{0.244 \, \lambda}{D} \qquad \text{(Milliradians)}$$

and the linear diameter of the Airy Disk, for an infinitely distant point source and a screen at the focal point of the optical system, is given by the equation:

$$d_{ad} = \frac{0.244 \, \lambda \, f_1}{D} \qquad \text{(Millimeters)}$$

where:

λ = Wavelength in Micrometers

f_1 = Focal length of Optics in Meters

D = Diameter of Optical Aperture in centimeters

The angular subtence of the Airy Disk, for a given radiation wavelength and optical aperture, can be determined from Figure 2.1.6.2. If the apertures in an optical system are not sufficiently large, diffraction effects can limit the angular resolution of the system.

2.2 Optics

2.2.1 The Lens -- The lens is an optical element that utilizes the phenomenon of refraction to collect, concentrate, redirect, and focus electromagnetic wave

Radiant Flux

Radial Distance

$d_{a.d.}$
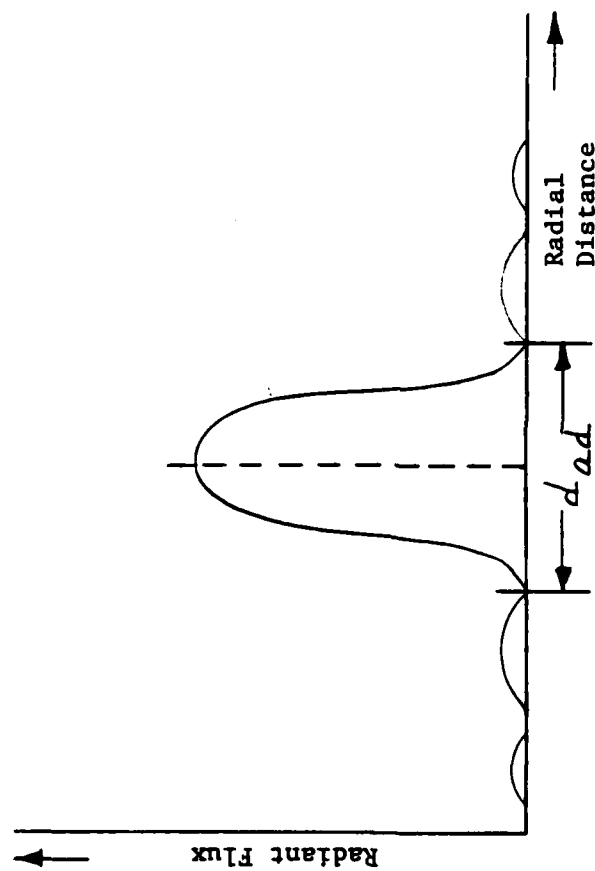
Figure 2.1.6.1 -- Distribution of Radiant Flux in Diffraction Limited Image of Point Source
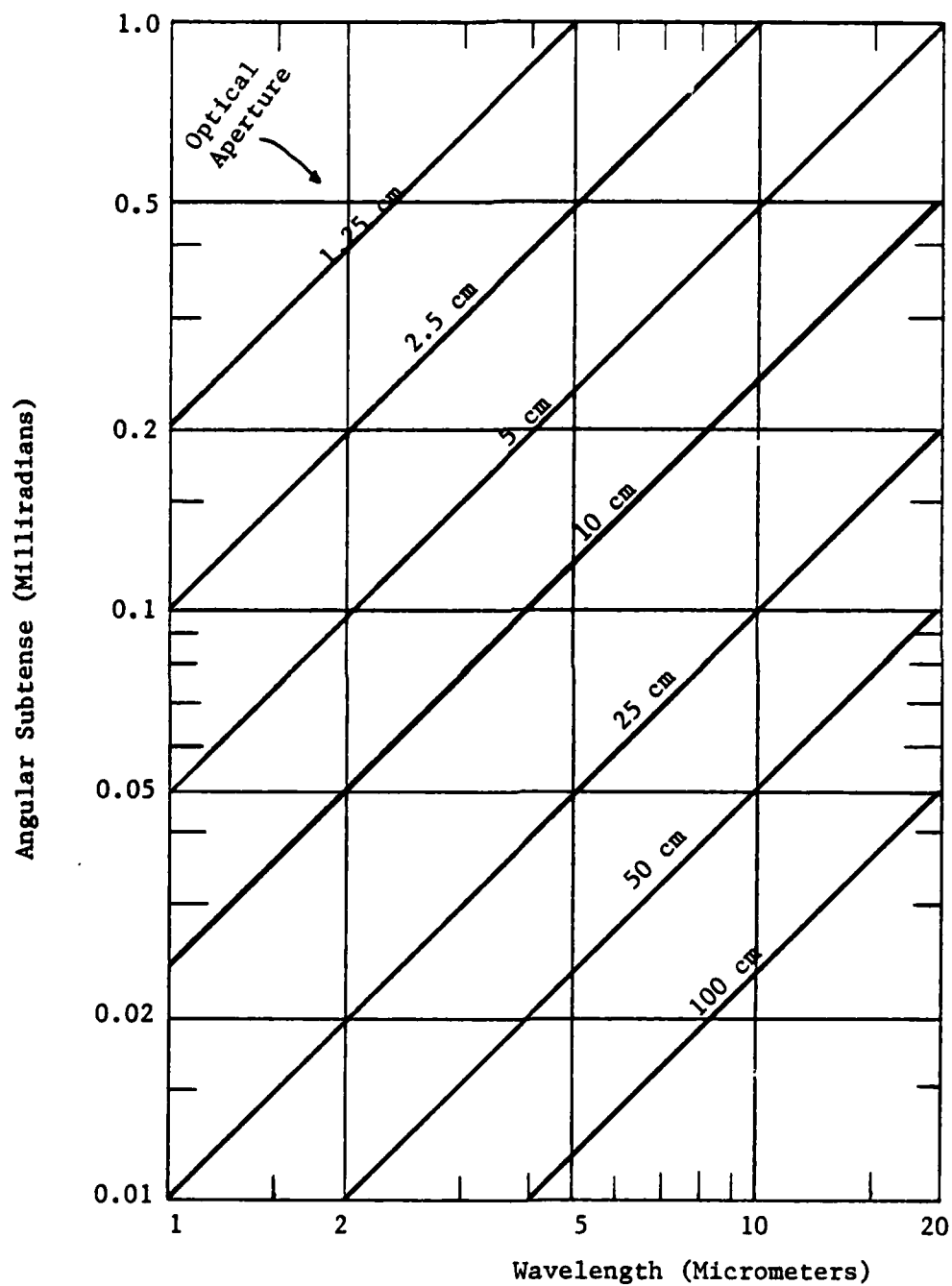
Figure 2.1.6.2 -- Angular Subtense of the Airy Disk

2.15b

radiation. The lens generally is characterized by curved surfaces (faces) and may consist of two or more lens elements, in tandem, with different geometries or indices of refraction.

A lens is considered a "thin lens" when its thickness is small in comparison with the radii of curvature of its surfaces, its focal length, and the object and image distances. When such is not the case, the lens must be considered a "thick lens". As will be seen, the same imaging formulae apply to thin and thick lenses provided that the object and image distances for a thick lens are measured from the principal points of the lens rather than from its center as for a thin lenses.

The Focal Points of a Lens -- As shown in Figure 2.2.1.1, focal points exist on either side of a lens. Rays emanating from the first focal point, F_1, (on the near side of the lens), emerge from the lens parallel to the optical axis as shown in Figure 2.2.1.1(a). Rays entering the lens parallel to the optical axis pass through the second focal point, F_2, (on the far side of the lens), as shown in Figure 2.2.1.1(b). The focal points lie at a distance, f, (the focal length), on either side of the lens. For a thin lens, the distances to the focal points are measured from the center of the lens as shown in the figure. (Thick lenses are discussed in a following paragraph).

The Lens Maker's Formula -- The focal length of a thin lens is determined by its index of refraction and the radii of curvature of its surfaces, (see Figure 2.2.1.2), and is given by the equation:

$$f = \left(\frac{1}{n-1} \right) \left(\frac{r_2 r_1}{r_2 - r_1} \right) \qquad \text{(cm)}$$

F_1, F_2 = Focal Points

f = Focal Length (Thin Lens)

(b) Source at Infinity

F_2

F_1

f f f

(a) Source at Focal Point

F_2

F_1

f f f
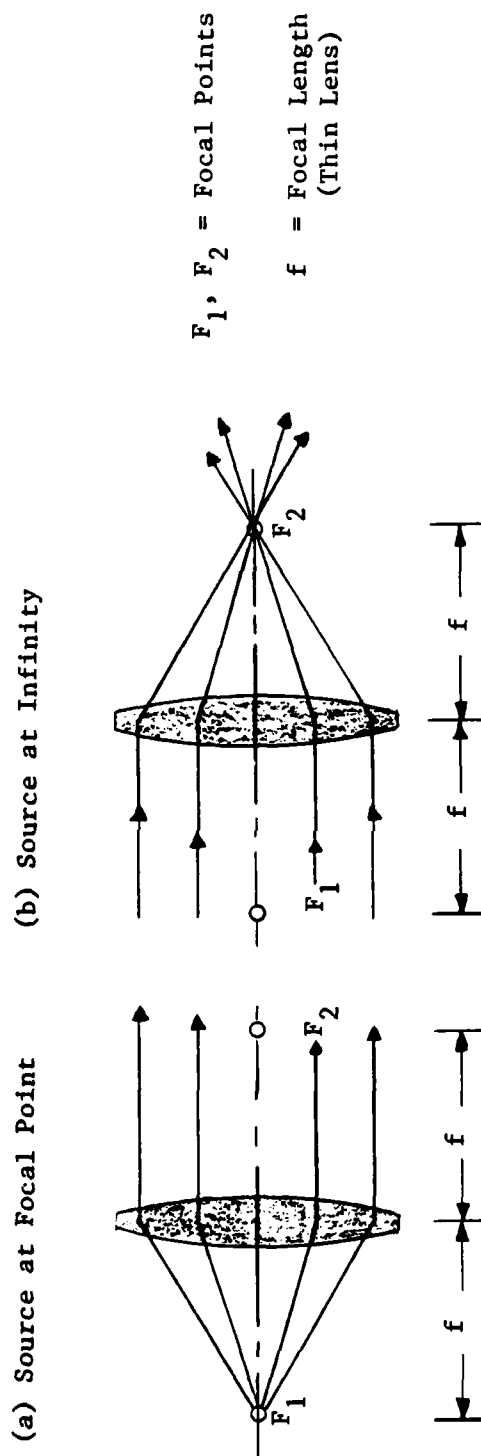
Figure 2.2.1.1 -- Focal Points of a Lens

$$f = \left(\frac{1}{n-1}\right)\left(\frac{r_1 r_2}{r_2 - r_1}\right)$$
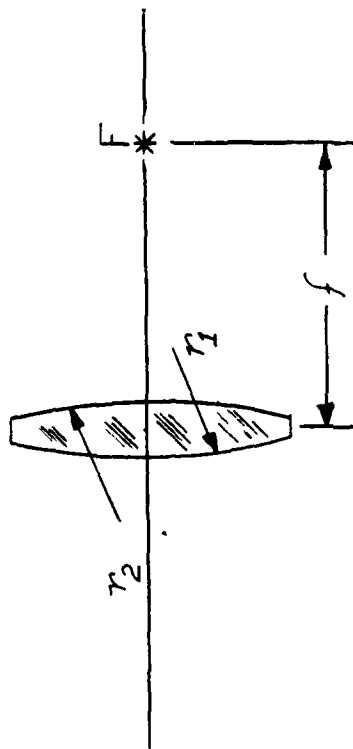
n = Lens Index of Refraction (N.D.)

r_1, r_2 = Lens Radii of Curvature (cm) (A Radius is Positive if Surface is Concave to the left).

When f > 0, the lens is said to be positive.

When f < 0, the lens is said to be negative.

Figure 2.2.1.2 -- Focal Length of a lens

where it is assumed that the medium on both sides of the lens has an index of refraction equal to unity and:

n = Index of Refraction of Lens Material (N.D.)

r_1 = Radius of Curvature of Left Hand Surface of Lens in Figure (cm).

r_2 = Radius of Curvature of Right-Hand Surface of Lens in Figure (cm).

(A radius of curvature is positive if the surface is concave to the left in the figure.)

Note that it is possible for a lens to have a negative focal length, indicating that the focal point is located on the opposite side of the lens to that shown in the figure.

Object/Image Geometric Construction (Ray Tracing) -- The image produced by a positive lens ($f > 0$) may be geometrically determined from the object by utilizing the following ray-tracing rules:

(1) A ray entering the lens parallel to its optical axis passes through the focal point on the far side of the lens.

(2) A ray entering the lens after having passed through the focal point on the near side of the lens exits from the lens parallel to the optical axis.

(3) A ray passing through the geometric center of a (thin) lens is undeflected by the lens.

Rays illustrating the three rules are shown, in Figure 2.2.1.3, emanating from the head of an arrow (the object) and converging on the head of the image of the arrow. Using this method, each point in an object can be traced to the corresponding point in its image.
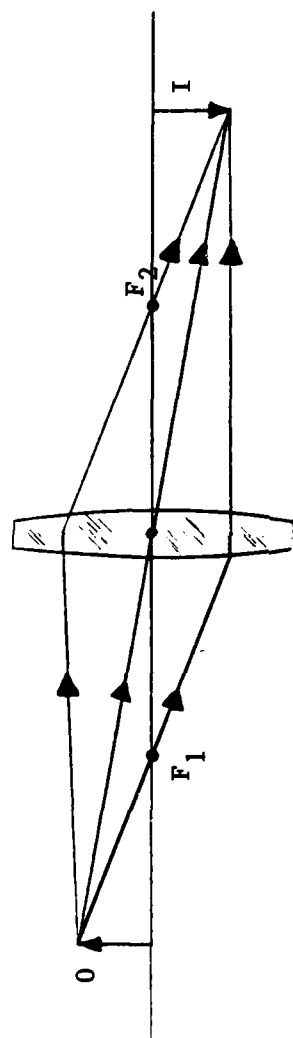
Figure 2.2.1.3 -- Geometric Method of Object - to - Image Construction for a Positive Lens (f > 0).

The Virtual Image -- When the rays forming an image actually emanate from the apparent position of that image, the image is termed "real". When the rays only appear to emanate from the image, as shown in Figure 2.2.1.4, the image is termed "virtual". (When the focal length of a lens is negative (f < 0), it creates a virtual image of an object beyond its focal point. P' Q' is the virtual image in Figure 2.2.1.4.) If a screen were placed at the position of an image, only a real image would appear on the screen. The rays to the right of the lens in the figure are, however, exactly as they would be if P' Q' were a "real" image. Thus, P' Q' forms the "object" for other optical elements to the right of the lens.

The virtual image produced by a negative lens, (f < 0), may be geometrically determined from the object by utilizing the following ray-tracing rules:

   (1) A ray entering the lens parallel to the optical axis is refracted
       so that it appears to emanate from the focal point on the near
       side of the lens.

   (2) A ray entering the lens after having passed through the focal point
       on the near side of the lens exits from the lens parallel to the
       optical axis.

   (3) A ray passing through the center of a (thin) lens is undeflected
       by the lens.

Rays illustrating these three rules are shown in Figure 2.2.1.4.

When the object is beyond the focal point of a lens with positive focal length (f > 0), a real image is formed, as shown in Figure 2.2.1.5(a). When the object is at the focal point, the image is formed at infinite distance $(d_i = \infty)$ as shown in Figure 2.2.1.5(b). When the object is inside the focal point, a virtual image is formed, as shown in Figure 2.2.1.5(c).
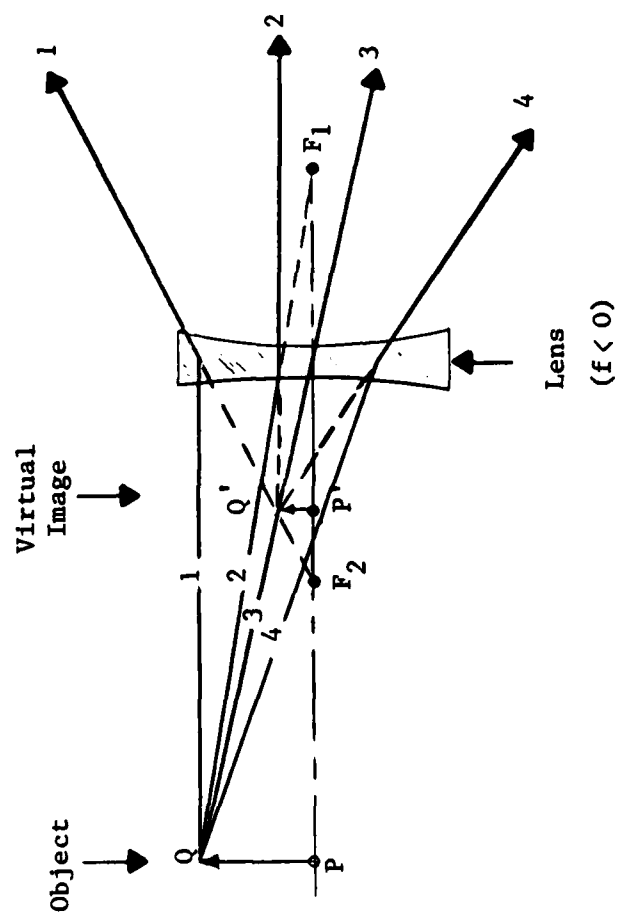
Figure 2.2.1.4 -- The Virtual Image Produced by a Negative Lens (f < 0)

2.18a
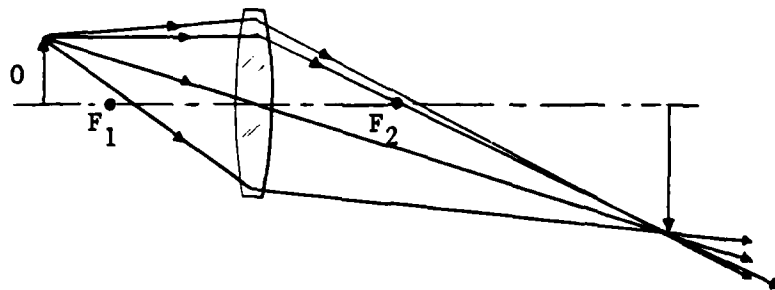
(a) Real Image $(|d_o| > |f|)$

(b) Image at Infinity $(|d_o| = |f|)$

I at Infinity
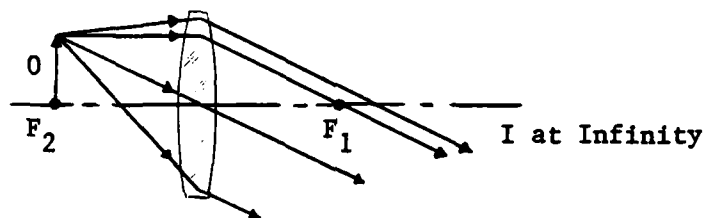
(c) Virtual Image $(|d_o| < |f|)$
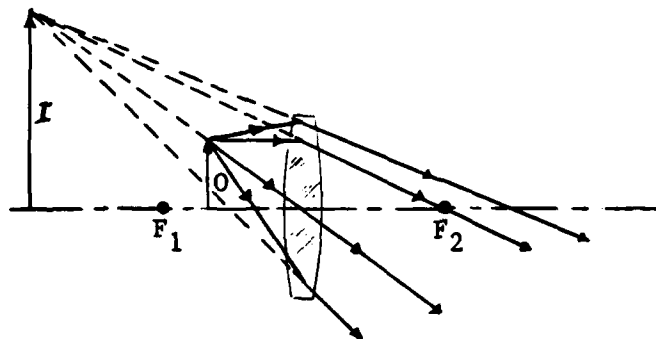
Figure 2.2.1.5 -- Effect of Object Location on Image

Multi-Lens Image Construction -- In Figure 2.2.1.6 is shown a four-lens optical system with the geometric construction used to determine the successive images (P, Q, R, and I) from the object (O). As can be seen from the figure, the real image from lens 1, (P), is inside the focal point of lens 2, thus producing a virtual image from lens 2, (Q). The virtual image from lens 2, Q, forms the object for lens 3, producing an image from lens 3, (R), which would be real except for lens 4. The image from lens 3, R, nevertheless, forms the object for lens 4. Since R is beyond lens 4, the graphical construction yields a real final image from lens 4, (I), on the same side of lens 4 as the image from lens 3.

Lens Imaging Characteristics -- The position and magnification of the image produced by a lens depend only upon the focal length of the lens and the position of the object with respect to the lens, as shown in Figure 2.2.1.7. Specifically:

$$d_i = \frac{d_o f}{d_o - f} \qquad \text{(cm)}$$

$$m = \frac{f}{f - d_o} \qquad \text{(N.D.)}$$

where: di = Image Distance (cm)

do = Object Distance (cm)

f = Focal Length of Lens (cm)

m = Magnification

If di is positive, the image is real. If di is negative, the image is virtual.

The sign conventions for object, image, and optical element parameters are dictated by the following rules:

(1) All distances are measured along the optical axis from the refracting or reflecting element to the object or image.

2.19
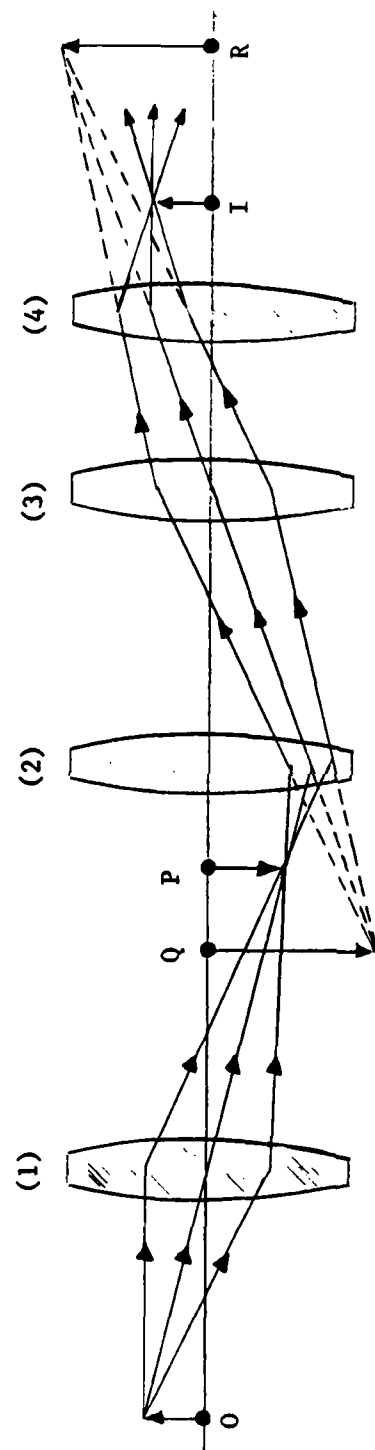
Figure 2.2.1.6 -- Multi-Lens Image Construction

2.19a
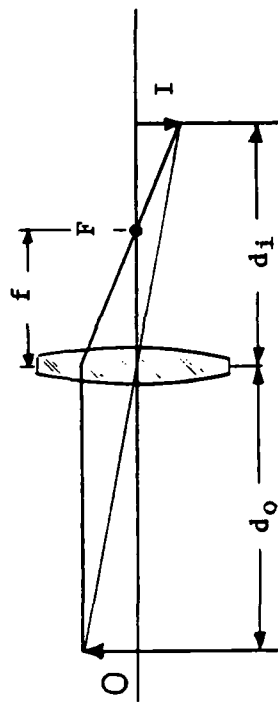
$$d_i = \frac{d_o f}{d_o - f} \quad (cm)$$

$$m = \frac{f}{f - d_o} \quad (N.D)$$

When $d_i > 0$, the image is real.

When $d_i < 0$, the image is virtual.

Figure 2.2.1.7 -- Lens Imaging Characteristics

(2) An object distance (d_o) is positive if its direction is opposite to that of the incident ray.

(3) An image distance (d_i) is positive if its direction is the same as that of the refracted or reflected ray.

(4) A radius of curvature is positive if the direction from the surface to the center of the optical element is the same as that of the refracted or reflected ray.

(5) An object or image dimension above the optical axis is positive.

The Thick Lens -- As previously stated, a "thick lens" is one for which its thickness (distance between surfaces) is not small in comparison with the radii of curvature of its surfaces, its focal length, and the object and image distances. Multiple lens systems also can be considered to be thick lenses. As indicated in Figure 2.2.1.8, the focal point, image, and object distances must be measured with respect to the Principal Points, H_1 and H_2. When these distances are taken in this manner, the same imaging formulae hold as for thin lenses. That is, the image distance is given by:

$$d_i = \frac{d_o\, f}{d_o - f} \qquad \text{(cm)}$$

and the image magnification is given by:

$$m = \frac{f}{f - d_o} \qquad \text{(N.D.)}$$

The focal length of a thick lens is given by the equation:

$$f = \left(\frac{1}{n-1}\right)\left[\frac{r_1\, r_2}{r_2 - r_1 + \left(\frac{n-1}{n}\right)t}\right] \qquad \text{(cm)}$$

and the principal points are located as shown in Figure 2.2.1.8, in which:

$$h_1 = \left(\frac{n-1}{n}\right)\left(\frac{t}{r_2}\right)f \qquad \text{(cm)}$$

$$h_2 = \left(\frac{n-1}{n}\right)\left(\frac{t}{r_1}\right)f \qquad \text{(cm)}$$
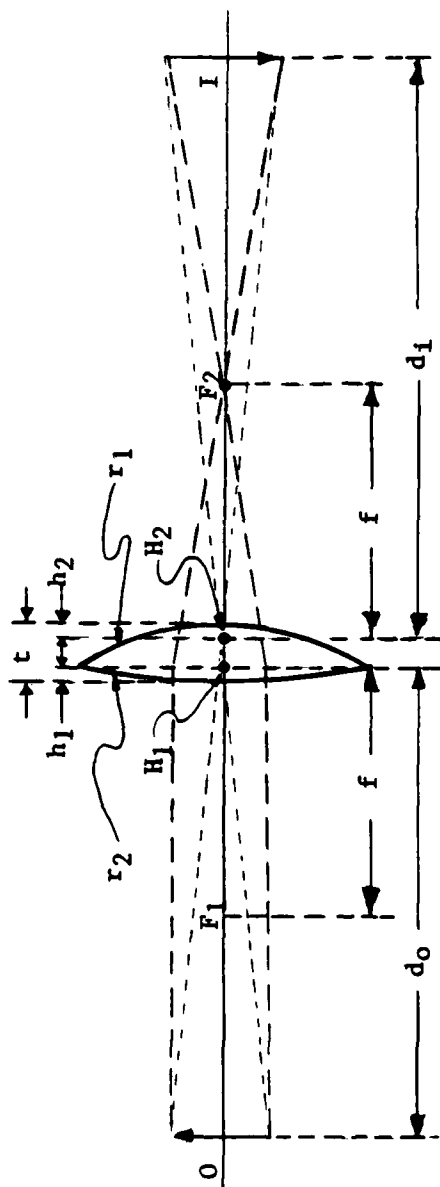
Figure 2.2.1.8--The Thick Lens

where:

d_i = Image Distance

d_o = Object Distance

f = Lens Focal Length

m = Image Magnification

n = Lens Index of Refraction

r_1 = Radius of Curvature of Surface No. 1

r_2 = Radius of Curvature of Surface No. 2

t = Thickness of Lens

Lens f-Number and Numerical Aperture -- The f-number of a lens is a measure of its radiation-gathering power.   It also affects the lens depth-of-field and the extent to which lens aberrations affect the quality of the image.   The f-number is defined by the equation:

$$f_N = f/D \quad (N.D.)$$

where:

f = Focal Length of Lens (cm)

D = Diameter of Lens (cm)

The Depth-of-Field is the range of object distances over which the image is not de-focused beyond a given limit on angular resolution, β, and is given by:

$$dF = \frac{d_o^2 f_N \beta}{f} = \frac{d_o^2 \beta}{D} \quad (cm)$$

where:

d_o = Object Distance (cm)

β = Angular Resolution Limit (Radians)

2.21

The numerical aperture of a lens is defined by the equation:

$$NA = \frac{1}{2 \, f_N} \qquad (N.A.)$$

where f_N is the f-number of the lens. Numerical aperture serves to provide a measure of lens radiation-gathering ability that increases with increasing ability. (f-number varies inversely with ability.)

Lens Aberrations -- Aberrations are those characteristics of optical elements, other than those associated with diffraction, which prevent the lens from imaging a point source as a point in the image plane. Both surface geometry and index of refraction variations contribute to aberration. Aberrations which are the result of more than one wavelength being present in the radiation are termed chromatic aberrations. All other aberrations are monochromatic aberrations. Aberrations cause an optical system to image a point source as a finite spot known as a blur circle or circle of confusion. As previously indicated, the effect of aberrations is a function of lens diameter, the size of the blur circle increasing rapidly with increasing numerical aperture.

The principal monochromatic aberrations are listed and defined below.

    Spherical Aberrations: Rays from a point on the optical axis are
    not brought to a common focus.

    Coma: The image of a point off the optical axis is an egg-shaped
    spot of finite size.

    Distortion: Straight lines are imaged as curved lines.

    Curvature of Field: The image of an object in a plane lies on a
    curved surface.

These monochromatic aberrations are a result of the inability of a lens with spherically ground surfaces to image an object perfectly. They are not due

to imperfections in the manufacture of the lens.   (In airborne systems, imperfections are generally held within limits which make their effects negligible.) Monochromatic aberrations can be corrected to any desired degree by utilizing non-spherical lenses or by multiple-lens systems as shown in Figure 2.2.1.9.

Chromatic aberrations are a result of the variation of the index of refraction of the lens material with the frequency or wavelength of the radiation. When more than one wavelength is present in the radiation from the object, the various frequency components are not refracted identically. Chromatic aberrations are of two kinds, defined below.

> Longitudinal Aberration: Different wavelengths are not imaged in the same plane.

> Lateral Aberration: The size of the image of an object varies with the wavelength of the radiation.

Chromatic aberrations can be corrected by utilizing multiple-element lenses with different indices of refraction as shown in Figure 2.2.1.10.

Types of Lenses -- The nomenclature and use of various types of lenses is indicated in Figure 2.2.1.11.

Multiple-Lens Systems -- The lens system of a simple non-imaging radiation detector is shown in Figure 2.2.1.12. The objective lens gathers radiant flux and delivers it to the field lens. The field lens delivers the radiant flux to the detector. Note that the flux is not focused to a point on the detector but irradiates the detector over its entire surface, thereby maximizing the signal-to-noise ratio.

2.23
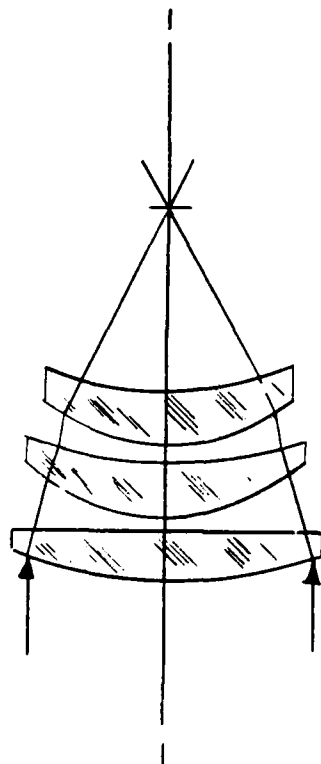
Figure 2.2.1.9--Correction of Lens Aberrations by the Use of Multiple-Lens Systems
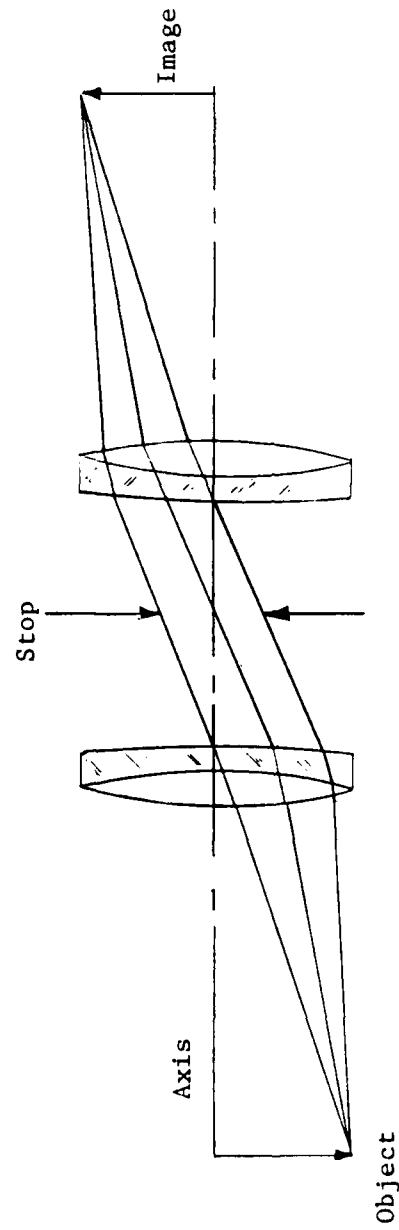
Figure 2.2.1.10 -- Correction of Lens Aberrations by the Use of Multiple Lenses of Different Refractive Index
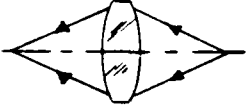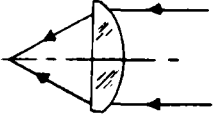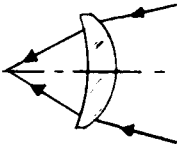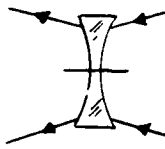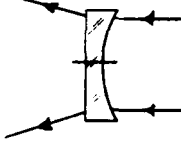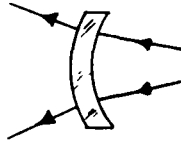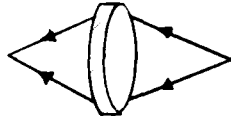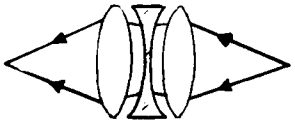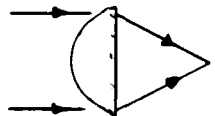
Lens	Type	Characteristics and Application
	Convex	Converging: General Use, Magnification
	Plano Convex	Converging: Used Often in Opposed Doubles to Reduce Spherical Aberration
	Menisus	Converging: Reduced Spherical Aberration
	Concave	Diverging: General Use, Demagnification
	Plano Concave	Diverging: Used in Multi-Element Combinations
	Menisus	Diverging: Reduced Spherical Aberration
	Doublet	Corrected for Chromatic Aberration
	Multi-Element	High Order of Aberrations Correction: Used in Complex Systems
	Aspheric	Corrected for Spherical Aberrations: Used in Condenser Systems

Figure 2.2.1.11 -- Types of Lenses

2.23c
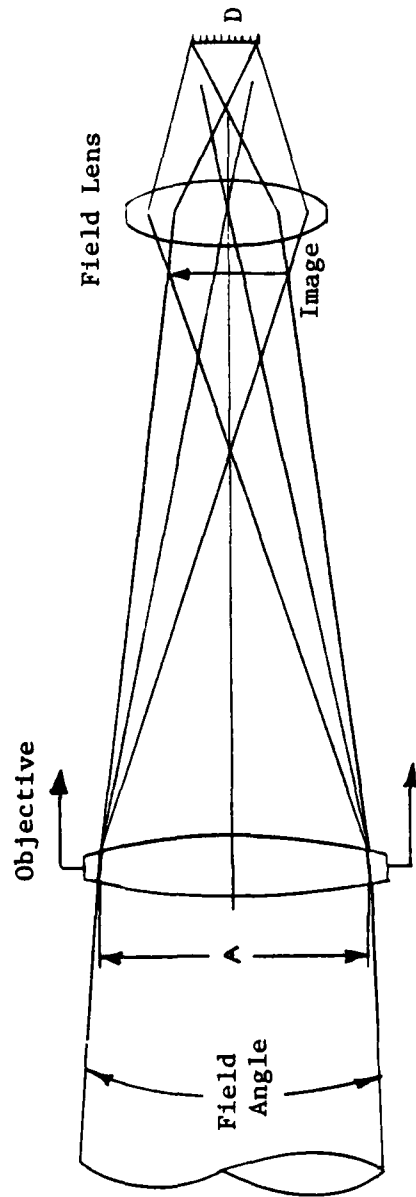
Figure 2.2.1.12 -- Lens System for a Non-Imaging Radiation Detector

2.23d

A relay lens system is shown in Figure 2.2.1.13. A relay lens system is used to transmit an image over an extended, narrow path without altering the size of the image or the field-of-view. A typical application is the periscope.

An afocal lens system focuses the final image at infinity for ease of viewing by the human eye. Two types of afocal lens systems commonly used in telescopes are shown in Figure 2.2.1.14.

A typical imaging sensor optical system is shown in Figure 2.2.1.15. In addition to a multiple-element objective and a field lens are shown a field stop (physical aperture), that determines the field of view, and an aperture stop, that determines the radiation-admitting area (aperture) of the system. As indicated by this example, field and aperture stops can be located at various points in the path of an optical system.

Final Image

Object
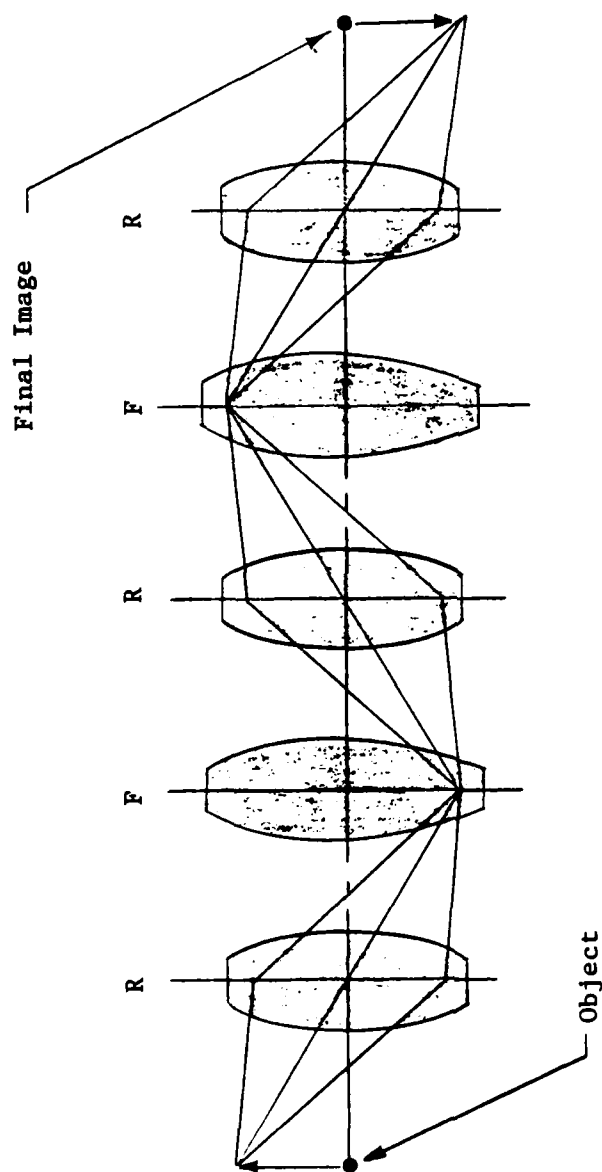
R = Relay Lens

F = Field Lens

Figure 2.2.1.13 -- Relay Lens System

2.24a

Gallilean Telescope
(Non-Inverting)

Astronomical Telescope
(Inverting)
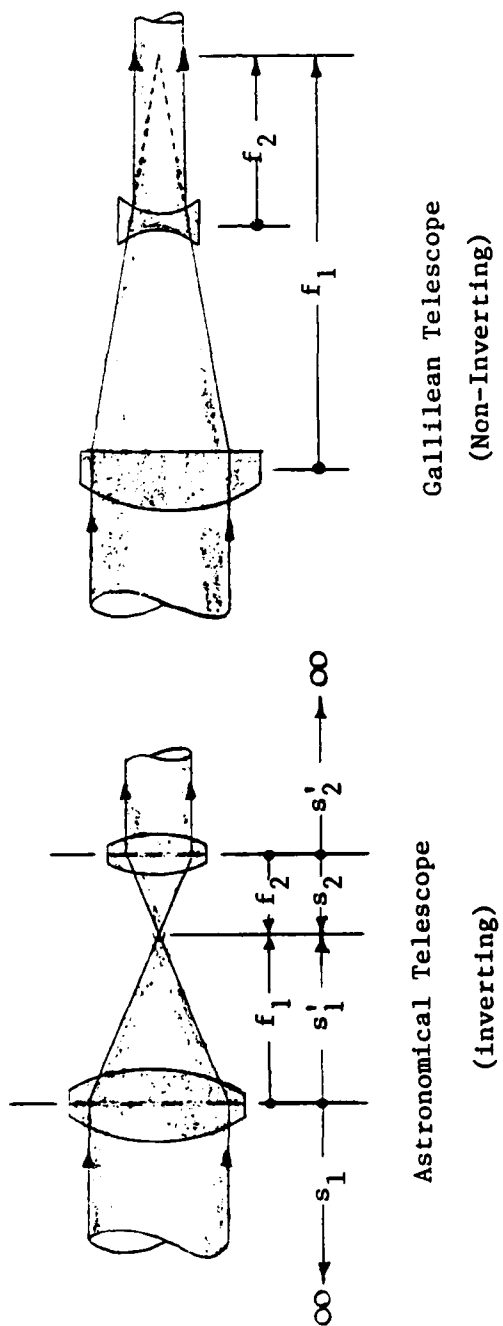
Figure 2.2.1.14 -- Afocal Lens Systems

2.24b

Final Image

Aperture Stop

Field Lens

Field Stop

Objective Lens

Entrance Pupil

Principal or Chief Ray

Object At ∞

1/2 Field Angle
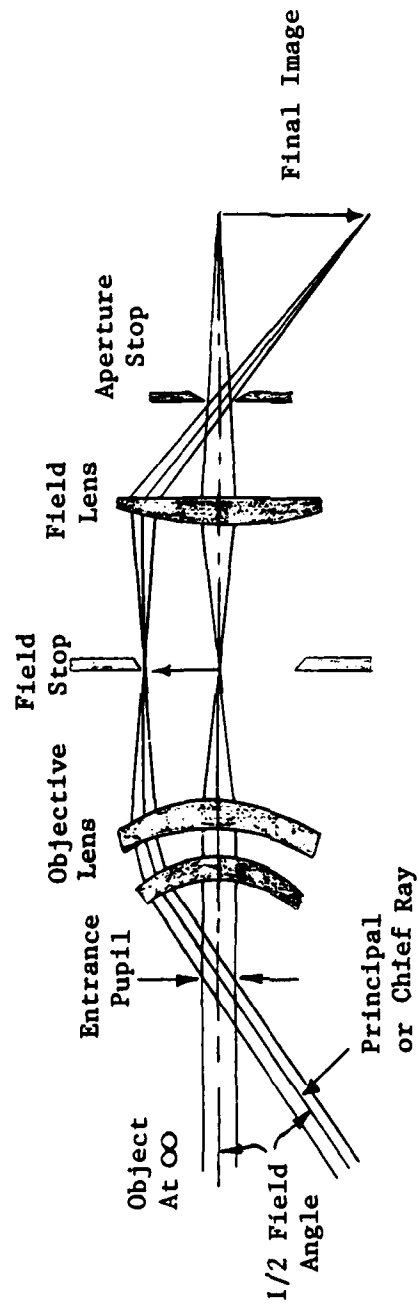
Figure 2.2.1.15 -- Optical System for a Typical Imaging Sensor

2.24c

2.2.2 The Mirror -- The mirror is an optical element that utilizes the phenomenon of reflection to collect, concentrate, redirect, and focus electromagnetic wave radiation. As an optical element, the mirror has many of the same characteristics and serves many of the same purposes as does the lens. The reflecting surfaces of a mirror may be curved or planar and may be partially or totally reflective. Mirrors possess one distinct advantage in comparison with lenses: they do not suffer from chromatic aberrations when "front-silvered". (There is no radiation path through a refracting medium and, hence, no variation of refractive index with frequency.)

The Spherical Mirror -- As with lenses, most mirrors are spherically ground. The focal point, (F), of a spherical mirror is located midway between the reflecting surface and the center of curvature, (c), as shown in Figure 2.2.2.1. Neglecting spherical aberrations, incident rays parallel to the optical axis are reflected (or appear to be reflected) through the focal point. Conversely, rays emanating from the focal point of a positive (concave) mirror are reflected parallel to the optical axis.

Object/Image Geometric Construction -- The image produced by a spherical mirror may be geometrically determined from the object by utilizing the following ray-tracing rules.

(1) An incident ray parallel to the optical axis of the mirror passes through the focal point after reflection.

(2) An incident ray passing through the focal point is reflected parallel to the optical axis.

(3) An incident ray passing through the center of focus is re-flected back upon itself.
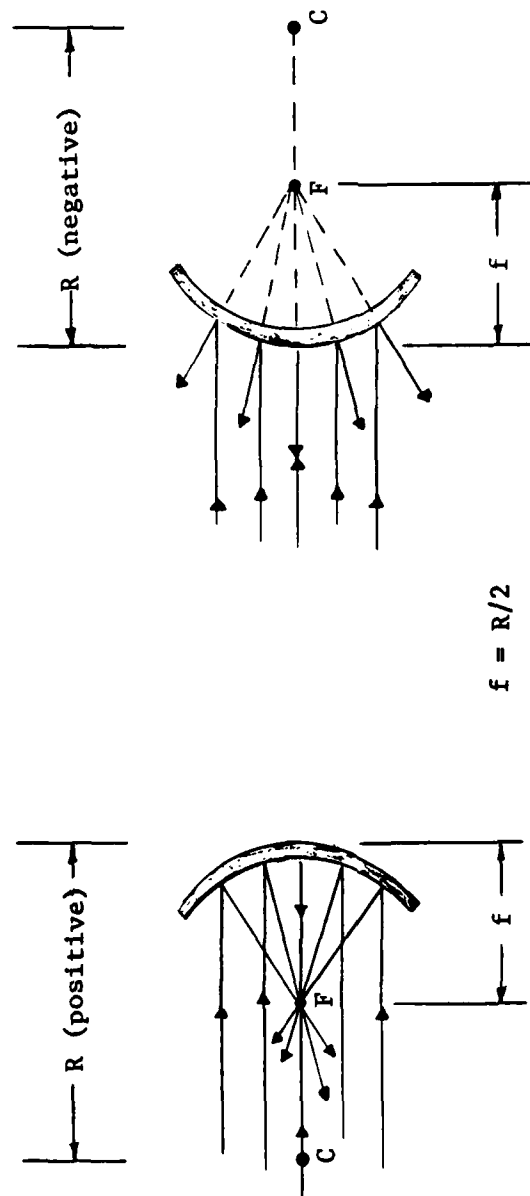
Figure 2.2.2.1 -- The Spherical Mirror

$f = R/2$

Rays illustrating these rules are shown, in Figure 2.2.2.2, emanating from the head of an arrow (the object) and converging on the head in the image of the arrow. Using this method, each point in an object can be traced to the corresponding point in its image. In Figure 2.2.2.3 is shown the virtual image produced by a negative (convex) mirror. Also shown are the construction lines corresponding to the following rules for the geometric method of constructing the image of an object, produced by a negative lens (f < 0).

(1) An incident ray parallel to the optical axis of the mirror is reflected so as to appear to emanate from the focal point on the far side of the mirror.

(2) An incident ray directed toward the focus on the far side of the lens is reflected parallel to the optical axis.

(3) An incident ray directed toward the center of curvature is reflected back upon itself.

Mirror Imaging Characteristics -- The position and magnification of the image produced by a spherical mirror depend only upon the focal length of the mirror and the position of the object with respect to the mirror, as shown in Figure 2.2.2.4. Specifically:

$$d_i = \frac{d_o f}{d_o - f} \quad \text{(cm)}$$

$$m = \frac{h_i}{h_o} = \frac{f}{f - d_o} \quad \text{(N.D.)}$$

where:

d_i = Image Distance

d_o = Object Distance

f = Focal Length of Mirror

h_i = Height (Size) of Image

h_o = Height (Size) of Object

m = Magnification

2.26
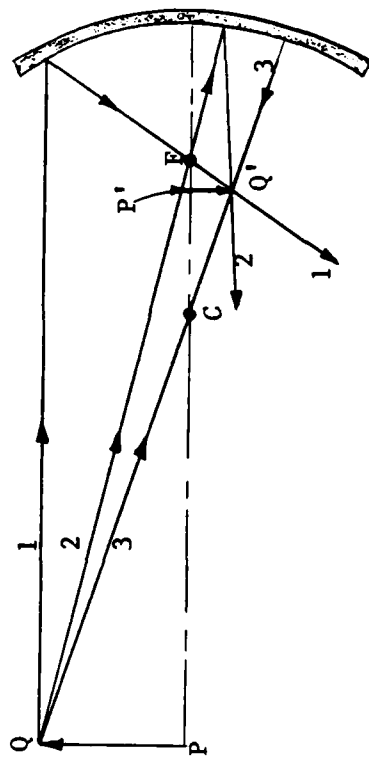
Figure 2.2.2.2 -- Object/Image Geometric Construction for a Spherical Mirror

2.26a
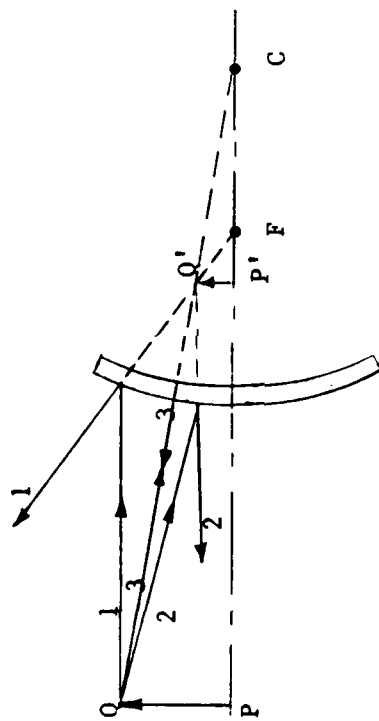
Figure 2.2.2.3 -- The Virtual Image Produced by a Negative (Convex) Mirror

$$d_i = \frac{d_o \cdot f}{d_o - f} \quad \text{(cm)}$$

When $d_i > 0$, the image is real
When $d_i < 0$, the image is virtual

$$m = \frac{h_i}{h_o} = \frac{f}{f - d_o} \quad \text{(ND)}$$

Figure 2.2.2.4 -- The Imaging Characteristics of the Spherical Mirror

If $d_i > 0$, the image is real.

If $d_i < 0$, the image is virtual.

As can be seen by comparison with the equations in Section 2.2.1 of this text, the above equations for a mirror are identical to those for a lens. The rules for assigning the signs of the above dimensions also are identical to those given for the lens in Section 2.2.1.

Mirror f-Number and Numerical Aperture -- The f-number and numerical aperture of a spherical mirror have the same meanings and forms as those, for a lens, presented in Section 2.2.1 of this text. That is:

$$f_N = f/D \qquad \text{(cm)}$$

and:

$$NA = \frac{1}{2 f_N} \qquad \text{(1/cm)}$$

where:

> D = Mirror Diameter (Aperture)

> f = Mirror Focal Length

The depth of field for a spherical mirror also is identical to that presented for a lens.

Mirror Aberrations -- The monochromatic aberrations of a spherical mirror are the same as those for a spherically-ground lens. As previously indicated, there are no chromatic aberrations for a front-silvered mirror. That is, there are no chromatic aberrations associated with the reflective process. As for the spherically-ground lens, the monochromatic aberrations defined in Section 2.2.1 are caused not by imperfections in manufacture of a spherically-ground mirror

buy by the inherent inability of a spherically-ground mirror to image perfectly. Mirror aberrations can be corrected by specially-ground (non-spherical) surfaces or by the use of specially-ground lenses as shown in Figure 2.2.2.5.

The Ellipsoidal Mirror -- The ellipsoidal mirror, consisting of a portion of the surface of an ellipsoid of revolution, possesses two focal points as shown in Figure 2.2.2.6. A point source placed at one focal point is perfectly imaged at the other. Planar, spherical, and paraboloidal mirrors are, in fact, special cases of the ellipsoidal mirror.

The Paraboloidal Mirror -- The paraboloidal mirror is a portion of a paraboloid of revolution. It is also an ellipsoidal mirror with one focal point at infinite distance. Thus, a paraboloidal mirror perfectly images, at its focal point, an object at infinite distance, as shown in Figure 2.2.2.7(a). Conversely, a point source placed at the focal point produces reflected rays parallel to the optical axis, as shown in Figure 2.2.2.7(b). (Note that a paraboloidal mirror has no spherical aberration.) Paraboloidal mirrors are widely employed in optical systems for which the object or target of interest is at a great distance in comparison with the dimensions of the system (most airborne applications).

The Planar Mirror -- The planar mirror is, in effect, an ellipsoidal mirror with both focal points at infinite distance. It perfectly images a point source as a point but produces only a virtual image (no real image and no focusing effect). The object/image geometry is simple ($d_i = d_o$), as shown in Figure 2.2.2.8, and the magnification is unity. The principal use of the planar mirror is the re-direction of the path of radiation.

(a) Schmidt

(b) Maksutov
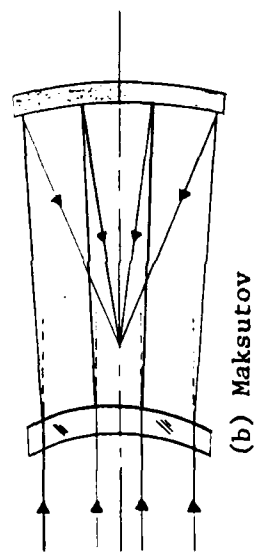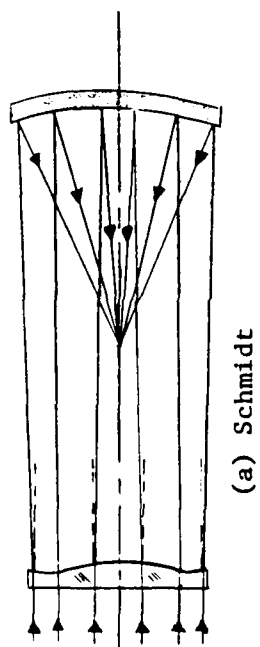
Figure 2.2.2.5--Correction of Mirror Aberrations by Means of Lenses
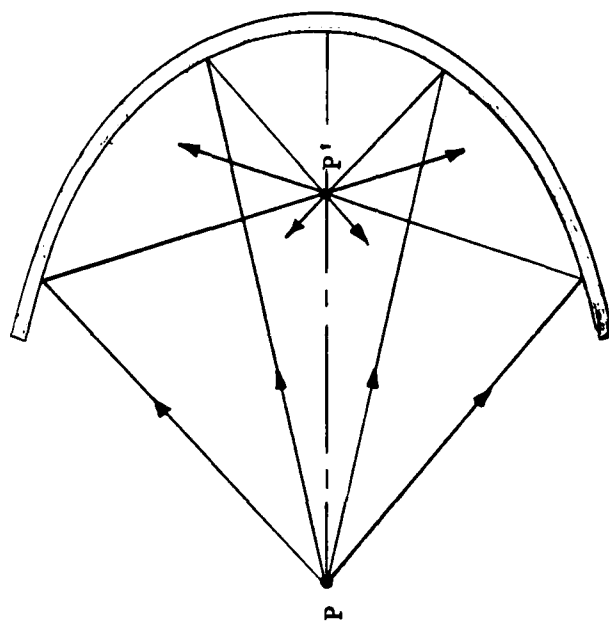
Figure 2.2.2.6 -- The Ellipsoidal Mirror
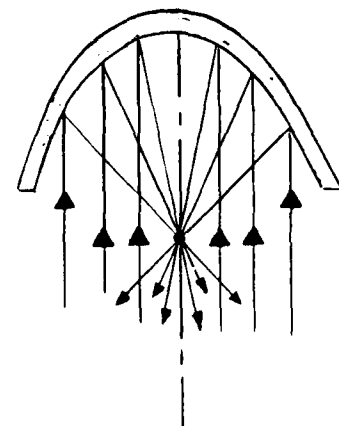
(b) Image at Infinity

(a) Object at Infinity
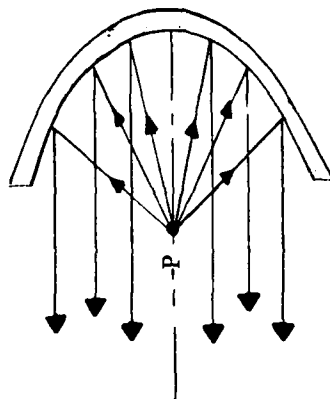
Figure 2.2.2.7--The Paraboloidal Mirror

$$d_i = d_o$$

$$m = \frac{h_i}{h_o} = 1$$

h_i

I

d_i

d_o

h_o

0
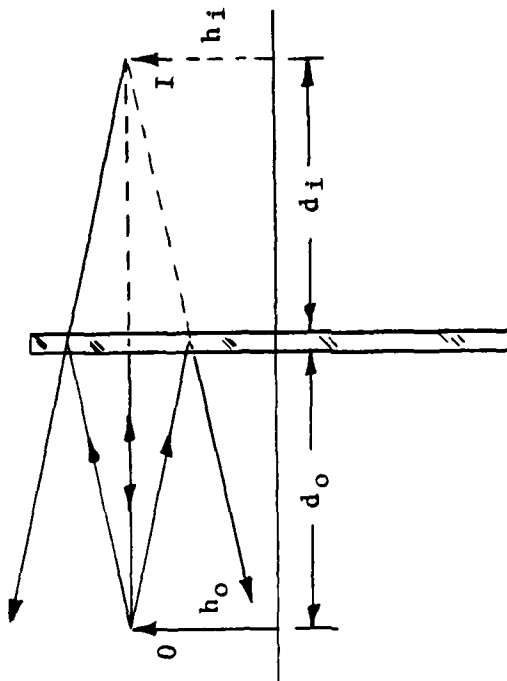
Figure 2.2.2.8 -- The Planar Mirror

2.28d

Types of Mirrors -- The nomenclature and use of various types of mirrors is
indicated in Figure 2.2.2.9.

Multiple-Mirror Systems -- In Figure 2.2.2.10 are shown several reflective
optical systems using primary and secondary mirrors. Such systems are employed
in airborne infrared target detection systems to avoid the problem caused by
the poor transmittance of many materials used in refractive optical systems.
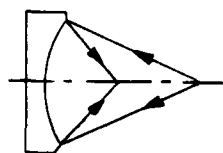
Concave Spherical   Converging: General Use
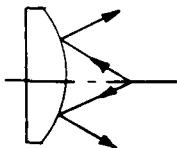
Convex Spherical   Diverging: General Use
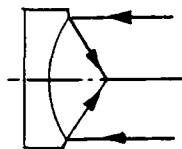
Paraboloidal   Accurately Focuses a Parallel Beam or Produces a Parallel Beam from a Point Source
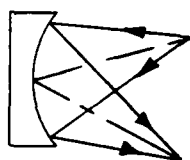
Conic:
Ellipsoidal   Refocuses a Diverging Bundle at Another Point (P) Displaced from the Point of Origin (O)
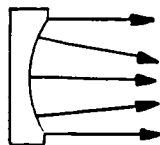
General
Aspheric   Used Mostly in Combination Systems of Two or More Components

Plane   Change Direction of Beam

Figure 2.2.2.9--Types of Mirrors

2.29a

(A) SIMPLE MIRROR

(B) NEWTONIAN TELESCOPE

(C) OFF-AXIS PARABOLOID

(D) FOLDED
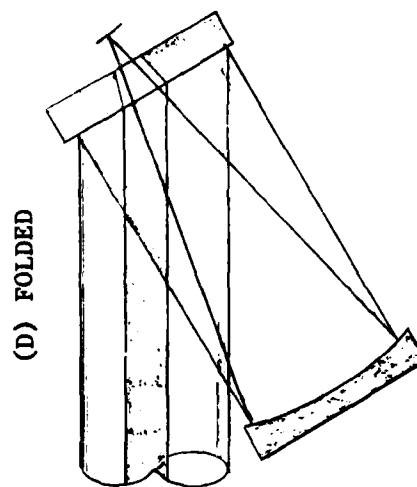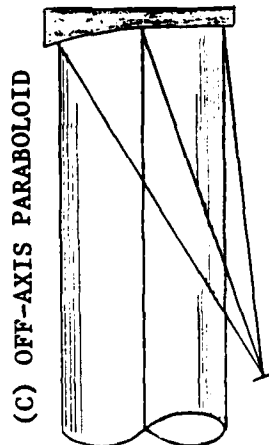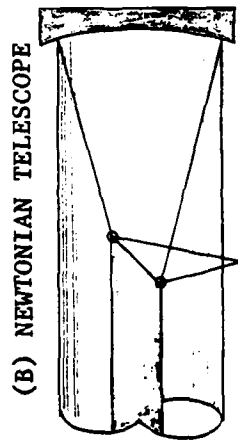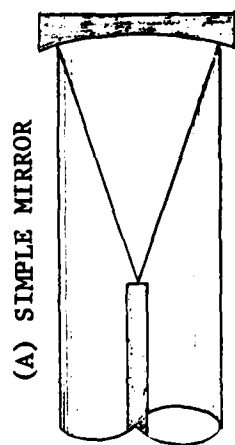
Figure 2.2.2.10--Multi-Mirror Optical Systems

2.2.3 The Prism -- The prism, or prismatic lens, can utilize both refraction and reflection to alter the propagation path of electromagnetic wave radiation. A prism is characterized by planar surfaces in contrast to the curved surfaces normally associated with a "lens". The principal applications of prisms, in electro-optical systems, are listed below and discussed in the following paragraphs.

Beam Angular Deflection (Reflection)
Beam Retro-Reflection
Beam Splitting (Partial Reflection)
Beam Deviation (Refraction)
Beam Lateral Displacement
Beam Polarization (Birefringence)
Beam Chromatic Dispersion
Image Inversion and Reversion
Image Rotation

Beam Angular Deflection -- Beam angular deflection entails alteration of the direction of propagation of a beam by internal reflection. Total reflection can be achieved by keeping the angle of incidence at the faces greater than the critical angle, as discussed in Section 2.1.5 of this text. The right angle prism shown in Figure 2.2.3.1(a) is used to deflect the beam path by 90°. The penta-prism shown in Figure 2.2.3.1(b) is used to deflect the beam path by twice the angle between the reflecting faces. The porro-prism shown in Figure 2.2.3.1(c) is used to deflect the beam by 180°.

Beam Retro-Reflection -- Retro-reflection changes the direction of propagation of a beam by 180° regardless of the angle of incidence. The corner reflector shown in Figure 2.2.3.2, so-called because its faces form the corner of a cube, provides retro-reflection.

Beam Splitting -- In a beam splitter, an internal, partially-silvered face is employed to "split" the beam into two beams as shown in Figure 2.2.3.3. A beam splitter is used to obtain two coherent beams.

(a) Right-Angle Prism

(b) Penta-Prism

(c) Porro-Prism
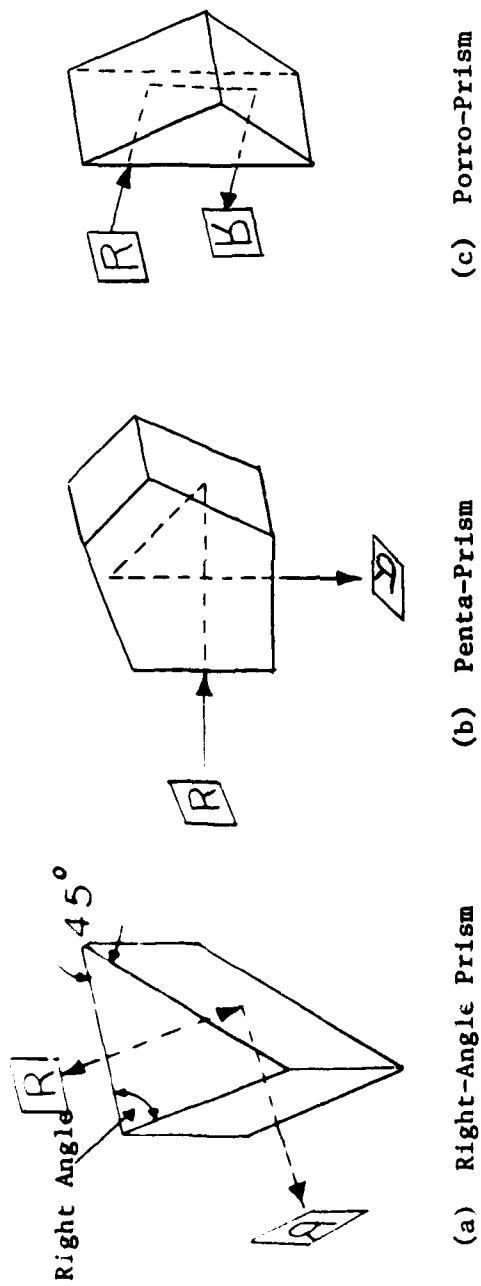
Figure 2.2.3.1 -- Beam Angular Deflection
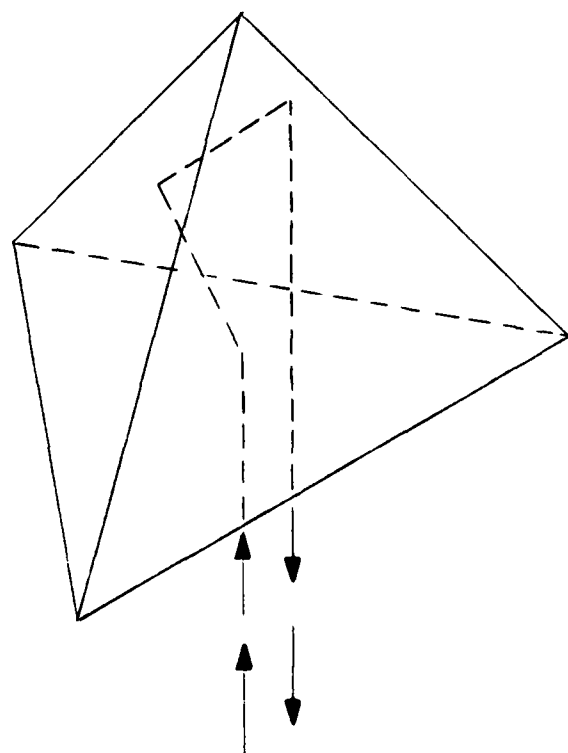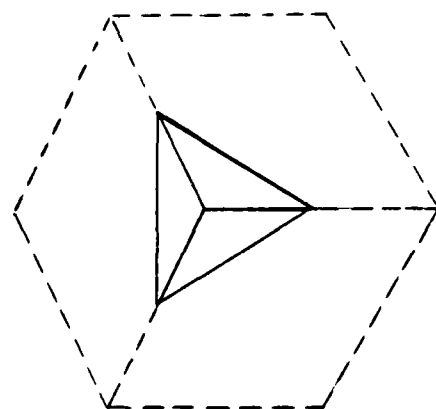
Corner Reflector

Figure 2.2.3.2—Beam Retro-Reflection

2.30b

Partially Silvered Internal Face

Exiting Beam

Exiting Beam

Entering Beam
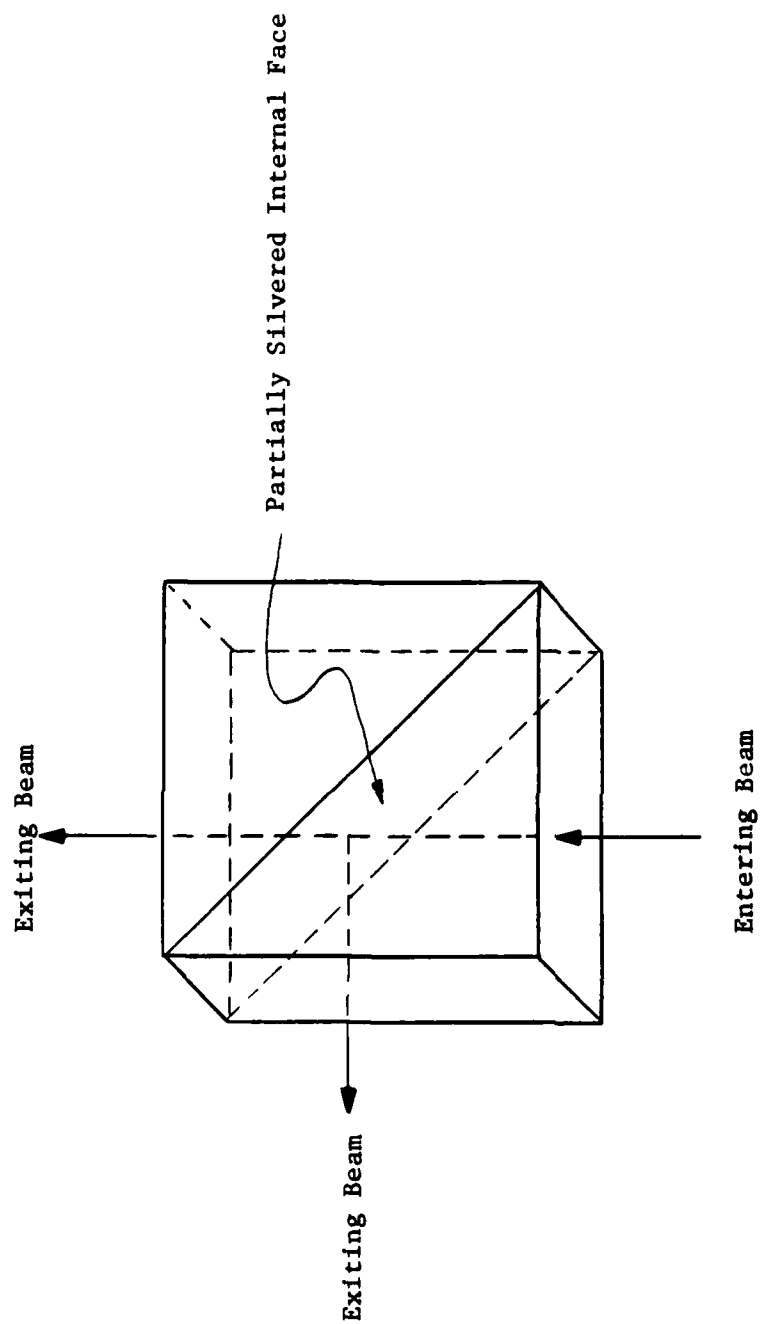
Beam-Splitting Prism

Figure 2.2.3.3--Beam-Splitting

2.30c

Beam Deviation -- Beam deviation effects alteration of the path of propagation of the beam by refraction. The wedge prism shown in Figure 2.2.3.4 deflects the beam through an angle δ given by the equation:

$$\delta = (n-1)\,\alpha \qquad \text{(Degrees)}$$

where:

n = Index of Refraction of Prism

α = Included Angle of Prism (Degrees)

Beam Lateral Displacement -- In beam lateral displacement, the path of propagation of the beam is shifted parallel to itself without changing the direction of propagation. The parallel prism shown in Figure 2.2.3.5 produces a beam lateral displacement, d, given by the equation:

$$d = w\,\theta_1\left(\frac{n-1}{n}\right) \qquad \text{(cm)}$$

where:

w = Width of Prism

θ_1 = Beam Angle of Incidence

n = Index of Refraction of Prism

Beam Polarization -- In a beam polarizing prism, the beam is resolved into two components with polarization at right angles. The Nicol Prism shown in Figure 2.2.3.6 employs a calcite crystal, sliced and re-attached with Canada Balsam cement. The calcite is birefringent; that is, it exhibits different indices of refraction to the components of the beam with polarization parallel to and transverse to its "optical axis". Because of the difference in index of refraction, the two

Wedge Prism

δ

γ
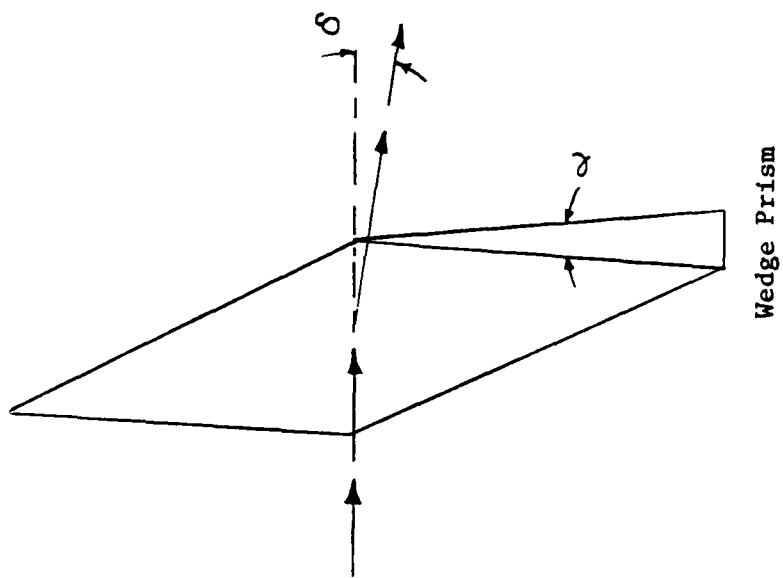
Figure 2.2.3.4 -- Beam Deviation

2.31a

$$d = \left(\frac{n-1}{n}\right) W \alpha_1$$

Parallel Prism
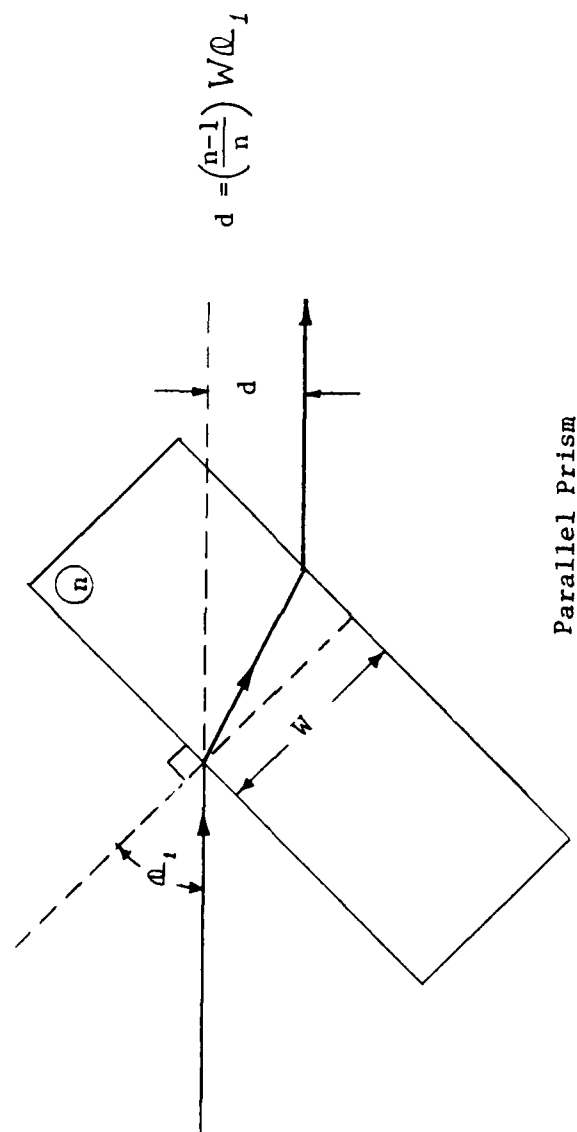
Figure 2.2.3.5--Beam Lateral Displacement
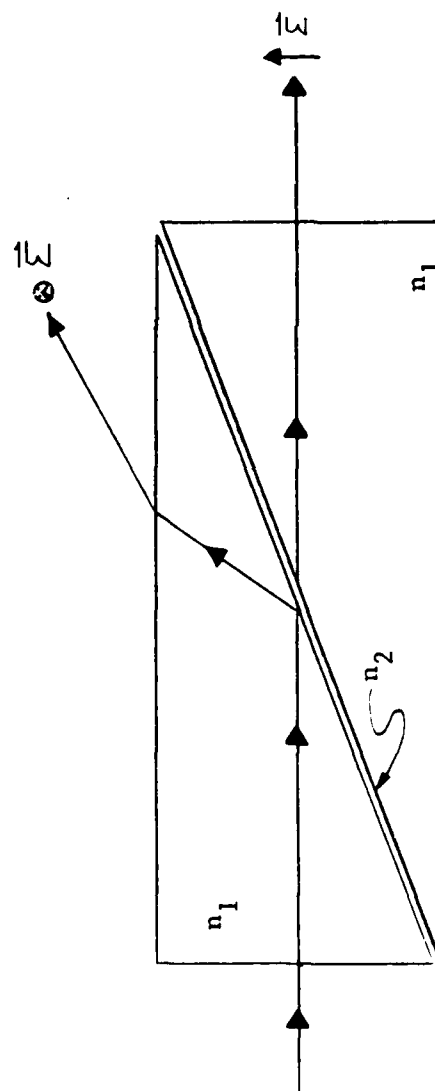
Figure 2.2.3.6 -- Beam Polarization

2.31c

components of the beam are refracted differently and reflected differently from the internal crystal/cement interface. One component is totally transmitted and the other is totally reflected by the interface, thereby effecting an angular separation between the two cross-polarized beams.

Beam Chromatic Dispersion -- In chromatic dispersion, the incident beam is dispersed (resolved into its component frequencies) by means of differential refraction, as shown in Figure 2.2.3.7. (Each frequency component is refracted differently because the index of refraction of the prism is dependent upon frequency.) The angular deflection, ∂_λ, of a component of wavelength, λ, is given by the equation:

$$\partial_\lambda = [n(\lambda) - 1]\,\alpha \qquad \text{(Degrees)}$$

where n (λ) is the (frequency-dependent) index of refraction and α is the included angle of the prism. Since $n(\lambda)$ increases with frequency, the higher-frequency components are deflected more than the lower-frequency components.

Image Inversion and Reversion -- The roof prism shown in Figure 2.2.3.8 reverses and inverts the image produced by radiation reflected from its inner surfaces.

Image Rotation -- The Pechan prism consists of two prisms cemented together as shown in Figure 2.2.3.9. The image of radiation reflected by the prism, as shown in the figure, is rotated through twice the angle through which the prism is rotated about the beam axis.

2.32
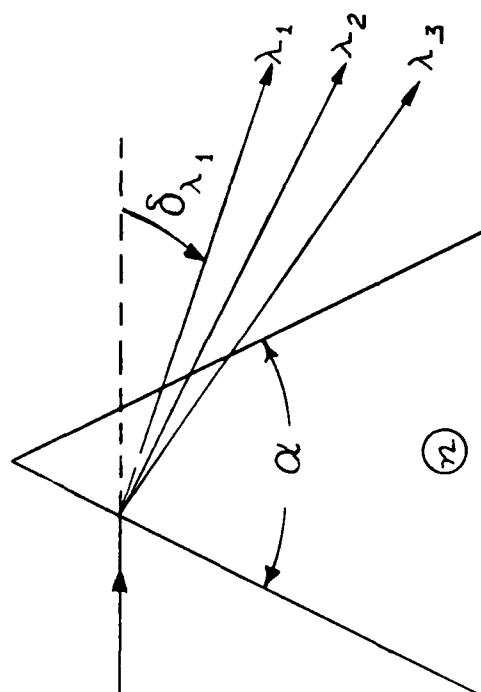
$$\delta_\lambda = [n(\lambda) - 1]\alpha$$

Figure 2.2.3.7 -- Beam Dispersion
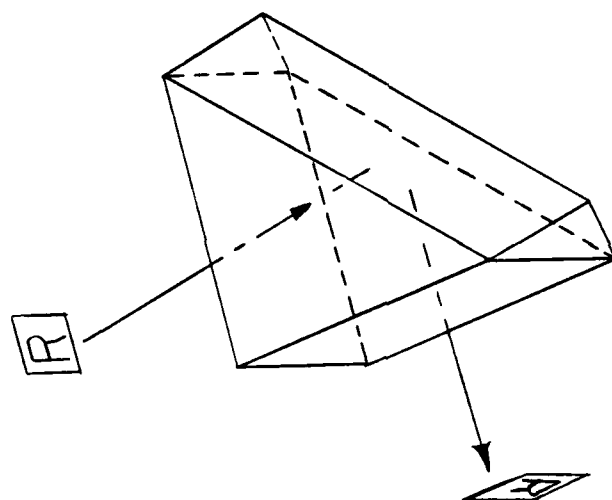
Roof Prism

Figure 2.2.3.8--Image Inversion and Reversion

2.32b
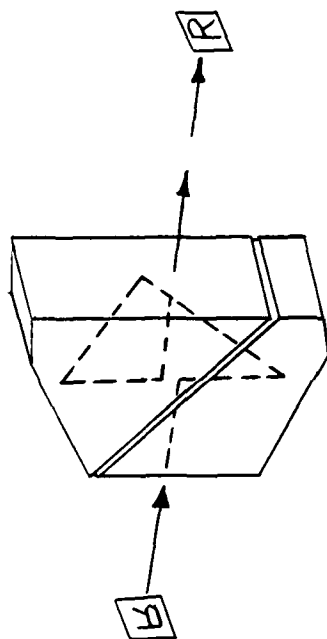
Pechan Prism

Figure 2.2.3.9—Image Rotation

2.32c

Beam Scanning Systems -- As previously indicated, a parallel prism produces a lateral displacement of the transmitted beam. The multi-faceted, rotating prism shown in Figure 2.2.3.10 produces a unidirection-linearly-scanned beam.

The rotating wedge prisms shown in Figure 2.2.3.11 produce varied scans, as shown in the figure, depending upon the relative rotation rates (w_1 and w_2) of the two prisms.

2.3 Physical Optics

2.3.1 Chromatic Filtering -- Chromatic (color) filtering is the selective alteration of the target/background clutter radiation spectrum. The selective alteration is dependent upon the temporal frequency (rather than spatial frequency) characteristics of the signal. (Spatial frequency is discussed in Section 2.3.2 of this text.) The primary purpose of chromatic filtering is to discriminate between the target and clutter (noise) radiation on the basis of spectral differences. Chromatic filtering also can be used to reduce chromatic aberrations by reducing the spectral bandwidth.

The   usual method of chromatic filtering is the interposition, into the optical path, of elements with temporal-frequency-dependent transmission characteristics. As with all such frequency filtering, there is some loss of target signal; but, if the spectral differences between the target and the clutter signals are sufficient, the frequency discrimination will result in an increased signal-to-noise ratio.

2.33
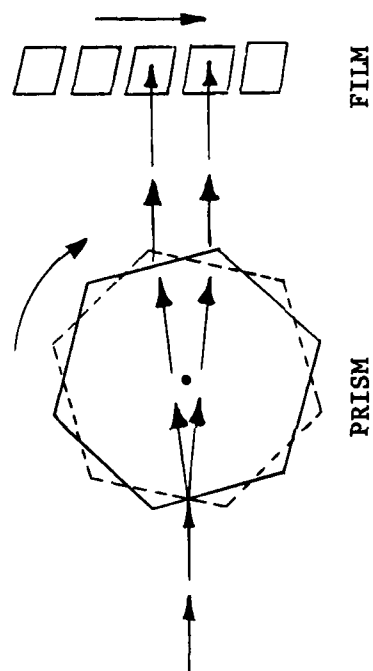
Figure 2.2.3.10--Parallel Prism Beam Scanner

FILM

PRISM

Axis of prism rotation

ω_1 ω_2

Rotating prisms   Optical system

Spiral scan
$n\omega_2 = \omega_1$

Circular scan
$\omega_2 = \omega_1$

Rosette scan
$n\omega_2 = -\omega_1$

Linear scan
$\omega_2 = -\omega_1$
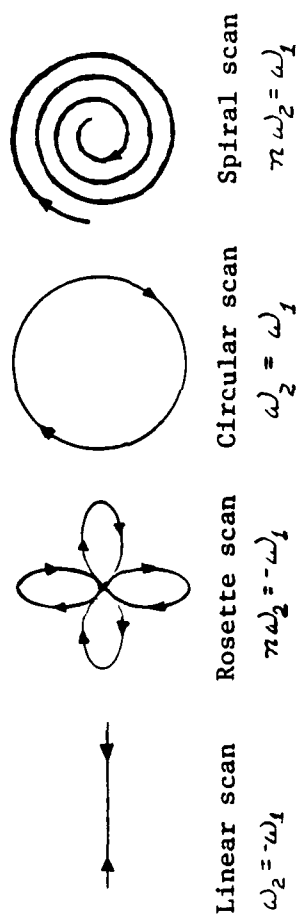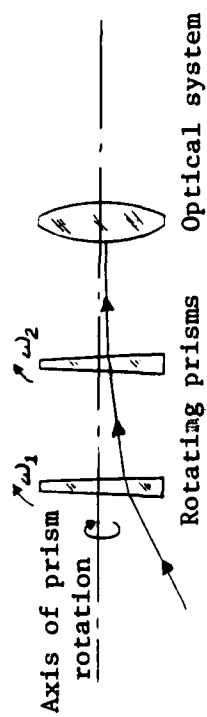
Figure 2.2.3.11--Wedge Prism Beam Scanner

There are two principal types of chromatic filter: the absorption filter and the interference filter. The absorption filter removes certain wavelengths from the incident radiation by selectively converting radiant energy to thermal energy. The thermal energy must then be dissipated, possibly creating a cooling problem. The interference filter removes specific wavelengths from the incident radiation by selective reflection. Selective reflection is achieved by utilizing wave interference between the transmitted beam and the radiation reflected by internal interfaces within the filter. (The filter consists of multiple layers, of thickness equal to an integral odd number of quarter-wavelengths of the radiation component to be removed.) Since the interference filter reflects, rather than absorbs, the rejected radiation, it does not create the heat-dissipation problem created by the absorption filter. In addition, the slope (sharpness) of the interference filter is much greater than that of the absorption filter.

The transmission characteristics of a number of chromatic filters are shown in Figure 2.3.1.1.

The conventional definitions for various chromatic filter parameters are given below.

> Bandpass Filter: A filter that transmits a band of wavelengths sharply bounded by extended regions of low transmittance.
>
> Bandwidth: The wavelength interval over which transmittance is 50% or more.
>
> Center Wavelength: The wavelength at the center of the pass band.
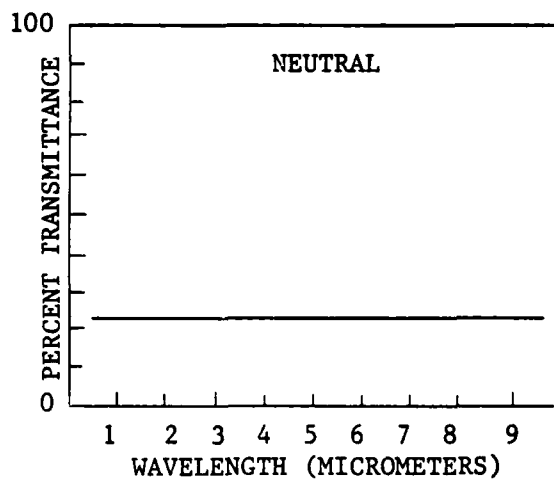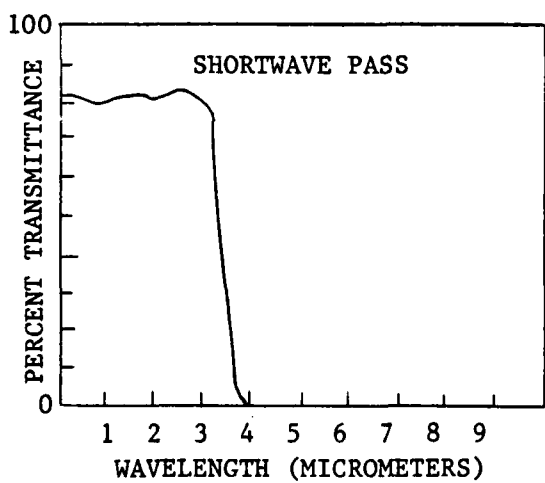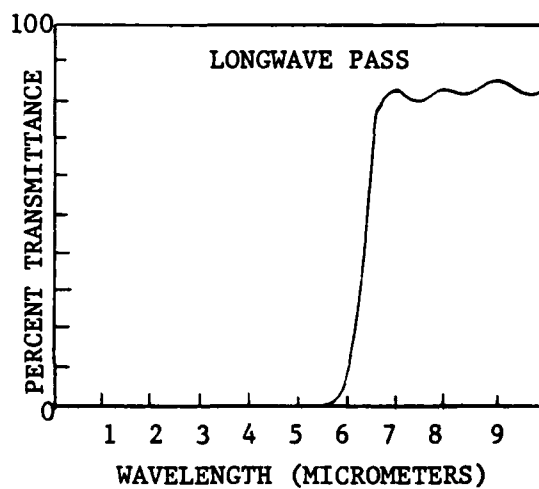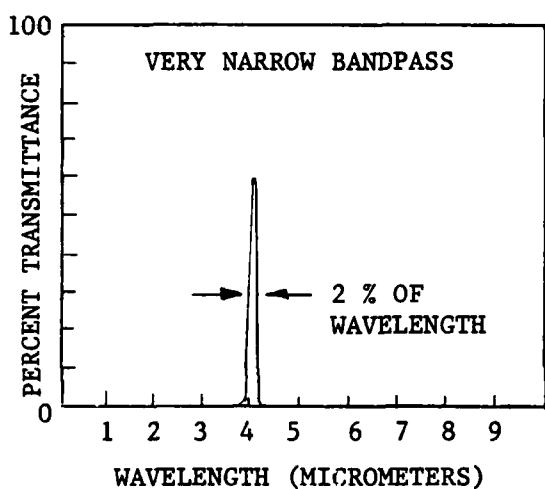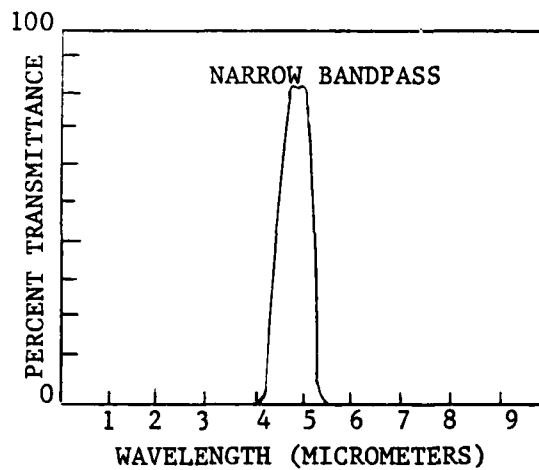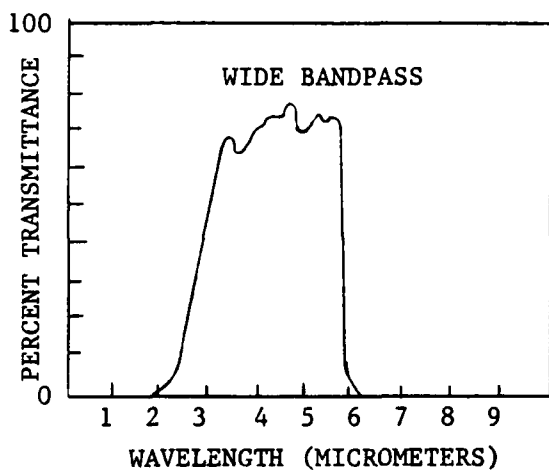
Figure 2.3.1.1--Typical Chromatic Filter Transmission
Characteristics

2.34a

Cut-on and Cut-off Wavelengths: The wavelengths at which transmittance is 5% of the peak value.

Longwave-Pass Filter: A filter that transmits all wavelengths greater than a specified cut-on value.

Shortwave-Pass Filter: A filter that transmits all wavelengths smaller than a specified cut-off value.

Slope: The ratio of the wavelength difference between the 5% and 80% of peak transmittance points to the center wavelength.

There are a number of "extraneous" factors which affect the performance of a chromatic filter. These factors, listed below, often are not included in the filter specifications, but must be considered in a comprehensive system evaluation. Off-band windows are especially important in the performance of interference filters.

Filter Off-Band Windows (Leaks)
Radiation Angle of Incidence
Structural Stability
Temperature Effects
Filter Aging

An example of chromatic filtering is the application illustrated in Figure 2.3.1.2. Shown in the figure are the approximate spectra for a sunlit cloud and a 1000°K blackbody. (The spectrum of a jet exhaust is similar to that of a 1000°K blackbody). As indicated, the radiation from the cloud could obscure a distant target, thereby degrading the performance of a heat-seeking missile or other infrared detector. If, however, a chromatic filter is employed, with a pass band as shown in the figure, the target-to-clutter signal ratio will be greatly improved.
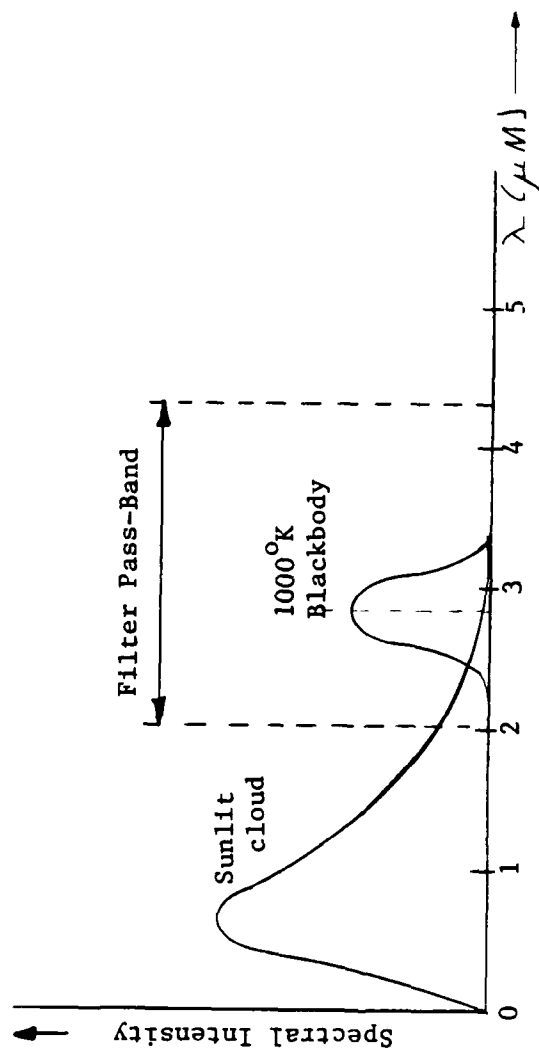
Figure 2.3.1.2 -- Example of Chromatic Filtering

2.3.2 *Fourier Optics* -- The temporal frequency of a time function is defined
as the number of times similar phenomena (events) occur per unit time. The
number of pulses per second in a pulse train is a familiar example. In an
exactly analogous manner, the spatial frequency of a space function (image)
is defined as the number of times similar phenomena (shapes) occur per unit
distance. The number of pickets per foot in a picket fence is a familiar
example. There exist many well-known mathematical techniques for dealing with
time functions (time averaging, time integration, time differentation, fre-
quency filtering, frequency-response analysis, Fourier analysis and synthesis,
Fourier and Laplace transforms, transfer functions, etc.) For every process
applied in the time domain, there exists an analogous process in the space
domain. The application of these space techniques to optical imagery (a
spatial process) is known as Fourier optics. The methods of Fourier optics are
identical to the analogous time-domain techniques except for one significant
difference--images are two-dimensional in space; time functions are one-
dimensional in time. For that reason, the implementation of the spatial
techniques is somewhat more complex than that for the temporal techniques.

The Optical Transfer Function -- A commonly applied technique for determining
the response of a dynamic system to a time function is the use of the transfer
    function, based upon Fourier or Laplace transforms. The advantage of the
transfer function approach is that the transfer function of a complex system
can be derived as the product of the transfer functions of the system components.
The spatial equivalent of the time-domain transfer function is called an optical
transfer function (OTF). The optical transfer function incorporates information
as to the effect of the system on both the amplitude and the phase of the
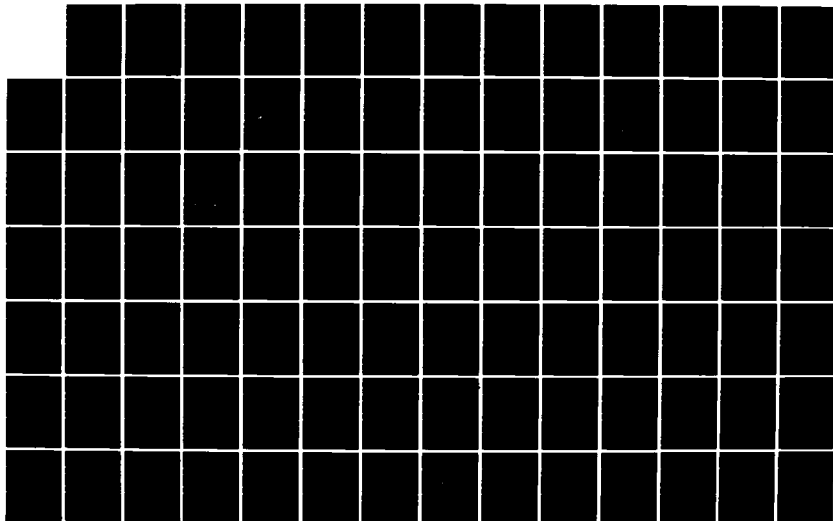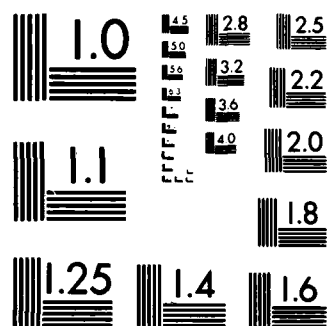
MICROCOPY RESOLUTION TEST CHART
NATIONAL BUREAU OF STANDARDS-1963-A

intensity distribution of the optical image.

The Point Spread Function -- Still another method of time-domain system
analysis utilizes the response of the system to an impulse (pulse of very
short time duration). The response of the system to any other input waveform
then can be determined by breaking the input into a series of very narrow
pulses (impulses) and summing the responses to the individual impulses. The
spatial domain equivalent of the time-domain impulse function is the point-
spread function (PSF).

The Modulation Transfer Function -- In order to determine the time response
of a dynamic system to a complex time function, it is common practice to
break the time function into its frequency components (determine the equivalent
Fourier series for the time function). The response of the system is then
determined from steady-state frequency response data for the system, and the
principle of linear superposition is applied to determine the response of the
system to the original complex waveform (signal amplitude time distribution)
by summing the system responses to the individual frequency components. The
spatial response (imaging performance) of an optical system to a complex space
function (object radiation intensity distribution) can be determined by employing
the spatial equivalent of the above time-domain technique. The spatial-domain
equivalent of the time-domain amplitude (frequency) response is called a
modulation transfer function (MTF). As with its time-domain counterpart, the
MTF of a multi-element optical system is equal to the product of the MTFs of
the individual elements.

2.37

Spatial Frequency Response of a Scanning Aperture -- An essential component of a scanning radiation sensor is a moving aperture of finite width that scans the sensor field of view. In the following development, the spatial frequency response, or modulation transfer function, of such a scanner is derived, for scanning in one direction only. The radiance of the target is assumed to vary sinusoidally in the scanned direction, (and without variation in the direction perpendicular to the scan), as shown in Figure 2.3.2.1, according to the equation:

$$N_T(x) = N_A \left[1 + Sin\left(\frac{2\pi x}{L}\right) \right] \qquad \text{(Watts/Cm}^2\text{-Sr)}$$

where:

$\qquad$ L = Period of Sinusoidal Variation (Cm)

$\qquad$ N_A = Amplitude of Sinusoidal Variation (Watts/Cm^2-Sr)

$\qquad$ X = Linear Distance in Scanned Direction (Cm)

At any instant, the instantaneous field of view of the scanner encompasses a small portion of the target, of width a, as shown in the figure. The response of the scanner is here assumed to be proportional to the average value of the radiant intensity of that small portion of the target, considered as a point source. The radiant intensity of the target is given by:

$$J_T(x) = J_A \left[1 + Sin\left(\frac{2\pi x}{L}\right) \right] \qquad \text{(Watts/Sr)}$$

where J_A is the amplitude of the target sinusoidal variation in target radiant intensity. $J_T(x)$ can be considered the optical input to the scanning process. The output of the scanning process is, then, the average value of radiant intensity over the instantaneous field of view, to which the sensor responds.

2.38

$$N_T(X) = N_A \left[1 + \cos \left(\frac{2\eta X}{L} \right) \right] \ (\text{Watts/cm}^2 - S_r)$$

Figure 2.3.2.1--Narrow Aperture Scanning Sinusoidal Radiance Target

2.38a

That average value is given by:

$$\bar{J_T}(x) = \frac{1}{a} \int_{x-a/2}^{x+a/2} J_T(x)\, dx \qquad \text{(Watts/Sr)}$$

or:

$$\bar{J_T}(x) = \frac{1}{a} \int_{x-a/2}^{x+a/2} J_A \left[1 + Sin\left(\frac{2\pi x}{L}\right) \right] dx \qquad \text{(Watts/Sr)}$$

or:

$$\bar{J_T}(x) = J_A + \left(\frac{J_A L}{\pi a}\right) Sin\left(\frac{\pi a}{L}\right) Cos\left(\frac{2\pi x}{L}\right) \qquad \text{(Watts/Sr)}$$

The spatial frequency response or modulation transfer function of the scanning process is defined as the (non-dimensional) ratio of the amplitude of the scanning process output to the amplitude of the scanning process input, as a function of the spatial frequency of the target sinusoidal variation in radiant intensity.

That is:

$$MTF = \frac{\bar{J_T}(Amp)}{J_T(Amp)} \qquad \text{(N.D.)}$$

where:

$$\bar{J_T}(Amp) = \left(\frac{J_A L}{\pi a}\right) Sin\left(\frac{\pi a}{L}\right) \qquad \text{(Watts/Sr)}$$

$$J_T(Amp) = J_A$$

Thus:

$$MTF = \frac{Sin\left(\frac{\pi a}{L}\right)}{\left(\frac{\pi a}{L}\right)} \qquad \text{(N.D.)}$$

2.39

This modulation transfer function is shown plotted versus (a/L) in Figure
2.3.2.2. (Note that (1/L) is the spatial frequency of the target sinusoidal
variation in radiant intensity.) That is:

$$SF_T = \frac{1}{L} \qquad \text{(cycles/Cm)}$$

The modulation transfer function is seen to go to zero at (a/L = 1). That is,
the cut-off spatial frequency of the scanner, SF_{co}, is given by:

$$SF_{co} = \frac{1}{a} \qquad \text{(Cycles/Cm)}$$

Thus, for $SF_T = SF_{co}$, the amplitude of the sinusoidal variation in the output of
the scanner vanishes.

The negative frequency response from (a/L = 1) to (a/L = 2) represents a spatial
frequency interval in which the sensor response is inverted (areas of high
target intensity appear as areas of low target intensity and vice versa). For
most purposes, the response of an optical system can be considered unusable
above the cut-off frequency.

If the aperture used in this example were of finite dimension in two directions,
with width a and height b, the full three-dimensional modulation transfer
function would be given by:

$$MTF = \left[\frac{\sin\left(\frac{\pi a}{L}\right)}{\left(\frac{\pi a}{L}\right)} \right]\left[\frac{\sin\left(\frac{\pi b}{L}\right)}{\left(\frac{\pi b}{L}\right)} \right] \qquad \text{(N.D.)}$$
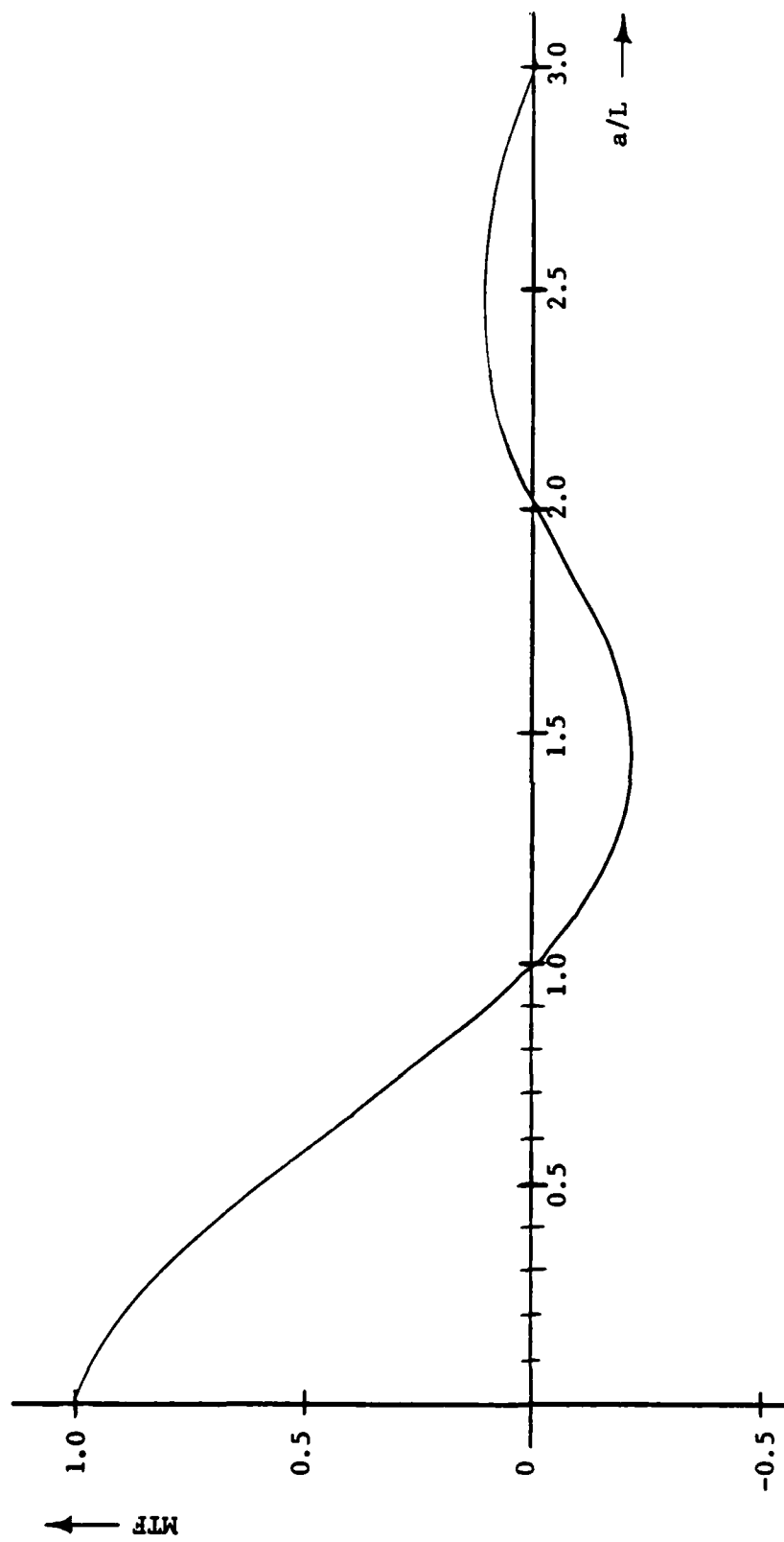
Figure 2.3.2.2 -- Modulation Transfer Function of Scanning Aperture

2.40a

where:

a = Aperture Dimension in x Direction.   (Cm)

b = Aperture Dimension in y Direction.   (Cm)

L_x = Target Spatial Period in x Direction. (Cm)

L_y = Target Spatial Period in y Direction. (Cm)

The magnitude of the modulation transfer function would appear as shown in Figure 2.3.2.3, where:

$k_x = 1/L_x$ = Target Spatial Frequency in x Direction. (Cycles/Cm)

$K_y = 1/L_y$ = Target Spatial Frequency in y Direction. (Cycles/Cm)
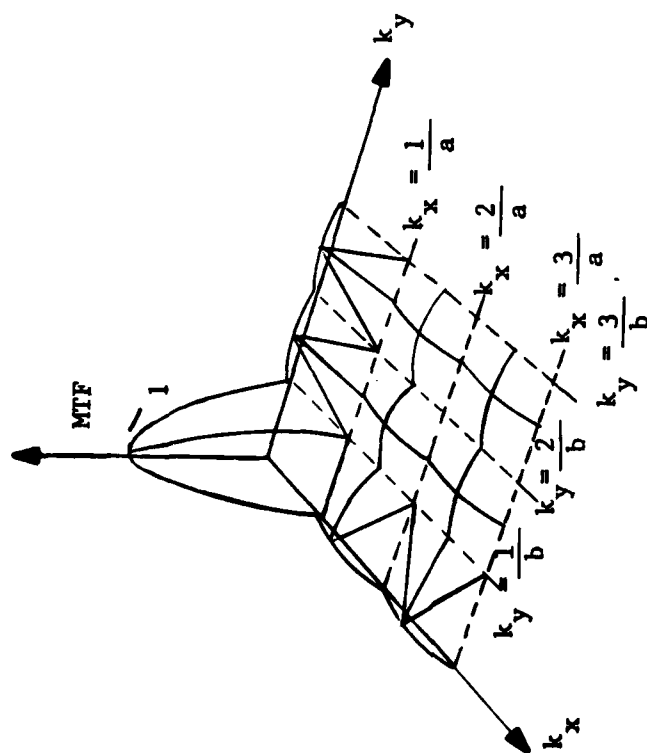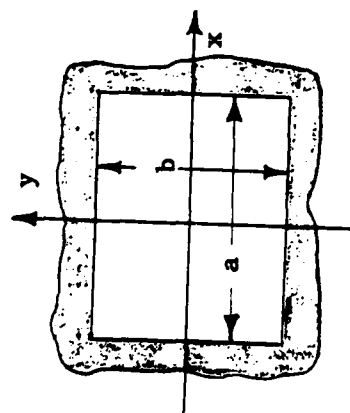
Figure 2.3.2.3 -- Modulation Transfer Function of a Rectangular Aperture

2.41a

2.3.3 Spatial Filtering -- As indicated in the preceding section of this text, optical components can be employed to modify the imaging characteristics of an optical system, in the space domain, just as electronic components can be used to modify the waveform shaping characteristics of an electronic system, in the time domain. The purpose of such spatial filtering is to improve the signal-to-noise ratio of the optical signal (target image). That is, spatial filtering is employed to discriminate between target and clutter on the basis of size and shape.

In the time domain, it is impossible to separate the characteristics of a signal as a function of time from its characteristics as a function of frequency. That is, the time history of a signal and the spectrum of that signal are equally valid descriptions of the same phenomenon. Similarly, the spatial characteristics (size and shape) of an image are inseparable from the spatial frequency characteristics of that image. Nevertheless, it is possible to distinguish two methods of implementing spatial filtering: filtering in the space (image) domain and filtering in the spatial frequency (spectrum) domain.

Filtering in the Space Domain -- Examples of filtering in the space domain are pattern recognition, map matching, target profile recognition, and the use of field stops to limit the field-of-view of an optical sensor. The filtering performed in these examples is accomplished by masks or reticles in the image plane. An example of space domain filtering is the field stop employed in the following example to discriminate between background radiation and a target of known area. As indicated in Figure 2.3.3.1, the sensor has two apertures, the area of the field-of-view, A_A, of the large aperture is equal to four times
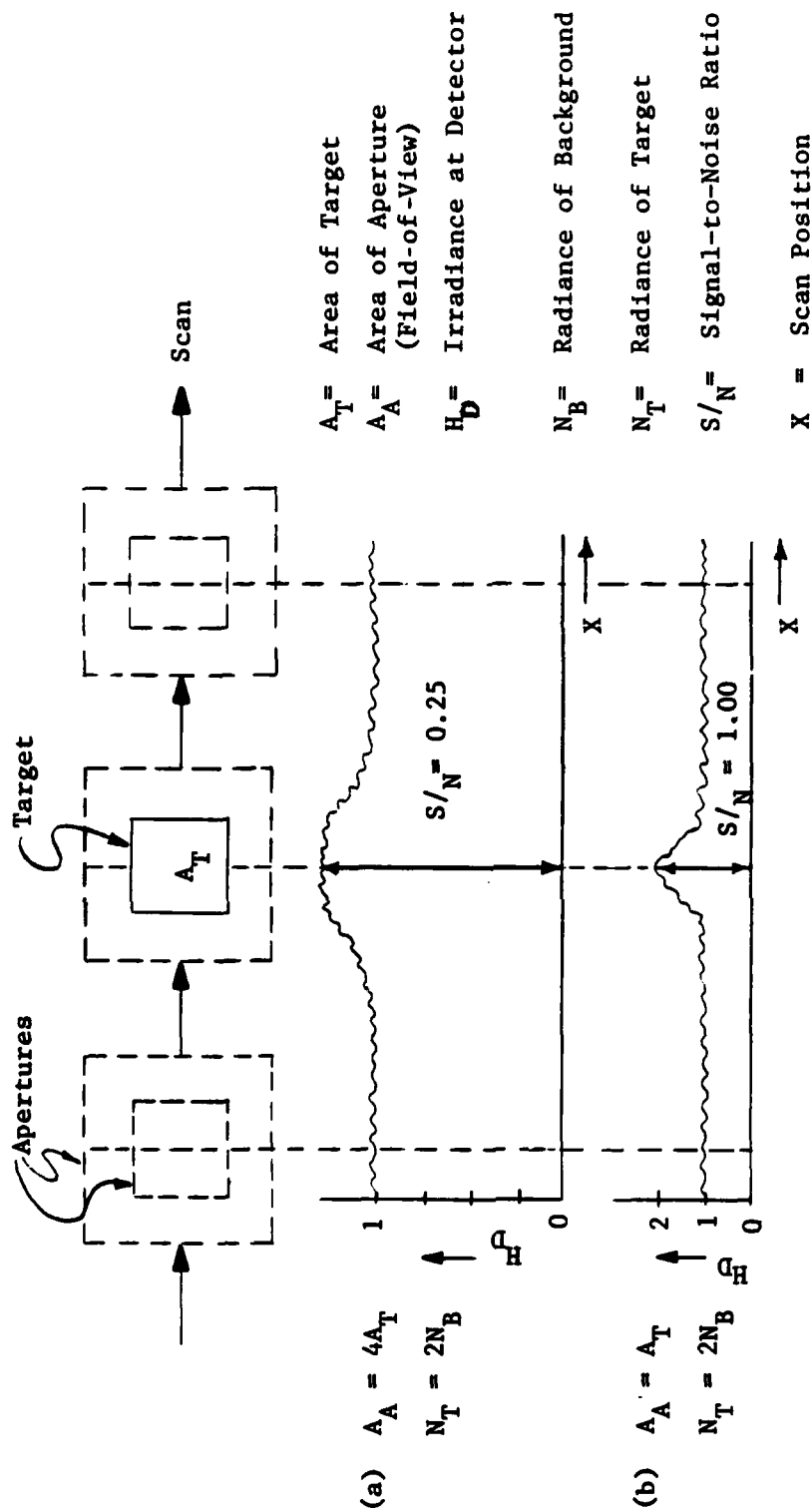
Figure 2.3.3.1 -- Filtering in the Space Domain

A_T = Area of Target

A_A = Area of Aperture (Field-of-View)

H_D = Irradiance at Detector

N_B = Radiance of Background

N_T = Radiance of Target

S/N = Signal-to-Noise Ratio

X = Scan Position

Scan

Target

Apertures

A_T

$S/N = 0.25$

$S/N = 1.00$

(a) $A_A = 4A_T$

$N_T = 2N_B$

(b) $A_A = A_T$

$N_T = 2N_B$

2.42a

the area of the target, shown as A_T. The area of the field-of-view of the small aperture is equal to that of the target. It is assumed that the radiance of the target is twice that of the background. The (normalized) irradiance at the sensor detector, (and hence the sensor response), is shown as a function of scan position for case (a) where $A_A = 4A_T$ and case (b) where $A_A = A_T$. As can be seen in the figure, the percentage increase in sensor output as the sensor scans the target is four times as large for $A_A = A_T$ than for $A_A = 4A_T$. Thus, the signal-to-noise ratio is improved by a factor of four by limiting the sensor field of view to the known area of the target.

Filtering in the Spatial Frequency Domain -- The optical Fourier transform of a (space domain) object represents the (spatial frequency domain) spectrum of that object. Filtering in the spatial frequency domain is accomplished by Fourier transforming the object in question into the spatial frequency domain, altering the resulting spectrum as desired, and transforming back into the space domain. The process of optical Fourier transformation can be implemented, with especial ease, for an object delineated by coherent radiation, by the apparatus depicted in Figure 2.3.3.2. The apparatus consists of a positive lens so positioned that the object, (a grid in the illustration), is imaged as shown. The distribution of the density of the radiant flux in the focal plane of the lens corresponds to the two-dimensional Fourier transform (spectrum) of the object with horizontal spatial frequency, k_x, in the horizontal direction and vertical spatial frequency, k_y, in the vertical direction. The irradiance in the focal plane is proportional to the spectral density at the frequencies represented by that point in the plane. The spectrum and corresponding image are shown in Figure 2.3.3.3. Spatial frequency filtering can be implemented simply by inserting a mask or reticle in the focal plane to block the radiation at those spatial frequencies to be attenuated or deleted in the desired image.

Object
y_0
x_o

Lens

Spatial
Spectrum
k_y
k_x

Focal Plane
of Lens
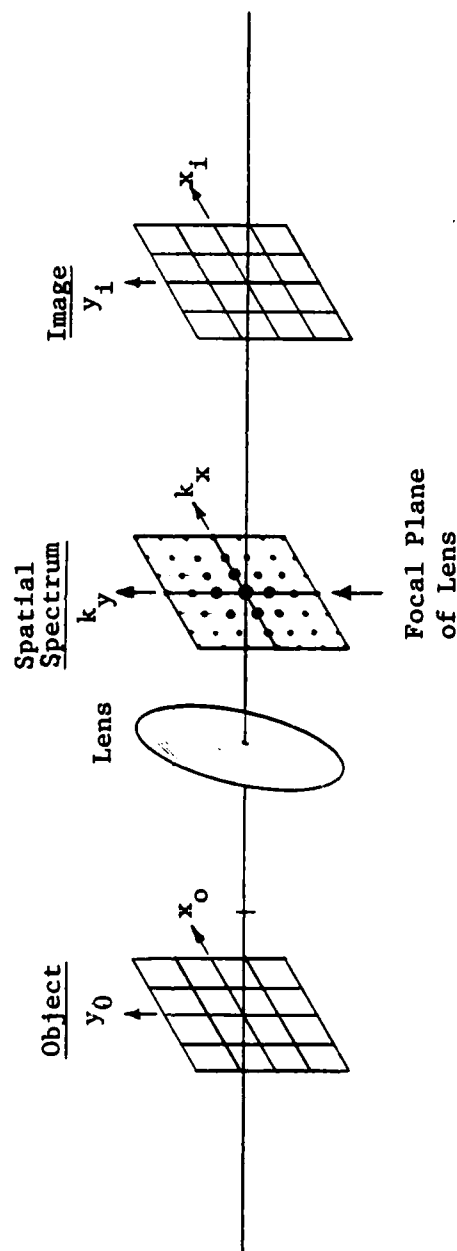
Image
y_i
x_i

x_o, y_o = Object Spatial Distribution

x_i, y_i = Image Spatial Distribution

k_x = Spatial Frequency in x Direction

k_y = Spatial Frequency in y Direction

Figure 2.3.3.2 -- Optical Fourier Transformation

2.43a

Image

y_1

x_1

Spectrum

k_y

k_x
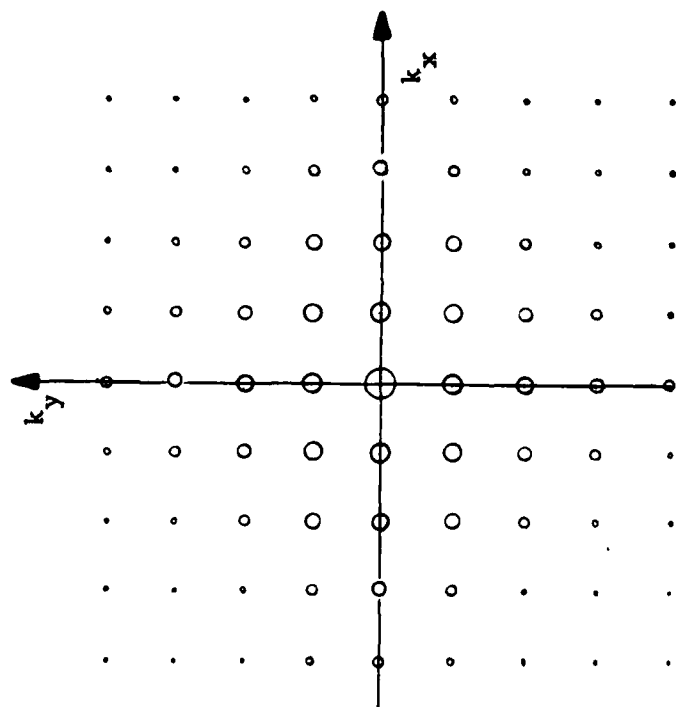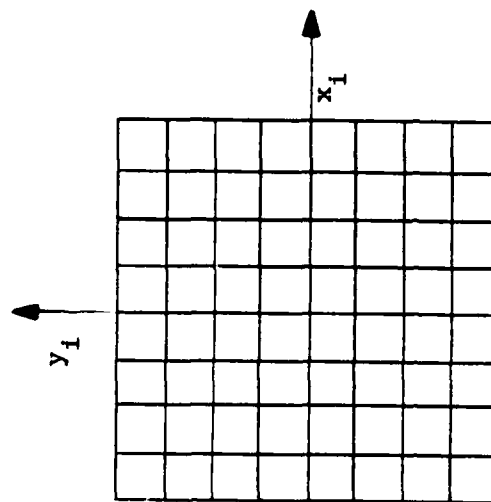
Figure 2.3.3.3 -- Fourier Transform (Spectrum) and Corresponding Image of Grid

2.43b

Such an optical spectral filter can be fabricated by exposing a photographic negative to the focal plane (Fourier spectrum) image of the space domain pattern to be deleted. For example, the horizontal lines, (which create spatial frequencies in the vertical direction), can be eliminated from the image by employing a mask which masks out all vertical frequencies except zero frequency. The resulting spectrum and image are shown in Figure 2.3.3.4.

Image

x_1

y_1

Spectrum

k_x

k_y
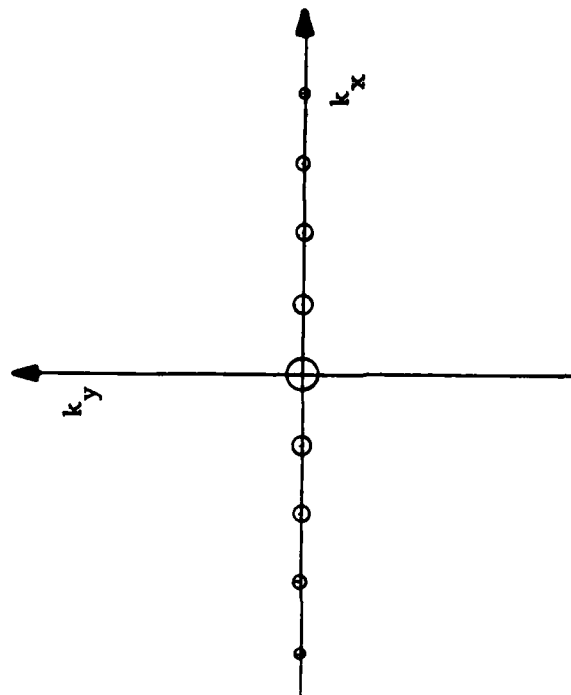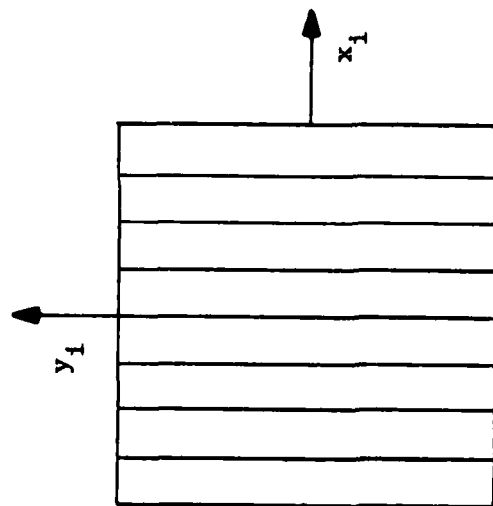
Figure 2.3.3.4 -- Fourier Transform (Spectrum) and Corresponding Image of Grid with Vertical Frequencies (Horizontal Lines) Deleted

2.3.4 Optical Time Modulation -- Optical time modulation is time-dependent amplitude modulation of the radiant flux in an optical system. Such modulation can be performed in a number of ways, but generally involves the attenuation or interruption of the flux by means of a shutter, Kerr cell, rotating reticle, or other active optical element. The process is a time-domain technique, (rather than a space-domain technique), and is intended to "time-color" the radiant "signal" in such a way as to distinguish it from other signals.

The radiant flux emitted by an active target sensor can be time modulated in order to distinguish the radiant flux emitted at one instant from the flux emitted at other instants of time, thereby providing an active ranging capability. Such time-coloring also allows the sensor to discriminate against noise from other emitters.

The radiant flux received by an optical sensor often is time-modulated in order to distinguish it from internal noise generated by processes, such as radiation detection, that take place at a point in the system beyond the modulator. The signals involved in a typical time-modulation arrangement are shown in Figure 2.3.4.1. The time-modulation depicted is a simple "chopping" action such as that due to a rotating, segmented reticle in the radiation path. In Figure 2.3.4.1(c) is shown the total sensor output waveform due to the input target radiation and to the internally-generated noise. The same signal, after chopping, is shown in Figure 2.3.4.1(d). In Figure 2.3.4.1(e) is shown the same signal after chopping and band-pass filtering tuned to the chopping rate of the time-modulator. Note that all of the output waveforms prior to band-pass filtering exceed the sensor threshold level even in the absence of a target

2.45

(a) Sensor Output Due to Target Radiation

(b) Sensor Output Due to Internal Noise

(c) Sensor Output Due to Target Plus Noise

(d) Sensor Output with Time Modulation

(e) Sensor Output with Time Modulation and Band-Pass Filtering
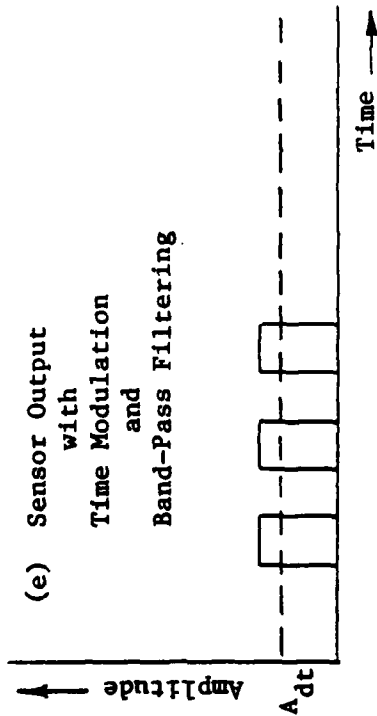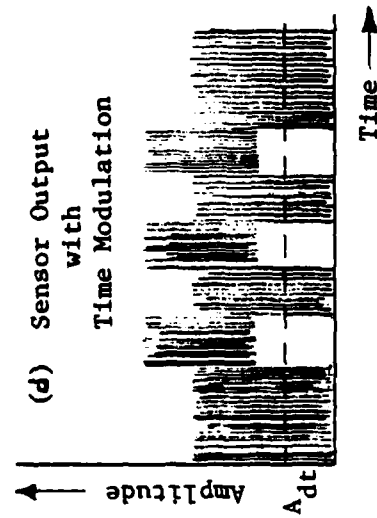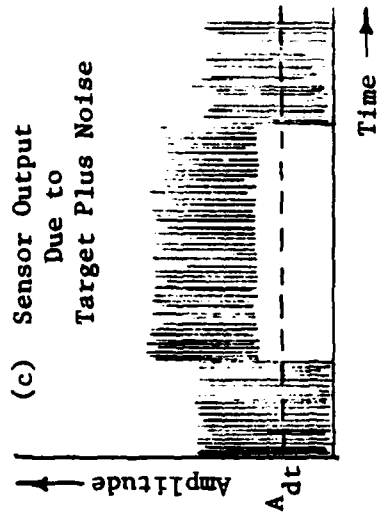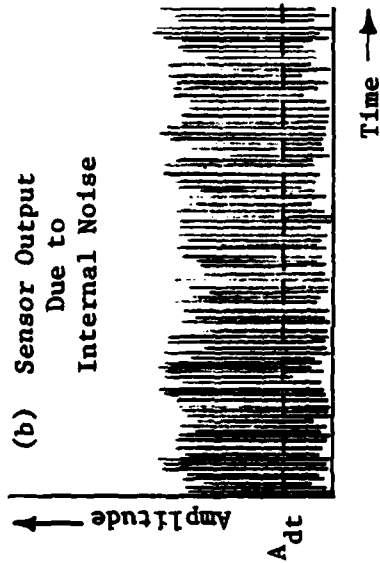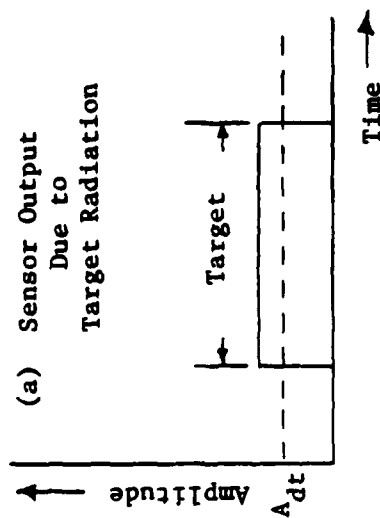
A_{dt} = Sensor Detection Threshold

Figure 2.3.4.1 -- Internal Noise Rejection by Optical Time Modulation

2.45a

signal. The final waveform, shown in Figure 2.3.4.1(e), exceeds the sensor

threshold level only during the period with a target signal present. Thus,

the time modulation and band-pass filtering discriminate against any signal

not modulated in the prescribed manner.

2.3.5 Image Scanning -- Image scanning can be considered quantization of the optical (image) information present in the sensor overall field-of-view. The information contained in one quantum is determined by the sensor instantaneous field-of-view. Usually, the scanning operation is performed by serially sampling the various instantaneous fields-of-view in a systematic manner. Such serial sampling results in a video signal representing the sampled (scanned) information serially in time. Thus, most image scanning can be considered space domain-to-time domain conversion. The purpose of such conversion is to allow time-domain signal processing techniques to be applied to the information signal representing the space distribution of radiation in the sensor field-of-view. Most of the signal processing required in optical systems can thus be performed utilizing time domain techniques more familiar to most engineers than are the alternative Fourier optics techniques. For example, digitization of the converted information allows the use of the formidable signal processing capabilities of the digital computer. In order to employ electronic signal processing devices, the optical signal (radiant flux) must be converted to an electrical signal (voltage or current). In some systems, the space-to-time and radiation-to-electronic signal conversions are performed simultaneously by moving a radiation detector in such a way as to scan the sensor field-of-view. In other systems, the radiation pattern is first converted to electrical form and is then scanned electrically. One such device is the vidicon TV camera tube described in Section 3.4.3 of this text. In still other systems, the optical information is scanned prior to detection. An example of this type of system is the forward-looking infrared sensor described in Section 3.4.5 of this text. In some systems, the scanned and converted information is stored and re-scanned to effect a scan conversion from one format to another.

2.47

As previously stated, the field-of-view scanning process can be considered a space-to-time conversion, performed to allow time-domain signal-processing techniques. Typical time-domain signal processing techniques applied to converted optical information include signal amplification, frequency filtering, limiting, threshold detecting, multiplexing, telemetering, and display. For an electro-optical target sensor, the end result of the scanning/conversion/ signal processing procedure is target detection, location, and/or display. Note that an oscilloscope display provides a time domain-to-space domain reconversion. The inherent signal-sampling nature of the scanning process introduces various sampled-data effects including reduction of effective target radiation power, a discontinuous information signal, frequency aliasing, and time/space distortion of the scanned field-of-view.

2.3.6 The Rotating Reticle -- A commonly encountered electro-optical system component is the rotating, segmented reticle. As shown in Figure 2.3.6.1, the reticle is positioned in an image plane in the optical path of the system so that the image of the radiation distribution within the sensor field-of-view is scanned by the rotating reticle. The reticle performs one or more of the following functions: optical time modulation, image scanning, spatial filtering, and chromatic filtering. These processes have been discussed in the preceding sections of this text. A rotating reticle application exemplifying all four functions is illustrated in Figure 2.3.6.2. The optical time modulation function is performed by the difference in transmissivity of the alternating segments of the reticle and serves to differentiate the signal due to incoming radiation from that due to internal noise sources. The image scanning function is performed by the movement of the leading edge of the opaque portion of the reticle across the field-of-view and provides the scan phase information required to determine the angular position of the target about the reticle spin axis. (The target position-to-phase conversion reticle is discussed in the next section of this text). The spatial filtering action is a result of the relative aperture size of a reticle segment in comparison with the image sizes of the target (essentially a point source) and the background clutter (the cloud). The detector output signal, (after space-to-time and radiation-to-electrical voltage conversions), is shown in the figure, as the reticle is scanned from left to right. The relatively high (temporal) frequency content of the signal due to the (small) target, compared to that due to the (large) cloud, is a direct consequence of the relatively high (spatial) frequency content of the target image compared with that of the cloud. A high-pass filter following the detector would then distinguish the target signal from that of the background clutter (cloud). The chromatic filtering function of the reticle is effected by the

2.49

Output

Electronics

Radiation Detector

Field Lens

Reticle

Image Plane

Objective Lens

W

Target

Field-of-View
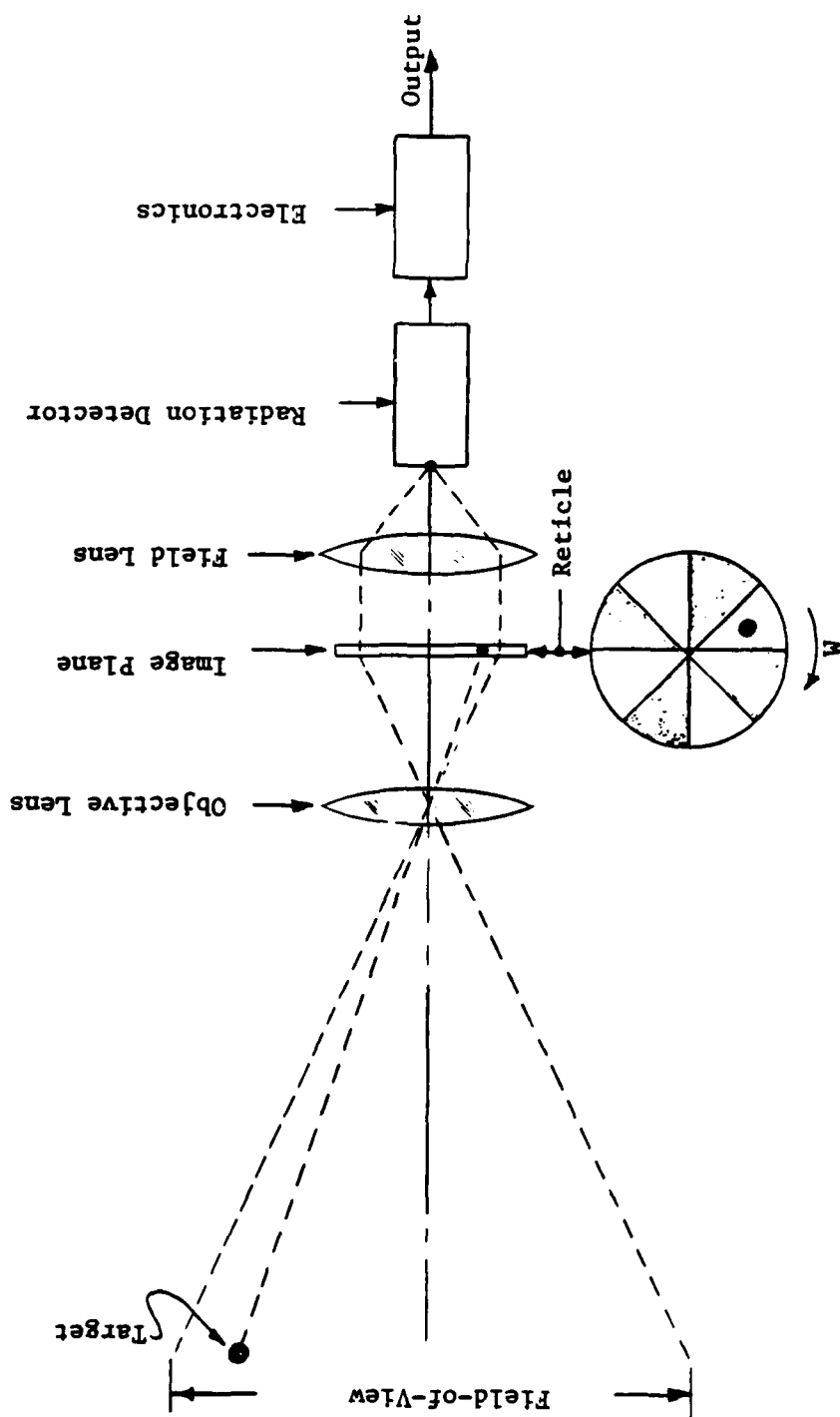
Figure 2.3.6.1 -- The Rotating Reticle

2.49a
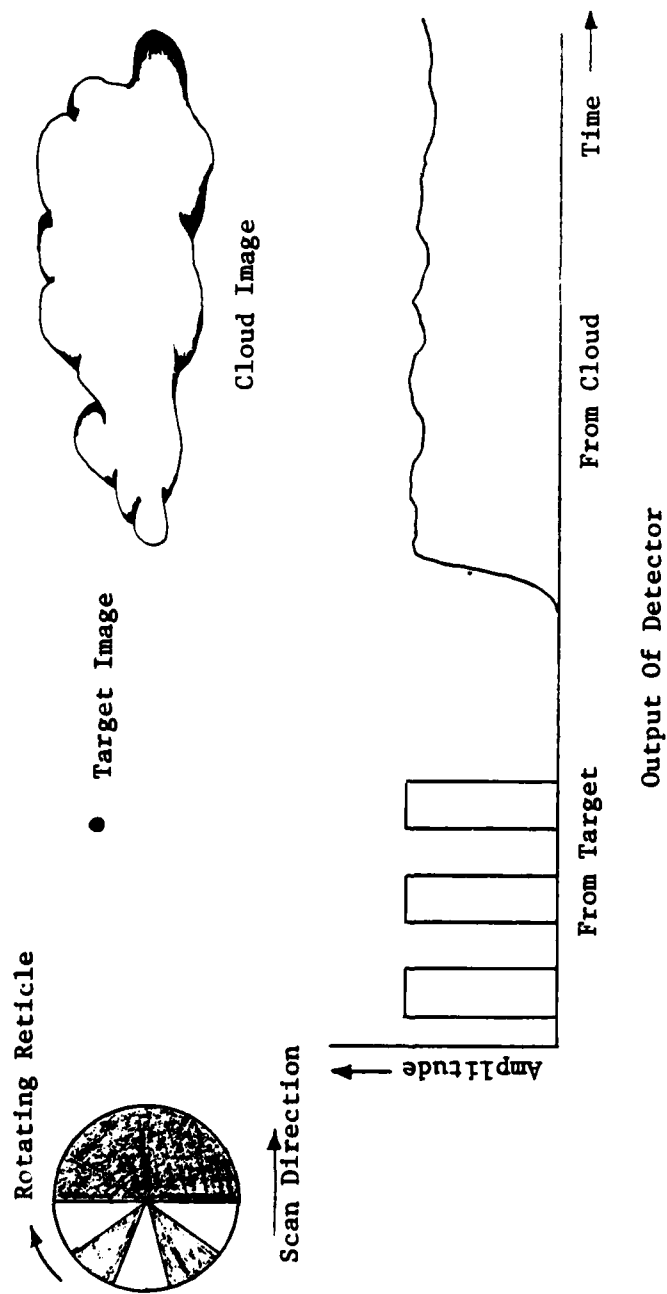
Figure 2.3.6.2-- Rotating Reticle Application

frequency (color) - selective transmissivity characteristics of the trans-
mitting segments of the reticle, which discriminate between target and back-
ground on the basis of spectral differences, as discussed in Section 2.3.1
of this text.

The rotating reticles described in the following paragraphs provide simul-
taneous image scanning, space-to-time conversion, and time modulation, as
indicated. The reticle illustrated in Figure 2.3.6.3 is half opaque and half
transparent. The relative time at which the opaque portion of the reticle
occults the target image (t), is a function of the angular position of the target,
(δ). This type of reticle thus provides pulse-train phase or pulse-position
modulation. The target is assumed to be a point source. In Figure 2.3.6.4
is shown a reticle designed to produce pulse amplitude modulation of the radiant
flux from an extended source (non-point-source) target. Due to the extent (size)
of the target and the finite width of the transparent segments of the reticle,
the amplitude of the flux modulation depends upon the radial distance of the target
from the center of the reticle. Thus, there is no modulation with an on-axis
target, as shown, and increasing modulation, (up to the point where the target
width just equals the segment width), as the target moves away from the axis.
Note that the opaque half of the reticle will provide phase modulation thus
allowing determination of target position in polar coordinates. In Figure
2.3.6.5 is shown a reticle designed to produce pulse width modulation of the
radiant flux from a point-source target. The width of the flux-transmitting
slot is constant with radius. The time interval during which the target is
visible, therefore, decreases with radial position of the target image. The

Target
Image

δ_1

Detector
Output

Time

$0 \ t_1$

(a)

Ref.

δ_1

δ_2

Detector
Output

Time

t_2

0

(b)

Ref.

δ_2
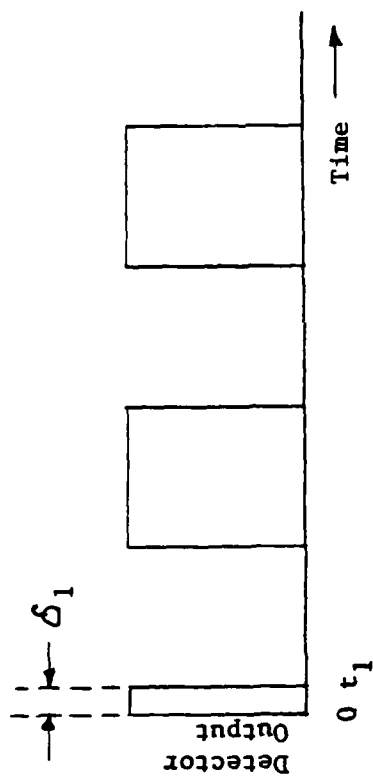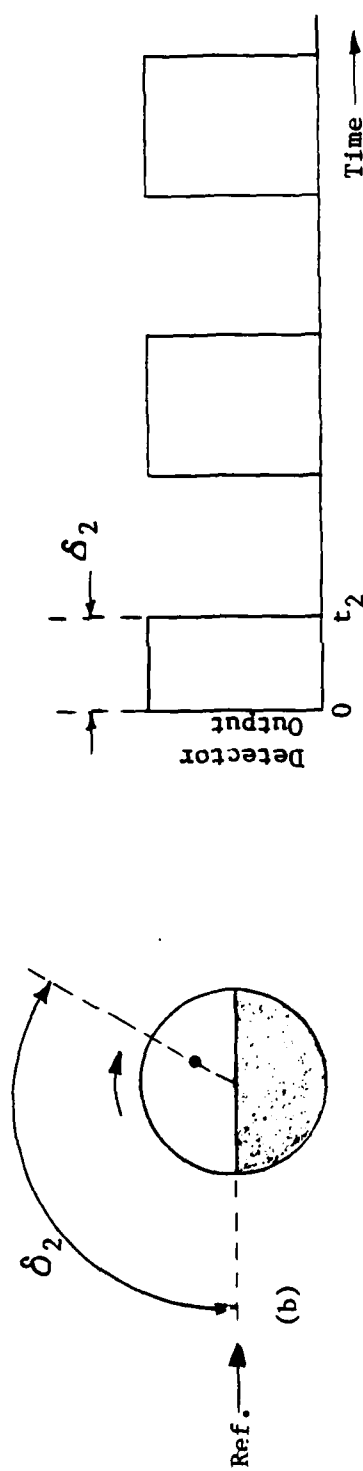
Figure 2.3.6.3-- Pulse-Phase-Modulating Rotating Reticle

2.50a

Image On Axis

Image Close To Axis

Image Away From Axis

Amplitude

Amplitude

Amplitude

Time

Time

Time

W
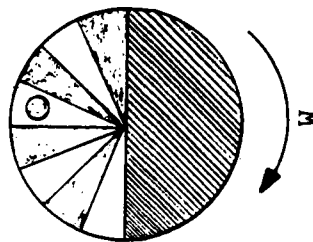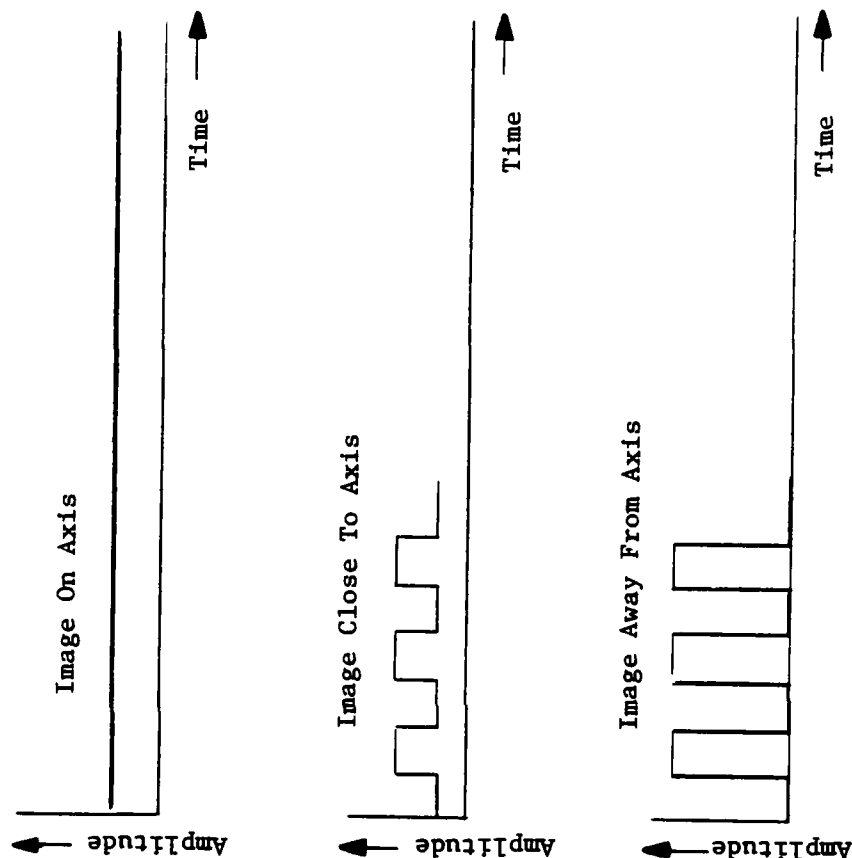
Figure 2.3.6.4-- Pulse-Amplitude-Modulating Rotating Reticle

2.50b
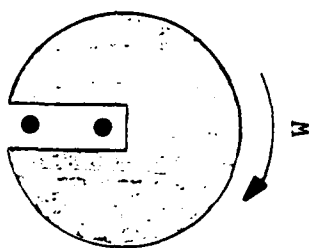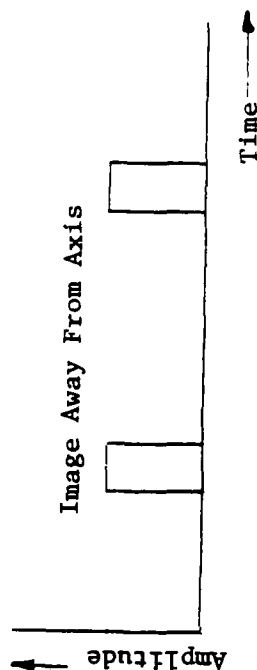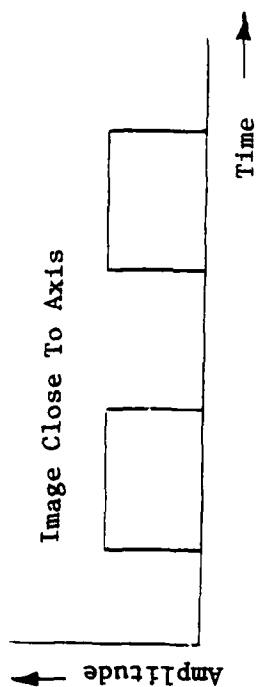
Figure 2.3.6.5-- Pulse Width Modulating Rotating Reticle

2.50c

result is pulse width modulation as shown in the figure. Note that the angular position of the target image also is indicated, by pulse position or phase. The alternate transmitting and opaque segments of the reticle shown in Figure 2.3.6.6 are arranged in tracks such that the number of segments in each track increases with the radius of the track. The radiant flux from a point-source target will thus be "chopped" at a frequency which increases with the radial distance of the target image from the center axis, thereby providing pulse frequency modulation of that flux. The reticle shown in Figure 2.3.6.7 spins about an axis offset from the center of the segmented pattern. The result is pulse frequency modulation of the radiant flux from a point target, as shown in the figure. From the frequency modulation, target image radial and angular position can be derived. The special-purpose rotating reticle shown in Figure 2.3.6.8 is designed to provide maximum amplitude modulation for point-source targets but discriminate against lineal targets. A sensor with such a reticle would respond to distant rocket plumes but reject linear clutter such as the earth-to-atmosphere interface (horizon).

2.51

Image Away from Axis

Image Close to Axis

Circular
Detector
Elements (10)

Phasing Portion

Target-Sensing
portion
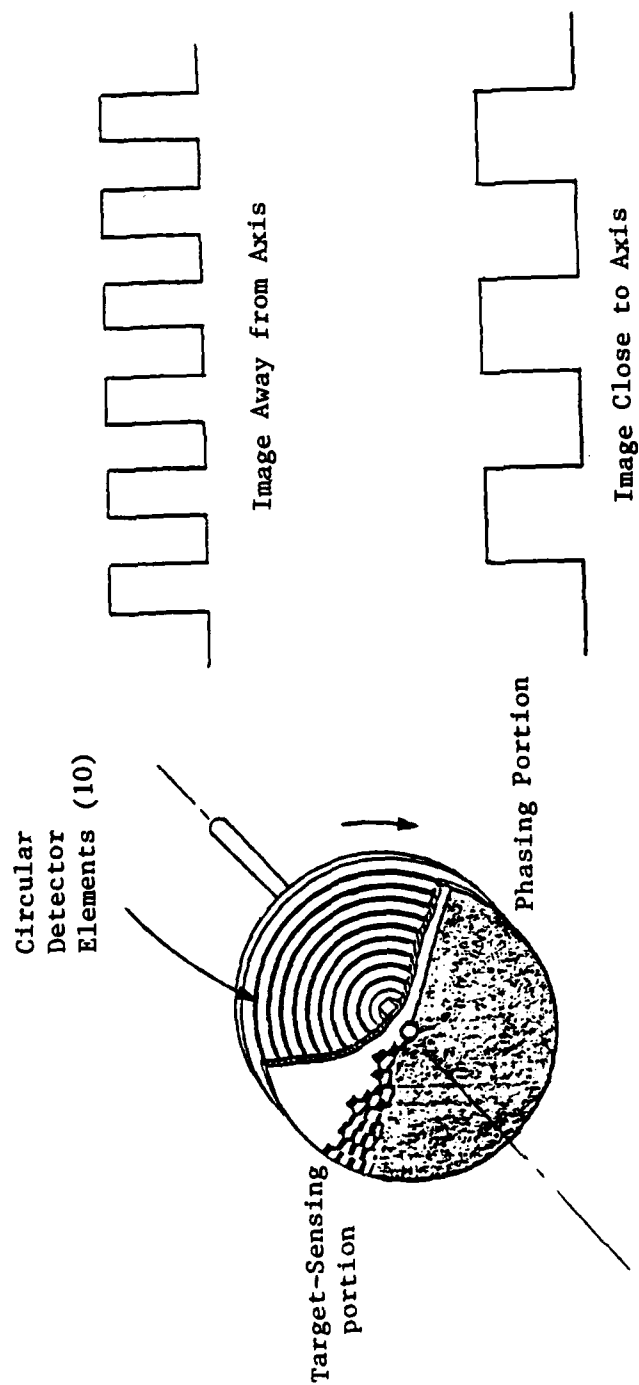
Figure 2.3.6.6-- Pulse Frequency Modulating Rotating Reticle

2.51a
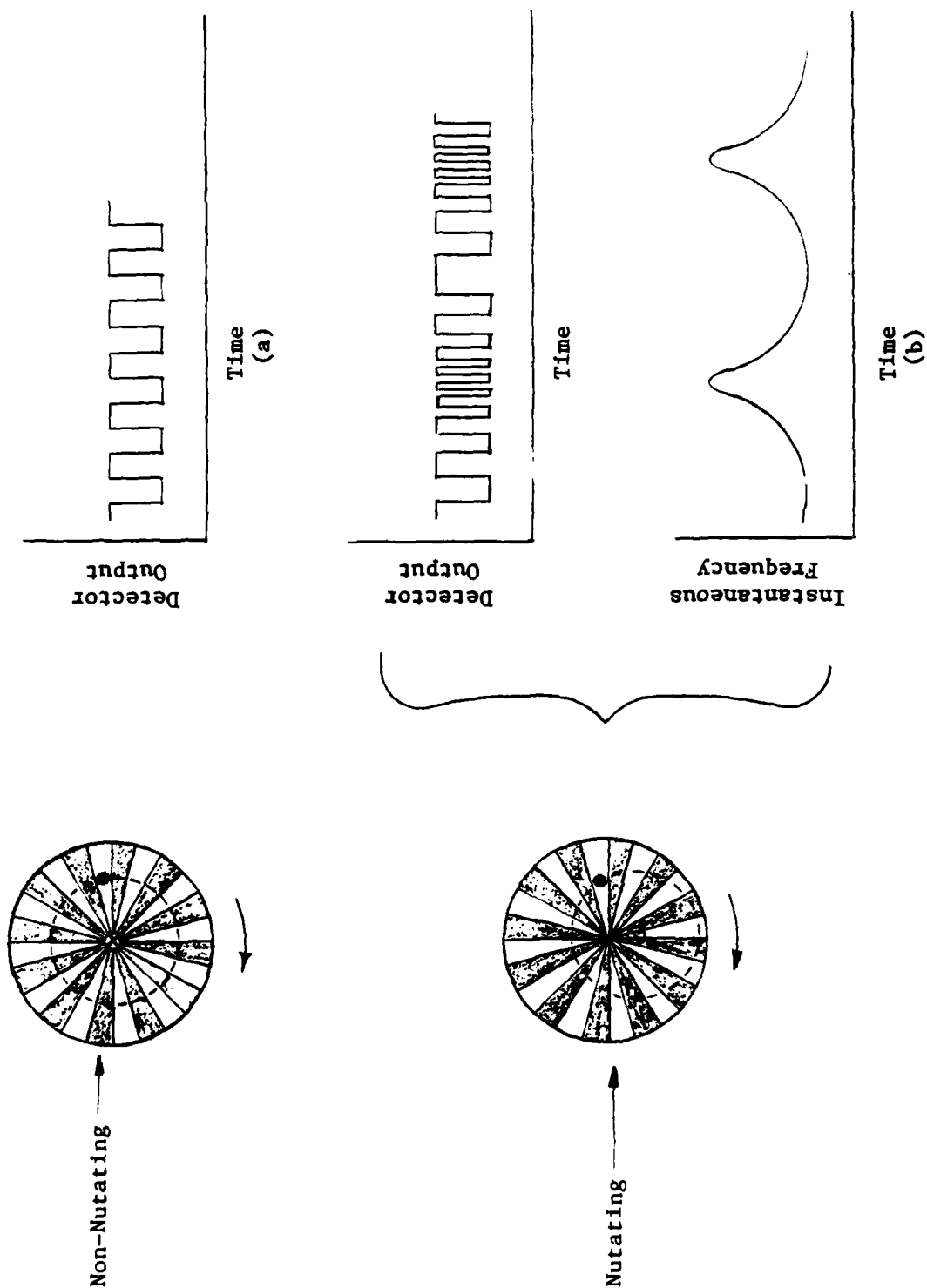
Figure 2.3.6.7 -- Nutating FM Rotating Reticle

2.51b
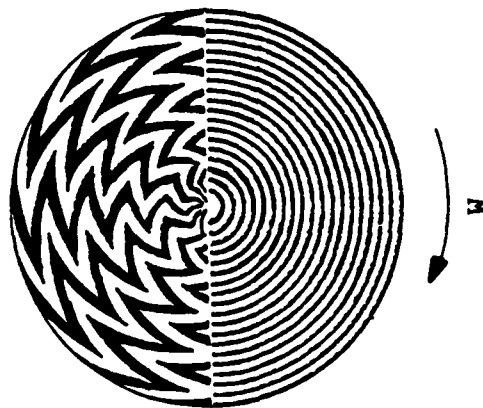
Figure 2.3.6.8-- Special Purpose Rotating Reticle

2.4 Radiation Detectors

2.4.1 Definition -- A radiation detector is a transducer of optical-frequency

radiant (electromagnetic wave) energy to electrical, or other, energy. (Except

for photographic devices, all of the radiation detectors of interest here con-

vert radiant energy to electrical energy.) The purpose of such conversion is

to provide a signal suitable for electronic processing. There are two basic

types of radiation detectors: thermal detectors and photon detectors. Thermal

detectors absorb radiant energy, thereby increasing in temperature. The in-

crease in temperature produces changes in the bulk physical properties of the

detector material. These changes are then measured as indications of radiant

energy absorbed (time integral of radiant flux). Photon detectors exhibit

measurable effects produced by the direct action of individual photons of

radiant energy on atomic electrons within the detector material (the photo-

electric effect). The principal types of radiation detectors in each category

are listed below.

Thermal Detectors	Photon Detectors
Calorimetric	Photoemissive
Fluid Expansion	Photoconductive
Evaporographic	Photovoltaic
Thermoelectric	Photoelectromagnetic
Bolometric	Photographic

The physical principles of operation and operating characteristics of the two

basic types of radiation detectors are discussed in the following paragraphs.

2.4.2 Thermal Detectors

The Calorimeter -- The calorimeter consists of a radiation-absorbing mass the temperature rise of which is measured, directly, as an indication of total radiant energy absorbed.

The Fluid-Expansion Thermometer -- The fluid-expansion thermometer consists of a radiation-absorbing liquid or gaseous mass the temperature rise of which is determined indirectly by measuring the change in volume of the fluid.

The Evaporograph -- The evaporograph consists of a radiation-absorbing screen the temperature rise of which is indicated indirectly by the rate of evaporation of a thin film of volatile substance. By focusing an image of the sensor field-of-view upon the screen, a thermal image is obtained.

The Thermocouple -- The thermocouple consists of a radiation-absorbing junction of two dissimilar electrical conductors. A voltage (contact potential) is developed across the junction, uniquely related to the temperature of the junction, thus indirectly indicating the absorbed radiant energy.

The Bolometer -- The bolometer is the thermal detector most frequently employed in airborne systems. It consists of a radiation-absorbing mass the electrical resistivity of which changes with temperature. Measurement of the resistivity thus provides an indirect indication of temperature rise and, hence, absorbed radiant energy. Commonly used bolometer materials are semiconductors (e.g. germanium), metallic oxides (thermistors), metals (platinum, nickel, silver, aluminum), and carbon (negative temperature coefficient).

Thermal Detector Characteristics -- The general characteristics of thermal-type radiation detectors are listed below and discussed in the following paragraphs.

> Response Time Large
> Detectivity Low
> Output Independent of Wavelength
> Heat Dissipation Required
> Cryogenic Cooling Not Required

The relatively slow response of the thermal-type radiation detector is a result of the time required to raise the temperature of the thermal mass. The long response time, (in the order of milliseconds), can be restrictive in a scanning sensor where target dwell times may be in the microsecond range.

The relatively low detectivity of the thermal detector results in a signal-to-noise ratio generally lower than that for a photon-type detector.

The most important advantage of the thermal-type detector is the fact that it responds to all wavelengths. (As discussed in Section 2.4.3 of this text, photon-type detectors do not respond beyond a certain wavelength).

The radiant energy absorbed by a thermal detector must be dissipated continuously in order for the detector to respond to a decreasing flux rate. Eventually, of course, all of the absorbed radiant energy must be dissipated. In situations involving continuing exposure to high-level radiation, heat dissipation can be a problem. Unlike photon detectors, however, cryogenic cooling is not usually required.

2.4.3 Photon Detectors

The Photoelectric Effect -- All electromagnetic radiation occurs in discrete
quanta called photons. Each photon contains an amount of energy, E_ν, determined
solely by the frequency of the radiation, according to the equation:

$$E_\nu = h f = \frac{hc}{\lambda} \quad \text{(Joules)}$$

where:

h = Planck's Constant = 6.63×10^{-34} (Watts-Sec^2)

c = Velocity of Propagation = 3×10^8 (Meters/Sec)

f = Frequency of Radiation (Hertz)

λ = Wavelength of Radiation (Meters)

The incident radiant flux, P, is related to the photon rate, Φ_ν, by the equation:

$$P \text{ (Watts)} = \Phi_\nu \text{ (Photons/sec)} \times E_\nu \text{ (Joules/Photon)}$$

or:

$$P = \frac{hc\Phi_\nu}{\lambda} \quad \text{(Watts)}$$

The electrons surrounding the nucleus of an atom exist in energy bands as
illustrated in Figure 2.4.3.1. Electrons in the lower energy states, E_o through
E_n, are bound to the atom in sharply-defined energy levels and take no part in
electrical conduction. Electrons in the non-discretized energy band (continuum)
above E_n but below that required to escape the material, (En + ϕ), are not bound
to the atom and are, therefore, free to take part in electrical conduction.
Electrons that have energies above the escape level take part in emission (escape
from the surface of the material). The work function, ϕ, is the minimum
incremental energy required to cause a bound electron to be emitted from the material.

Emitted Electrons

Conduction Electrons

Bound Electrons

$\emptyset$

E_n

E_2

E_2

E_1

E_0

Energy Level

E = Energy Level

$\emptyset$ = Work Function
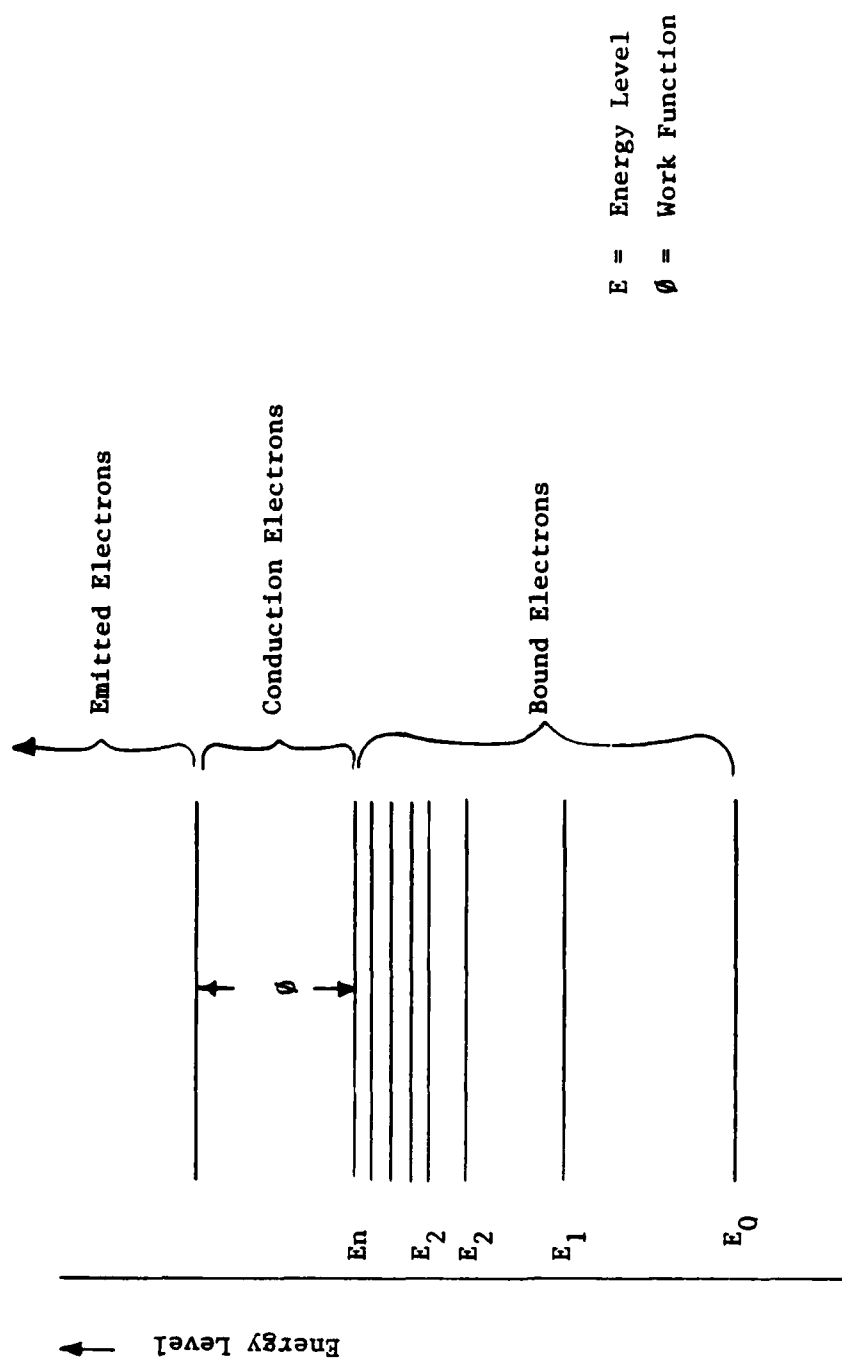
Figure 2.4.3.1-- Energy Levels of Atomic Electrons

2.55a

An incident photon of radiation can interact directly with an atom to raise

the energy level of a bound electron to the conduction band or even to the

point of emission. Both of these events are termed the photoelectric effect.

When the freed electron remains within the material, the process is called

photoconduction. When the freed electron is emitted from the surface of the

material, the process is called photoemission. In either case, the photon

of radiation is annihilated.

As previously indicated, the energy contained in a photon of radiation is pro-

portional to the frequency of the radiation. In order for photoconduction to

occur, the incident photon must possess enough energy, (the radiation must be

of high enough frequency), to raise the energy level of a bound electron into

the conduction band. In order for photoemission to occur, the incident photon

energy must be even higher as indicated in Figure 2.4.3.2. Thus photon-type

radiation detectors exhibit a cut-off wavelength beyond which (cut-off frequency

below which) they do not respond.

The Photoemissive Radiation Detector -- A photoemissive radiation detector

usually takes a form similar to that shown in Figure 2.4.3.3. It consists of

an evacuated vessel in which two electrodes are located. One of the electrodes,

the cathode, is coated with a photoemissive material. The external circuit

consists of a voltage supply (the battery) and an electrical-current-measuring

device (the ammeter). Photons of sufficient energy striking the surface of the

coated electrode produce photoemissive photoelectrons which flow to the positive

electrode (anode), thus causing an electrical current in the external circuit,
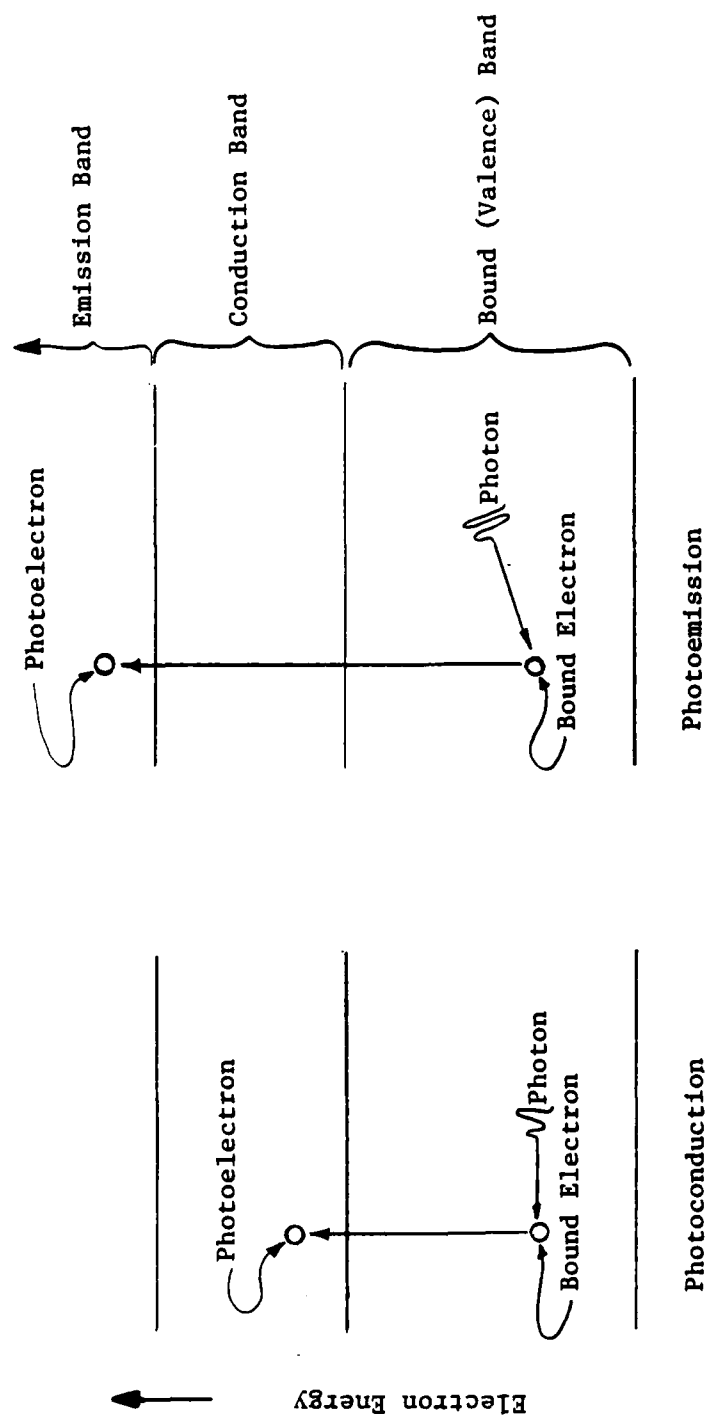
Figure 2.4.3.2-- The Photoelectric Effect

Photoemissive Material

Electrode

Vacuum

Photoelectron

Electrode

Photon

I

V

+

−
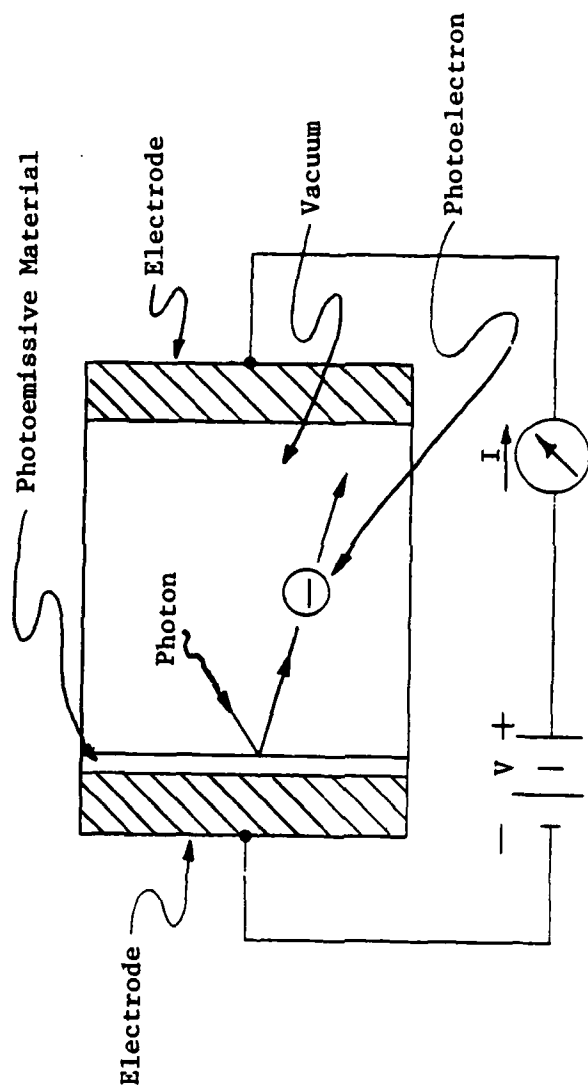
Figure 2.4.3.3-- Photoemissive Radiation Detector

2.56b

indicated by the ammeter. Photoemissive detectors include vacuum phototubes, photomultipliers, channeltrons, and others. In order for an electron to escape from a photoemissive surface, the absorbed photon energy, E_ν, must exceed the work function of the material. The excess energy is converted to kinetic energy of the emitted electron according to the equation:

$$E_\nu - \phi = \tfrac{1}{2} m_e v_e^2 \quad \text{(Joules)}$$

In order for an electron just to escape ($v_e = 0$), the photon energy must be:

$$E_\nu = \frac{hc}{\lambda} = \phi \qquad \text{(Joules)}$$

Thus, the cut-off wavelength of a material is given by the equation:

$$\lambda_{cutoff} = \frac{hc}{\phi} \qquad \text{(Meters)}$$

where:

h = Planck's Constant = 6.63×10^{-34} (Watts-Sec^2)

c = Velocity of Light = 3×10^8 (Meters/Sec)

m_e = Mass of Electron (Grams)

v_e = Escape Velocity of Electron (Meters/Sec)

λ = Radiation Wavelength (Meters)

ϕ = Work Function of Material (Joules)

The Photoconductive Radiation Detector -- A photoconductive radiation detector consists of a piece of semiconductor material with two electrodes attached as shown in Figure 2.4.3.4. The external circuit consists of a voltage source (the battery) and a current measuring device (the ammeter). Photons entering the semiconductor material produce photoconductive photoelectrons within the semiconductor material (and corresponding "holes" in the bound states of the atoms). Under the influence of the externally-applied electric field, the

2.57
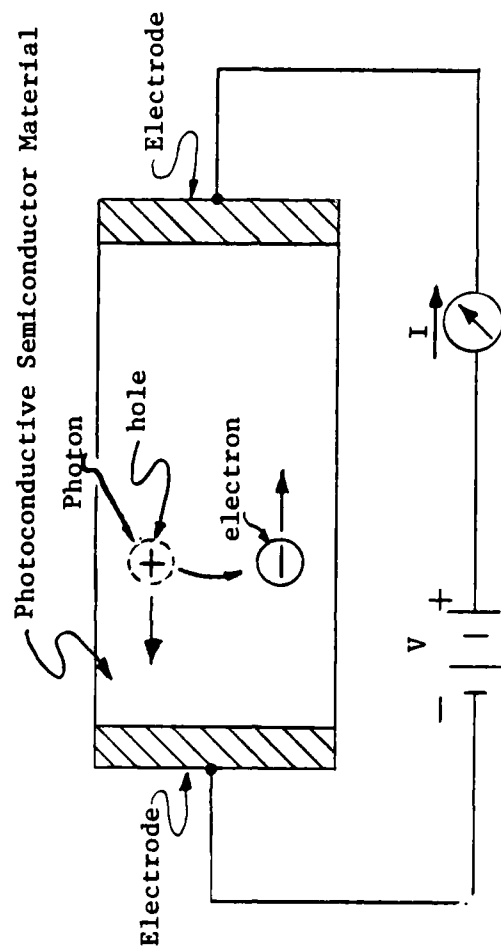
Figure 2.4.3.4-- Photoconductive Radiation Detector

photoelectrons move toward the positive electrode and the "holes" move toward the negative electrode thus causing a measureable electrical current to flow in the external circuit. Since the energy required to induce photoconduction is less than that required to induce photoemission, photoconductive detectors can respond to longer-wavelength radiation. Photoconductive materials include Si, Se, Ge:Hg, Ge:Cu, Ge:Zn, In Sb, PbS, PbSe, PbTe, PbSnTe, and Hg:Cd:Te.

The Photovoltaic Radiation Detector -- A photoconductive radiation detector consists of a semiconductor diode as shown in Figure 2.4.3.5. The external circuit consists of an electrical voltage-measuring device (the voltmeter). Photons entering the semiconductor material produce photoelectrons and corresponding "holes". As a result of the difference in energy levels in P-type and N-type semiconductor materials, the photoelectrons tend to migrate into the N-type material and the holes tend to migrate into the P-type material, thus producing an electric potential (voltage) across the P-N junction. This voltage is measured by the external voltmeter. The photon energy required for photovoltaic detection is essentially the same as that for photoconduction. Therefore, the cut-off wavelengths are approximately the same. Typical photovoltaic radiation detector (photodiode) materials are Si, InAs, and InSb.

The Photoelectromagnetic Radiation Detector -- A photoelectromagnetic radiation detector is constructed as shown in Figure 2.4.3.6. Two pairs of electrodes are attached to a photoconductive semiconductor bar, at right angles, as shown. The power electrodes are connected to an external voltage source (the battery). The output electrodes are connected to a voltage-measuring device (the voltmeter). A magnetic field is impressed as shown (perpendicular to the plane of the drawing).
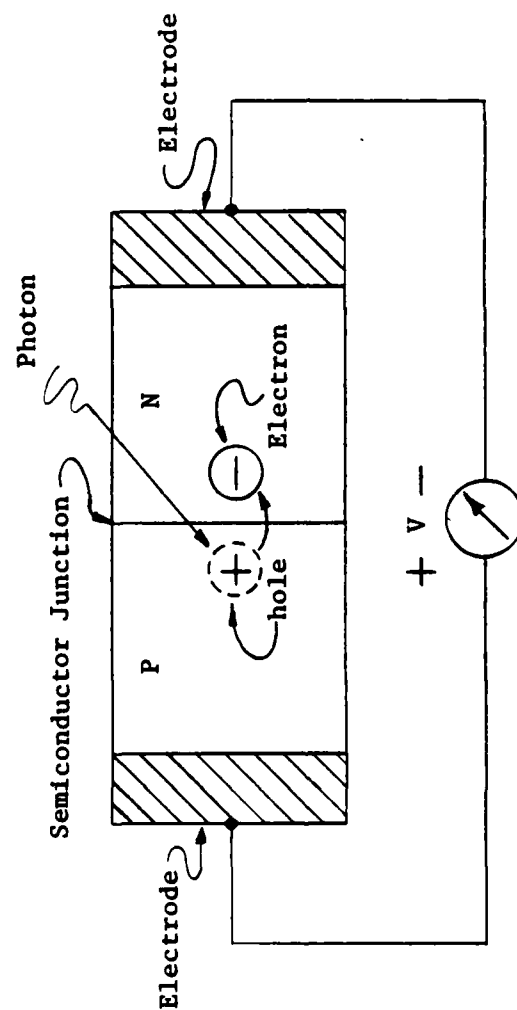
Figure 2.4.3.5-- Photovoltaic Radiation Detector

2.58a
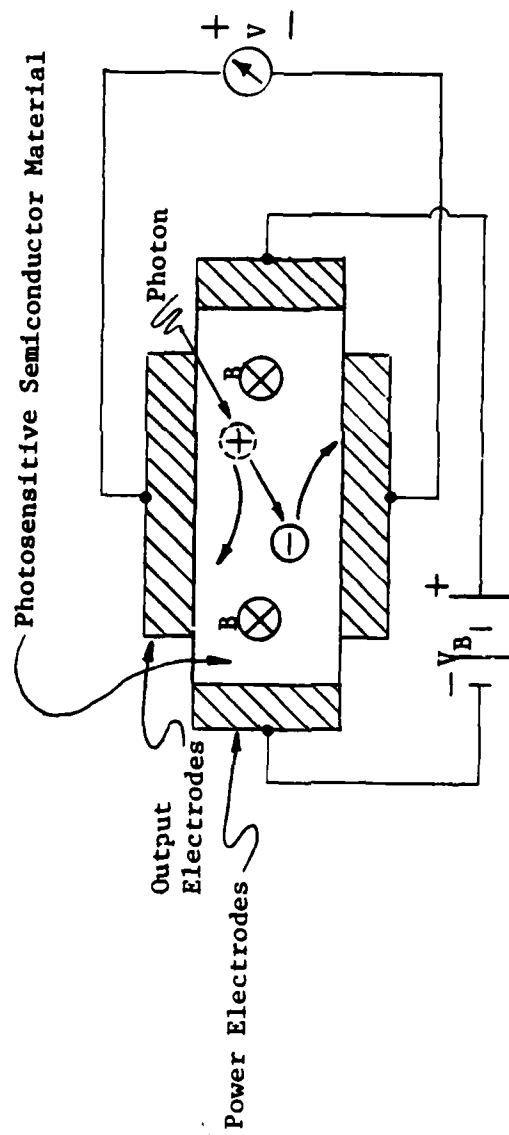
Figure 2.4.3.6-- Photoelectromagnetic Radiation Detector

Photons entering the semiconductor bar produce photoelectrons (and holes) which move under the combined effects of the electric and magnetic fields. The photoelectrons (and holes) move in curved paths with the result that an excess of electrons is accumulated at one output electrode and a scarcity of electrons at the other. Thus, a voltage is generated across the output electrodes.

The Photographic Radiation Detector -- The photographic radiation detector consists of a thin film of a photosensitive material. The photosensitive material undergoes a chemical change when exposed to radiation of sufficient energy (of sufficiently high frequency) to release electrons from atoms within the substance. When the radiation incident upon the photosensitive film represents an image (focused on the film), that image can be made evident by further chemical processing.

Photon Detector Characteristics -- The general characteristics of photon-type radiation detectors are listed below and discussed in the following paragraphs.

> Response Time Small
> Detectivity High
> Output Dependent Upon Wavelength
> Cryogenic Cooling Required

The interaction between an absorbed photon and the absorbing atom (the photoelectric effect) is essentially instantaneous. Photon detectors are therefore characterized by a relatively fast response (in the order of microseconds). This characteristic generally makes photon detectors more suitable for rapid-scan sensors than are the much slower thermal detectors.

The signal-to-noise ratio at the output of a photon-type radiation detector is, generally, larger than that for a thermal-type detector. Thus, the detectivity, (a direct measure of signal-to-noise ratio), is, in general, higher.

The most unfortunate characteristic of photon detectors is the existence of a cut-off wavelength beyond which the detector will not respond. (The cut-off wavelength is, as previously indicated, a result of the minimum photon energy (frequency) required to produce the photoelectric effect.) Unfortunately, many targets of military significance are at temperatures so low (infrared radiation wavelength so large) that photon detectors do not respond well to their radiations.

Most photon-type detectors perform well only at extremely low (cryogenic) temperatures. (Detectivity generally decreases rapidly with increasing temperature). For that reason, most radiation sensors utilizing photon-type detectors must incorporate relatively elaborate cryogenic cooling mechanisms.

2.4.4 Radiation Detector Characteristics -- The principal characteristics of radiation detectors can be categorized as indicated by the following list.

Sensitivity: Output for a given input.

Noise Equivalent Input: Input required to obtain S/N = 1.

Spectral Response: Response dependence on wavelength.

Dynamic Response: Response dependence on time.

Electrical Characteristics: Output level, impedance, power requirements, etc..

Environmental Limitations: Cooling required, moisture, shock, acceleration, etc. limitations.

2.4.5 Definitions of Symbols -- The symbols defined below are pertinent to a discussion of the performance characteristics of radiation detectors.

A_d = Effective Area of Detector (cm^2)

c = Velocity of Propagation of Radiation (cm/sec)

$\dot{D}$ = Detectivity of Detector (1/Watts)

D^* = Specific Detectivity of Detector (cm - $\sqrt{Hz}$/Watt)

D_λ^* = Spectral Spec. Det. of Detector (cm - $\sqrt{Hz}$/Watt-μM)

E_ν = Energy of One Photon (Joules)

f = Frequency (Hz)

f_c = Optical Modulation (Chopper) Frequency (Hz)

f_1 = Optical Focal Length (cm)

G = Gain (ND)

h = Planck's Constant (Watts - Sec^2)

H = Irradiance (Watts/cm^2)

H_s = Irradiance due to Signal (Watts/cm^2)

I = Electrical Current (Amps)

k = Boltzmann's Constant (Watt-Sec/Deg)

M_e = Mass of Electron (gms)

NEI = Noise Equivalent Irradiance of Detector (W/cm^2)

NEP = Noise Equivalent Power of Detector (Watts)

q_e = Charge of Electron (coulombs)

Q = Photon Irradiance (Photons/sec-cm^2)

Q_b = Q due to background "noise" (Photons/sec-cm^2)

Q_s = Q due to target signal (Photons/sec-cm^2)

r_d = Radius of Detector (cm)

r_t = Radius of Target (cm)

R_d = Resistance of Detector (ohms)

R_t = Range to Target (cm)

R = Responsivity of Detector (Volts/Watt)

t = Time (sec)

T = Temperature (Degrees, Kelvin)

v_e = Velocity of Electron (cm/sec)

V = Voltage (Volts)

V_N = Voltage due to Noise (Volts)

V_s = Voltage due to Signal (Volts)

α = Angle (Radians)

$[\Delta f]$ = Noise Equivalent Bandwidth (Hz)

η = Responsive Quantum Efficiency of Detector (ND)

θ = Angular Field-of-View (cone angle) (Rad.)

λ = Wavelength of Radiation (μM)

λ_c = Cutoff Wavelength of Detector (μM)

μ = Microns (Micro-)

τ = Transmittance of Medium (ND)

τ_d = Time comstant of Detector (Secs)

τ_e = Electrical Carrier (charge) Lifetime (Secs)

Ω = Solid Angle Field-of-View (stearadians)

2.4.6 Radiation Detector Parameters -- The principal parameters describing the input/output relationships of radiation detectors are discussed in the following paragraphs.

Responsivity: R (Volts/Watt) -- The responsivity of a radiation detector is the ratio of the output quantity to the input quantity. For example, for a photovoltaic detector:

$$\mathcal{R} = \frac{V_s}{H_s A_d}$$

The output voltage is then given by:

$$V_s = \mathcal{R} A_d H_s \quad \text{(Volts)}$$

Responsivity is of limited value in specifying detector performance because, nearly always, it is not the output level but, rather, the signal-to-noise ratio that determines system performance. Responsivity does not reflect the noise level. Responsivity also is generally dependent upon many factors, including: radiant flux signal amplitude and frequency characteristics, radiation wavelength, temperature, detector area, optical modulation (chopper) frequency, and the bandwidth of the measurement system.

Noise Equivalent Power: NEP (Watts) -- The noise equivalent power of a radiation detector is that input flux (power) required to produce a signal-to-noise ratio equal to unity. Thus, for a photovoltaic detector:

$$NEP = \frac{V_N}{\mathcal{R}}$$

The output signal-to-noise voltage ratio is then given by:

$$\left(\frac{V_s}{V_N} \right) = \left(\frac{A_d}{NEP} \right) H_s \quad \text{(N.D.)}$$

NEP depends upon the same factors that influence the responsivity. Unlike responsivity, however, it takes into consideration the noise present.

Noise Equivalent Irradiance: NEI (Watts/cm^2) -- The noise equivalent irradiance of a radiation detector is that input irradiance required to produce an output signal-to-noise voltage ratio equal to unity. Thus, for a photovoltaic detector:

$$NEI = \frac{V_N}{\mathcal{R} A_d}$$

The output signal-to-noise voltage ratio is then given by:

$$\left(\frac{V_S}{V_N}\right) = \left(\frac{1}{NEI}\right) H_S \qquad \text{(N.D.)}$$

NEI depends upon the same factors that influence detector responsitivity. Like NEP, it reflects the noise level as well as the signal level.

Detectivity: D(1/Watts) -- The detectivity of a radiation detector is the reciprocal of the noise equivalent power. That is:

$$D = \frac{1}{NEP} = \frac{\mathcal{R}}{V_N}$$

The output signal-to-noise ratio is then given by:

$$\left(\frac{V_S}{V_N}\right) = \left(D A_d\right) H_S \qquad \text{(N.D.)}$$

Detectivity is defined in order to provide a measure of detector sensitivity directly proportional to the sensitivity. Detectivity depends upon the same factors that influence detector responsivity.

Specific Detectivity: $D^*(\sqrt{Cm-Hz}/Watt)$ -- The specific detectivity of a radiation detector is defined as the detectivity, D, multiplied by the square roots of detector area and the bandwidth of the measurement system. That is:

$$D^* = \sqrt{A_d}\,\sqrt{\Delta f}\; D = \frac{\sqrt{A_d}\,\sqrt{\Delta f}\;\mathcal{R}}{V_N}$$

The output signal-to-noise voltage ratio is then given by:

$$\left(\frac{V_S}{V_N}\right) = \left(\frac{\sqrt{A_d}\; D^*}{\sqrt{\Delta f}}\right) H_S \qquad \text{(N.D.)}$$

The specific detectivity is defined in order to provide a measure of detector sensitivity relatively independent of detector area and system bandwidth. It, otherwise, depends upon the same factors that influence detector responsivity.

Responsive Quantum Efficiency: η (N.D.) -- The responsive quantum efficiency of a photon-type radiation detector is defined as the ratio of detector photo-electric events to incident photons. (Not all incident photons produce photo-electrons.) Thus, for a photovoltaic detector:

$$\eta = \frac{V_S}{V_{S(\eta=1)}} = \frac{(V_S/V_N)}{(V_S/V_N)_{(\eta=1)}}$$

The output voltage of a photovoltaic detector is then given by:

$$V_S = (\eta\,\mathcal{R}\,A_d)\, H_S \qquad \text{(Volts)}$$

or:

$$V_S = \left(\frac{\eta\,\mathcal{R}\,A_d\,hc}{\lambda}\right) Q_S \qquad \text{(Volts)}$$

where Q_S is the photon irradiance (photons per second per square centimeter).

2.4.7 Typical Radiation Detection Parameter Values -- Tables of typical

radiation detector material parameters are presented in Figures 2.4.7.1(a)

through 2.4.7.1(d). Plots of detector material specific detectivity versus

wavelength are shown in Figure 2.4.7.2. The dotted curves in Figure 2.4.7.2

represent the theoretical upper limits on photon detector detectivity dis-

cussed in Section 2.4.9 of this text.

Detector Material	Operating Mode[a]	Useful Wavelength Range[b] (μ)	Wavelength of Peak Response (μ)	Resistance[c] (Ohm)	Time Constant (μ sec)	D^* (500°K B.B.)[d] ($\frac{cm-(Hz)^{\frac{1}{2}}}{Watts}$)	D^* (Peak Resp.)[d] ($\frac{cm-(Hz)^{\frac{1}{2}}}{Watts}$)
THERMAL DETECTORS							
Room-temperature operation							
Thermocouple	Thermo-electric	1-40	N/A	1-10	25,000	$3\text{-}12\times10^8(5)$	$6\text{-}15\times10^8(5)$
Thermistor bolometer	bolometer	0.2-40	N/A	$1\text{-}5\times10^6$	2,000	$0.3\text{-}1.2\times10^8(15)$	$1\text{-}3\times10^8(15)$
Low-temperature operation							
Carbon bolometer (2.1°K)	bolometer	40-100	N/A	0.12×10^6	10,000	$4\times10^{10}(13)$	$4\times10^{10}(13)$
Germanium bolometer (2.1°K)	bolometer	5-2000	N/A	12×10^3	400	$8\times10^{11}(200)$	$8\times10^{11}(200)$

a. PV = photovoltaic, PC = photoconductive, PEM = photoelectromagnetic
b. Wavelengths between which D* exceeds 0.2 of its peak value.
c. Value shown is for a square element. For PV detectors the value is the dynamic impedance dV/dI.
d. All D* values given for a detector viewing a hemispherical surround at a temperature of 300°K at the frequency indicated.

Figure 2.4.7.1(a) -- Radiation Detector Material Parameters

Detector Material	Operating Mode[a]	Useful Wavelength Range[b] (μ)	Wavelength of Peak Response (μ)	Resistance[c] (Ohm)	Time Constant (μ sec)	D^* (500°K B.B.)[d] $\left(\frac{cm-(Hz)^{\frac{1}{2}}}{Watts}\right)$	D^* (Peak Resp.)[d] $\left(\frac{cm-(Hz)^{\frac{1}{2}}}{Watts}\right)$
PHOTON DETECTORS							
Room-temperature							
Silicon	PV	0.5-1.05	0.84	$0.1-1\times10^6$	100	$10^{10}-10^{11}$(90)	$1-5\times10^{12}$(90)
Lead Sulfide (PbS)	PC	0.6-3.0	2.3-2.7	$0.5-10\times10^6$	50-500	$1-7\times10^8$(800)	$50-100\times10^9$(800)
Indium arsenide (InAs)	PV	1-3.7	3.2	20	~1	$1-3\times10^8$(900)	$3-7\times10^9$(900)
Indium arsenide (InAs)	PEM	1.4-3.8	3.4	-	~1	-	6×10^9(1000)
Operation at 195°K							
Lead Sulfide (pbS)	PC	0.5-3.3	2.6	$0.5-5\times10^6$	800-4000	$0.7-7\times10^9$(800)	$20-70\times10^{10}$(800)
Indium arsenide (InAs)	PV	0.5-3.5	3.2	-	~1	$1-5\times10^9$(1800)	$3-25\times10^{10}$(1800)

a. PV = photovoltaic, PC = photoconductive, PEM = photoelectromagnetic.
b. Wavelengths between which D^* exceeds 0.2 of its peak value.
c. Value shown is for a square element. For PV detectors the value is the dynamic impedance dV/dI.
d. All D^* values given for a detector viewing a hemispherical surround at a Temp. of 300°K at the frequency indicated.

Figure 2.4.7.1(b) -- Radiation Detector Material Parameters (Con't)

Detector Material	Operating Mode[a]	Useful Wavelength Range[b] (μ)	Wavelength of Peak Response (μ)	Resistance[c] (Ohm)	Time Constant (μ sec)	D^* (500°K B.B.)[d] $\left(\frac{cm-(Hz)^{\frac{1}{2}}}{Watts}\right)$	D^* (Peak Resp.)[d] $\left(\frac{cm-(Hz)^{\frac{1}{2}}}{Watts}\right)$
Indium arsenide (InAs)	PEM	1.3-3.6	3.2	--	~1	3×10^9 (1000)	20×10^{10} (1000)
Indium antimonide (InSb)	PC	0.5-6.5	5.1	20	~1	1×10^9 (800)	$0.5-0.9\times10^{10}$ (800)

a. PV = photovoltaic, PC = photoconductive, PEM = photoelectromagnetic.
b. Wavelengths between which D^* exceeds 0.2 of its peak value.
c. Value shown is for a square element. For PV detectors the value is the dynamic impedance dV/dI.
d. All D^* values given for a detector viewing a hemispherical surround at a temperature of 300°K at the frequency indicated.

Figure 2.4.7.1(b) -- Radiation Detector Material Parameters (Con't)

Detector Material	Operating Mode[a]	Useful Wavelength Range[b] (μ)	Wavelength of Peak Response (μ)	Resistance[c] (Ohm)	Time Constant (μ sec)	D^* (500°K B.B.)[d] $\left(\frac{\text{cm-(Hz)}^{\frac{1}{2}}}{\text{Watts}}\right)$	D^* (Peak Resp.)[d] $\left(\frac{\text{cm-(Hz)}^{\frac{1}{2}}}{\text{Watts}}\right)$
Operation at 77°K							
Lead Sulfide (PbS)	PC	0.7-3.8	2.9	$1\text{-}10\times10^6$	500-3000	$3\text{-}8\times10^9(800)$	$8\text{-}20\times10^{10}(800)$
Indium arsenide (InAs)	PV	0.6-3.2	2.9	10×10^6	~2	$3\text{-}8\times10^9(1800)$	$20\text{-}70\times10^{10}(1000)$
Lead telluride (PbTe)	PC	1-5.4	5.0	$50\text{-}500\times10^6$	~5	$1\times10^9(90)$	$0.8\times10^{10}(90)$
Indium antimonide (InSb)	PV	0.6-5.6	5.1	$1\text{-}50\times10^3$	~1	$3\text{-}20\times10^9(900)$	$3\text{-}8\times10^{10}(900)$
Indium antimonide (InSb)	PC	0.7-5.9	5.3	$2\text{-}10\times10^3$	1-10	$3\text{-}10\times10^9(900)$	$2\text{-}6\times10^{10}(900)$
Gold-doped germanium (p-type)	PC	1-9	5.4	$0.1\text{-}10\times10^6$	~1	$1\text{-}3\times10^9(800)$	$0.3\text{-}1\times10^{10}(800)$
Mercury-cadmium-telluride	PV	6-15	10.6	5-50	0.01	$10^9\text{-}10^{10}(900)$	-

a. PV = photovoltaic, PC = photoconductive, PEM = photoelectromagnetic.
b. Wavelengths between which D^* exceeds 0.2 of its peak value.
c. Value shown is for a square elemtn. For PV detectors the value is the dynamic impedance dV/dI.
d. All D^* values given for a detector viewing a hemispherical surround at a Temp. of 300°K at the frequency indicated.

Figure 2.4.7.1(c) -- Radiation Detector Material Parameters (Con't)

Detector Material	Operating Mode[a]	Useful Wavelength Range[b] (μ)	Wavelength of Peak Response (μ)	Resistance[c] (Ohm)	Time Constant (μ sec)	D^* (500°K B.B.)[d] ($\frac{cm-(Hz)^{\frac{1}{2}}}{Watts}$)	D^* (Peak Resp.)[d] ($\frac{cm-(Hz)^{\frac{1}{2}}}{Watts}$)
Operation below 50°K							
Zinc-doped germanium-Silicon alloy (Ge-Se:Zn) (48°K)	PC	2-15	10.5	0.1×10^6	~1	5×10^9 (100)	1×10^{10} (100)
Mercury-doped germanium (Ge:Hg) (30°K)	PC	3-14	11	$2-100 \times 10^3$	~1	$3-9 \times 10^9$ (900)	$1-1.5 \times 10^{10}$ (900)
Cadmium-doped germanium (Ge:Cd) (28°K)	PC	6-24	17	20×10^3	~1	4×10^9 (400)	1.2×10^{10} (400)
Copper-doped germanium (Ge:Cu) (4.2°K)	PC	6-29	23	$0.5-1 \times 10^6$	~1	$5-10 \times 10^9$ (1800)	$1.5-3 \times 10^{10}$ (1800)
Zinc-doped germanium (Ge:Zn) (4.2°K)	PC	7-40	37	0.3×10^6	~0.01	$3-4 \times 10^9$ (800)	$0.9-1.2 \times 10^{10}$ (800)

a. PV = photovoltaic, PC = photoconductive, PEM = photoelectromagnetic.
b. Wavelengths between which D^* exceeds 0.2 of its peak value.
c. Value shown is for a square element. For PV detectors the value is the dynamic impedance dV/dI.
d. All D^* values given for a detector viewing a hemispherical surround at a temperature of 300°K at the frequency indicated.

Figure 2.4.7.1(d) -- Radiation Detector Material Parameters (Con't)

Figure 2.4.7.2 -- Specific Detectivity of Detector Materials
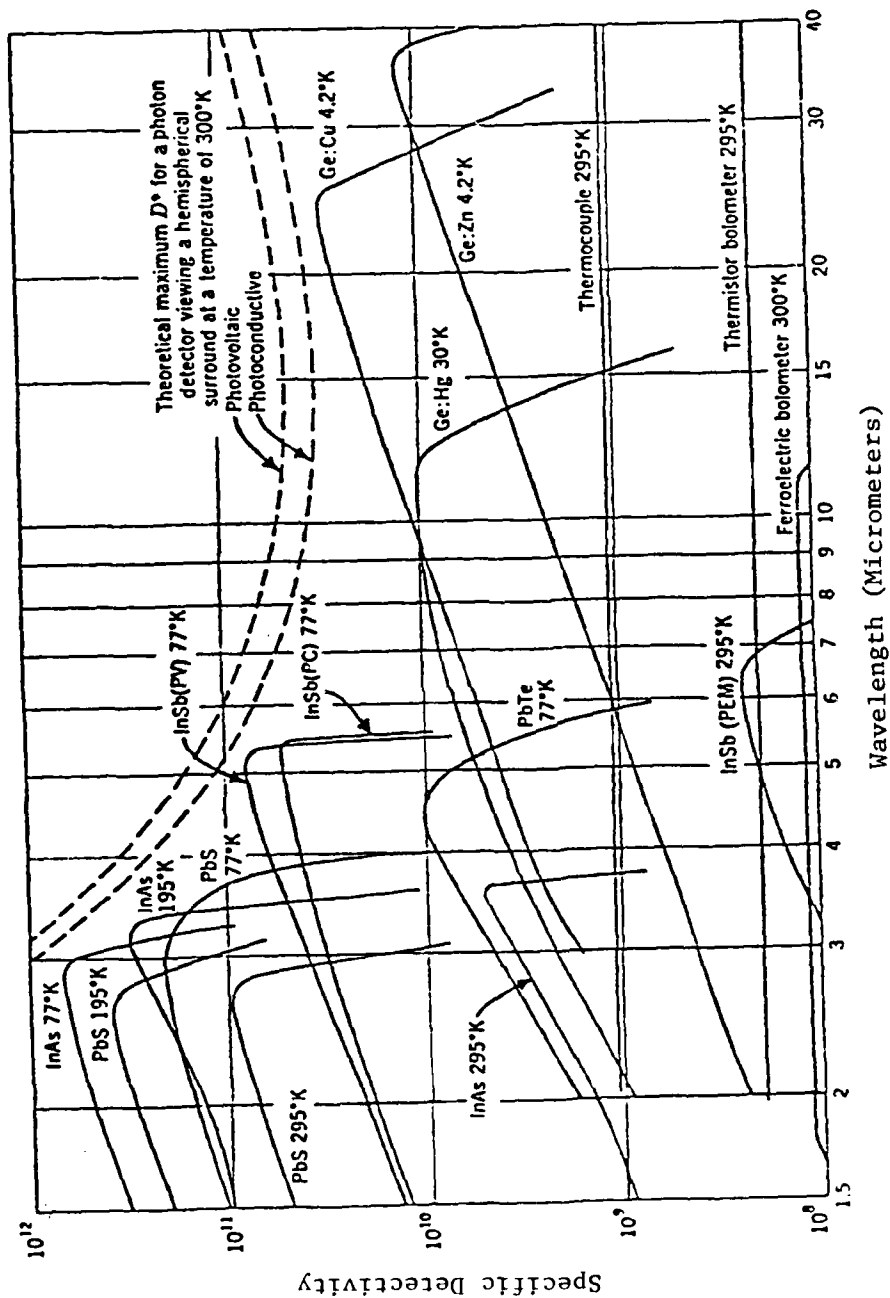
Detector is assumed to view a hemisphere at a temperature of 300°K. Chopping frequency is 1800 Hz for photon detectors except InSb for which it is 1000 Hz.

2.68

2.4.8 Radiation Detector Noise -- As previously indicated, signal-to-noise ratio, (rather than signal alone), generally determines system performance. For that reason, noise assumes an importance equal to that of the signal itself. In a radiation sensor, two fundamentally-different types of noise are evident: externally-generated noise produced by background clutter in the sensor field-of-view, and internally-generated noise produced by the sensor system itself.

Externally-Generated Noise -- Externally-generated noise can be reduced only by limiting the response of the sensor system. Sensor response characteristics that often can be limited to increase the signal-to-noise ratio include: field-of-view, spectral response (bandwidth), spatial response (spatial frequency response or angular resolution), time response, and threshold sensitivity.

Field-of-View Limiting -- The sensor field-of-view can be reduced by means of appropriate optical design, including the use of field stops. Limiting the field-of-view discriminates against clutter of spatial extent greater than that of the intended target.

Spectral Response Limiting -- Limiting the spectral response of the system can be accomplished by selection of the radiation detector or by the use of chromatic filters. In either case, the result is to discriminate against the clutter on the basis of frequency (wavelength).

Spatial Response Limiting -- The spatial response of the system can be limited by spatial filtering, generally achieved by the use of reticles or by controlling the shape and size of the radiation detector. Spatial filtering discriminates against clutter on the basis of size and shape.

2.69

Time Response Limiting -- The time response of the sensor is limited by frequency filtering of the signal after conversion from the space domain to the time domain. A typical example is the use of an electronic low-pass (smoothing) filter to attenuate the time response of a scanning system to a flare (very strong point-source).

Threshold Sensitivity Limiting -- The threshold sensitivity of a radiation sensor can be adjusted to discriminate against low-level clutter.

Limiting the response of the radiation sensor by any of these methods degrades the performance of the system to some extent. The use of these techniques is, there-fore, restricted by the required performance of the system.

Internally-Generated Noise -- The major sources of internally generated noise are radiation effects, thermal effects, and electronic effects. Radiation effects are caused by extraneous radiation reaching the radiation detector. Thermal effects are short-term effects due to thermal noise and long-term effects due to component heating. Electronic effects are caused by inadvertent electric and magnetic coupling and by the discrete nature of electronic phenomena. The dominant source of noise in a radiation sensor is the radiation detector itself. Radiation detector noise is the vector sum of the six types of noise discussed in the following paragraphs.

Thermal (Johnson) Noise -- Thermal noise is caused by the thermal motion of the electrons in a resistive component. The power amplitude of thermal noise is

2.70

proportional to the absolute temperature of the component. The RMS value of
the thermal (Johnson) noise voltage is given by the equation:

$$V_J = \left[4\,k\,R\,(\Delta f)\,T \right]^{1/2} \quad \text{(Volts, rms)}$$

where:

k = Boltzmann's Constant

R = Component Resistance (Ohms)

T = Component Absolute Temperature (Deg., K)

(Δf) = Noise Bandwidth of Measuring System (Hertz)

Note that thermal noise is white (i.e., not a function of frequency). Since the
other major types of detector noise decrease with frequency, thermal noise generally
dominates at high frequencies. As suggested by the above equation, thermal noise
can be reduced by lowering the temperature of the detector or reducing the band-
width of the system.

Contact Noise -- Contact noise is caused by fluctuations in the contact resistance
at discontinuities and interfaces between materials of differing electrical
properties. Because the power varies inversely with frequency, contact noise
is sometimes called "1/f" (one-over-f) noise. It also is sometimes called "excess
noise" and "current noise". The rms value of the contact noise voltage is given
by the equation:

$$V_c = C_n\,R\,\bar{I}\left[\frac{\Delta f}{f}\right]^{1/2} \quad \text{(Volts)}$$

where:

C_n = Constant Characteristic of Material (N.D.)

$\bar{I}$ = Average Detector Current (Amps)

R = Detector Resistance (Ohms)

2.71

Because of its (1/f) characteristic, contact noise generally dominates at very low frequencies in a radiation detector. For the same reason, it is usually negligable above a few hundred hertz and therefore can be eliminated by optical modulation above that frequency.

Generation/Recombination Noise -- Generation/recombination noise is caused by fluctuations in the rates at which charge carriers (electrons and holes) are generated and destroyed within a semiconductor. Such carriers are created by photon absorption and by the motion of electrons in the semiconductor material. The rms amplitude of the generation/recombination noise voltage is given by the equation:

$$V_{GR} = \bar{I} \, R \left[\frac{4 \tau (\Delta f)}{n (1 + 4\pi^2 \tau^2 f^2)} \right]^{1/2} \qquad \text{(Volts, rms)}$$

where:

        f = Frequency (Hertz)

        $\bar{I}$ = Average Detector Current (Amsp)

        n = Carrier Charge Population (N.D.)

        R = Detector Resistance (Ohms)

    (Δf) = System Noise Bandwidth (Hertz)

        τ = Carrier Charge Lifetime (Secs)

Generation/recombination noise is generally dominant at mid-frequencies in photon detectors and can be reduced by "doping" of the semiconductor material and by limiting the system bandwidth.

2.72

Shot Noise -- Shot noise is caused by random fluctuations in the rate of arrival of electrons at an internal junction in an electrical circuit. (It is called "shot" noise because, at low current levels, it sounds like shotgun pellets (shot) sprinkled on a tin roof). The rms amplitude of the shot noise voltage is given by the equation:

$$V_S = R\left[2\,q_e\,\overline{I}\,(\Delta f)\right]^{1/2} \quad \text{(Volts, rms)}$$

where:

$\overline{I}$ = Average Detector Current (Amps)

q_e = Electronic Charge = 1.6×10^{-19} Coulombs

R = Detector Resistance (Ohms)

(Δf) = System Noise Bandwidth (Hertz)

Shot noise is generally dominated by other noise processes though it can be significant in photon detectors. Shot noise can be reduced by limiting system bandwidth.

Photon Noise -- Photon noise is caused by random fluctuations in the rate of arrival of photons at the detector in a radiation sensor. (Photon noise is the radiative analog of shot noise.) The rms value of the photon noise voltage is given by the equation:

$$V_P = R\left[2\,q_e\,\overline{I}_r\,(\Delta f)\right]^{1/2} \quad \text{(Volts, rms)}$$

where:

$\overline{I}_r$ = Average Detector Currend due to Photon Absorption (Amsp)

q_e = Electronic Charge (Coulombs)

R = Detector Resistance (Ohms)

(Δf) = System Noise Bandwidth (Hertz)

2.73

Although photon noise is caused by photons originating external to the sensor, it is considered internal noise because it arises as the result of an internal process (photon absorption). Although photon noise is usually dominated by other noise processes, it can be significant in background-limited detectors. Photon noise can be reduced by limiting the bandwidth of the system.

Temperature Noise -- Temperature noise is caused by fluctuations in the rate at which heat is absorbed and dissipated by the detector. It is not thermal (Johnson) noise, however, but is caused by variations in the electrical properties of the detector with temperature (temperature coefficients). Temperature noise is generally significant only in thermal-type radiation detectors and is usually dominated by other noise processes. Temperature noise can be minimized by proper cooling and thermal isolation of the detector.

Total Internally-Generated Noise -- The combined effects of the dominant internal noise sources in a radiation detector are shown in Figure 2.4.8.1. The individual noise voltages are assumed to be statistically independent and are, therefore, root-sum-squared according to the equation:

$$V_{Noise} = \left[V_c^2 + V_{GR}^2 + V_J^2 \right]^{1/2} \quad \text{(Volts, rms)}$$

Note that, in the low-frequency range, contact (1/f) noise dominates; in the mid-frequency range, generation/recombination noise dominates; and in the high-frequency range, thermal (Johnson) noise dominates.

Background-Limited Infrared Photodetection (BLIP) -- The goal of radiation sensor design is to reduce the internally-generated noise to the level where the external

$V_N \cong V_J$

$V_N \cong V_{GR}$

$V_N \cong V_C$

High

Mid

Low

Frequency (Hertz) →

V_{Noise} (volts, rms)
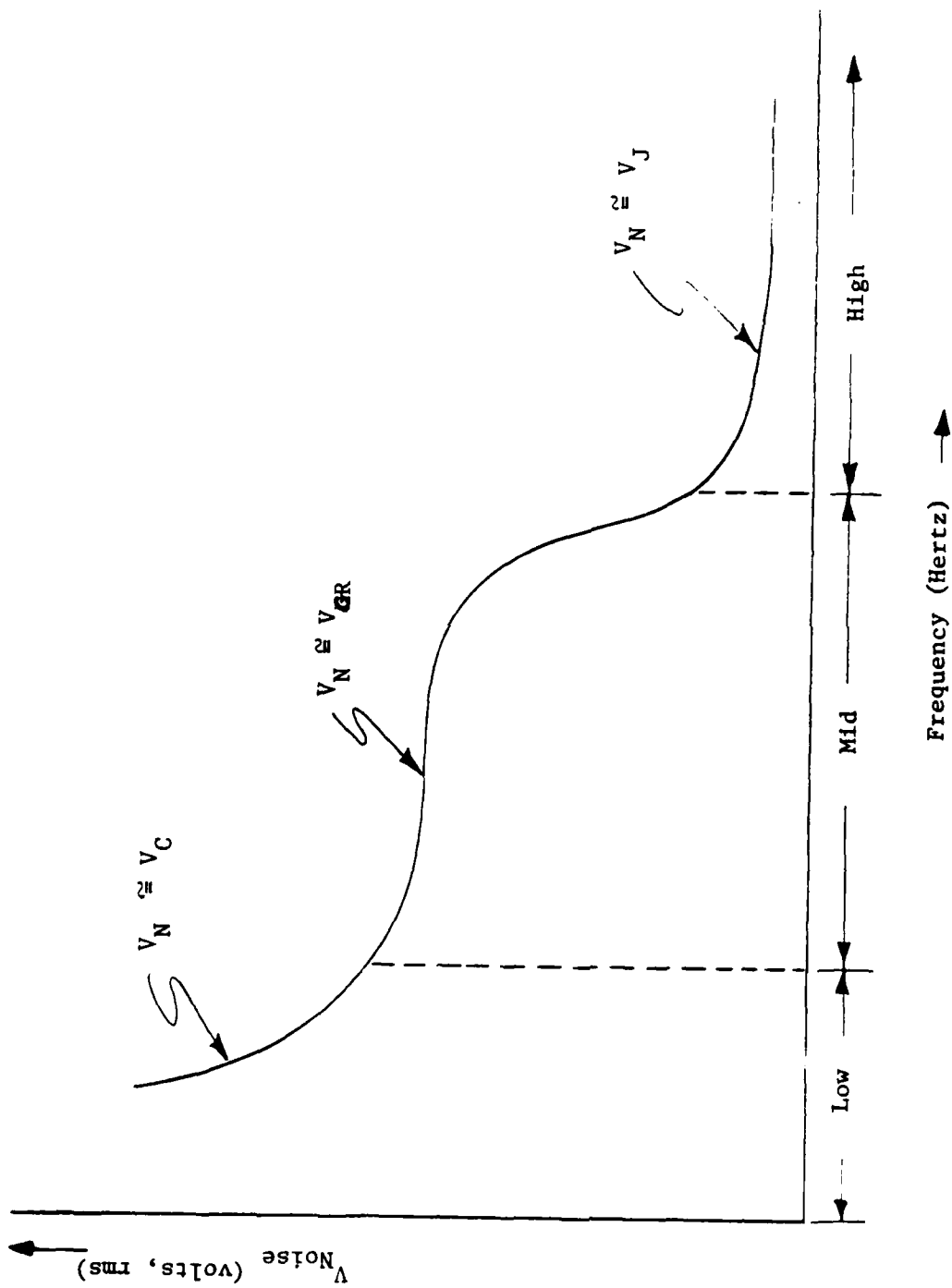
Figure 2.4.8.1 -- Radiation Detector Noise

2.74a

(target background) noise is dominant. Such a sensor is said to be in BLIP operation. Further increase in signal-to-noise ratio can be obtained by employing temporal, chromatic, or spatial filtering to discriminate between target and clutter. A theoretical limit exists in the specific detectivity (D*) that can be achieved for a given detector field-of-view and target background temperature (background radiation level.) The theoretical limit on specific detectivity is given by the equation:

$$D^*_{Limit} = \left(\frac{\lambda}{2hc}\right)\left[\frac{\eta}{Q_b}\right]^{1/2} \qquad (Cm-Hz/Watt)$$

where:

c = Velocity of Propagation (cm/Sec)

h = Planck's Constant

Q_b = Background Photon Flux (Photons/Sec)

η = Responsive Quantum Efficiency (N.D.)

λ = Wavelength (cm)

The theoretical limits for photovoltaic and photoconductive detectors are plotted versus wavelength in Figure 2.4.8.2 for a detector viewing a hemisphere with a background temperature of 300°K.
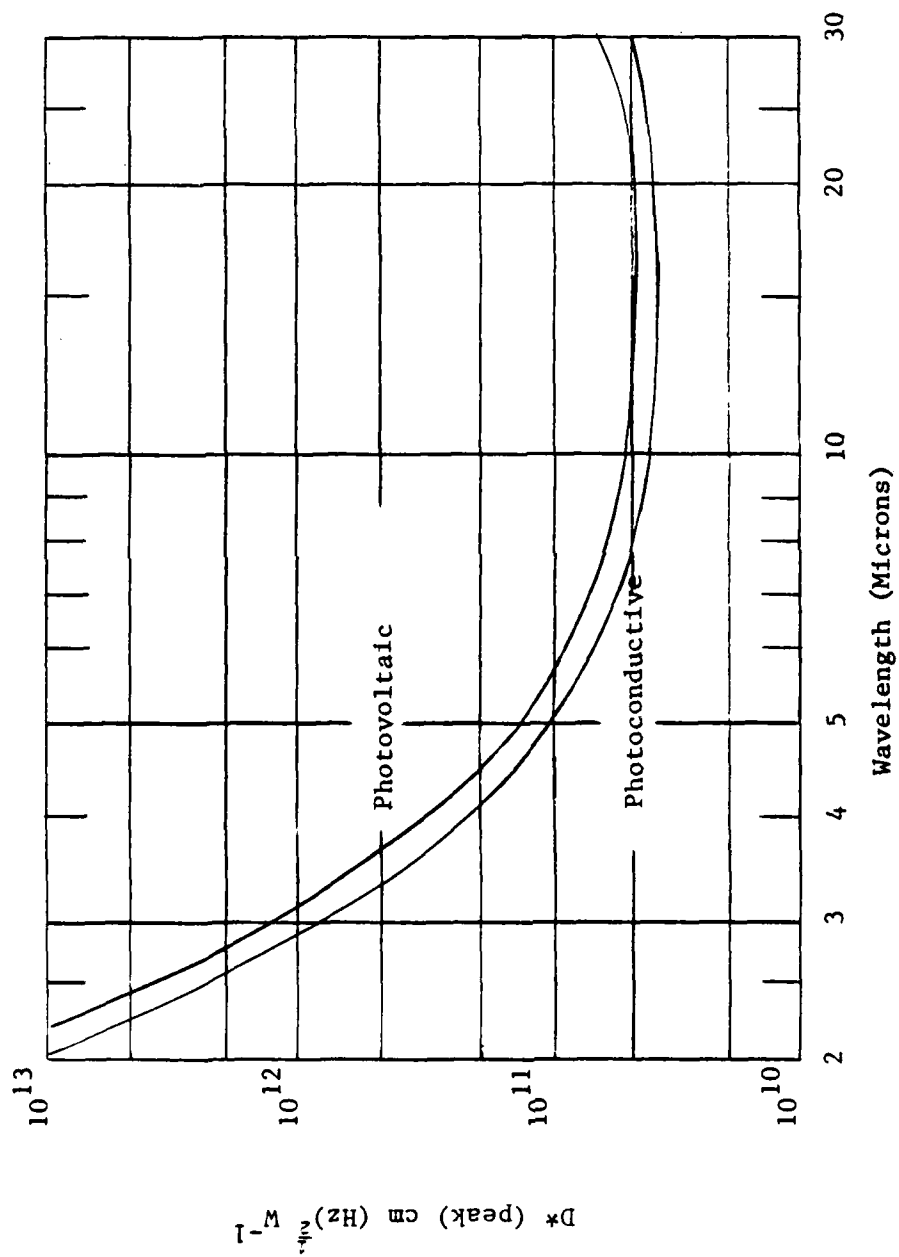
Figure 2.4.8.2 -- Theoretical Limits on Specific Detectivity

2.75a

2.5   The Laser

2.5.1   The Lasing Principle -- The word laser is an acronym for the words:

Light Amplification by Stimulated Emission of Radiation. The laser is based

upon the fact that electromagnetic radiation can interact directly with the

atomic structure of a material in such a way as to result in the absorption

and/or emission of electromagnetic radiation by the material. The structure

of an atom can be represented by the Bohr model as shown in Figure 2.5.1.1(a).

(Refer to Section 2.3.1 of the text on communications for a discussion of the

Bohr model of the atom). The protons and neutrons are assumed to be located in

a nucleus at the center of the atom. The electrons are assumed to orbit about

the nucleus in "shells" as shown in the figure. In actuality, the "shells"

are energy levels as shown in the energy diagram in Figure 2.5.1.1(b). Each

"level" represents a fixed, discrete energy and can be occupied by no more than

a specific number of electrons. An electron can be raised from one energy level

to a higher energy level by absorbing energy from a photon of electromagnetic

radiation. (In a laser, this process is called pumping.) Conversely, it can

fall to a lower energy state by emitting energy in the form of a photon of

electromagnetic radiation. (This process is called radiative decay). Other,

non-radiative processes exist by which the energy level of the electrons can

be changed.) In radiative absorption or decay, the frequency of the radiation

involved is determined entirely by the difference in energy of the two levels

between which the transition occurs. That is:

$$\Delta E = h f \qquad \text{(Joules)}$$

2.76

(b) Energy Diagram

$^2S_{12}$ $^2P_{32}$ $^2D_{52}$

7s
6s
5s

7p
6p
5p
4p

6d
5d
4d

3d

Metastable State

Radiative Decay Transition

Non-Radiative Decay Transition

Ground State

E_3 E_2 E_1

$3p$ $3s$

$4s$

Pumping Transition

Energy

Electron Orbits

Electron

Nucleus

Ground State Orbit

E_3 E_2 E_1
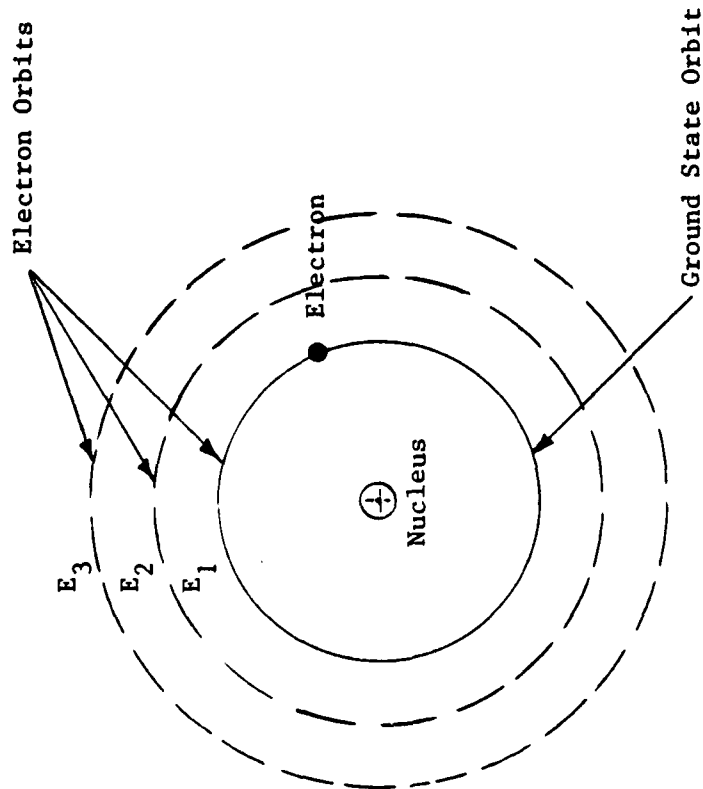
(a) Bohr Model
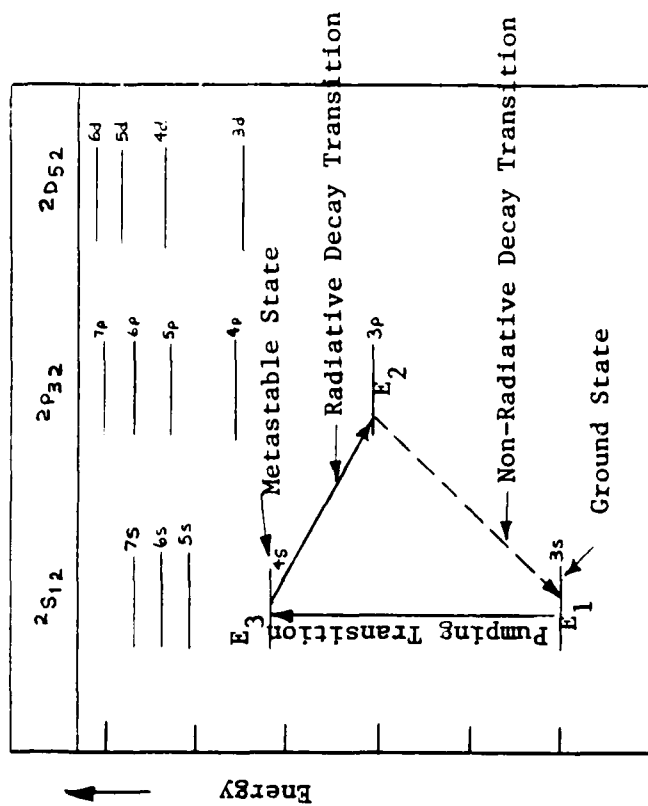
Figure 2.5.1.1 -- Electron Energy Levels in the Atom

where:

>   f = Frequency of Radiation Absorbed or Emitted (Hz)
>
>   h = Planck's Constant = 6.63×10^{-34} (Watts-Sec^2)
>
> ΔE = Difference in Energy between Transition Levels (Joules)

Thus, in Figure 2.5.1.1(b), the "pumping transition" shown requires an energy

input equal to $(E_3 - E_1)$. The "radiative decay transition" shown produces

radiation of a frequency given by the equation:

$$f = \frac{\Delta E}{h} = \frac{E_3 - E_2}{h} \qquad \text{(Hertz)}$$

In a laser, the electrons in the lasing material are raised to higher, metastable

energy states (pumped) by one of several methods to be discussed later. Some

of the electrons in the higher energy levels then fall back to lower energy levels

by emitting a photon of electromagnetic radiation (radiative decay). In order

for the radiant flux contributed by newly-emitted photons to add to that of the

existing photons, (constructive interference), the emitted photons must be coherent

and in phase with the existing photons. Such synchronous emission is achieved in

the laser by passing the previously-emitted radiation through the lasing material.

The electromagnetic fields created by the passing photons encourage the radiative

decay of metastable electrons in a manner that produces photons in phase with the

passing photons. In most implementations, the laser photons are passed repeatedly

through the lasing material, inducing ever-increasing rates of radiative decay,

(increase of flux), on each pass.

2.5.2 The Optical Resonator -- A typical laser implementation is shown in the

schematic drawing of Figure 2.5.2.1. The lasing substance shown in the figure

is a ruby rod pumped by the xenon lamp also shown. Two mirrors M1 and M2, are
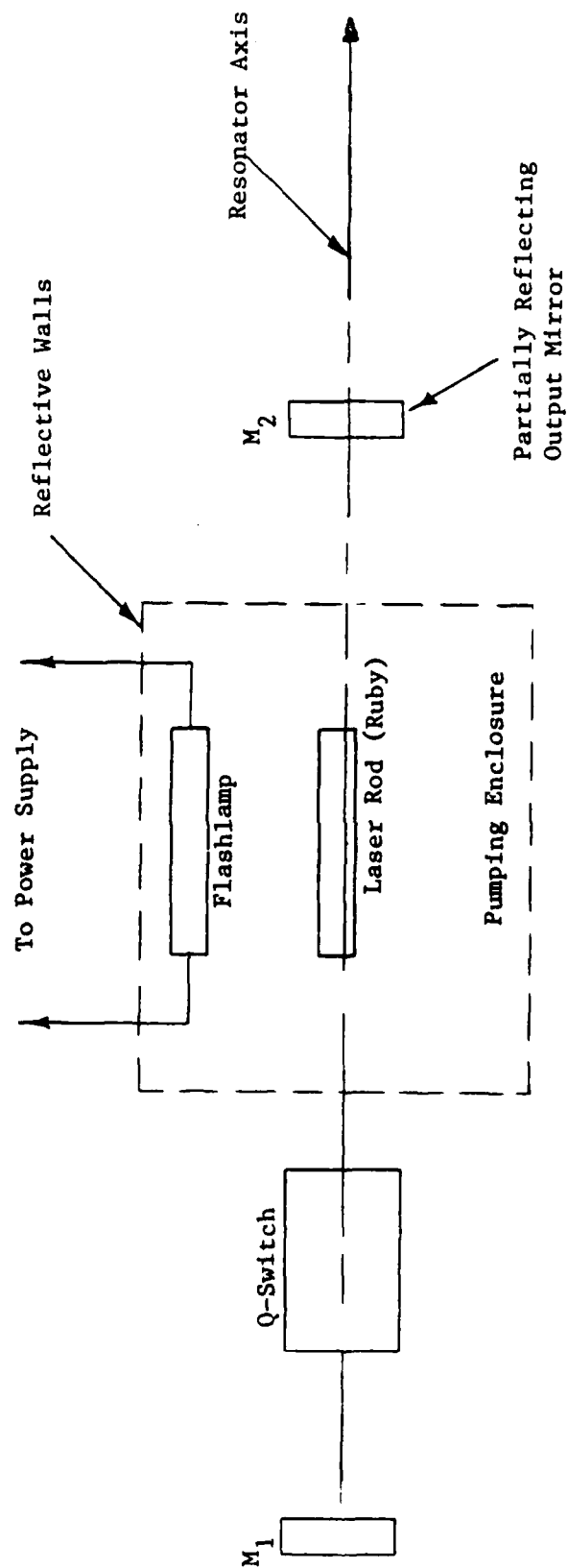
Figure 2.5.1.2 -- The Optical Resonator

2.77a

positioned so as to reflect axially-emitted photons back and forth through the laser rod. This arrangement is called an optical resonator or optical cavity. In order for the reflected photons to induce synchronous emission, the phase of a reflected photon must be the same each time it arrives back at a given point in the lasing material. In order for that condition to exist, the length of the optical cavity (the distance between mirrors M1 and M2) must be equal to an exact multiple of one-half wavelength of the radiation. Because of the very large number of wavelengths between the mirrors in a typical optical resonator, the spacing between cavity resonant frequencies (wavelengths) is very small. For that reason, many of the resonant frequencies of a typical optical cavity will normally fall within the spectral bandwidth of the photons produced by a given radiative decay transition. Therefore, the angular alignment of the mirrors is generally more critical than the distance between the mirrors. A useful output is taken from the optical resonator by using a partially-silvered mirror at one end of the cavity, as shown. Non-axially emitted photons are not reflected directly back and forth along repetitive paths and eventually are lost to the lasing process. The axially-propagated photons pass repeatedly through the ruby rod, their numbers being enhanced by stimulated emission (synchronous radiative decay) on every pass. The positive (regenerative) feed-back created by the lasing process causes the radiant flux in the laser beam to increase rapidly and would quickly deplete the population of electrons in the higher energy states if it were not for the Q-switch shown in the figure. The Q-switch is a device that attenuates the radiant flux in the beam as it passes back and forth through the optical resonator, thereby creating negative (degenerative) feedback. If pulsed operation is desired, the Q-switch is

2.78

alternately opened and closed to its limits. While the switch is closed, thereby blocking the beam, the laser rod is pumped by the xenon lamp. When the Q-switch opens, the lasing process begins. Due to the positive feedback, the radiant flux increases very rapidly until it depletes the upper-energy-level electrons, thereby terminating the pulse. The Q-switch then closes and the pumping process begins again. If continuous operation is desired, the Q-switch is partially opened to a flux level such that the negative feedback due to the Q-switch just balances the positive feedback due to the lasing process. The level of radiant flux can thus be controlled and modulated by means of the Q-switch.

2.5.3 Laser Implementation -- The lasing process has been demonstrated in numerous materials including gasses (xenon, argon, krypton, carbon dioxide, nitrogen, helium-neon, and deuterium fluoride), liquids (rare earth salts and various dyes), non-crystalline solids (neodymium-doped glasses), crystalline solids (ruby, yttrium-aluminum-garnet, and various crystalline substances doped with iron-group and rare-earth salts), and semiconductors (gallium arsenide and silicon). Typical methods of pumping laser materials are optical (radiation), chemical (gasses and liquids), electric discharge (gasses), and electronic (semiconductors). Efforts are currently under way to employ nuclear pumping. Several types of Q-switch are employed. The simplest Q-switch is a rotating mirror used in the optical path of an optical resonator. The optical circuit is completed only periodically, when the mirror reflects the radiation in the required direction. Many resonator designs use a Pockels Cell as a Q-switch. The Pockels Cell consists of a polarizer and an analyzer (two, crossed, polarizing filters) with an electrically-activated

birefringent crystal between them. With no activating voltage on the crystal, no radiation passes through the crossed polaroids. When the birefringent crystal is activated, the plane of polarization of the beam is rotated and radiation is passed. With semiconductor lasers, the "Q" of the optical resonator can be changed by modulating the pumping current, thus eliminating the need for a separate Q-switch. A schematic drawing of a semiconductor laser is shown in Figure 2.5.3.1. The laser radiation is generated only in the immediate vicinity of the p-n junction, as shown. The ends of the semiconductor are polished and act as the reflecting mirrors in a resonant cavity. The beamwidth and bandwidth of a semiconductor laser are generally much wider than those of optically-pumped lasers.

Pumping Current

P-N Junction

p

n

L
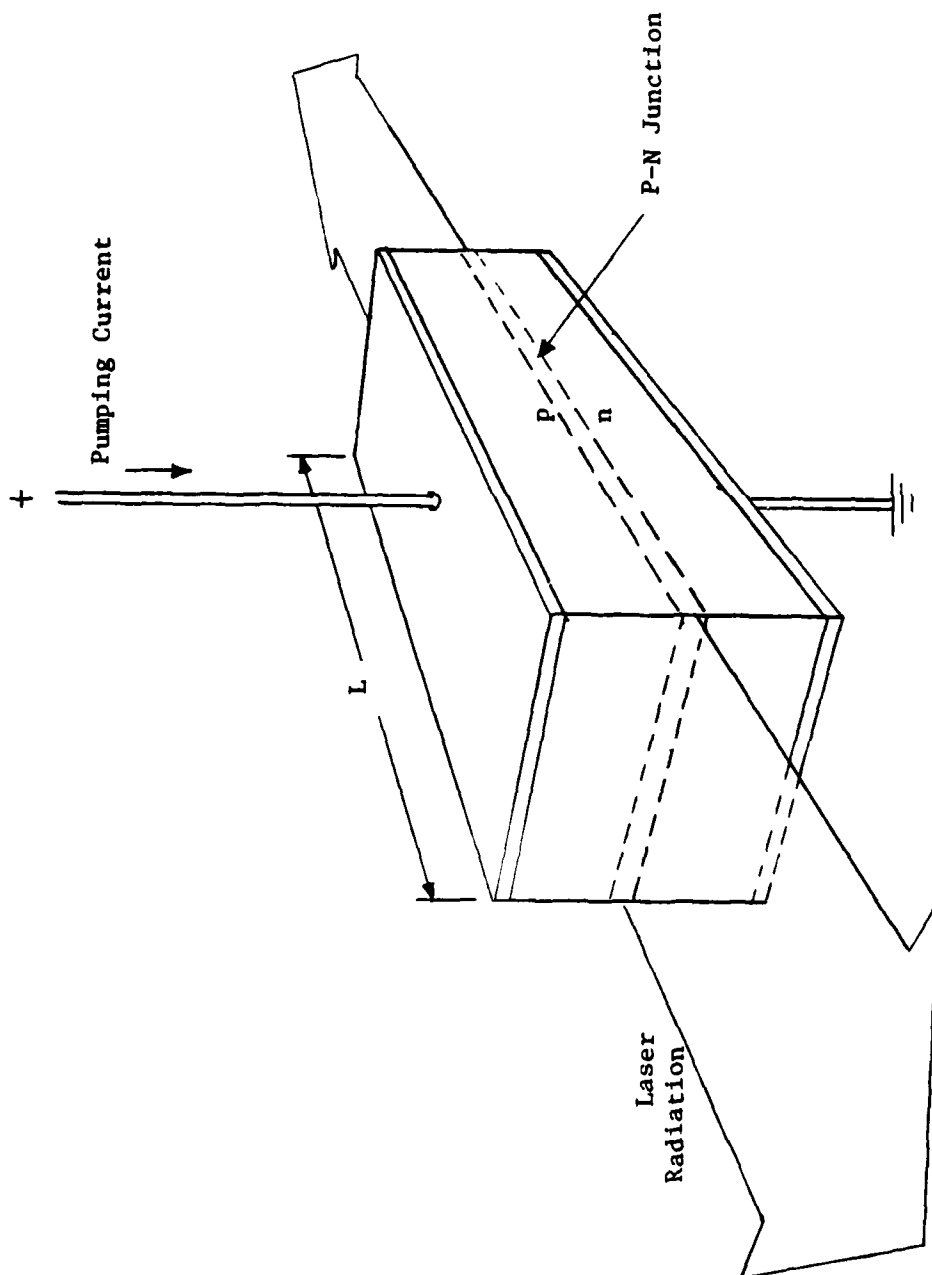
Laser
Radiation

Figure 2.5.3.1 -- The Semiconductor Laser

2.80a

2.5.4 Laser Radiation Characteristics -- Four characteristics of laser radiation are of special significance with respect to airborne systems requirements: temporal coherence, spatial coherence, energy density, and frequency.

Temporal Coherence -- Laser radiation exhibits a high degree of phase correlation in time (temporal coherence). That is, it has narrow bandwidth (is highly monochromatic) and displays excellent frequency (or phase) stability with time. These characteristics are a result of the "stimulated" emissions involved in the lasing process. Temporal coherence allows the use of very narrow-band, (low noise), systems and provides the necessary stability for precise frequency and phase measurements. In addition, it minimizes the effects of chromatic aberrations in an optical system.

Spatial Coherence -- The emissions of a laser are spatially coherent; that is, they exhibit a high degree of phase correlation in space. The emissions at various points in a beam cross-section are, therefore, in phase. Such spatial coherence allows the radiation to be directed into a very narrow (collimated) beam. Narrow (angular) beamwidth provides high directive gain and excellent angular resolution in an optical sensor.

Energy Density -- Lasers are inherently capable of producing very short, high-energy pulses. That characteristic, in combination with the narrow beamwidth discussed above, allows the energy in a laser pulse to be concentrated in both space and time. Such high-energy pulses not only provide a high signal-to-noise ratio in communications applications but make possible the use of a laser as a direct-radiation weapon.

2.81

Frequency -- The frequency of laser radiation is dictated by the energy levels associated with the forces by which electrons are bound to the nuclei of atoms. These energy levels are such that the frequency of laser radiation falls in the range of 10^4 to 10^6 gigahertz. (See Figure 2.5.4.1) The short wavelengths associated with these frequencies (0.3 to 30 micrometers) make optical-frequency systems much less susceptible to diffraction effects than are radio-frequency systems. For that reason, optical sensor systems offer much better target resolution and imaging capability than do RF systems, for hardware (apertures) of the same size. Optical frequencies also provide far greater communication system bandwidth than do radio frequencies.

The characteristics of a number of existing lasers are presented in Figure 2.5.4.2.
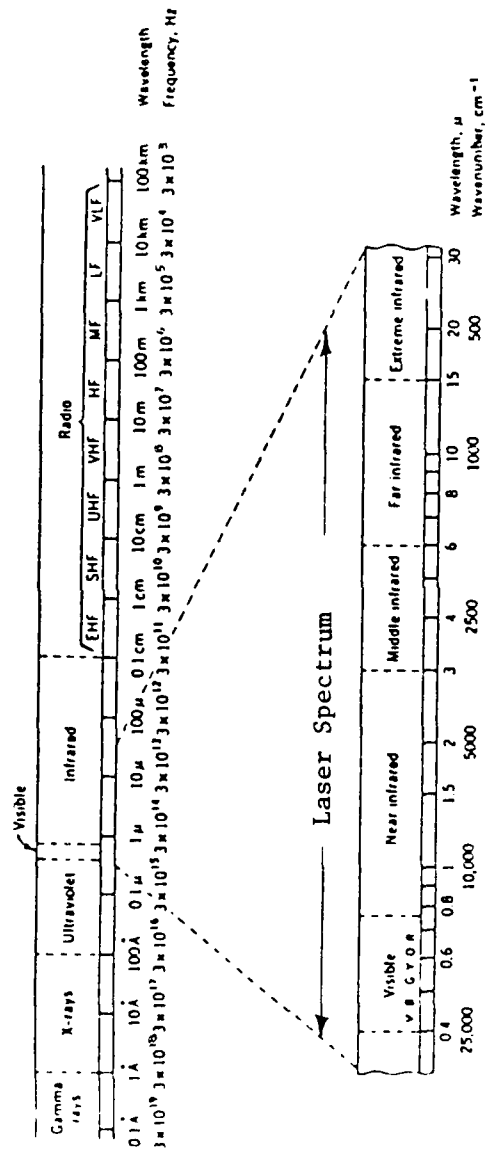
Figure 2.5.4.1 -- Laser Radiation Spectrum

Lasing Material	Pulse Width (Sec)	Peak Output (Watts)	Pulse Energy (Joules)	Efficiency (%)	Wavelength (μ meters)
Nd:Glass	20×10^{-12}	1×10^{11}	2	-	1.06
Nd:YAG	20×10^{-12}	1×10^{2}	2×10^{-9}	-	1.06
Nd:Glass	20×10^{-9}	3×10^{9}	6×10^{1}	-	1.06
Nd:YAG	20×10^{-9}	5×10^{3}	5×10^{-4}	0.2	1.06
GaAs	20×10^{-9}	1×10^{2}	2×10^{-6}	10	0.90
Ruby	20×10^{-9}	1×10^{9}	2×10^{1}	-	0.69
Dye	20×10^{-9}	2×10^{6}	4×10^{-2}	0.4	0.50 (Tunable)
Nd:Glass	1×10^{-3}	1×10^{6}	1×10^{3}	1	1.06
Ruby	1×10^{-3}	4×10^{5}	4×10^{2}	1	0.69
YAG	Cont.	1×10^{2}	-	3	1.06
GaAs	Cont.	1×10^{0}	-	20	0.84
CO_2	Cont.	1×10^{3}	-	20	10.6
He/Ne	Cont.	5×10^{-2}	-	.05	0.63

Figure 2.5.4.2 -- Laser Characteristics

2.6 Electro-Optical Sensors

2.6.1 Generalized E/O System -- The block diagram of a generalized electro-optical system is shown in Figure 2.6.1.1. As indicated in the figure, an E/O system can include both active (transmitting) and passive (receiving) sub-systems. Active devices include both coherent (laser) and non-coherent illuminators. (Laser systems are discussed in Section 2.5 of this text). The receiving portion of an E/O system can be one of two types: a point-source sensor or an imaging sensor. (Various point-source-detecting and imaging sensors are described in Section 2.6.2 of this text). Both types of sensor process and detect optical-frequency electromagnetic radiation, process the detector output signal, and provide an indication or display. A point source sensor senses the total radiant flux within its instantaneous field-of-view and indicates the intensity of the radiation sensed. An imaging sensor pro-duces an image of the radiant flux distribution within its overall field-of-view. As indicated in Figure 2.6.1.1, the sensor output can be employed to track a target automatically. Also depicted in the figure is the common practice of bore-sighting an optical system with other devices such as radar antennas, visual sights, and weapon delivery systems.

Figure 2.6.1.1 -- Generalized Electro-Optical System

2.6.2 Types of Electro-Optical Sensors -- Electro-optical sensors can be categorized according to the method of scanning employed. In the following paragraphs, the various methods of scanning are defined and examples of the application of each method are presented.

Point-Source Sensors -- As previously indicated, a point-source sensor senses the total radiant flux within its instantaneous field-of-view. An example of a non-imaging point-source sensor is the ALR-21 air-to-air missile launch warning sensor shown in Figure 2.6.2.1. The radiant flux within a 30° field-of-view is filtered and focused upon a point-source detector, thereby indicating a radiation source within that field-of-view.
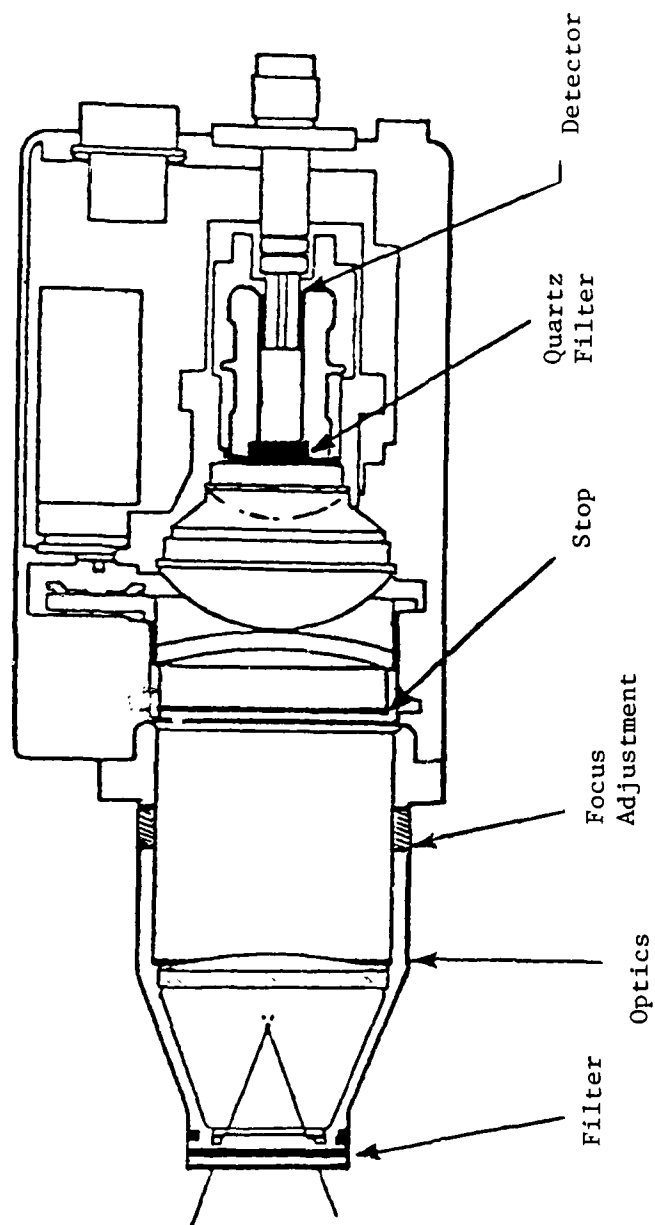
Figure 2.6.2.1 -- AN/ALR-21 Point Source Sensor Head

Detector

Quartz
Filter

Stop

Focus
Adjustment

Optics

Filter

Non-Scanned Imaging Sensors -- A non-scanned imaging sensor simultaneously forms an image of the radiation pattern within its field-of-view. An example of such a sensor is the photographic camera shown in Figure 2.6.2.2. The radiant flux is focused upon a photosensitive film within which a photoelectric process occurs, thereby causing visible particles to be deposited, upon development of the film, in proportion to the radiant energy absorbed. The result is a visible image of the radiation pattern within the field-of-view. Currently available photosensitive materials respond to radiation of wavelengths up to about 1.3 micrometers.

Another example of a non-scanned imaging sensor is the phosphor-screen image converter shown in Figure 2.6.2.3. Infrared radiation from the object, O, is focused on an internal phosphor screen to form the image I_1. The radiant energy absorbed by the phosphor screen is re-emitted at visible wavelengths, thereby producing a visible image which is viewed through the eyepiece or re-focused at I_2 for further processing. The phosphor screen is generally "activated" by radiation from an internal radiative source. Suitable phosphors, which include zinc sulfide, respond to radiation wavelengths up to about 2 micrometers.

Intensification of the image in an image converter can be achieved by the arrangement shown in Figure 2.6.2.4. This arrangement, known as an image converter/intensifier, converts the electromagnetic radiation pattern into a pattern consisting of electrons. Energy is added to the electron stream, to intensify the image, and the electron stream is then re-converted to electromagnetic radiant energy. This process is performed by focusing the input radiation from the target
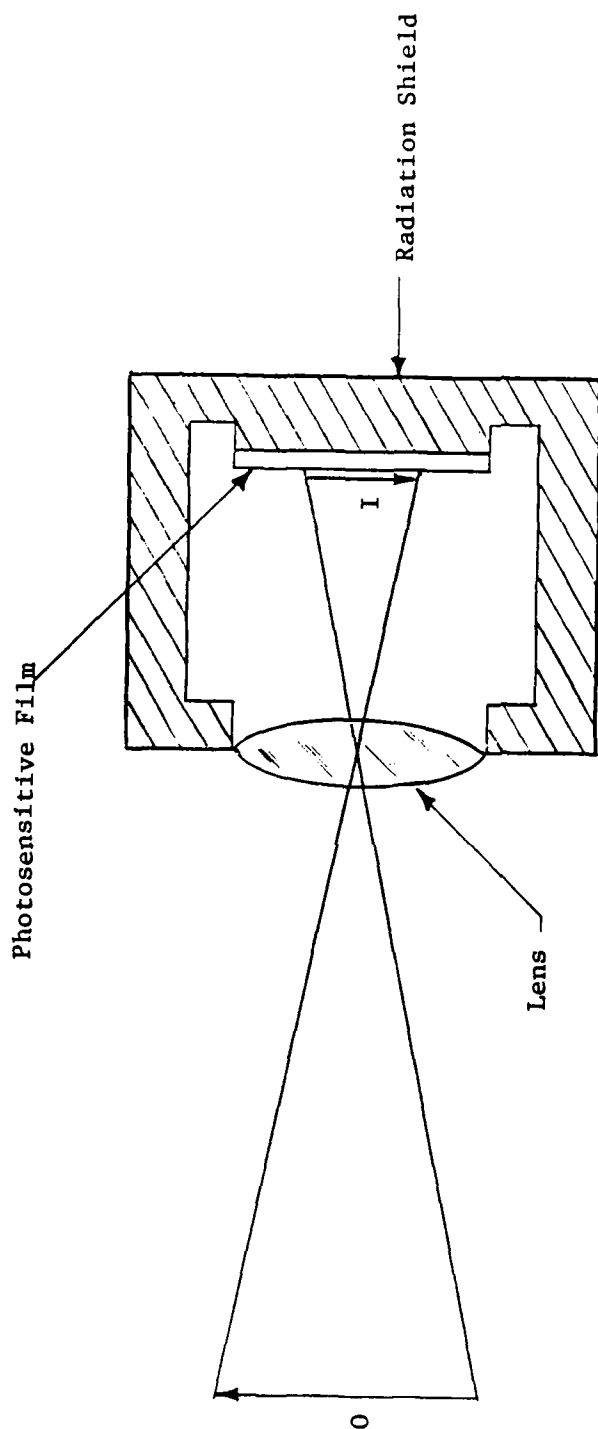
Figure 2.6.2.2 -- Photographic Camera

Radiation Shield

Photosensitive Film

Lens

I

O

2.85a
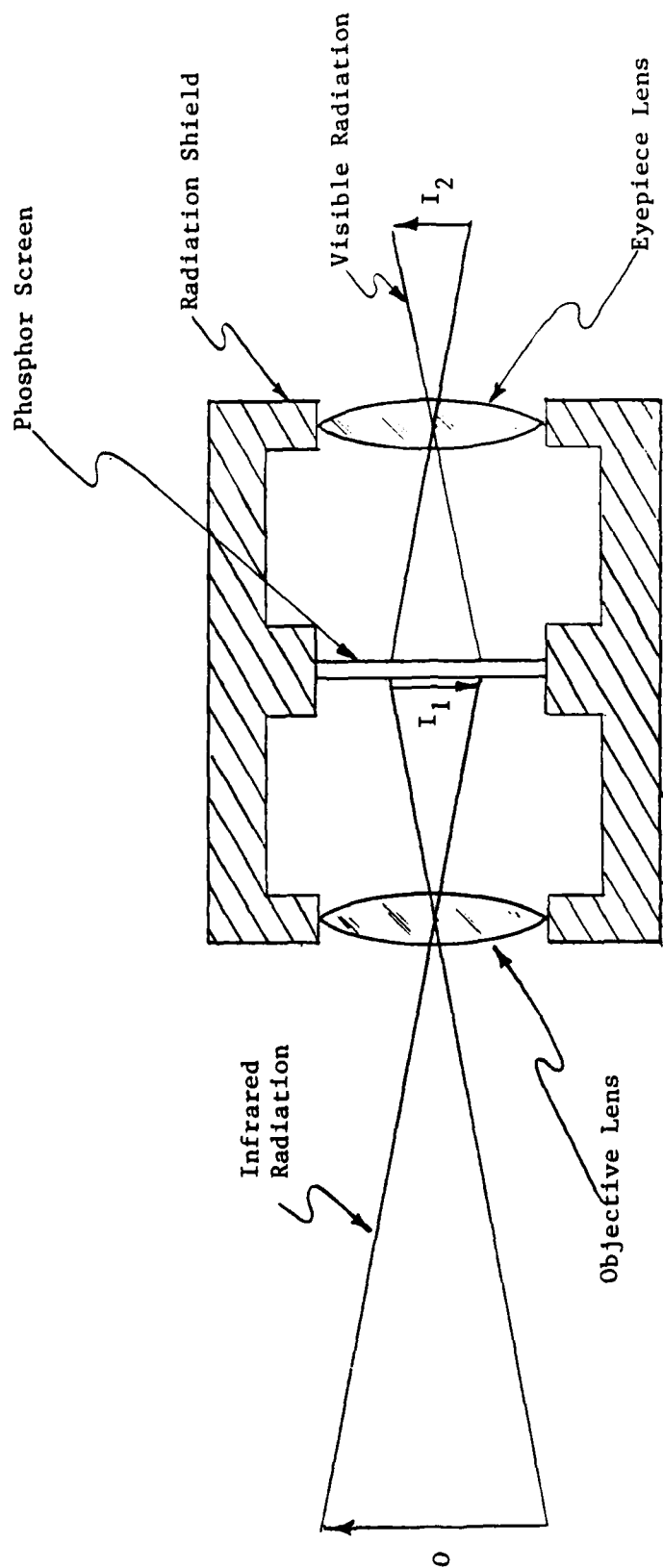
Figure 2.6.2.3 -- The Image Converter

2.85b
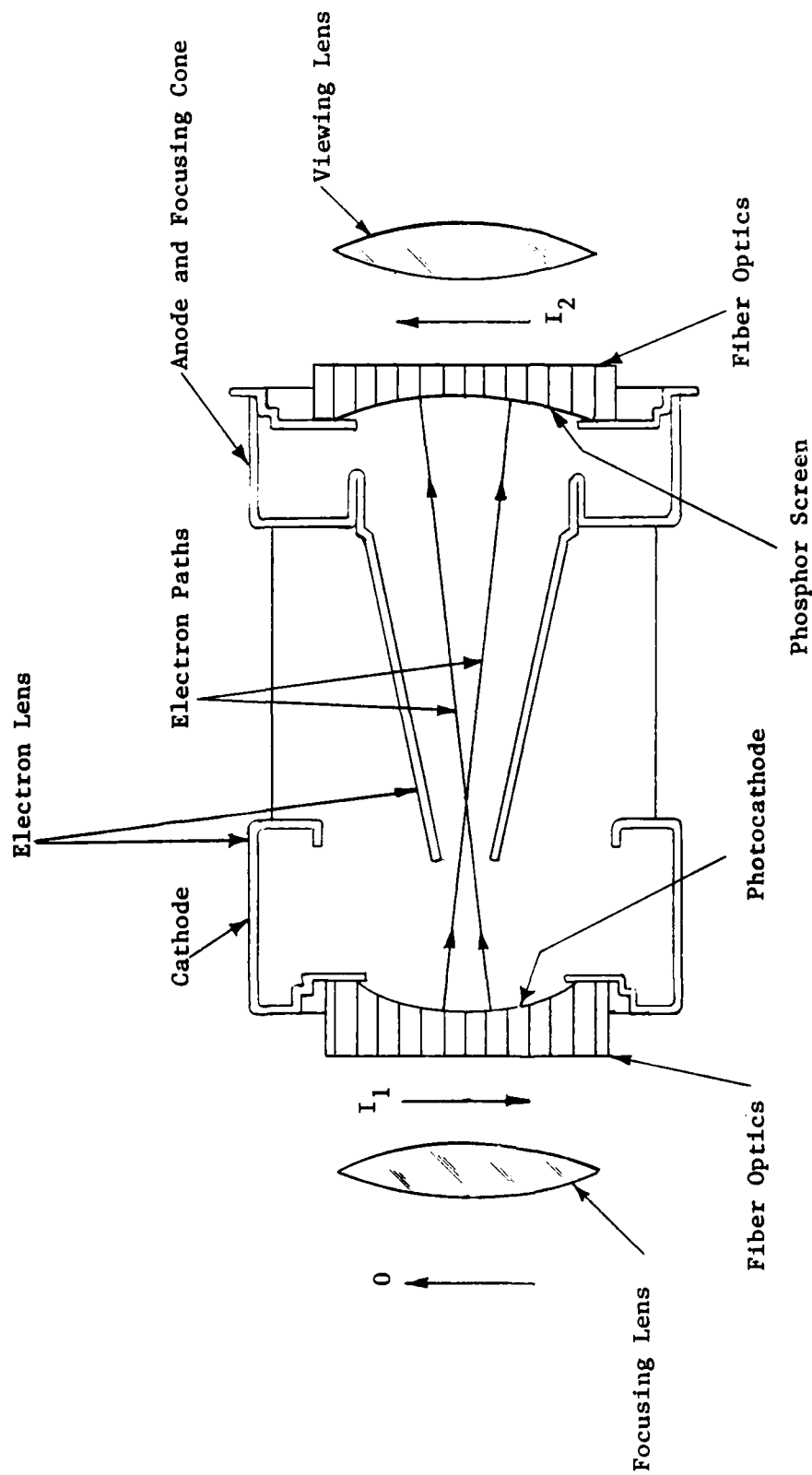
Figure 2.6.2.4 -- The Image Converter/Intensifier

2.85c

(object) onto a photocathode. The photoelectrons emitted by the photocathode are focused and accelerated toward the phosphor screen by the electron lens structure shown in the figure. The photoelectrons impinging upon the phosphor screen produce an image in the form of electromatic radiation which is then viewed through an eyepiece or further processed optically. The fiber optic plates shown in the figure are employed to interface between the planar-image electromagnetic radiation optics and the spherical-image electron optics. The photoemissive materials employed in photocathodes respond to radiation wavelengths up to about 2 micrometers. Image intensifiers can be used in tandem, as shown in Figure 2.6.2.5, to achieve more image intensification than possible with a single stage. As previously indicated, an image intensifier converts the radiant image into a stream of electrons in order to employ electronic techniques for amplification. The conversion allows the application of other electronic techniques as well. One such technique, illustrated in Figure 2.6.2.6, is the use of magnetic deflection coils to deflect the electron stream in such a way as to compensate for inadvertent motion of the sensor, thus stabilizing the image against such motion. Sensor motion (line-of-sight jitter) is a major problem in airborne sensors. The schematic drawing of a typical telescope/image converter/intensifier combination (infrared scope or starlight scope) is shown in Figure 2.6.2.7.
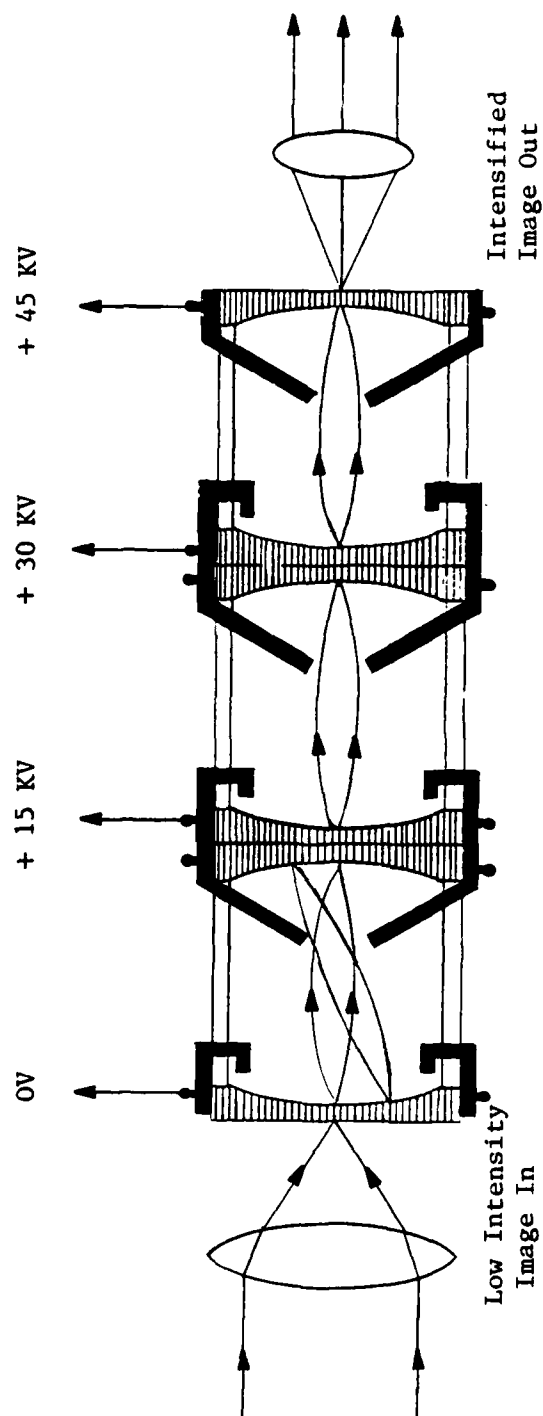
Figure 2.6.2.5 -- Multi-Stage Image Intensifier

+ 45 KV   + 30 KV   + 15 KV   0V

Intensified
Image Out

Low Intensity
Image In
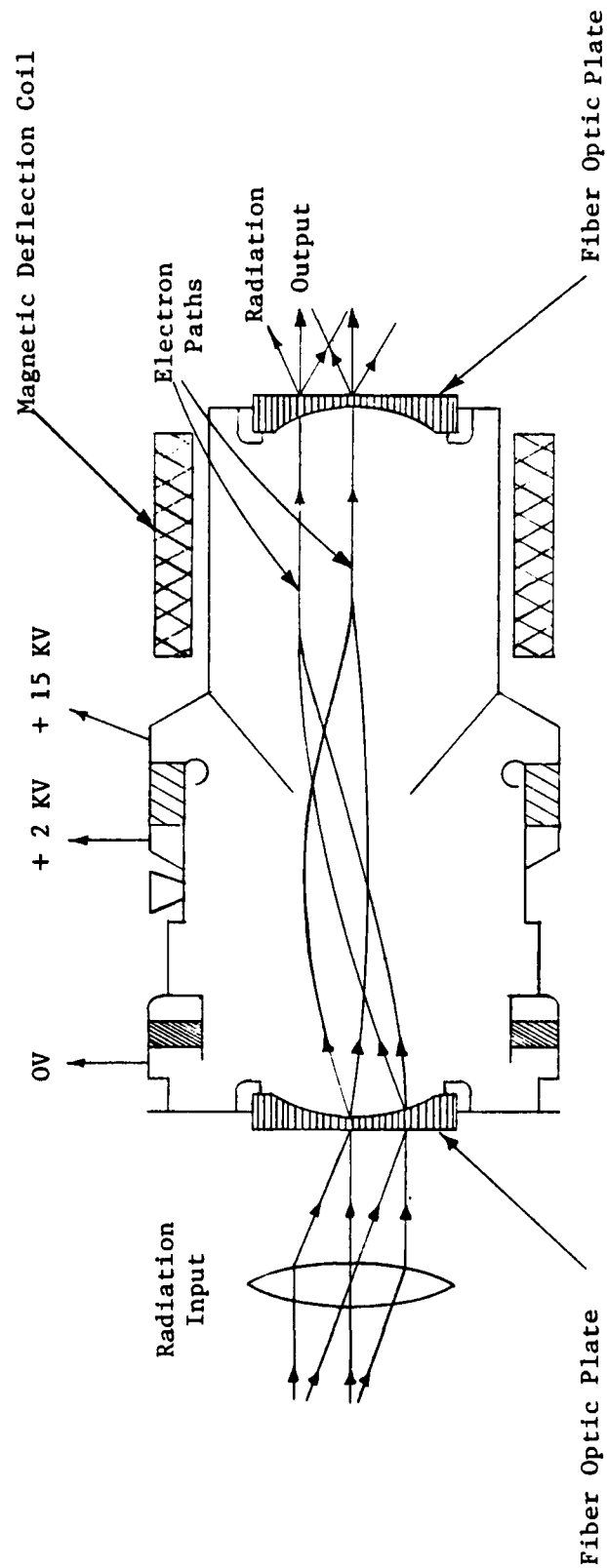
Figure 2.6.2.6 — Stabilization of Image by Magnetic Deflection Coils

2.86b
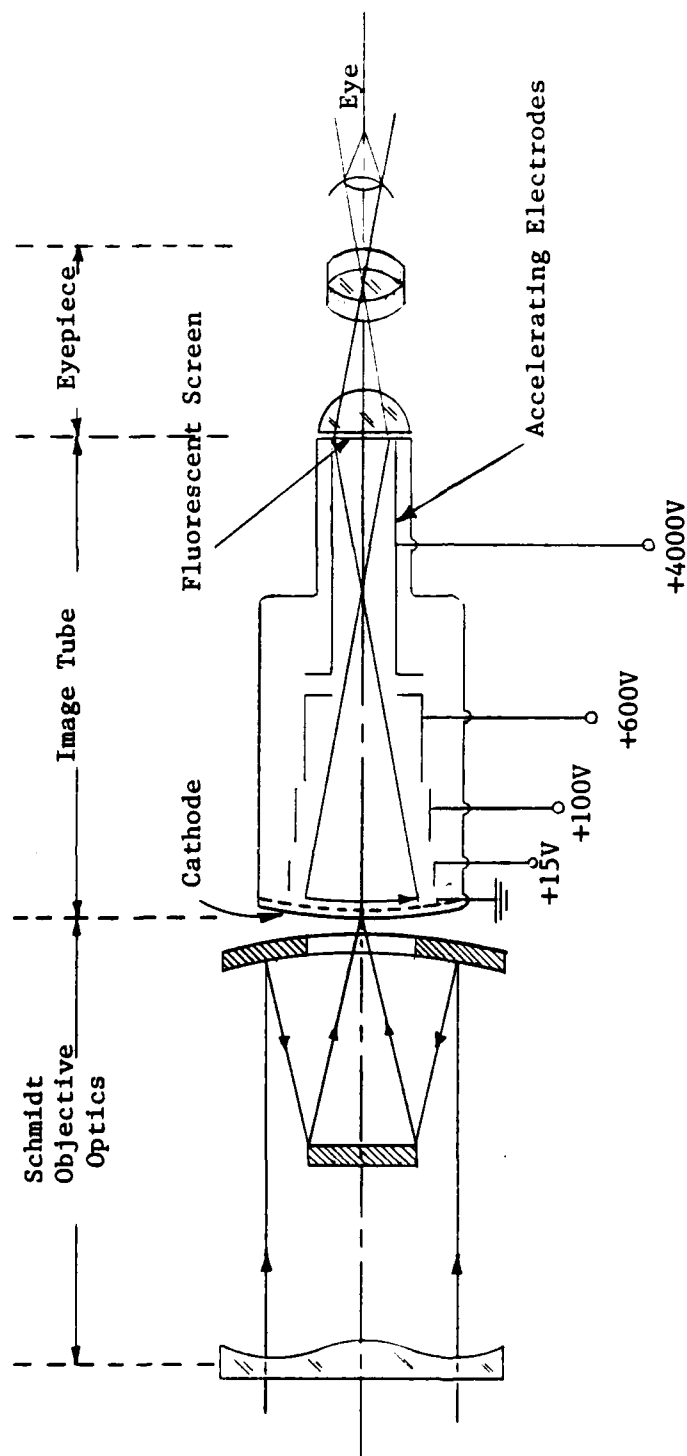
Figure 2.6.2.7 -- Telescopic Image Converter/Intensifier

Eye

Accelerating Electrodes

Eyepiece

Fluorescent Screen

+4000V

Image Tube

+600V

+100V

Cathode

+15V

Schmidt
Objective
Optics

Electron-Beam-Scanned Imaging Sensors -- Electron-beam-scanned imaging sensors
scan the overall field-of-view by deflecting an internal electron beam. One
such device, the vidicon television camera tube, is shown in Figure 2.6.2.8.
In the vidicon, the incoming   radiation is focused onto an internal screen
composed of photoconductive material. An image is thus formed on the screen
consisting of areas of greater and lesser conductivity, the conductivity of
the screen being more or less proportional to the irradiance of the screen at
that point. A narrow beam of electrons is deflected in such a way as to scan
the back of the photoconductive screen as shown in the figure. When the electron
beam impinges upon an irradiated area of the screen, the electrons are conducted
through the screen to a transparent, conductive signal plate and into an ex-
ternal circuit, as shown in Figure 2.6.2.8. The resulting current in the ex-
ternal circuit constitutes the output signal from the sensor. Beam electrons
not conducted through the photoconductive screen are collected by a grid (mesh),
also shown in the figure. Suitable photoconductive materials are available
which respond to radiation up to about 13 micrometers in wavelength. An electron-
multiplying target screen can be employed in a vidicon to increase the output
of the sensor. A camera tube employing such a device, called an SEC (secondary
electron conduction) vidicon, is illustrated in Figure 2.6.2.9. In an SEC
vidicon, a photoemissive screen is irradiated by the incoming radiation, thus
producing an photoelectron stream "image" as in the image converter/intensifier.
The photoelectrons are accelerated toward and focused upon an internal screen,
called the "target". When the accelerated electrons strike the target, electrons
within the target are ejected, (due to secondary emission), thereby leaving areas
deficient in electrons on the target screen. The target screen is then scanned
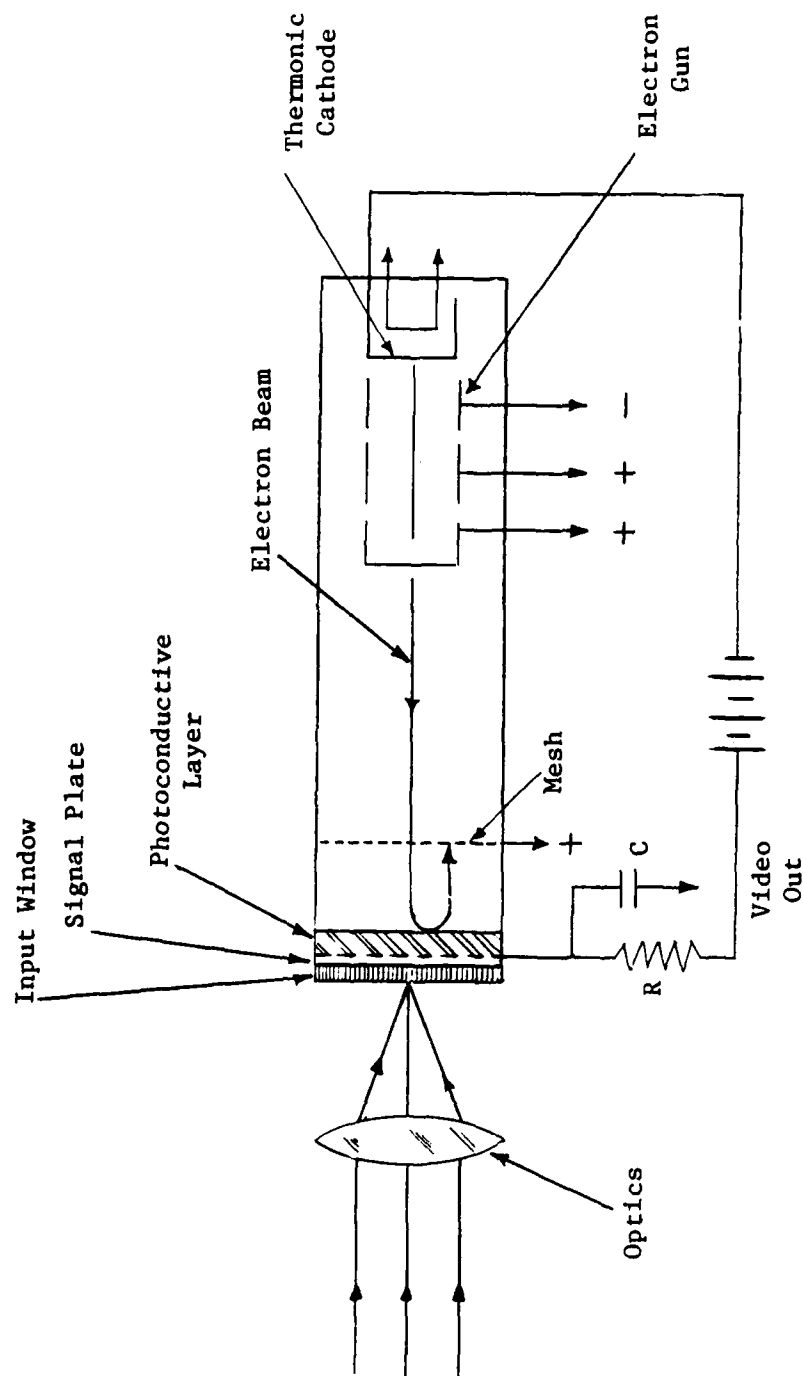
Figure 2.6.2.8 -- The Vidicon Television Camera Tube

2.87a
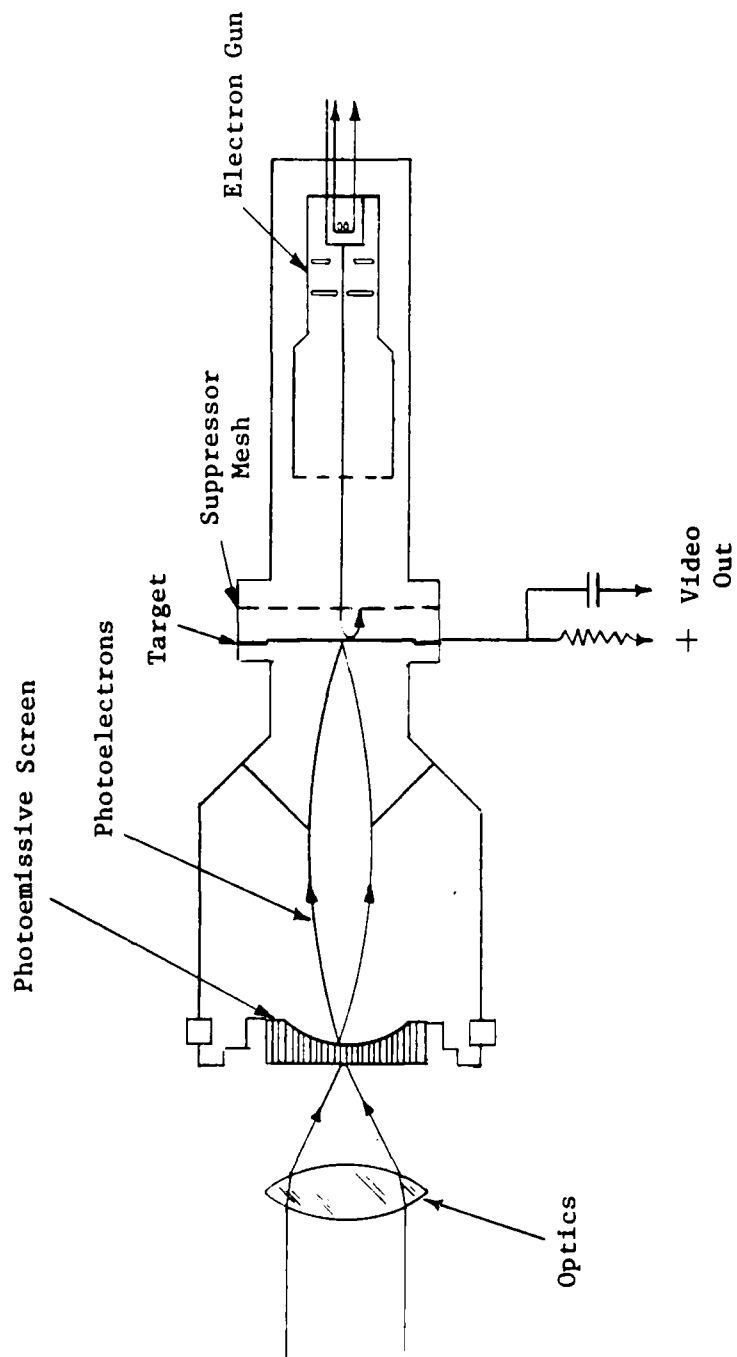
Figure 2.6.2.9 -- The SEC Vidicon Television Camera Tube

from behind by a narrow electron beam. When the electron beam impinges upon

an area of the screen deficient in electrons, electrons from the beam flow

into the target and out into the external circuit, thus producing an output

signal.

Another type of electron-beam-scanned TV camera tube is the image orthicon

shown in Figure 2.6.2.10. In an image orthicon, the incoming radiation is

focused upon a photocathode, thus producing an electron-cloud "image" of the

field-of-view. These photoelectrons are accelerated toward a target screen

as shown in the figure. The accelerated electrons strike the target screen

producing secondary emission as shown in the target detail drawing and leaving

areas of the screen deficient in electrons. The screen is then scanned from

behind by a narrow beam of electrons. Where the scanning beam impinges upon

an electron-deficient area of the target screen, the beam loses electrons to

the screen. The electrons remaining in the beam (not absorbed by the target)

constitute the output signal and are returned to an electron multiplier in

the base of the camera tube. The electron multiplier, a device which amplifies

current by cascading secondary emission, greatly increases the output current.

The image orthicon is, therefore, much more sensitive than a vidicon.

The image dissector television camera tube shown in Figure 2.6.2.11 can be con-

sidered an electron-beam-scanned imaging sensor. However, instead of scanning

an irradiated target screen with a narrow electron beam, the image dissector

uses magnetic deflection coils to scan the entire electron "image" across a

point source detector. The process is accomplished as follows. The incoming

radiation from the target is focused upon a photocathode (photoemissive screen).

The resulting photoelectrons are accelerated and focused upon an "imaging"
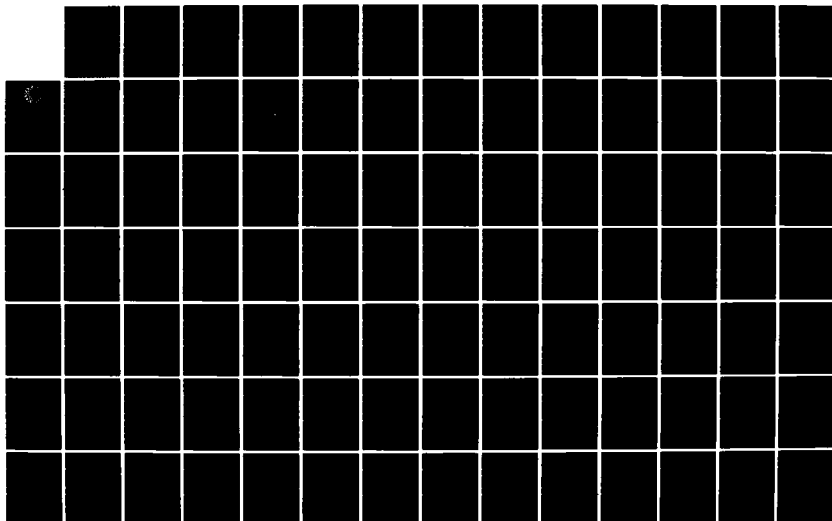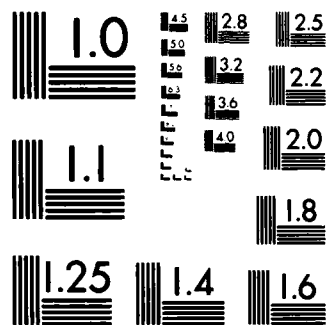
MICROCOPY RESOLUTION TEST CHART

NATIONAL BUREAU OF STANDARDS-1963-A
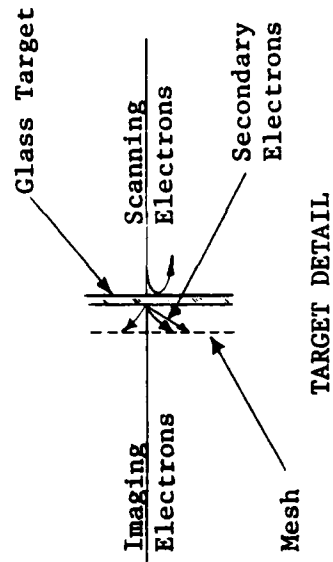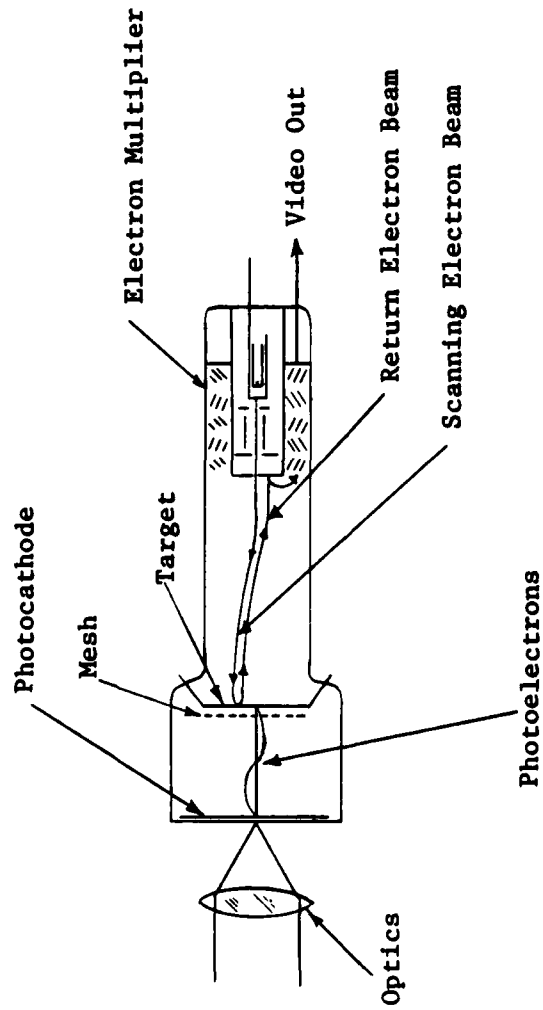
Figure 2.6.2.10 -- The Image Orthicon Television Camera Tube

2.88a
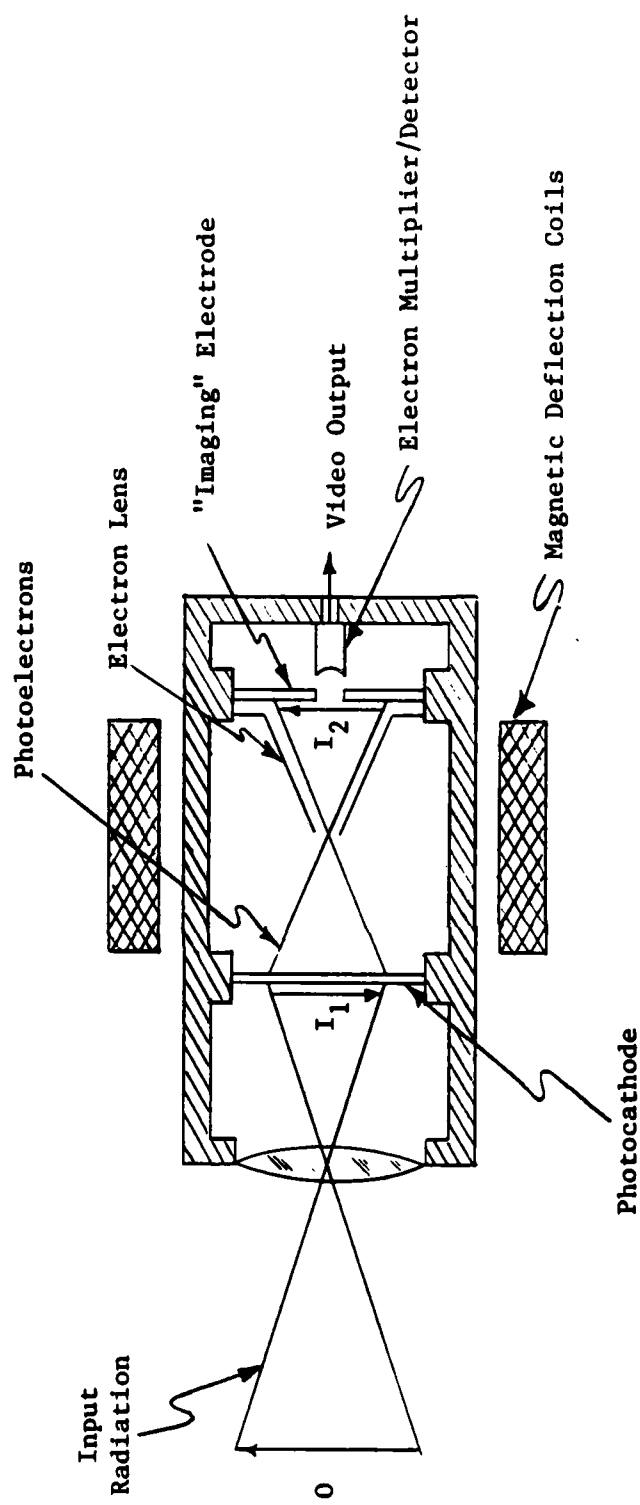
Figure 2.6.2.11 -- The Image Dissector Television Camera Tube

electrode (anode) as shown in the figure. In the center of the imaging

electrode is an aperture behind which is positioned a point-source detector.

In order to scan the field-of-view, magnetic deflection coils are used to

deflect the entire photoelectron stream (image) across the aperture in the

imaging electrode. The advantage of the image dissector over the vidicon

and image orthicon is the greater resolution afforded by a point-source

detector.

Electronically-Scanned Imaging Sensors -- Electronically-scanned imaging sensors scan the sensor field-of-view by utilizing a two-dimensional array of point-source radiation detectors and serially sampling their outputs electronically. The solid-state television camera "tube" shown in Figure 2.6.2.12 is an example of an electronically-scanned imaging sensor. The incoming radiation from the target is focused upon a two-dimensional array of semiconductor photodiodes. (Such an array may contain more than 65,000 (256 x 256) individual photodiodes.) The outputs of the photodiodes, representing the two-dimensional radiation pattern within the sensor field-of-view, are sampled by a time-multiplexer as shown in the figure. An m-by-n array of photodiodes can be sampled by energizing one of m excitation lines, as shown in the array detail drawing, and taking the output from one of n output lines. Note that, in this type of sensor, no electron beams are involved.

Output Lines

Excitation Lines
Photodiode Array Detail

Scanned
Output

Photodiode Matrix

Photodiode Outputs

Electronic
Scanner
(Multiplexer)

Excitation Lines

I

O

2.90a
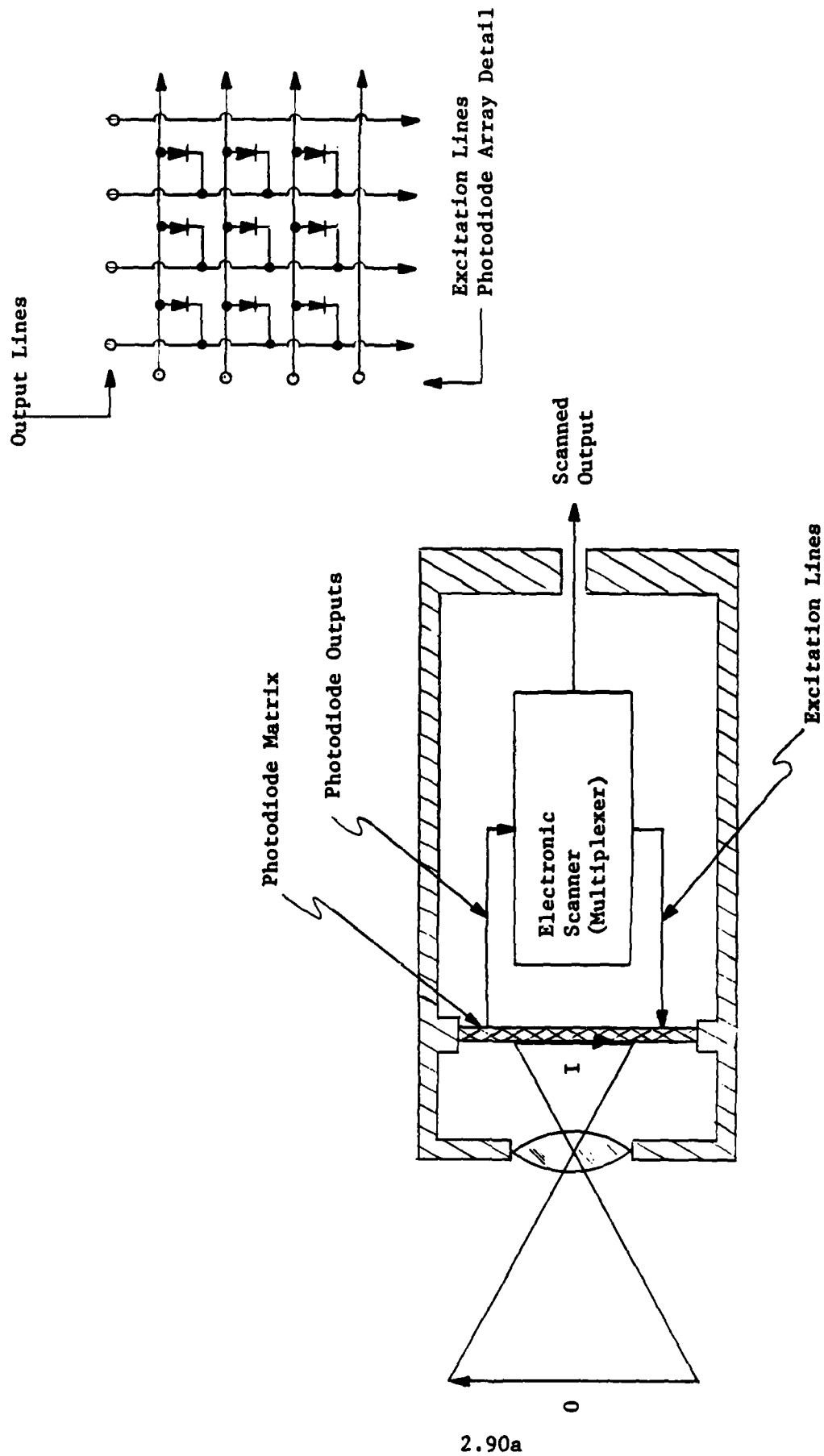
Figure 2.6.2.12 -- The Solid-State, Electronically Scanned Television Camera Sensor

Optically-Scanned Imaging Sensors -- Optically-scanned imaging sensors employ point-source radiation detectors and scan the field-of-view by deflecting the incoming radiation or by moving the radiation detector elements. The scanning motion can be effected by moving components in the optical system, moving the detectors only, or moving the entire sensor. Scanning of the two-dimensional field-of-view can be performed by scanning a point-source detector in two dimensions or by scanning a lineal array (line) of detectors in a single dimension. An example of the latter (one-dimensional scanning of a linear detector array) is the airborne I/R ground mapping arrangement shown in Figure 2.6.2.13. The lineal array of detectors is mounted on the underside of an aircraft so as to view a narrow strip of ground transverse to the ground track. Thus, the forward motion of the aircraft provides the required one-dimensional scanning motion for the sensor, the detectors viewing a "swath" of terrain parallel to the ground track. The individual outputs of the detectors are amplified and used to drive light-emitting diodes mounted in a lineal array similar to that of the detectors. Photosensitive film is transported past the LED array in a direction transverse to the array thus irradiating a "swath" of film and reproducing the ground I/R radiation pattern viewed by the detector array. In order to reproduce the radiation pattern without distortion, the rate at which the film is transported past the LED array must be proportional to the ground speed of the aircraft. The need for synchronization between sensor field-of-view scanning and display implementation is common to all scanned imaging sensors and is shown explicitly in the figure.

A two-dimensional scanning mechanism for an airborne ground mapper is shown in Figure 2.6.2.14. With such a mechanism, a single detector element is used,

2.91
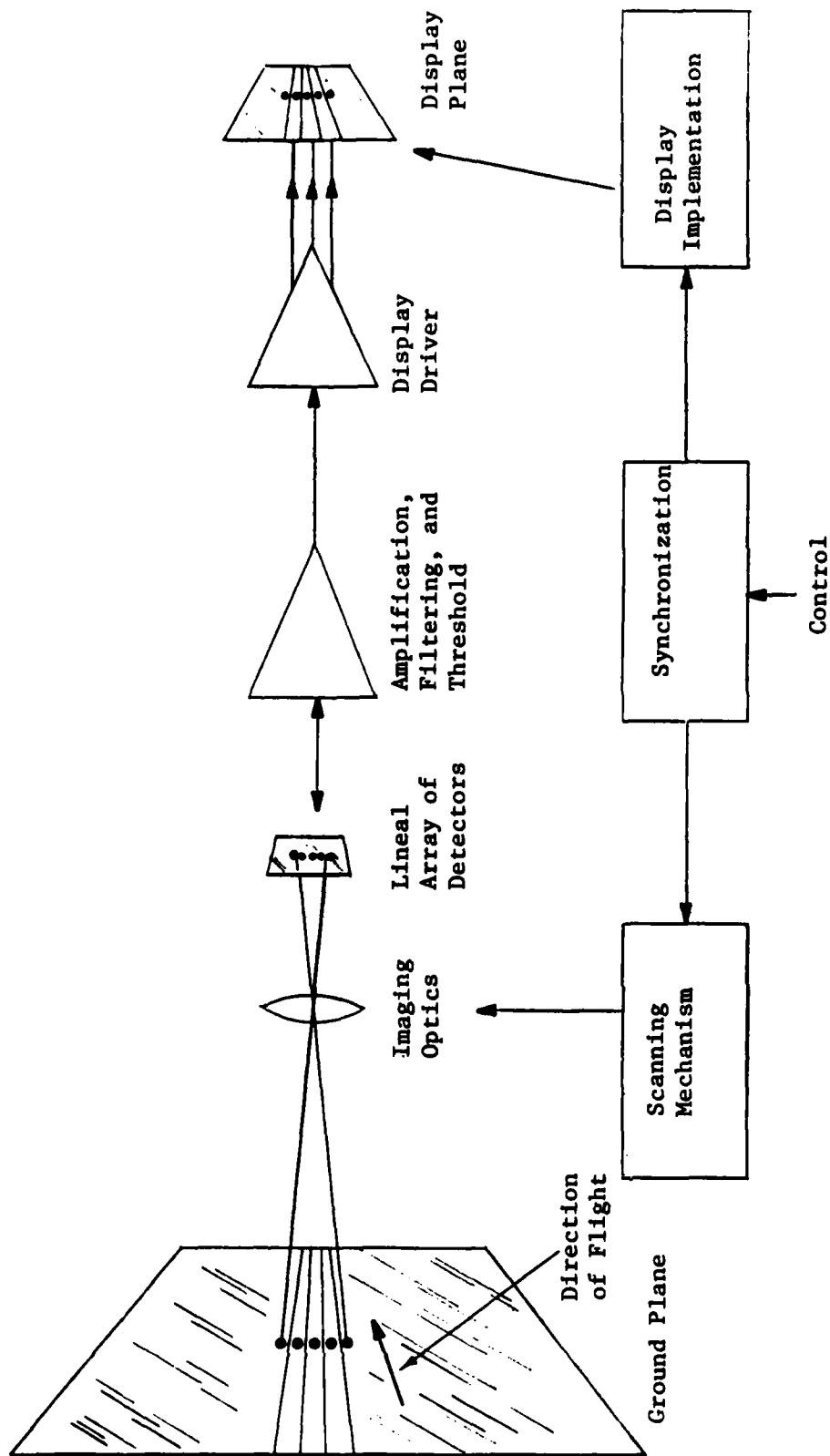
Figure 2.6.2.13 -- One-Dimensionally Scanned Ground Mapper

2.91a

Infra-Red Detector

Field Lens

Scanning Mirror

Optical Axis

Elemental Area

Ground Strip

Direction of Flight
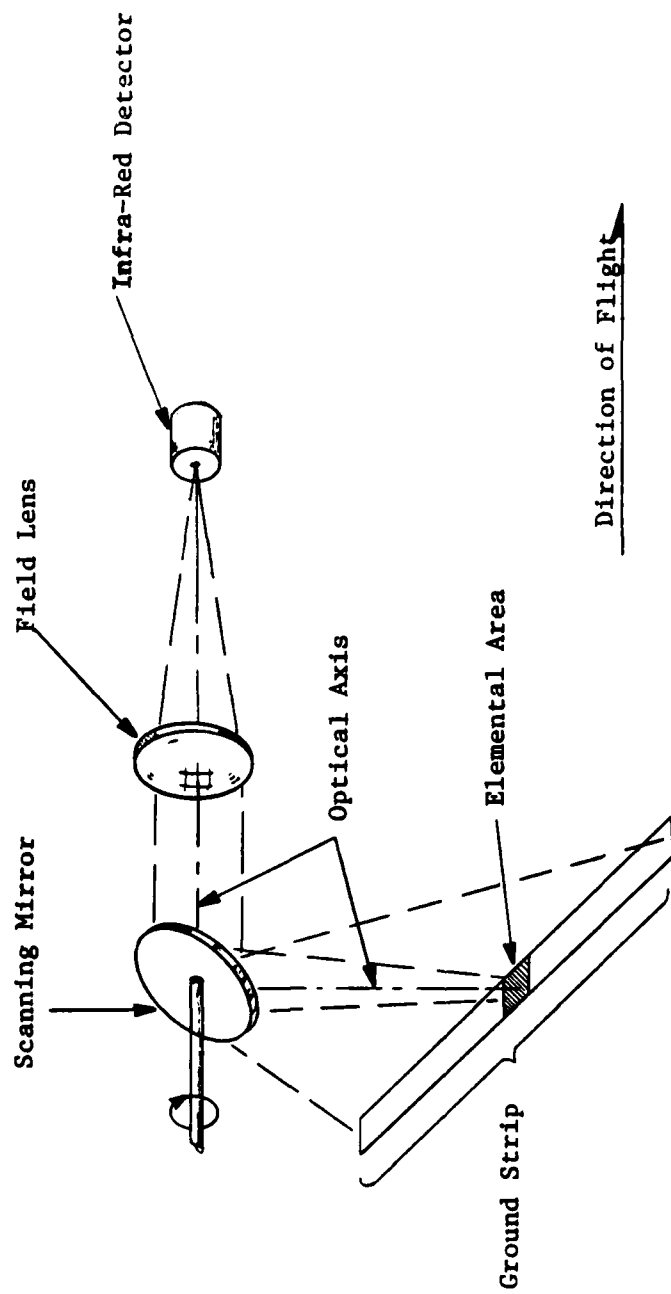
Figure 2.6.2.14 -- Two-Dimensionally-Scanned Ground Mapper

the cross-track scanning being provided by the rotating mirror. Along-track scanning is provided by the motion of the aircraft. Unless measures are taken to remove distortion in this type of system, distortion will be present due to geometry (for large angles off the vertical) and due to lateral motion (drift) of the aircraft.

A modern airborne forward-looking infrared sensor (FLIR) is shown in Figure 2.6.2.15. In this system, a one-dimensional scan is effected by rotating a conical array of planar mirrors about the conical axis. The rotating mirrors, in conjunction with a lineal array of detector elements, provide two-dimensional coverage of the sensor field-of-view. The outputs of the detectors are used to drive a lineal array of light-emitting diodes which is scanned by another conical array of planar mirrors mounted cn the same shaft as that scanning the detectors. Thus, synchronous de-scan (for display) is ensured. In this system, the de-scanned output is not viewed directly. Instead, the de-scanned LED outputs are viewed by a TV camera, the purpose of which is scan conversion. The scan conversion is necessary to put the sensor output in a format suitable for display on a cathode-ray tube.
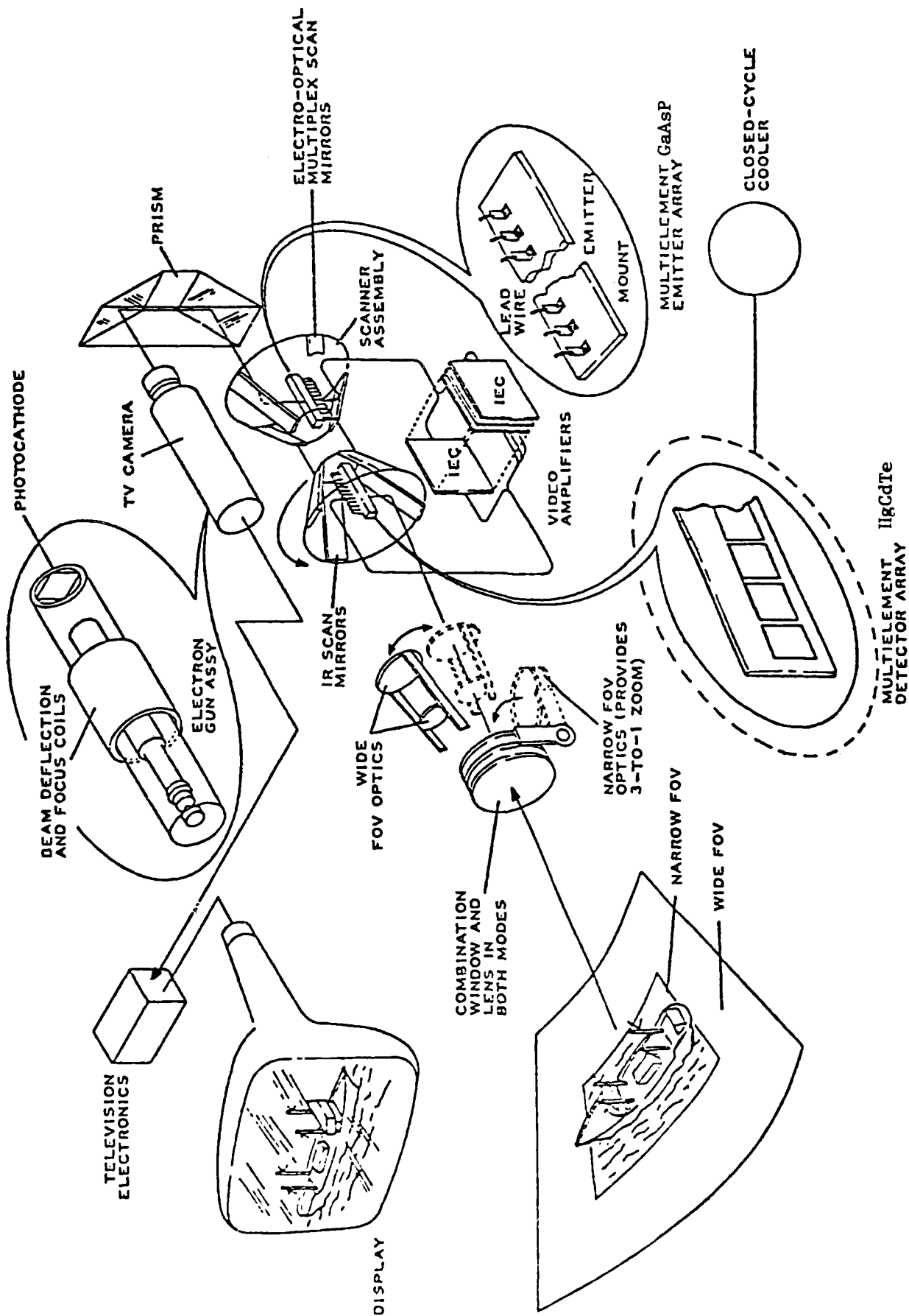
Figure 2.6.2.15 -- Airborne Forward-Looking Infrared Sensor

2.92a

2.6.3 Electro-Optical Target Tracking Systems -- An electro-optical target

tracking sensor conforms to the general principles discussed in Section 2.17 of

the text on radar systems. The reader is, therefore, referred to that text for

a general discussion of the principles of closed-loop tracking sensors. The

material in this section will be confined to a description of a typical infrared

target-tracking system -- that employed in the Sidewinder air-to-air guided

missile.

A block diagram for a missile target tracking and guidance system such as that

employed in the Sidewinder is presented in Figure 2.6.3.1. As shown therein,

two closed control loops are involved: the tracking-head positioning loop and

the missile guidance loop. The tracking-head loop functions in the following

manner. The angular position of the sensor tracking head is compared with that

of the target line-of-sight as indicated by the direction-of-arrival of the

infrared radiation from the target. The tracking angle error is sensed (in

this case, by a rotating reticle), amplified, and used to drive the sensor head

positioning servo, thus nulling the tracking angle error. The missile guidance

loop functions in a manner similar to that of the sensor head positioning loop.

The missile flight path (longitudinal axis) angle is compared with the sensor

head tracking angle. The missile flight path angle error is sensed (in this

case, by magnetic pickoff coils), amplified, and used to position the missile

control fins, thus nulling the missile guidance error.

A detail drawing of the Sidewinder tracking head is shown in Figure 2.6.3.2(a).

The incoming radiation is focused, by a Cassegrainian telescope, on a lead

sulfide point-source radiation detector. The entire telescope is integral with

a gyro rotor (mounted on bearings not shown in the figure), thus providing
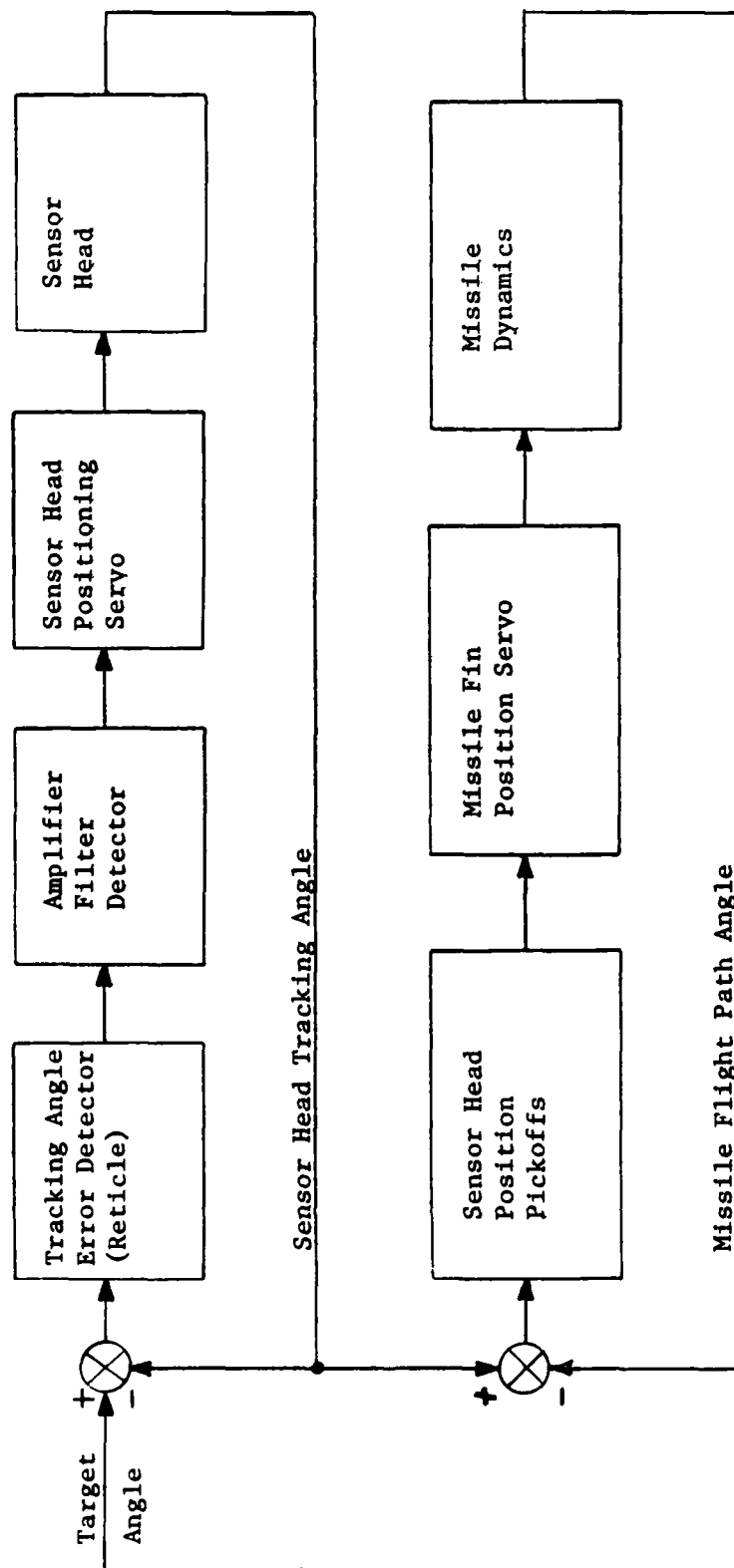
Figure 2.6.3.1 -- Guided Missile Tracking and Guidance System

2.93a

(b) Reticle

(a) Tracking Head

Gyro Rotor Tracking Head

Cell Window

Pb S Cell

Reticle

Spherical Primary M   )r

Support Disc and Filter

IR Dome

Incident Radiation

Secondary Mirror

Optical Axis
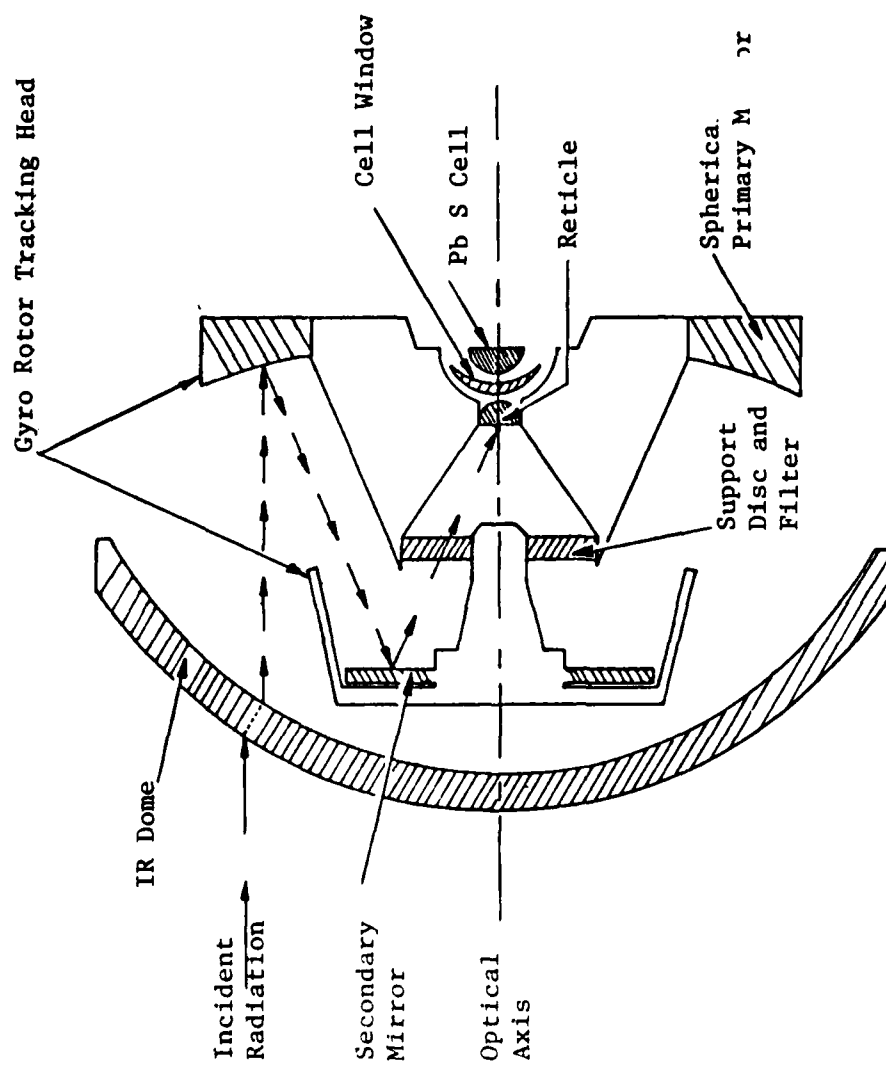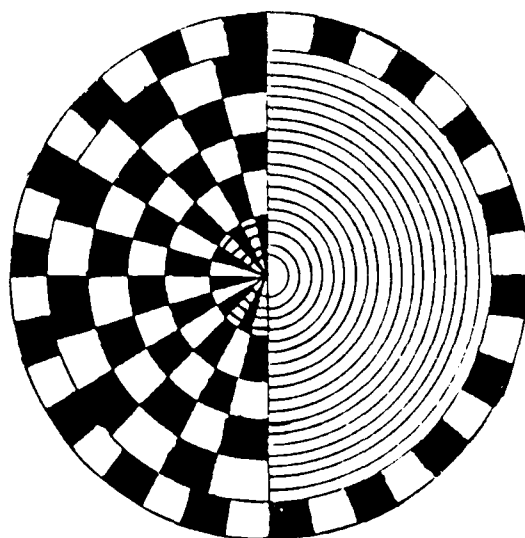
Figure 2.6.3.2 -- Sidewinder Missile Tracking Head and Reticle

2.93b

gyroscopic stabilization of the tracking angle. Also integral with the rotor are an interference-type chromatic filter, (used to discriminate against sunlit clouds), and a reticle. Since the entire gyro rotor/telescope assembly rotates, the reticle is also rotated. The reticle employed, shown somewhat simplified in Figure 2.6.3.2(b), is a combination of the phase-modulating and amplitude-modulating rotating reticles discussed in Section 2.3.6 of this text.

The I/R tracking system described above treats the target as essentially a point source. That is, no effort is made to image the target. When an imaging sensor is employed, more precise tracking can be effected. That is, some feature of the target image can be tracked such as the edge (contrast tracking) or the centroid (angle-gate tracking), or shape (pattern recognition tracking). The implementation of image feature tracking is, or course, more complex; but, once the feature to be tracked has been identified, the tracking principles are the same as those for the tracking system discussed above.

2.6.4 Laser Ranging and Target Designating Systems -- A laser ranger closely

resembles the ranging radars discussed in the text on radar systems. The reader

is, therefore, referred to that text for a description of ranging principles

and techniques. The reader also is referred to Section 2.5 of this text for a

discussion of the principles of Laser Operation . Due to the great difference

between radio frequencies and optical frequencies, the implementation and hard-

ware of laser rangers are somewhat different from those of RF systems. A block

diagram for a laser ranger is presented in Figure 2.6.4.1. The laser pulse is

initiated by a signal from the timer. The outgoing laser pulse is sensed by the

photodiode the output of which is used to start a timer in the range computing

unit. When the target return (incoming) pulse is detected by the sensor receiver,

the range timer is stopped and the computed range is displayed or output for

other purposes. Because of the difficulty in acquiring a target with an active

laser sensor, an aiming device is bore-sighted with the laser as shown in the

figure.

A laser target designator is used to illuminate a target for a weapon delivery

sensor. The laser radiation is encoded, usually by pulse modulation, in order

to provide rejection of ambient or jamming radiation. The scenario for a laser-

designated air-to-ground guided weapon delivery is shown in Figure 2.6.4.2.

The target is acquired by an auxiliary sensor, the laser beam is placed on the

target and maintained until weapon impact. A sensor in the guided weapon (such

as a laser-guided bomb) tracks and homes on the radiation reflected by the

illuminated (designated) target.
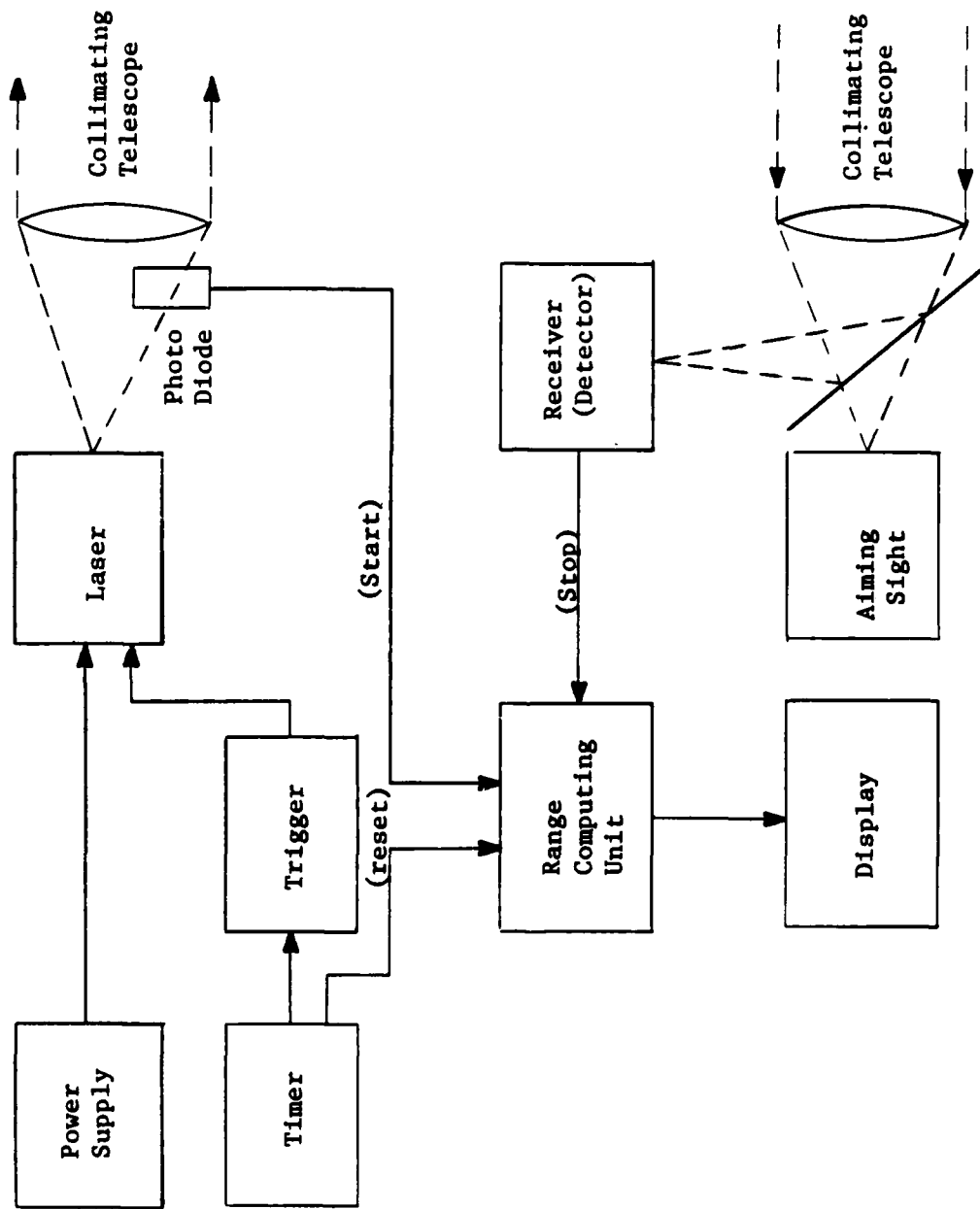
Figure 2.6.4.1 -- Block Diagram for a Laser Ranger

2.95a
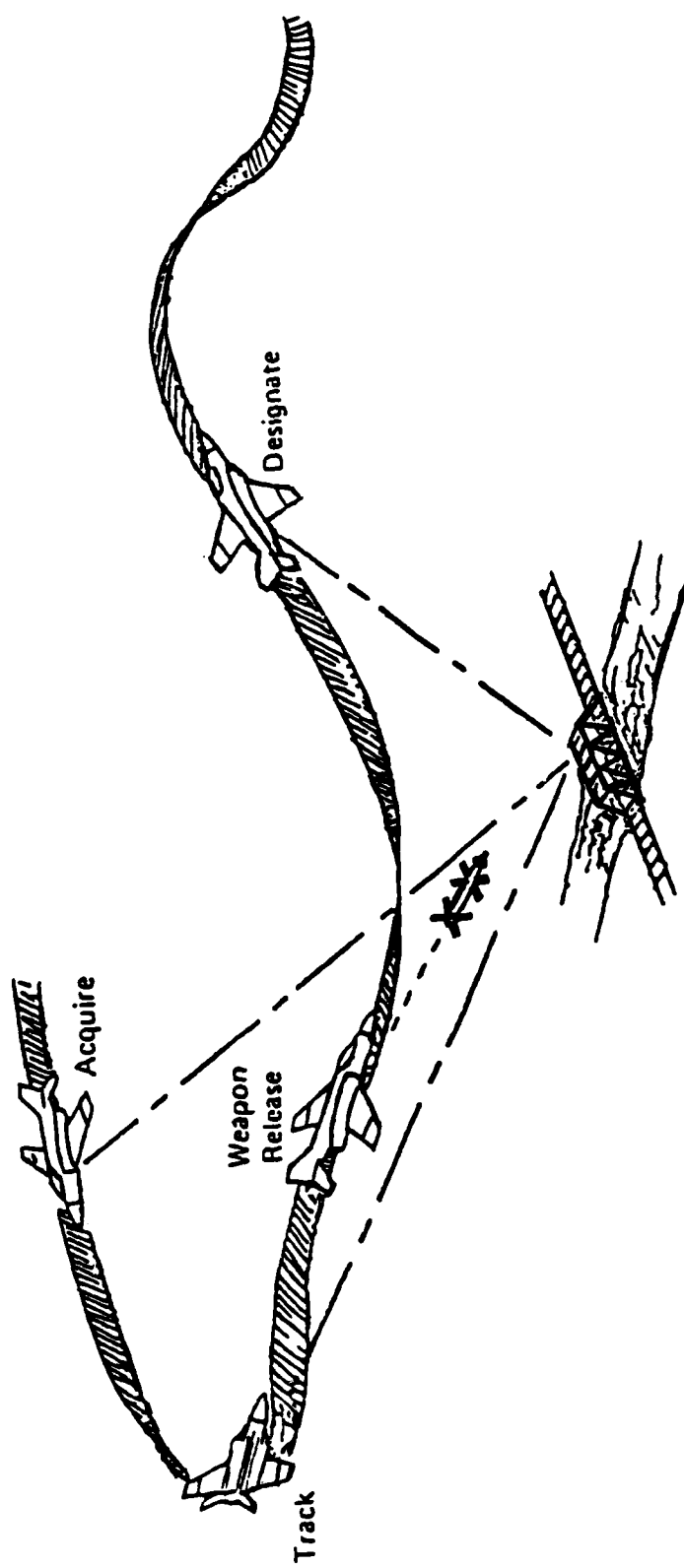
Figure 2.6.4.2 -- Laser Designated Weapon Delivery

2.95b

3.0 Electro-Optical System Characteristics

3.1 General Characteristics -- Electro-optical systems share nearly all of

the communications system characteristics discussed in Section 3.0 of the text

on communications system test and evaluation. Similarly, electro-optical sensors,

especially active sensors, share most of the radar system characteristics dis-

cussed in Section 3.0 of the radar text. Because of the commonality of character-

istics, the reader is referred to the material in those texts.

3.2 Definitions of E/O System Characteristics -- The principal characteristics

of E/O systems are listed below and defined and discussed in the following

paragraphs.

> Angular Resolution
> Bandwidth
> Beamwidth
> Bearing Accuracy
> Blind Ranges
> Boresight Accuracy
> Field-of-View
> Image Definition
> Instantaneous Field-of-View
> Line-of-Sight Limits
> Line-of-Sight Slew Rate, Max.
> Line-of-Sight Stability
> Maximum Range
> Minimum Resolvable Differential Temperature (MRΔT)
> Misfire Rate
> Modulation Transfer Function
> Noise-Equivalent Temperature Difference (NEΔT)
> Pointing Accuracy
> Power Output
> Pulse Amplitude
> Pulse Amplitude Stability
> Pulse Energy
> Pulse Width
> Pulse Repetition Frequency (PRF)
> PRF Accuracy
> PRF Stability
> Range Accuracy
> Range Resolution
> Spatial Frequency Response
> Spectrum
> Temporal Frequency Response
> Thermal Resolution
> Time Response

Angular Resolution -- The minimum line-of-sight angular separation for which two

point sources can be distinguished. For a point-source detecting system, the

angular resolution is generally limited by the instantaneous field-of-view. (A

discussion of E/O system angular resolution is presented in Section 3.3.5 of this

text.)

Bandwidth (Color or Temperature Bandwidth) -- The range of optical frequencies to which an E/O system responds. More precisely, the temporal frequency span between the half-power points in the optical frequency response of a system. Often stated in terms of wavelength. (See Section 2.5.3 of the text on Communications Systems for a discussion of bandwidth). For a photon-detection system, the bandwidth is limited by the response of the detector.

Beamwidth -- The angular separation between two radial lines extending from the origin to the half-power points of the main lobe in the radiation pattern of a radiating system. Also called beam divergence. (See Section 2.6.7 of the text on Communications Systems for a discussion of radiation pattern beamwidth.) Because of the high optical frequencies, electro-optical systems are not often diffraction limited and, therefore, exhibit radiation beamwidths much smaller than those for RF systems, for a given size radiating element.

Bearing Accuracy -- The maximum error within which an E/O sensor is capable of determining the bearing (azimuth or elevation) of a target. For an optical system, bearing accuracy depends upon angular resolution and boresight accuracy.

Blind Ranges -- The ranges at which a target cannot be detected by a pulsed, active E/O sensor due to ecliping of the target return by the transmitted pulse. Range gating produces similar effects.

Boresight Accuracy -- The maximum angular error within which the line-of-sight of an E/O sensor or illuminator can be aligned with a reference axis or with another sensor. The inherent accuracy of optical systems is such that boresight errors are a major contributor to system errors.

3.3

Field-of-View (FOV) -- The angular extent of the line-of-sight positions at which an E/O sensor or illuminator can respond. Field-of-view is determined by instantaneous field-of-view and the scan or slew limits of the system. (See Instantaneous Field-of-View).

Image Definition -- The ability of an E/O imaging sensor to yield an undistorted, "sharp" image of the radiation pattern within the field-of-view. Image definition usually is limited by the angular resolution of the detector and the resolution of the display.

Instantaneous Field-of-View (IFOV) -- The angular extent of the line-of-sight positions at which an E/O sensor responds at any one time. For a non-scanned sensor the IFOV is identical to the FOV. For a scanned, point-source detector, the IFOV is determined by the focal length of the optics and the dimensions of the detector element or field stop. For an electronically-scanned sensor the IFOV is determined by electron optics internal to the sensor. (A discussion of sensor instantaneous field-of-view is presented in Section 2.3.4 of this text).

Line of-Sight Limits -- The maximum excursions of the sensor line-of-sight in a scanned or slewed E/O sensor. In most E/O systems, the line-of-sight limits are imposed by mechanical considerations.

Line-of-Sight Slew Rate, Max. -- The maximum angular rate at which an E/O sensor line-of-sight can be changed. In most E/O systems, the line-of-sight slew rate limits are imposed by mechanical considerations.

Line-of-Sight Stability -- The maximum line-of-sight deviation from commanded line-of-sight position, due to mechanical vibrations or other inadvertent perturbations. Both short-term deviations (LOS jitter) and long-term deviations (LOS drift) are included.

Maximum Range -- The maximum range at which a given system function (detection, recognition, track acquisition, or tracking) can be performed for a target and environment of specified characteristics, with a specified probability. (An expression for maximum range is developed in Section 3.3.1 of this text.)

Minimum Resolvable Differential Temperature (MRΔT) -- The minimum difference in temperature to which an infrared sensor is capable of responding. Also called Thermal Resolution. (A discussion of E/O sensor thermal resolution is presented in Section 3.3.3 of this text.)

Misfire Rate -- The rate of firing failures (pulse drop-outs) in the transmissions of an active E/O system (illuminator).

Modulation Transfer Function (MTF) -- The amplitude ratio (ratio of image intensity or contrast to target intensity or contrast) versus-spatial frequency response characteristics of an E/O system. Also called Spatial Frequency Response. (A discussion of the modulation transfer function is presented in Section 2.3.2 of this text.)

Noise-Equivalent Temperature Difference (NEΔT) -- The difference in target temperature required to produce a change in the output of an infrared sensor just equal to the output due to ambient noise. Equivalently, the difference in target temperature required to produce a signal-to-noise ratio of unity.

Pointing Accuracy -- The maximum angular error within which an E/O system line-of-sight can be aligned with that of another sensor or with a reference direction. Pointing accuracy is determined by bearing resolution and line-of-sight stability.

Power output -- The radiant flux output from an active E/O system. Both average power and peak power are significant. (See Section 2.2 of the text on Radar Systems for a more detailed discussion of peak and average powers.)

Pulse Amplitude -- The "peak" radiant flux associated with a single pulse. More precisely, the value of radiant flux (in watts) which, when multiplied by the pulse width (in seconds), yields a total energy (in Joules) equal to the actual energy contained in the pulse. (See Section 2.2 of the text on Radar Systems for a more detailed discussion of pulse peak power.)

Pulse Amplitude Stability -- The maximum deviation of pulse amplitude from a fixed value. Short-term and long-term stabilities often are separately specified.

Pulse Energy -- The total energy (in Joules) contained in a pulse, equal to the product of pulse peak power and pulse width.

Pulse Width -- The time span between the fifty-percent-of-peak-power points of a pulse. (See Section 2.2 of the text on Radar Systems for a more detailed discussion of pulse parameters.)

Pulse Repetition Frequency (PRF) -- The rate of occurrence of pulses in a pulse train.

Pulse Repetition Frequency Accuracy -- The maximum deviation of PRF from a specified value.

Pulse Repetition Frequency Stability -- The maximum deviation of PRF from a fixed value.

Range Accuracy -- The maximum error within which an E/O system can determine the range of a target. For active systems that range directly, ranging accuracy depends upon range resolution. For passive systems that determine range by measuring altitude and line-of-sight depression angle (elevation), range accuracy depends upon bearing accuracy and altitude-measurement accuracy.

Range Resolution -- The minimum separation in range for which two targets can be distinguished. For active systems that range directly, range resolution is limited by pulse width. For passive systems that determine range by measuring line-of-sight depression angle (elevation) and altitude, range resolution depends upon bearing (angular) resolution.

Spatial Frequency Response -- The amplitude ratio (ratio of image intensity or contrast to target intensity or contrast)-versus-spatial frequency characteristics of an E/O system. Also called Modulation Transfer Function. (The spatial frequency response of a rectangular aperture is derived in Section 2.3.2 of this text).

Spectrum -- The power density-versus-temporal frequency characteristics of a given radiant signal. Equivalently, the temporal frequency content of a signal. The spectrum is generally specified in terms of spectral radiant flux as a function of wavelength, for an optical system.

Temporal Frequency Response -- The amplitude ratio-versus-temporal frequency characteristics of an E/O system. Both the carrier frequency (color) response and the video frequency (intensity time variation) response of an E/O system are significant.

Thermal Resolution -- See Minimum Resolvable Temperature Differential.

Time Response -- The response characteristics of a system with respect to variations in the input with time. Often stated in terms of time constants. Closely related to temporal frequency response.

3.3 Discussions of Major E/O System Characteristics

3.3.1 The E/O Sensor Range Equation -- The maximum range at which an electro-optical sensor can perform a given function depends upon the function to be performed, the characteristics of the target, the target background, the transmittance of the atmosphere, the characteristics of the sensor, and the signal-to-noise ratio required to attain given probabilities of success and failure. In the following development, an expression is derived for the maximum range at which a given function can be performed.

For a target of intensity J_T (Watts/Stearadian) and an atmospheric transmittance of τ_a (N.D.), the irradiance H_s (Watts/Cm^2) at the aperture of a sensor at range R (Cm) is given by:

$$H_s = \left(\tau_a / R^2 \right) J_T$$

The radiant flux P_d (Watts) incident upon the radiation detector element is, then, given by:

$$P_d = A_{so} \, \tau_{so} \, H_s = \tau_a \, A_{so} \, \tau_{so} \, J_T / R^2$$

where:

A_{so} = Aperture of Sensor Optics (Cm^2)

τ_{so} = Transmissivity of Sensor Optics (N.D.)

The detector output signal-to-noise ratio (Vs/Vn) (N.D.) is, then, given by:

$$\left(V_S / V_N \right) = D_d \, P_d = \tau_a \, A_{so} \, \tau_{so} \, D_d \, J_T / R^2$$

where D_d (1/Watts) is the detectivity of the detector.

The range attainable for a given signal-to-noise ratio is then given by:

$$R = \left[\frac{T_a\, A_{so}\, T_{so}\, D_d\, J_T}{(V_s/V_N)} \right]^{1/2} \quad (cm)$$

If the minimum signal-to-noise ratio required for a given system function (detection, recognition, track acquisition, or tracking) is designated by $(V_s/V_n)_{Min}$, the maximum attainable range is given by the equation:

$$R_{Max} = \left[\frac{T_a\, A_{so}\, T_{so}\, D_d\, J_T}{(V_s/V_N)_{Min}} \right]^{1/2} \quad (cm)$$

or, separating the various terms for identification:

$$R_{Max} = \left\{ \underset{\text{Target}}{\left[J_T \right]} \underset{\text{Atmosphere}}{\left[T_a \right]} \underset{\text{Optics}}{\left[A_{so} T_{so} \right]} \underset{\text{Detector}}{\left[D_d \right]} \underset{\substack{\text{Signal} \\ \text{Processing}}}{\left[1/(V_s/V_N)_{Min} \right]} \right\}^{1/2}$$

This equation assumes that all of the target radiant flux entering the sensor aperture is delivered to the detector. If, due to internal aperture stops or optics, all of the target flux is not incident upon the detector, that factor must be included in the optics term. For a pulsed system, $(V_s/V_n)_{Min}$ should be interpreted as the required value of the ratio of the peak signal to rms noise. If the detectivity of the detector (D_d) is expressed in terms of specific detectivity (D^*), the area of the detector (A_d) and bandwidth of the system (Δf) will appear explicitly in the range equation. Because of uncertainties in determining appropriate values for parameters such as τ_a and D_d, the maximum range of an E/O sensor must be verified by measurement under actual operating conditions.

3.3.2 The Active E/O Sensor Range Equation -- The irradiance at an E/O sensor
receiver produced by a target illuminated by a laser or other illuminator de-
pends upon the characteristics of the illuminator, the characteristics of the
target, the transmittance of the atmosphere, and the ranges from illuminator
to target and target to sensor. In the following developments, expressions are
derived for sensor irradiance, for both monostatic and bistatic sensor systems.

The target irradiance, H_T, produced by an illuminator of radiant intensity J_I
is given by the equation:

$$H_T = \frac{\tau_{aI}\, J_I}{R_{IT}^2} \qquad (\text{Watts/Cm}^2)$$

where:

$\qquad J_I$ = Radiant Intensity of Illuminator (Watts/Sr)

$\qquad R_{IT}$ = Range from Illuminator to Target (Cm)

$\qquad \tau_{aI}$ = Transmittance of Atmospheric Path from Illuminator to
$\qquad\qquad$ Target (N.D.)

The transmittance of the atmospheric path, for range R, is given by:

$$\tau_a = e^{-\sigma_a R} \qquad (\text{N.D.})$$

where:

$\qquad \sigma_a$ = Extinction Coefficient of Atmosphere along Path (1/Cm)

For a diffuse target smaller that the illuminator beam, the radiant flux re-
flected by the target depends upon the target area, A_T. The radiant intensity,
J_T, of a target viewed normally and radiating into a hemisphere is, then:

$$J_T = \frac{H_T\, A_T\, \rho_T}{\pi} \qquad (\text{Watts/Stearadian})$$

3.11

where:

A_T = Area of Target (Cm^2)

ρ_T = Reflectivity of Target (N.D.)

The irradiance at the receiver, H_R, produced by the radiant flux from the target is given by:

$$H_R = \frac{\tau_{aT}\, J_T}{R_{TR}^2} \qquad (Watts/Cm^2)$$

where:

R_{TR} = Range from Target to E/O Receiver (Cm)

τ_{aT} = Transmittance of Atmospheric Path from Target to Receiver (N.D.)

Combining the above equations, the irradiance received by an E/O sensor due to a target illuminated by a non-colocated (bistatic) illuminator is:

$$H_R = \left(\frac{\tau_{aI}\, \tau_{aT}\, A_T\, \rho_T}{\pi\, R_{IT}^2\, R_{TR}^2} \right) J_I \qquad (Watts/Cm^2)$$

For a monostatic active sensor:

$$R_{IT} = R_{TR} = R$$

and:

$$\tau_{aI} = \tau_{aT} = \tau_a$$

The expression for irradiance at the sensor then becomes:

$$H_R = \left(\frac{\tau_a^2\, A_T\, \rho_T}{\pi\, R^4} \right) J_I \qquad (Watts/Cm^2)$$

3.12

For a diffuse target larger than the illuminator beam, the radiant flux intercepted and reflected by the target is independent of the target area, A_T. The radiant flux reflected by the target, P_T, is then:

$$P_T = \rho_T \, \tau_{aI} \, P_I \qquad \text{(Watts)}$$

where:

P_I = Radiant Flux emitted by Illuminator (Watts)

ρ_t = Reflectivity of Target (N.D.)

τ_{aI} = Transmittance of Atmospheric Path from Illuminator to Target (N.D.)

The radiant intensity of the target, viewed normally and radiating into a hemisphere, is then:

$$J_T = \frac{P_T}{\pi} = \frac{\tau_{aI} \, \rho_T \, P_I}{\pi} \qquad \text{(Watts/Sr)}$$

Thus, the irradiance at the sensor receiver due to a target illuminated by a non-colocated (bistatic), narrow-beam illuminator is given by:

$$H_R = \frac{\tau_{aI} \, \tau_{aT} \, \rho_T \, P_I}{\pi \, R_{TR}^2} \qquad \text{(Watts/Cm}^2\text{)}$$

where:

R_{TR} = Range from Target to Receiver (Cm)

τ_{aT} = Transmittance of Atmospheric Path from Target to Receiver (N.D.)

Note that the target return is independent of the range from illuminator to target. This expression applies to the case of a laser designator for which the laser beam (spot) is usually smaller than the target. Specular reflection by the target and non-normal illumination and viewing angles must be considered in

actual practice. For the case of a monostatic, active, narrow-beam sensor:

$$R_{IT} = R_{TR} = R$$

$$\tau_{2I} = \tau_{2T} = \tau_2$$

and the irradiance at the sensor is given by:

$$H_R = \frac{\tau_2^2 \, \rho_T \, P_I}{\pi \, R^2}$$

3.3.3 Infrared Sensor Thermal Resolution or Minimum Resolvable Differential

Temperature (MRΔT) -- In the final analysis, the true measure of I/R sensor

performance is its ability to detect a temperature differential. (The difference

in temperature between target and clutter or signal-to-noise ratio). The

minimum resolvable differential temperature of an I/R sensor is a function of

the characteristics of the target, the background clutter, the transmittance of

the atmosphere, the range to the target, the characteristics of the sensor, and

the signal-to-noise ratio required to attain specified probabilities of detection

and false alarm. In the following development, an expression is derived for the

minimum resolvable temperature differential for an infrared sensor, assuming a

target of Area A_T viewed normally and radiating into a solid angle Ω.

In Section 3.3.1 of this text, an expression was derived for the sensor signal-to-

noise ratio, (Vs/Vn), produced by a given target radiant intensity, (J_T). Em-

ploying that expression and identifying the minimum signal-to-noise ratio required

for detection with the minimum differential in target intensity required for

detection, we have:

$$\left(V_S/V_N\right)_{Min} = \left(\frac{T_a \, A_{SO} \, T_{SO} \, D_d}{R^2}\right) \left(\Delta J_T\right)_{Min} \quad \text{(N.D.)}$$

In order to derive an expression relating the minimum required change in target

intensity with the minimum required change in target temperature, consider a

target radiating a flux P_T (Watts) into a solid angle Ω (Stearadians). The

radiant intensity of such a target is given by:

$$J_T = P_T / \Omega \qquad \text{(Watts/Stearadian)}$$

For a target of area A_T (Cm^2) and radiant emittance W (Watts/Cm^2):

$$J_T = \frac{W\, A_T}{\Omega} \qquad \text{(Watts/Stearadian)}$$

The differential radiant intensity (ΔJ_T) produced by a differential in radiant emittance (ΔW) is then:

$$\Delta J_T = \frac{A_T\,(\Delta W)}{\Omega} \qquad \text{(Watts/Sr)}$$

Generally, the radiant emittance of the target is a function of wavelength, λ. The radiant emittance, W, then can be expressed in terms of the spectral radiant emittance, W_λ, by the equation:

$$W = \int_{\Delta\lambda} W_\lambda\, d\lambda \qquad \text{(Watts/Cm}^2\text{)}$$

where $\Delta\lambda$ is the wavelength interval (bandwidth) of interest. This integral c in be approximated by the equation:

$$W = \left(W_\lambda\right)_{Av} (\Delta\lambda) \qquad \text{(Watts/Cm}^2\text{)}$$

where $(W_\lambda)_{Av}$ is the average value of W_λ over the wavelength interval ($\Delta\lambda$). The change in target spectral radiant emittance (ΔW), produced by a change in target temperature, (ΔT), is then:

$$\Delta W = \left(\frac{\partial W_\lambda}{\partial T}\right)_{Av} (\Delta\lambda)\,(\Delta T) \qquad \text{(Watts/Cm}^2\text{)}$$

where $\left(\frac{\partial W_\lambda}{\partial T}\right)_{Av}$ is the average rate of change of target spectral radiant emittance with temperature, over the wavelength interval ($\Delta\lambda$). Substituting this expression for (ΔW) into the previously derived expression for (ΔJ_T), we have, for the change in target radiant intensity, (ΔJ_T), due to a change in target temperature, (ΔT):

$$(\Delta J_T) = (A_T/\Omega)\left(\frac{\partial W_\lambda}{\partial T}\right)_{Av} (\Delta\lambda)\,(\Delta T) \qquad \text{(Watts/Sr.)}$$

The minimum change in target radiant intensity is thus related to the minimum change in target temperature by the equation:

$$(\Delta J_T)_{Min} = (A_T/\Omega)\,(\partial W_\lambda/\partial T)_{Av}\,(\Delta\lambda)\,(\Delta T)_{Min} \text{ (Watts/Sr)}$$

Substituting this expression for $(\Delta J_T)_{Min}$ into the previously derived expression for $(Vs/Vn)_{Min}$, we have, for the detector signal-to-noise ratio produced by the minimum detectable target differential temperature:

$$(Vs/V_N)_{Min} = \left(\frac{A_T\,\tau_a\,A_{so}\,\tau_{so}\,D_d\,(\partial W_\lambda/\partial T)_{Av}\,(\Delta\lambda)}{\Omega\,R^2}\right)(\Delta T)_{Min}$$

or, solving for the minimum resolvable differential temperature:

$$(MR\Delta T) = \frac{\Omega\,R^2\,(Vs/V_N)_{Min}}{A_T\,\tau_a\,A_{so}\,\tau_{so}\,D_d\,(\Delta\lambda)\,(\partial W_\lambda/\partial T)_{Av}} \text{ (K. Deg.)}$$

where:

A_{so} = Effective Optical Aperture of Sensor (Cm^2)

A_T = Area of Target (Cm^2)

D_d = Detectivity of Detector (1/Watts)

R = Range to Target (Cm)

$(Vs/Vn)_{Min}$ = Minimum detector signal-to-noise ratio required for detection (N.D.)

$(\Delta\lambda)$ = Sensor Bandwidth (Micrometers)

$\left(\dfrac{\partial W_\lambda}{\partial T}\right)_{Av}$ = Average value of the rate of change of W_λ with temperature over the bandwidth of the sensor (Watts/Cm^2-μm-K°)

τ_a = Transmittance of Atmosphere (N.D.)

τ_{so} = Transmittance of Sensor Optics (N.D.)

Ω = Solid Angle into which Target Radiates (Stearadians)

For a blackbody target, an expression can be derived for the rate of change of target spectral radiant emittance with respect to temperature. For such a target:

$$W_\lambda = \frac{2\pi h c^2}{\lambda^5 \left(e^{hc/\lambda kT} - 1\right)} \qquad \text{(Watts/Cm}^2 - \mu\text{m)}$$

Taking the partial derivative of W_λ with respect to temperature, we have:

$$\left(\frac{\partial W_\lambda}{\partial T}\right) = \left(\frac{2\pi h^2 c^3}{k \lambda^6 T^2}\right)\left[\frac{e^{hc/\lambda kT}}{\left(e^{hc/\lambda kT} - 1\right)^2}\right] \qquad \text{(Watts/Cm}^2 - \mu\text{m} - \text{K}^\circ\text{)}$$

where:

        C = Velocity of Light (Cm/Sec)

        h = Planck's Constant (Watts-Sec^2)

        k = Boltzmann's Constant (Watts-Sec/Deg)

        T = Absolute Temperature (°K)

        λ = Wavelength (Micrometers)

If the target cannot be assumed to be a blackbody, the value of $\left(\frac{\partial W_\lambda}{\partial T}\right)_{Av}$ must be determined experimentally. Note that the presence of $\left(\frac{\partial W_\lambda}{\partial T}\right)_{Av}$ in the expression for (MRΔT) implies the possibility of minimizing $\left(\frac{\partial W_\lambda}{\partial T}\right)_{Av}$ in the bandwidth of a sensor in order to reduce the detectability of the target.

In practice, the minimum resolvable differential temperature of an I/R sensor depends upon factors not included in the equation derived above, including: dynamic effects (e.g., dwell time in a scanning system), the optical resolution of the optics, the signal processing employed, and the type of display. Further complexities arise from the necessity of determining "average" values of the

system parameters (e.g., τ_a, τ_{so}, D_d, Etc.). In the final analysis, the MRΔT of a system must be verified by empirical testing.

Note that for (Vs/Vn) = 1, the derived equation for MRΔT yields the Noise Equivalent Differential Temperature (NEΔT).

3.3.4 E/O Sensor Field-of-View -- The total field-of-view, (FOV), of a fixed (non-scanning) E/O sensor is identical to its instantaneous field-of-view (IFOV). For a scanning sensor, however, the total field-of-view is determined primarily by the angular limits of its scanning mechanism. Both the total and the instantaneous fields-of-view are of importance and must be determined in an E/O sensor evaluation. The FOV of a scanned sensor depends upon factors peculiar to the scanning mechanism and does not require further discussion. For a large class of scanned point-source detecting sensors, however, the instantaneous field-of-view is determined by the characteristics of the optical system and the dimensions of the detector element. The geometry involved in such a sensor is illustrated in Figure 3.3.4.1. At any instant of time, a detector element of diameter D_d "sees" a "spot" of diameter D_{IFOV} at range R_T. The geometry shown assumes that R_T is much greater than the focal length of the optical system, FL_o, thus placing the detector at the focal point of the optical system. The diameter of the instantaneous field of view, D_{IFOV}, is given by the equation:

$$ D_{IFOV} = \frac{D_d\, R_T}{FL_o} \qquad \text{(Meters)} $$

where:

D_d = Diameter of Detector (Meters)

FL_o = Focal Length of Optics (Meters)

R_T = Range to Target (Meters)

The (one-dimensional) angular field-of-view, θ_{IFOV}, is given by:

$$ \theta_{IFOV} = Tan^{-1} \left[\frac{D_{IFOV}}{R_T} \right] \approx \frac{D_{IFOV}}{R_T} = \frac{D_d}{FL_o} \qquad \text{(Radians)} $$

Detector Area = A_d

Optics

IFOV

D_d

FL_o

Ω_{IFOV}

R_T
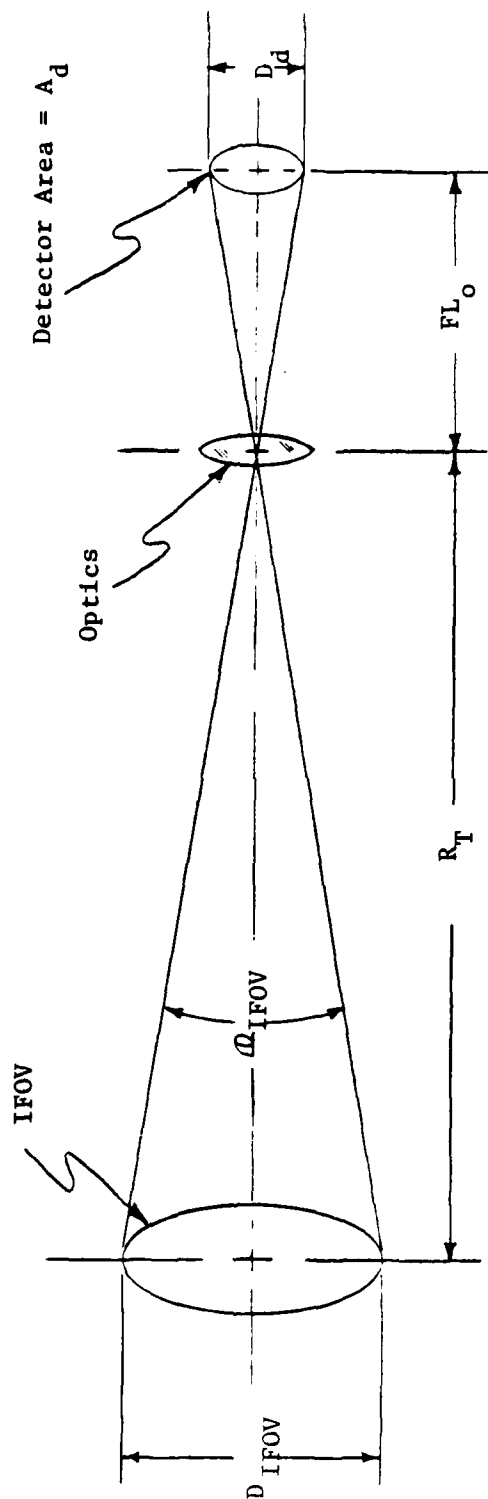
D_{IFOV}

A_d = Detector Element Area (Meters^2)

D_{IFOV} = Diameter of IFOV at Range R_T (Meters)

D_d = Diameter of Detector Element (Meters)

FL_o = Focal Length of Optics (Meters)

R_T = Range to Target (Meters)

Ω_{IFOV} = Angular Field of View (Radians)

Ω_{IFOV} = Solid Angle Field of View (Stearadians)

Figure 3.3.4.1 -- Instantaneous Field of View of Point - Source Detecting Sensor

3.20a

and the solid (two-dimensional) angular field-of-view, Ω_{IFOV}, is given by:

$$\Omega_{IFOV} = A_d / (FL_o)^2$$

where:

A_d = Area of the Detector (Meters^2)

In most systems, the sensor field-of-view is dominated by the geometrical considerations presented above. A number of other considerations, however, can be important. For example, a field stop can be used to limit the irradiated portion of the detector element. When such a stop is used, the effective (irradiated) diameter of the detector must be used in the equations for IFOV. (Maximization of the detector output signal-to-noise ratio requires that the entire detector be irradiated.) Another possible contributor to sensor instantaneous field-of-view is diffraction effects. When diffraction is a significant factor, the diffraction-produced incremental field-of-view, (one-half the angular subtense of the Airy Disk), must be added to that determined by the detector size. The incremental angular field-of-view due to diffraction, δ_{IFOV} is given by:

$$\delta_{IFOV} = \frac{0.122 \, \lambda}{D_o} \quad \text{(Milliradians)}$$

where:

D_o = Diameter of Optical Aperture (Cm)

λ = Wavelength of Radiation (μm)

Other effects, such as optical aberrations, can enlarge the sensor instantaneous field-of-view. When such effects are significant, the angular subtense of the associated blur circle must be added to the angular field-of-view of the sensor.

3.3.5   E/O Sensor Angular Resolution -- The angular resolution of an E/O sensor depends upon the factors listed below.

>   Optical Aberrations
>   Diffraction Effects
>   Detector Element Field-of-View
>   Electronic Effects
>   Display Limitations
>   Line-of-Sight Jitter

Optical Aberrations -- The loss of angular resolution due to optical aberrations in a well-designed system generally is negligable. When such effects are significant, an incremental angular resolution equal to one-half the diameter of the resulting blur circle must be added to the system instantaneous field-of-view.

Diffraction Effects -- Diffraction effects generally are not dominant. The incremental angular resolution due to diffraction effects, (one-half the diameter of the Airy Disk), is given by:

$$\partial \theta_R = \frac{0.122\ \lambda}{D_o} \qquad \text{(Milliradians)}$$

where:

D_o = Diameter of Optical Aperture (Cm)

λ = Wavelength of Radiation (μm)

Detector Element Field-of-View -- For a point-source-detecting sensor, the angular resolution is generally determined by the detector element geometrical instantaneous field-of-view. That is, two point sources should be resolvable if the angular separation of their lines-of-sight is at least equal to the sensor angular instantaneous field-of-view, θ_{IFOV}, as defined in Section 3.3.4 of this text. Thus, the angular resolution of a point-source-detecting E/O sensor, θ_R,

generally is given by:

$$\theta_R = \theta_{IFOV} = Tan^{-1}\left[\frac{D_{IFOV}}{R_T}\right] \cong \frac{D_{IFOV}}{R_T} = \frac{D_d}{FL_o} \quad \text{(Radians)}$$

where:

D_d = Diameter of Detector Element (Meters)

D_{IFOV} = Diameter of Sensor IFOV (Meters)

FL_o = Focal Length of Optics (Meters)

R_T = Range to Target (Meters)

θ_{IFOV} = Sensor Angular IFOV (Radians)

Electronic Effects -- For a non-point-scanning imaging E/O sensor, the angular resolution is generally determined by electronic effects. Usually dominant are those effects due to dispersions associated with the electron "optics" of such devices. As is the case with conventional optical systems, the focusing ability of "electron-optical" systems is limited. Another important electronic effect is the diffusion of charges in semiconductor materials such as those used in photosensitive screens. In addition, a narrow electron beam "mushrooms" when striking a target, thus effectively increasing the diameter of the beam and, therefore, the resolution of an electron-beam-scanned sensor.

Display Limitations -- Two major factors contribute to loss of angular resolution due to display limitations: the limited size of a display that feasibly can be mounted in the cockpit of an aircraft, and the visibility of the display due to viewing distance and the brightness of the display with respect to ambient light. In actual practice, the resolution of an airborne sensor is sometimes limited by the display.

Line-of-Sight Jitter -- A major contributor to loss of in-flight angular resolution in airborne electro-optical sensors is line-of-sight jitter due to airframe vibrations and other sources of LOS instability. In Figure 3.3.5.1 is plotted a curve showing total angular resolution, (with line-of-sight jitter), θ_R, versus rms line-of-sight jitter, α. (Both quantities are plotted normalized with respect to the angular resolution without line-of-sight jitter, θ_{R_0}.) This curve, empirically derived by Philco-Ford, can be used to determine total angular resolution for a given stable-line-of-sight angular resolution and a given line-of-sight jitter.
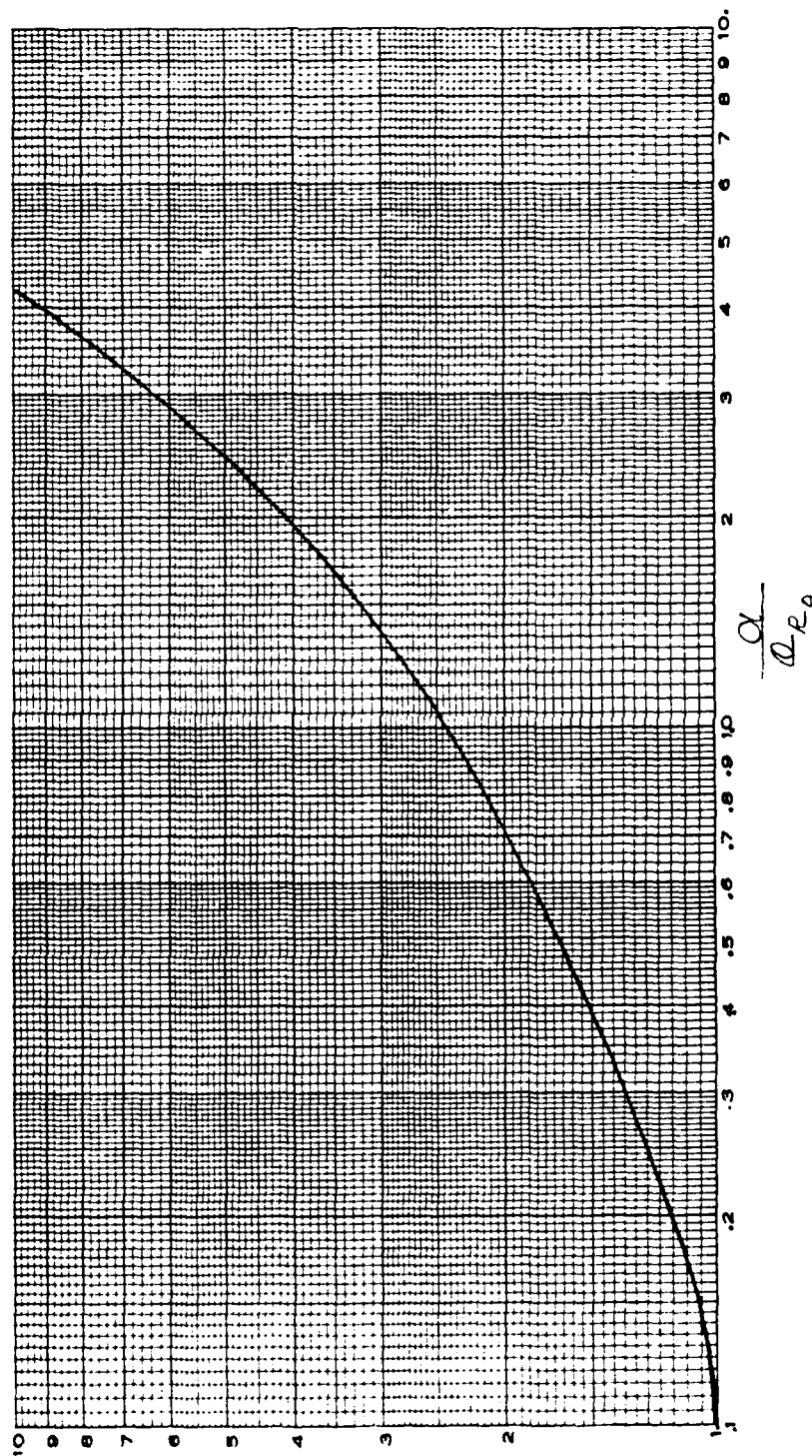
α = RMS Value of Sensor Line-of-Sight Jitter (Rad.)

α_R = Sensor Angular Resolution with Line-of-Sight Jitter (Rad.)

α_{R_0} = Sensor Angular Resolution without Line-of-Sight Jitter (Rad.)

Figure 3.3.5.1 -- Effect of Line-of-Sight Jitter on Sensor Angular Resolution

3.24 a

3.3.6 E/O Sensor Spatial Response -- The spatial frequency response of a linear E/O Sensor to an arbitrary target shape (spatial distribution of radiant intensities) can be determined analytically by decomposing the spatial distribution into its component spatial frequencies (Fourier analysis); subjecting each component to the attenuation and phase shift dictated by the optical transfer function of the sensor; and recombining the attenuated components (Fourier synthesis). The result will be the system response to the original target. This Fourier optics technique can be employed to determine the response of an E/O sensor scanning aperture to a bar target (target with radiant intensity varying as a rectangular or square wave). In the following development, the spatial response of a rectangular scanning aperture to a bar target is determined by direct integration. The response of an E/O sensor to a bar target is of interest since the spatial response (e.g., cut-off frequency) of E/O sensors is most frequently determined using such targets.

In Figure 3.3.6.1 is shown an E/O sensor scanning a bar target with bars of high radiant intensity shown shaded and inter-bar spaces (of low intensity), of width equal to that of the bars, shown unshaded. The fundamental spatial frequency of the target, SF_T, is determined by the angular subtense of one cycle of the target, θ_{1C}, (illustrated in the figure), which, in turn, depends upon the linear width of one cycle of the target, W_{1C}, and the range to the target, R_T. That is:

$$SF_T = \frac{1}{\theta_{1C}} \qquad \text{(Cycles/Radian)}$$

$$\theta_{1C} = \frac{W_{1C}}{R_T} \qquad \text{(Radians)}$$
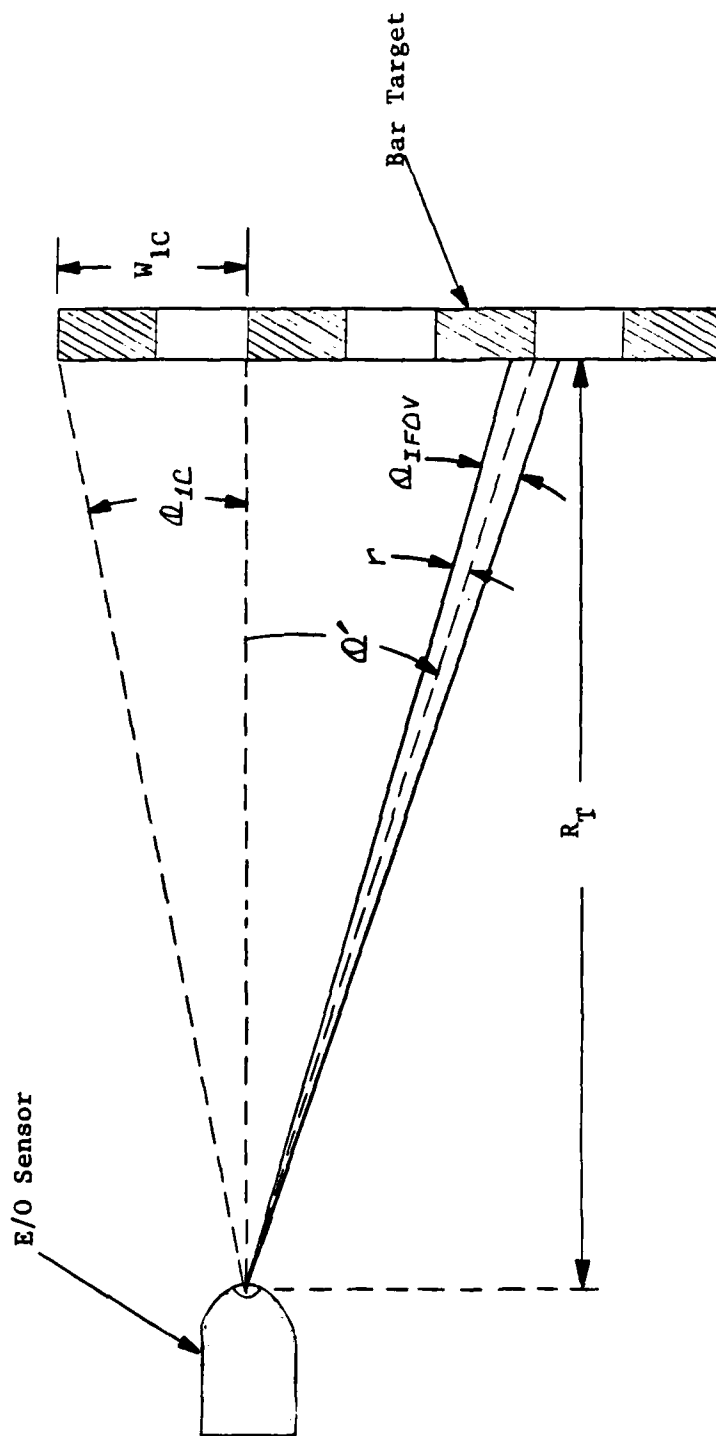
Figure 3.3.6.1 -- E/O Sensor Scanning Bar Target

3.25a

where:

R_T = Range to Target (Meters)

W_{1C} = Linear Width of one cycle of the target (Meters)

Θ_{1C} = Angular Subtense of one cycle of the target (Radians)

Also illustrated in Figure 3.3.6.1 is the sensor angular instantaneous field-of-view, Θ_{IFOV}, and the scanning angle, Θ'. The width of the angular instantaneous field-of-view is equal to 2r. Thus, the angular field-of-view of the sensor, for a scan angle of $\Theta = \Theta'$, extends from $\Theta = \Theta'-r$ to $\Theta = \Theta'+r$, as shown in Figure 3.3.6.2. As discussed in Section 2.3.2 of this text, the output of the sensor for $\Theta = \Theta'$, is proportional to the average value of the target radiant intensity, $\bar{J}_T(\Theta')$. That is:

$$\bar{J}_T(\Theta') = \frac{1}{2r} \int_{\Theta'-r}^{\Theta'+r} J_T(\Theta) \, d\Theta$$

The spatial response of the scanning aperture to the bar target is defined as the amplitude of the variations in output radiant intensity, as the target is scanned, to the amplitude of the variations in input (scanned) radiant intensity. That is, the aperture spatial response is the amplitude ratio, AR, given by:

$$AR = \frac{\bar{J}_T(Max) - \bar{\bar{J}}_T(Min)}{J_T(Max) - \bar{J}_T(Min)} \quad \text{(N.D.)}$$

The maximum values of the input radiant intensity are equal to J_A. The minimum values of input radiant intensity are zero. Thus:

$$AR = \frac{1}{J_A}\left[\bar{J}_T(Max) - \bar{J}_T(Min)\right] \quad \text{(N.D.)}$$
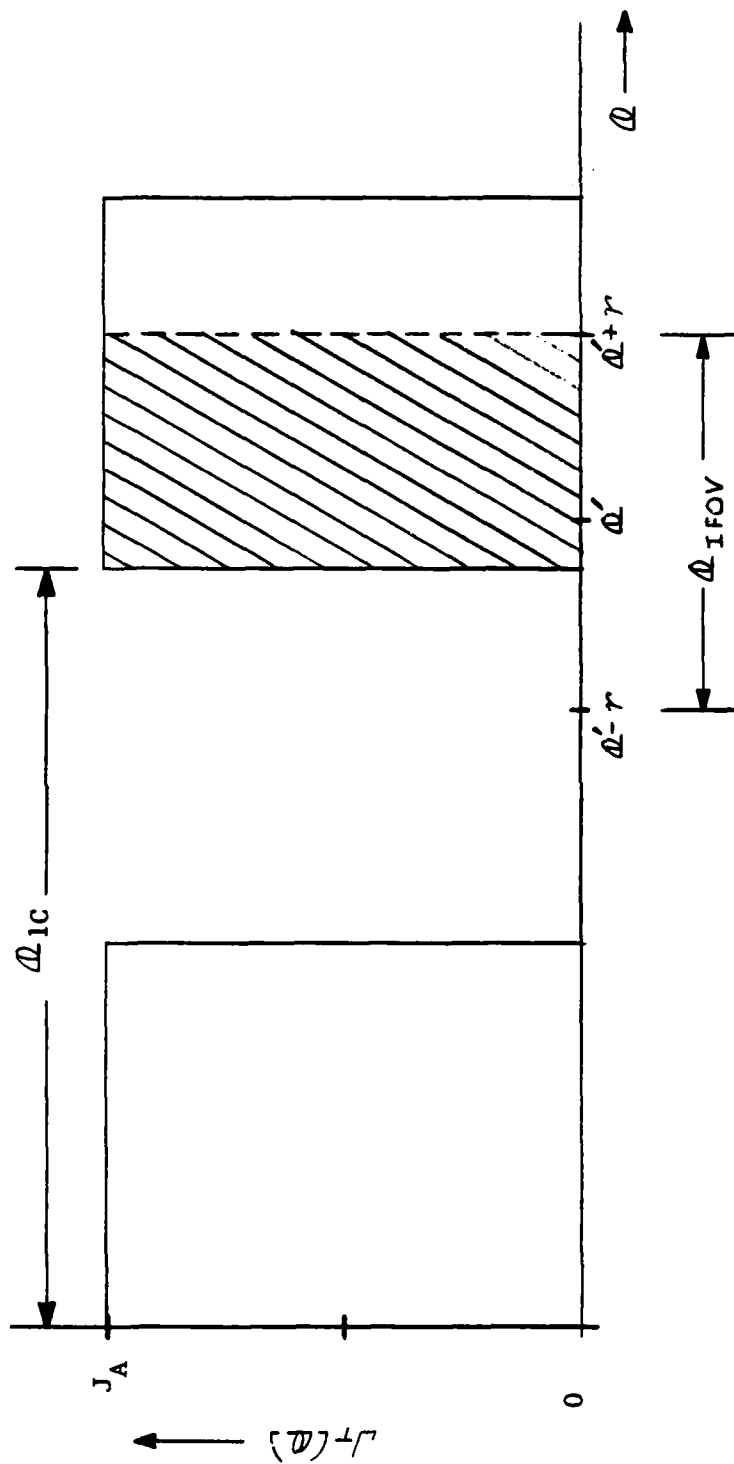
$J_T(\alpha)$ = Bar Target Radiant Intensity

α = Sensor Scan Angle

α' = Sensor Instantaneous Scan Angle

α_{IFOV} = Sensor Instantaneous Field-of-View

Figure 3.3.6.2 -- Bar Target Radiant Intensity

The maximum values of the aperture output, $\bar{J}_{T(Max)}$, occur at scan angles given by:

$$\theta' = \frac{\theta_{1c}}{4} + n\,\theta_{1c}$$

where n is an integer.

Evaluating the expression for $\bar{J}_T$ at $\theta' = \theta_{1C}/4$, there are two cases of interest the case for which the sensor instantaneous field-of-view is equal to or less than one target bar width, and the case for which the sensor instantaneous field-of-view is greater than one bar width. For the former case, $0 \stackrel{\geq}{=} r \stackrel{\leq}{=} \theta_{1c}/4$ and:

$$\bar{J}_{T(Max)} = \frac{1}{2r} \int_{\theta'-r}^{\theta'+r} (J_A)\,d\theta = J_A$$

For the latter case, $\theta_{1c}/4 \stackrel{\geq}{=} r \stackrel{\leq}{=} \theta_{1c}/2$ and:

$$\bar{J}_{T(Max)} = \frac{1}{2r} \int_{\theta'-r}^{\theta'-\theta_{1c}/4} (0)\,d\theta + \frac{1}{2r} \int_{\theta'-\theta_{1c}/4}^{\theta'+\theta_{1c}/4} (J_A)\,d\theta + \frac{1}{2r} \int_{\theta'+\theta_{1c}/4}^{\theta'+r} (0)\,d\theta$$

or:

$$\bar{J}_{T(Max)} = \frac{J_A\,\theta_{1c}}{4r} = \frac{1}{2}\left(\frac{\theta_{1c}}{\theta_{IFOV}}\right) J_A$$

The minimum values of the aperture output, $\bar{J}_{T(Min)}$, occur at scan angles given by:

$$\theta' = \frac{3\,\theta_{1c}}{4} + n\,\theta_{1c}$$

where n is an integer.

Evaluating the expression for $\bar{J}_T$ at $\theta' = \frac{3\theta_{1C}}{4}$, we must, again, consider the two cases.

3.27

For $0 \leqq r \leqq \theta_{Ic}/4$,

$$\bar{J}_{T(Min)} = \frac{1}{2r} \int_{\theta'-r}^{\theta'+r} (0) \, d\theta = 0$$

For $\theta_{Ic}/4 \leqq r \leqq \theta_{Ic}/2$,

$$\bar{J}_{T(Min)} = \frac{1}{2r} \int_{\theta'-r}^{\theta'-\theta_{Ic}/4} (J_A) \, d\theta + \frac{1}{2r} \int_{\theta'-\theta_{Ic}/4}^{\theta'+\theta_{Ic}/4} (0) \, d\theta + \frac{1}{2r} \int_{\theta'+\theta_{Ic}/4}^{\theta'+r} (J_A) \, d\theta$$

or:

$$\bar{J}_{T(Min)} = \left[1 - \frac{1}{2} \left(\frac{\theta_{Ic}}{\theta_{IFOV}} \right) \right] J_A$$

The aperture output, for the two cases, is shown plotted versus scan angle in Figure 3.3.6.3. Thus, for the case where the sensor IFOV is equal to or less than one target bar width, the aperture spatial response (amplitude ratio) AR is given by:

$$AR = \frac{\bar{J}_{T(Max)} - \bar{J}_{T(Min)}}{J_{T(Max)} - J_{T(Min)}} = 1$$

and for the case where the sensor IFOV is greater than one target bar width, the aperture spatial response is given by:

$$AR = \left(\frac{\theta_{Ic}}{\theta_{IFOV}} - 1 \right)$$

As previously indicated, the spatial frequency of the target, SF_T, is given by:

$$SF_T = \frac{1}{\theta_{Ic}}$$

(Cycles/Radian)

and the aperture cut-off frequency, SF_{co}, is given by:

$$SF_{co} = \frac{1}{\theta_{IFOV}}$$

(Cycles/Radian)

3.28

(a) For $\Omega \leqq r \leqq \dfrac{\vartheta_{IC}}{4}$, $J_{TC(MAX)} = J_A$ and $J_{T(MIN)} = 0$

J_A

J_T

$\overline{J}_T\ (MAX)$

$\overline{J}_T\ (MIN)$

0 $\quad \dfrac{\vartheta_{IC}}{4} \quad \dfrac{3\vartheta_{IC}}{4} \quad \dfrac{5\vartheta_{IC}}{4} \quad \vartheta'$
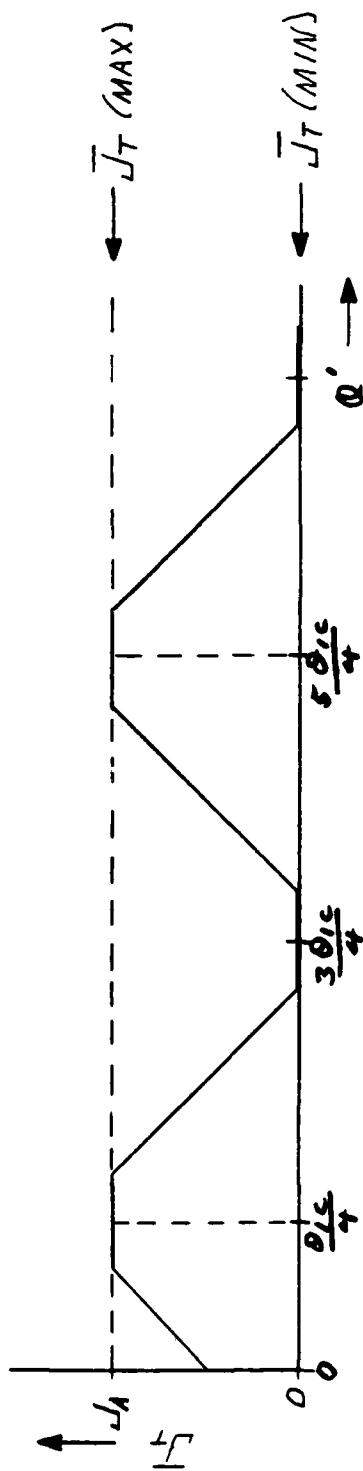
(b) For $\dfrac{\vartheta_{IC}}{4} \leqq r \leqq \dfrac{\vartheta_{IC}}{2}$, $J_T(MAX) = \dfrac{1}{2}\left(\dfrac{\vartheta_{IC}}{\vartheta_{IFOV}}\right)J_A$ and $J_T(MIN) = \left[1 - \dfrac{1}{2}\dfrac{\vartheta_{IC}}{\vartheta_{IFOV}}\right]J_A$

J_A

J_T

$\overline{J}_T\ (MAX)$

$\overline{J}_T\ (MIN)$

0 $\quad \dfrac{\vartheta_{IC}}{4} \quad \dfrac{3\vartheta_{IC}}{4} \quad \dfrac{5\vartheta_{IC}}{4} \quad \vartheta'$
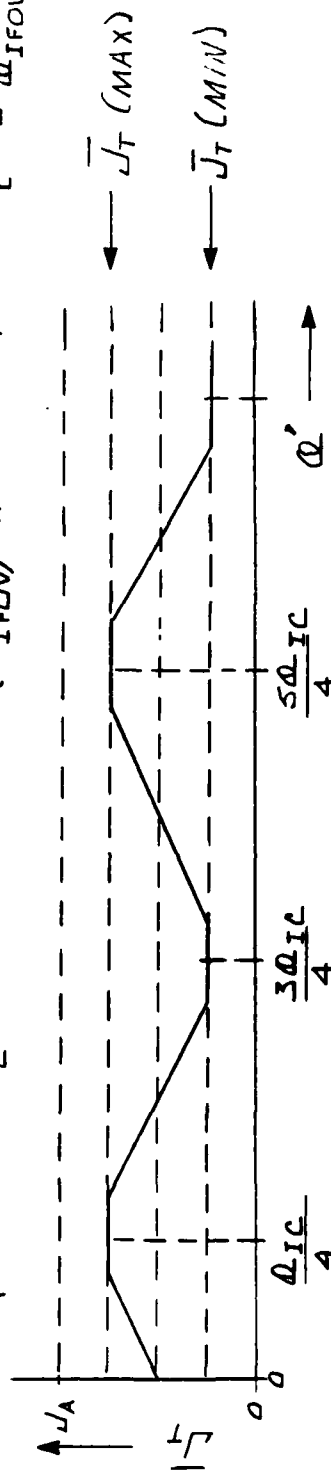
Figure 3.3.6.3 -- Radiant Intensity Output of a Rectangular Scanning Aperture due to a Bar Target

Thus:

$$\frac{\theta_{IFOV}}{\theta_{ic}} = \frac{SF_T}{SF_{co}}$$

The spatial response (amplitude ratio) of a rectangular aperture to a bar target is shown plotted versus spatial frequency ratio in Figure 3.3.6.4.

The target spatial frequency at which the aperture response (amplitude ratio) just begins to fall off is seen, from Figure 3.3.6.4, to be given by:

$$\frac{SF_T}{SF_{co}} = \frac{1}{2}$$

or:

$$SF_T = \frac{1}{2} SF_{co}$$

This spatial frequency, sometimes called the resolution spatial frequency, SF_R, is that target spatial frequency for which the sensor IFOV is equal to one bar width. That is:

$$\theta_{IFOV} = \frac{1}{2} \theta_{ic} \qquad \text{(Radians)}$$

At the resolution spatial frequency, the sensor responses to (images of) adjacent bars just begin to merge and the radiant intensity output of the scanning aperture is similar to that shown in Figure 3.3.6.5. The resolution spatial frequency, SF_R, is related to the cut-off spatial frequency, SF_{co}, the angular resolution, θ_R, and the angular instantaneous field-of-view, θ_{IFOV}, by the equations:

$$SF_R = \frac{1}{2} SF_{co} \qquad \text{(Cycles/Radian)}$$

$$SF_R = \frac{1}{2\theta_R} = \frac{1}{2\theta_{IFOV}} \qquad \text{(Cycles/Radian)}$$

For $0 \leq \alpha_{IFOV} \leq \dfrac{\alpha_{IC}}{2}$, $\quad AR = 1$

For $\dfrac{\alpha_{IC}}{2} \leq \alpha_{IFOV} \leq \alpha_{IC}$, $\quad AR = \dfrac{\alpha_{IC}}{\alpha_{IFOV}} - 1$

$$AR = \frac{\overline{J_T(MAX)} - \overline{J_T(MIN)}}{J_T(MAX) + J_T(MIN)}$$

Spatical Response (AR)

$\dfrac{SF_T}{SF_{CO}}$ $\left(\dfrac{\alpha_{IFOV}}{\alpha_{IC}}\right)$
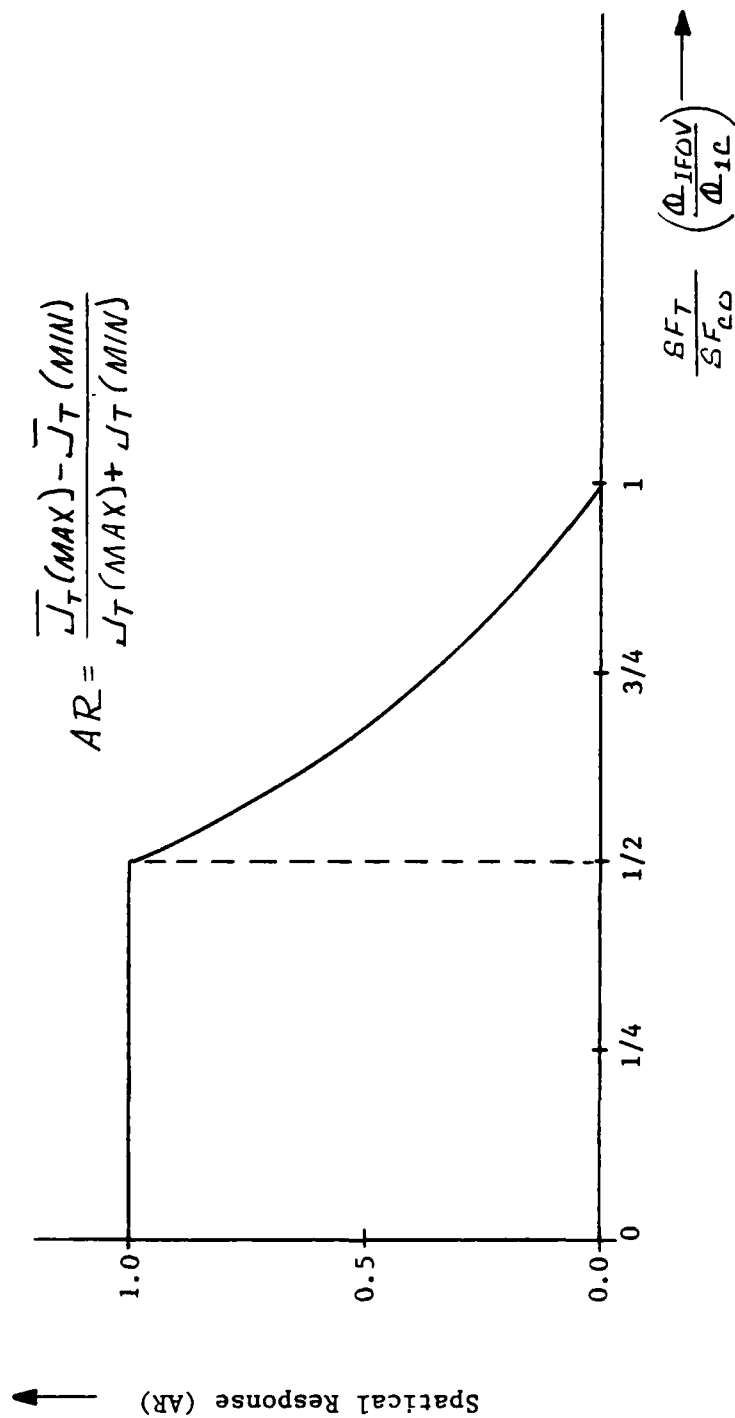
Figure 3.3.6.4 -- Spatial Response of a Rectangular Scanning Aperture to a Bar Target

3.29a
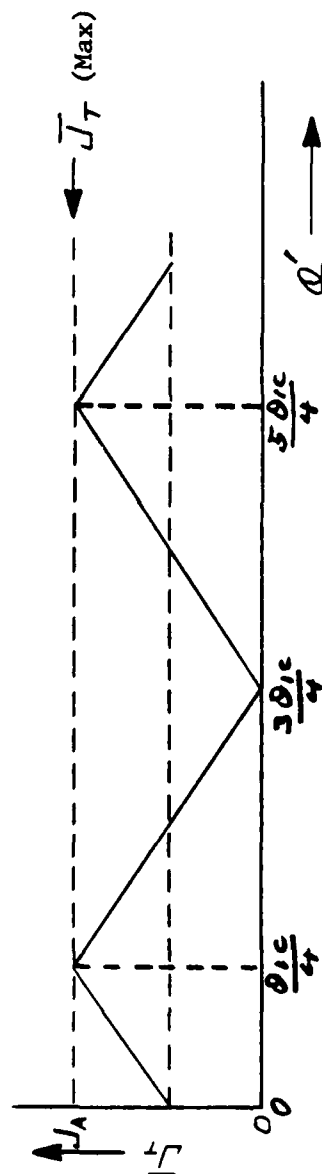
Figure 3.3.6.5 -- Radiant Intensity Output of a Rectangular Scanning Aperture due to a Bar Target of Spatial Frequency Equal to the Scanning Aperture Resolution Spatial Frequency

3.3.7 E/O Sensor Display Limitations -- The angular resolution of an imaging

sensor often is limited by the resolution of the display. For a spot-scanned,

(or LED matrix), display, the angular resolution depends upon the size of the

scanning spot, (or individual LED), and upon the rise time (or bandwidth) of

the display electronics.

When the scanning motion is continuous, (as it is in the horizontal direction

in most horizontally-scanned CRT displays), the angular resolution of the dis-

play is equal to the angular subtence of the scanning spot in the horizontal

direction.

Thus:

$$\theta_R = \frac{(\text{Linear Width of Scan Spot}) \times (\text{Angular FOV of Display})}{(\text{Linear Width of Display})}$$

When the display angular field of view is limited by electronic bandwidth, the

angular resolution is that angle for which the scan time is just equal to the

reciprocal of the electronic system bandwidth.

Thus:

$$\theta_R = \frac{\dot{\theta}_{scan}}{[BW]_E} \qquad (\text{Deg})$$

Where:

$$\dot{\theta}_{scan} = (\text{Angular Scan Rate}) \ (\text{Deg/Sec})$$

$$\dot{\theta}_{scan} = (\text{Deg/Line}) \times (\text{Lines/Frame}) \times (\text{Frames/Sec})$$

$$[BW]_E = \text{Electronic Bandwidth (Hertz)}$$

3.30

When The scanning motion is discontinuous, (as it is in the vertical direction in a horizontally-scanned CRT or in either direction in an LED matrix display), sampled-data effects require that each cycle of the bar target be sampled at least twice, in accordance with the Nyguist sampling theorem. That is, the angular resolution is equal to twice the angular subtence of the scanning spot, line width, or individual LED. Thus:

$$\theta_R = \frac{2X(\text{Linear Width of Scan Spot})X(\text{Angular FOV of Display})}{(\text{Linear Width of Display})}$$

It should be noted that the Nyguist sampling theorem applies to any discontinuous (sampled-data) scanning process, including that associated with a FLIR optical scanner.

3.4 Typical Electro-Optical System Characteristics

The characteristics of typical electro-optical systems are included in a separate, classified document devoted to hardware descriptions. Included therein are descriptions of low-light-level TV sensors, forward-looking infrared (FLIR) sensors, photographic cameras, and laser ranger/designator systems.

4.0   Electro-Optical System Performance Test and Evaluation

4.1   The Philosophy of Testing

4.1.1   Stages of Testing -- Testing can be categorized as developmental,

functional, or operational, depending upon the stage of development of the

test item. Developmental testing is concerned with the evaluation of design

features for the purpose of design development. The end result of developmental

testing is the proposed final design. Functional testing is concerned with the

performance evaluation of the final design as a whole. The principal method of

evaluation is the quantitative measurement of the ability of the test item to

perform its intended functions. The end result of functional testing is final

design acceptance or rejection. Operational testing is concerned with the evalua-

tion of the final design and production implementation of the test item. Of

primary interest is the ability of the test item to accomplish its intended

operational mission. The end result of operational testing is acceptance or re-

jection of the test item for service use and the recommendation of operational

procedures.

4.1.2   Testing Criteria -- The basic purpose of any stage of testing determines

the criteria used to evaluate the test results. The testing criteria, in turn,

are reflected in the tests to be performed and the test methods employed. Test-

ing criteria derive from one of three objectives: data acquisition, determination

of specification compliance, and evaluation of mission performance. In develop-

mental testing the intent is to acquire comprehensive information on the

characteristics of the item under test. Usually, no a-priori criteria are

imposed for performance acceptance or rejection. Functional testing, however, is primarily intended to evaluate the performance of the test item against specific criteria -- that is, for specification compliance. As previously indicated, operational testing is primarily concerned with mission performance. While some specific, quantitative requirements are imposed, test criteria for operational testing often are of a qualitative nature.

It should be recognized that the three stages of testing; developmental, functional, and operational; are not mutually exclusive. That is, the differences are primarily ones of emphasis. For example, functional testing often produces data that result in a design change. Thus, functional testing often takes on some aspects of developmental testing. For that reason, it is necessary, in functional testing, to test to a depth sufficient to allow engineering analysis of the problem. A "go" or "no-go" answer often is not sufficient. On the other hand, functional testing cannot ignore mission suitability in evaluating a new design. Compliance with published specifications is not sufficient if functional testing reveals an operational problem. Thus, while the following sections of this text will be concerned primarily with quantitative tests for specification compliance, it should be noted that functional testing should reflect mission requirements, including non-quantitative considerations when appropriate.

4.1.3 Test Regimes -- Functional airborne system tests are performed in the laboratory, in the aircraft on the ground, and in flight. For various reasons, testing is usually performed in that order. Tests performed on the bench in the laboratory are most convenient, quickest, cheapest, and safest. Flight

tests are least convenient, take the longest time, are most costly, and present the greatest danger to personnel and equipment. They also are most susceptible to uncertainties in the weather and availability of equipment. For the above reasons, tests should be performed in the laboratory, before installation in the aircraft, when feasible. Tests that can only be performed installed in the aircraft should be performed on the ground when feasible. Flight tests should be performed only when necessary and only when laboratory and ground tests have reduced the uncertainties to the greatest extent feasible. Of course, some tests can be performed only in flight; and, in any event, flight performance eventually must be demonstrated.

Flight tests sometimes can be performed in a test-bed aircraft. Such an arrangement allows in-flight tests to be performed with instrumentation far more extensive than would be possible with the system installed in the aircraft for which it was intended. In addition, a test bed aircraft can be employed for which flight operations are more convenient, less hazardous, and less costly. Testing in a test bed aircraft, however, cannot satisfy all flight testing requirements. The performance characteristics of all airborne systems are, to some extent, susceptible to the environment of the installation. Other factors influenced by the vehicle are the electrical power, cooling, electromagnetic interference, vibration, acceleration, and other environmental effects. In a digital system, software interaction is an important area for evaluation.

An alternative to some flight testing is flight simulation testing. The most useful "simulations" incorporate actual flight hardware for the system under test,

utilizing simulations only for generating external stimuli. Such a hybrid test simulation can, in fact, perform tests not possible in actual flight. Test "flights" can, for example, be rerun exactly, or with controlled modifications. The ability of a simulation to exactly duplicate test conditions is especially valuable in testing digital systems, where one-at-a-time modifications of the inputs are necessary to exercise the various logic branches of the software. Furthermore, real-time interrupts in a test simulation make possible the examination of internal system quantities not available in an actual flight situation.

This text is devoted to test methods peculiar to electro-optical system parameter determination and performance testing. Topics of general concern to airborne systems test and evaluation, such as test planning, test performance, instrumentation, data acquisition, and data analysis, are discussed in the text on Integrated Airborne Systems Test and Evaluation.

In the following sections, brief descriptions are given of the methods employed to determine system compliance with the major electro-optical system functional specifications. General testing, such as environmental, electromagnetic compatibility, reliability, and maintainability testing, is discussed in a separate text devoted to tests common to all airborne systems.

4.2 Infrared Scanner (FLIR) Performance Testing

4.2.1 Angular Resolution -- The angular resolution of an infrared imaging
system can be determined indirectly by determining its spatial frequency response.
The angular resolution, Θ_R, is related to the cut-off spatial frequency, $(SF)_{co}$,
by the equation:

$$\Theta_R = \frac{1}{(SF)_{co}}$$
(Radians)

For a discussion of methods of determining spatial frequency response, see Sections
4.2.19 & 4.2.20 of this text. A direct, in-flight method of determining the
angular resolution of an E/O sensor utilizes a resolution array of point source
(small, high-intensity) targets as shown in Figure 4.2.1.1. The process is as
follows:

(a) Fly prescribed flight path toward E/O target array, at constant altitude.

(b) Determine aircraft position (range to target) by range instrumentation
and record as a function of time.

(c) Acquire E/O target on sensor.

(d) Utilizing a video recorder or cockpit camera, record E/O sensor display
imagery.

(e) Determine E/O sensor linear resolution, as a function of time, by noting
the apparent number of E/O sources discerrible at any given time.

(f) Correlate range and resolution data to obtain resolution as a function
of range.

(g) Calculate E/O sensor angular resolution, Θ_R, as the ratio of linear
resolution, W_R, to range, R. That is:
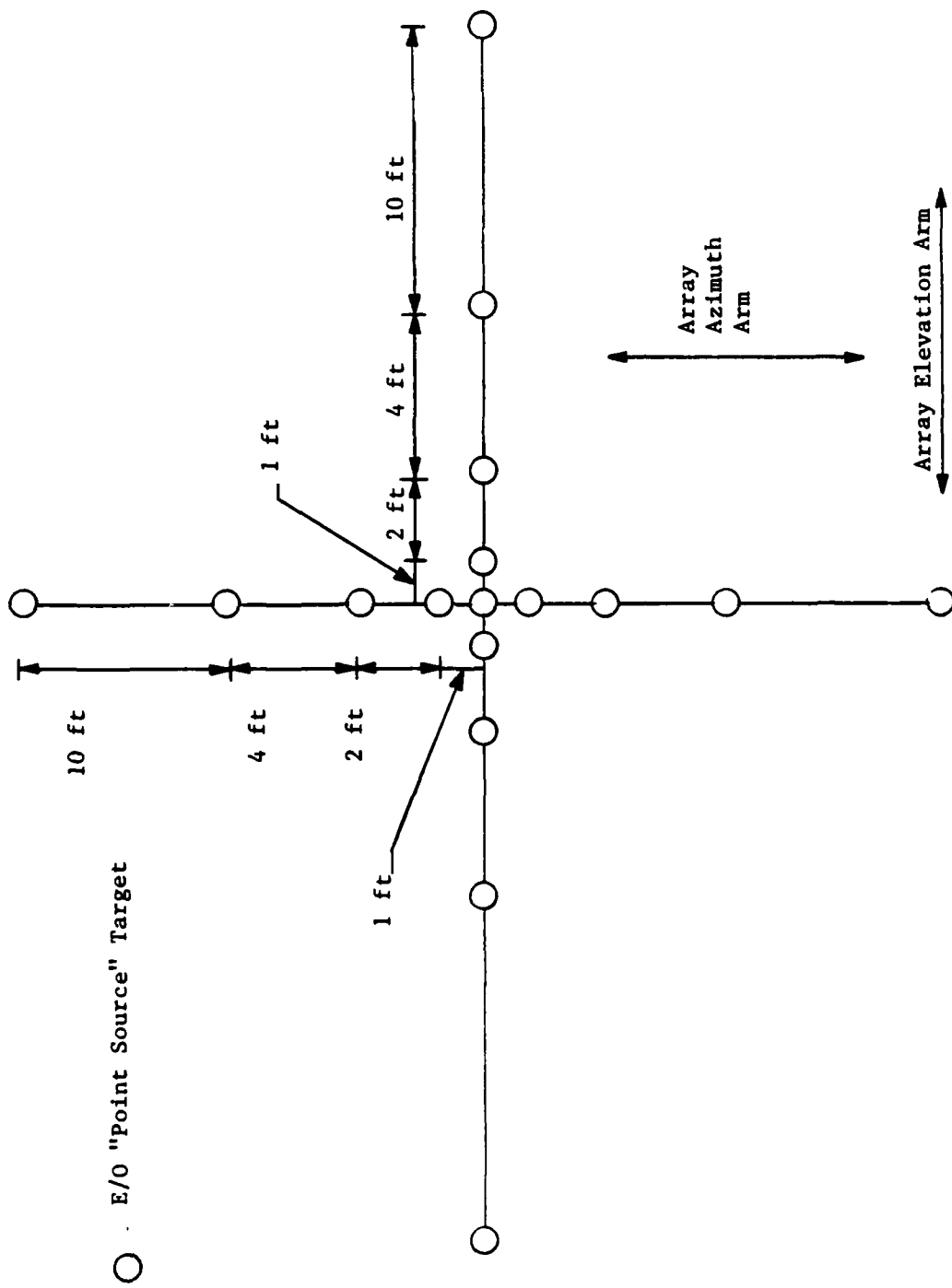
Figure 4.2.1.1--Air-to-Ground E/O Target Resolution Array

○ E/O "Point Source" Target

10 ft
4 ft
2 ft
1 ft

10 ft
4 ft
2 ft
1 ft

Array Azimuth Arm
Array Elevation Arm

$$\theta_R = \frac{W_R}{R}$$

where:

R = Slant range to target at time of observation (Meters)

W_R = Minimum resolvable linear target separation (Meters)

The minimum resolvable linear target separation is derived from the apparent number of discernible targets according to the following table. (Both azimuth and elevation resolution can be determined from the array shown in the figure. The table applies (separately) to either axis.)

No. Targets	1	3	5	7	9
Linear Resolution (Feet)	>10	<10	<4	<2	<1

If the target array is not oriented perpendicular to the sensor line-of-sight, a correction must be made for geometric distortion.

Angular resolution can be directly measured on the ground, utilizing a scaled-down version of the resolution array and an optical collimator. The collimator "collimates" the radiation from a nearby target so that it appears to the sensor as a distant target. The 180-inch collimator employed at NAVAIRTESTCEN is described in Section 4.6.2 of this text.

Imaging "granularity" in some sensors produces inconsistent results in tests employing point sources. In such cases, the granularity itself should be evaluated.

4.2.2 Bandwidth (Optical Bandwidth, Temperature Bandwidth) -- The range of optical radiation frequencies to which an I/R sensor responds can be determined through the use of a suitable I/R source and a monochrometer as shown in Figure 4.2.2.1. The monochrometer is a device that transmits only radiation within a narrow bandwidth. In order to determine the response bandwidth of an I/R system, the source/monochrometer must be calibrated (the spectral radiant intensity determined as a function of frequency or wavelength). The bandwidth of the response of the I/R sensor is determined by the following procedure.

(a) Adjust monochrometer to desired wavelength and record wavelength.

(b) Record quantitative sensor output.

(c) Calculate ratio of sensor output to sensor input radiant flux.

(d) Repeat steps (a) through (c) to obtain data beyond the half-power points of the sensor response curve in both directions.

(e) Calculate bandwidth of sensor as the frequency span between the half-power points.
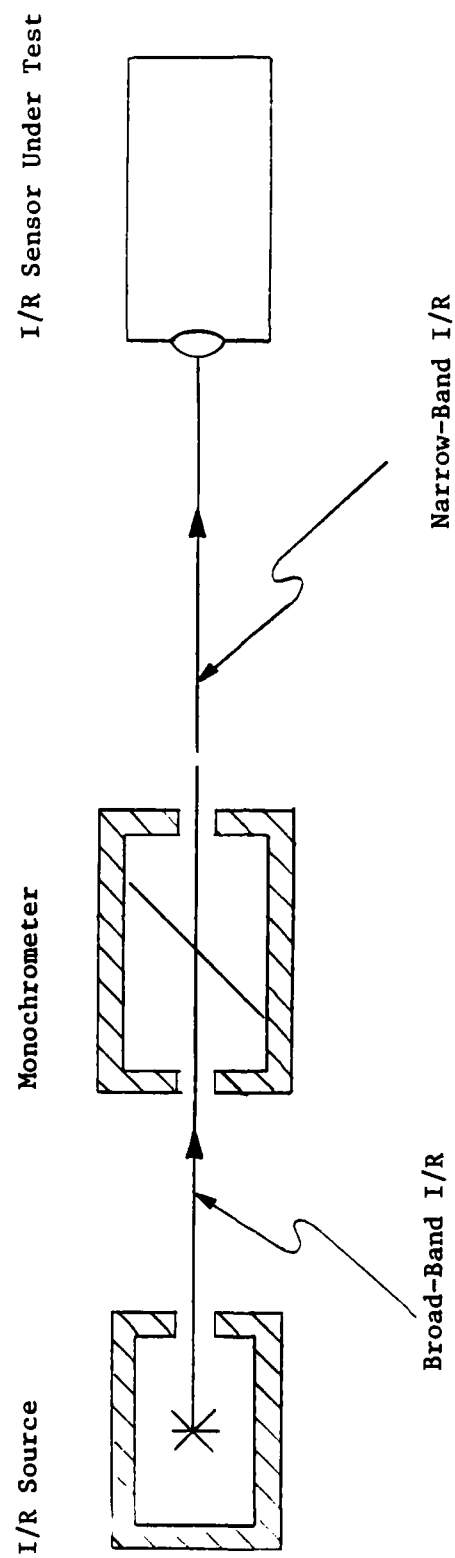
Figure 4.2.2.1 -- I/R Sensor Bandwidth Determination Test Setup

4.7a

4.2.3 Bearing Accuracy -- In-flight determination of bearing accuracy can be
performed according to the following procedure.

  (a) Fly prescribed flight path, at constant altitude, toward well-defined
      target of known position.

  (b) Acquire target on sensor.

  (c) Vary bearing to target and record indicated bearing as a function of
      time.

  (d) Track aircraft using range instrumentation and calculate test aircraft-
      to-target bearing (truth data) from range data and aircraft heading.

  (e) Compare target bearing indicated by sensor to truth data, by time
      correlating data.

4.2.4 Blind Ranges (Active Sensors) -- The blind ranges produced by eclipsing

in an active, pulsed E/O   sensor are generally greater than the maximum

useful range of the sensor (because of the large pulse repetition interval

usually employed). When significant blind ranges, including the minimum range,

exist, they can be determined by the following procedure.

   (a) Fly prescribed flight path, at constant altitude, toward well-defined
       target of known position.

   (b) Acquire target on sensor.

   (c) Continue to close on target monitoring sensor indication for dropouts.

4.2.5 Boresight Accuracy -- The alignment of the E/O sensor line-of-sight
reference (boresight) with the aircraft armament datum line is determined
employing a special test fixture, incorporating an I/R target and collimator
(or autocollimator), which bolts to the airframe and provides an on-boresight
target. The following procedure is employed.

   (a) Affix test fixture to aircraft.

   (b) Set sensor line-of-sight reference to zero azimuth and zero elevation.

   (c) Note indicated position of test target in relation to sensor LOS
       reference (boresight).

The relative alignment of the boresight of an E/O sensor with respect to the
boresights of other sensors and systems can be determined by simultaneously
acquiring a known target on the boresight of the respective sensors and com-
paring their indicated positions. Both on-the-ground and in-flight procedures
are employed.

4.2.6 Field-of-View (FOV) -- The overall field-of-view of an E/O sensor can be determined on the ground utilizing a target and a collimator; on the ground using a fixed, distant target; or in flight. When a fixed target is employed, the sensor boresight line-of-sight is slewed until the target appears at the extremities of the field-of-view and the corresponding sensor slew angles are noted. When a target moving relative to the aircraft is employed, the target is moved to the extremities of the FOV and the angular FOV of the sensor is calculated from the known (measured) target positions.

4.2.7 Image Definition -- The clarity of the imaging capability of an E/O
sensor is best determined indirectly by determining its spatial frequency
response in accordance with the procedures discussed in Section 4.2.19 of this
text. In any event, image definition should be evaluated employing a target/
collimator arrangement as described in Section 4.6.2 of this text. While
actual, distant targets are more realistic, they are difficult to define
quantitatively and their images suffer from atmospheric effects. Qualitative
checks should, however, be performed, in flight, on representative, mission-
related targets.

4.2.8 Instantaneous Field-of-View (IFOV) -- The instantaneous field-of-view of a scanned point-source-detecting E/O sensor can be determined indirectly by determining its angular resolution. The angular instantaneous field-of-view, Θ_{IFOV}, is related to the angular resolution, Θ_R, by the equation:

$$\Theta_{IFOV} = \Theta_R \qquad \text{(Radians)}$$

This equation neglects all resolution-limiting effects except the finite size of a detector element. (See Section 3.3.4 of this text.) In order to minimize the effects of other factors on resolution, and hence IFOV, the sensor response should be monitored directly at the detector output.

The sensor instantaneous field-of-view can be determined directly using a point (very small, intense) source and a collimator. The sensor scanning motion is halted and the point source position in the sensor field-of-view is altered, noting the positions at which the source leaves the field-of-view of a given detector element. This method often is impractical since it requires that the scanning motion be halted and that the output of a single detector element be accessible.

4.2.9 Line-of-Sight Slew Limits -- In order to determine the LOS slew angle limits, the E/O sensor is slewed to the limit of its travel about all axes. The angular limits can be measured directly from the sensor head gimbals or calculated from linear measurements from a reference to the sensor boresight. The azimuth and elevation look angles also can be read from the sensor direction indicators.

4.2.10 Line-of-Sight Slew Rates -- The maximum sensor line-of-sight slew rates are most readily determined by commanding sensor head slew from one limit to the opposite limit and timing the transit with a stop watch. In-flight determination of the maximum automatic (tracking) slew rates can be effected by flying a path with respect to the target calculated to produce a prescribed maximum LOS slew rate. (The maximum LOS slew rate is equal to the ratio of the ground speed of the aircraft to the aircraft-to-target distance-of-closest-approach. The distance-of-closest-approach is decreased, in successive runs, until target track is broken due to excessive LOS slew rate.

4.2.11 Line-of-Sight Drift Rate - The long-term LOS instability (drift rate) of an E/O sensor is best determined on the ground, utilizing the following procedure, illustrated in Figure 4.2.11.1.

(a) Align the sensor LOS reference (e.g. cross-hairs) on a prominent, fixed point target, at a known distance.

(b) After various time intervals, note the positions of the points in the target plane at which the sensor reference is then directed.

(c) Calculate the sensor drift rate according to the formula:

$$\overset{\circ}{\theta} = \frac{Tan^{-1}\left[D(t_1)/R\right]}{t_1 - t_0}$$

where: $D(t_1)$ = Linear Drift Distance at Range R (Meters) at Time t.

R = Range from sensor to Target Plane (Meters)

t_1 = Time of Measurement (Seconds)

t_0 = Time of Initial Alignment (Seconds)

The drawing in Figure 4.2.11.1 depicts a measurement of azimuth drift. The same procedure is employed to determine drift in elevation.
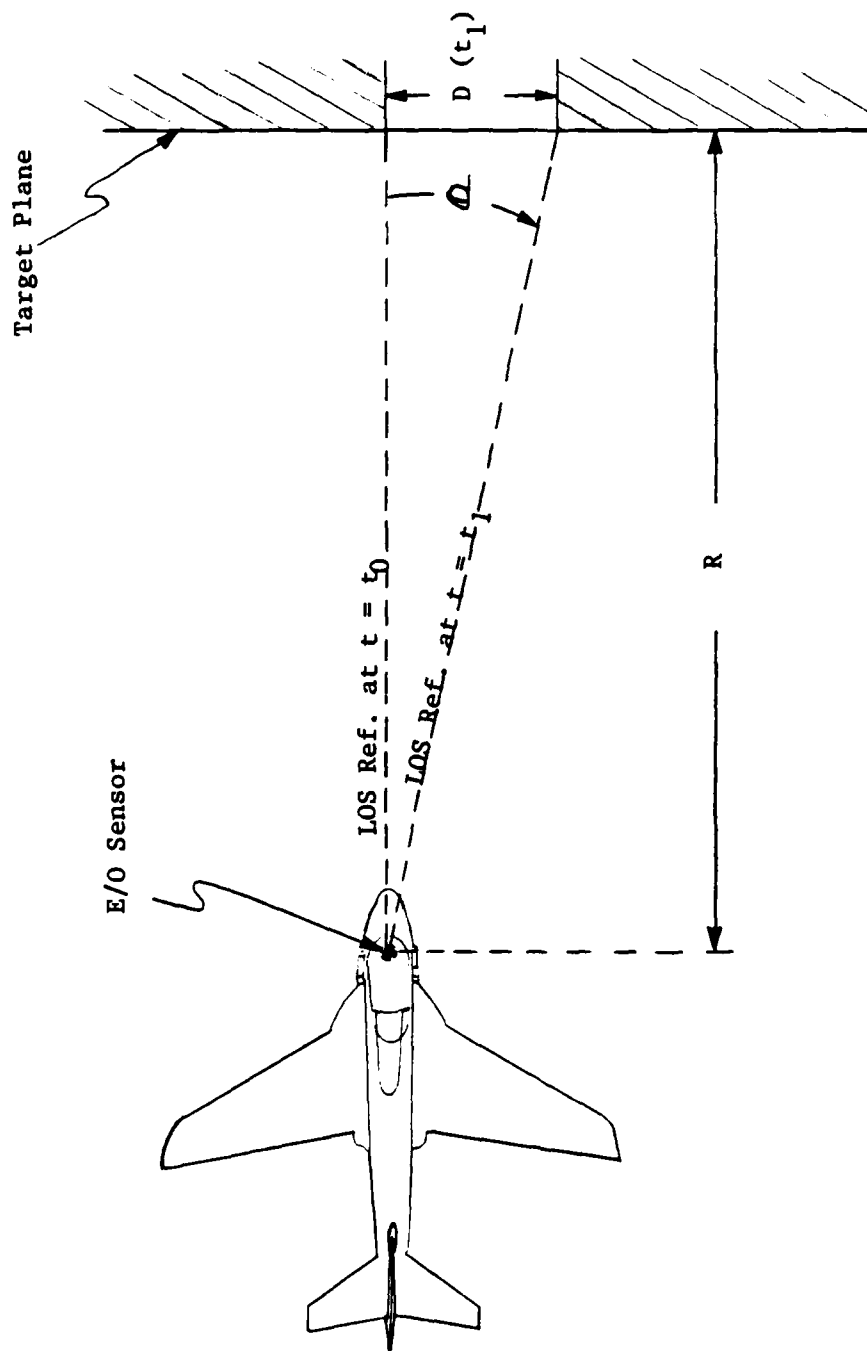
Figure 4.2.11.1 -- E/O Sensor Line-of-Sight Drift Rate Test Setup

4.16a

4.2.12 Line-of-Sight Jitter -- The short-term LOS instability (jitter) of E/O sensor must be determined in flight since in-flight vibration is a major contributor to LOS jitter. The usual method of measurement of LOS jitter is indirect and utilizes the measurable loss of sensor angular resolution due to LOS jitter. The method of determination of angular resolution and the method of deriving LOS jitter from in-flight measurements are presented in Section 4.2.20 of this text. A direct method of determining the LOS jitter of an E/O imaging sensor is to record the displayed image of a well-defined source, (utilizing a camera or video recorder), and measure the actual jitter in the displayed image.

4.2.13 Maximum Ranges for Detection and Recognition -- The maximum ranges at

which an E/O sensor provides detection and recognition of a target must be de-

termined in flight, and can utilize an E/O sensor bar target as described in

Section 4.6.1 of this text or a mission-related target of known location. The

E/O bar target has the advantage of known, controlled characteristics. Mission-

related targets have the advantage of realism. Although the radiant intensity

of some mission-related targets can be measured by independent instrumentation,

quantitative sensor evaluation generally requires the use of a specially de-

signed target such as the bar target described herein. The procedure for de-

termining the maximum detection and recognition ranges is as follows:

(a) Fly prescribed flight path, at constant altitude, toward well-defined
target at known location.

(b) Determine aircraft position (range to target) by range (ground) in-
strumentation or by on-board ranging system and record as a function
of time.

(c) Align sensor line-of-sight to place E/O target of known anticipated
position in field-of-view of sensor.

(d) Acquire target on sensor. (Note time of acquisition as time of
detection.)

(e) Continue observing E/O target on sensor until target features (bars
for a bar-target) become distinguishable. (Note time of feature
definition as time of recognition.)

(f) Correlate aircraft-to-target range times with detection and
recognition times to obtain maximum ranges for detection and
recognition. Note that the maximum detection and recognition
ranges are a function of the radiant and spatial characteristics of
the target, the ambient background illumination, and the atmospheric
conditions at the time of the test. To be meaningful, the maximum
ranges must be associated with specific target characteristics and
test conditions.

4.18

E/O Target

Slant Range

Sensor Line – of – Sight

Range Tracking System

E/O Sensor

Altitude
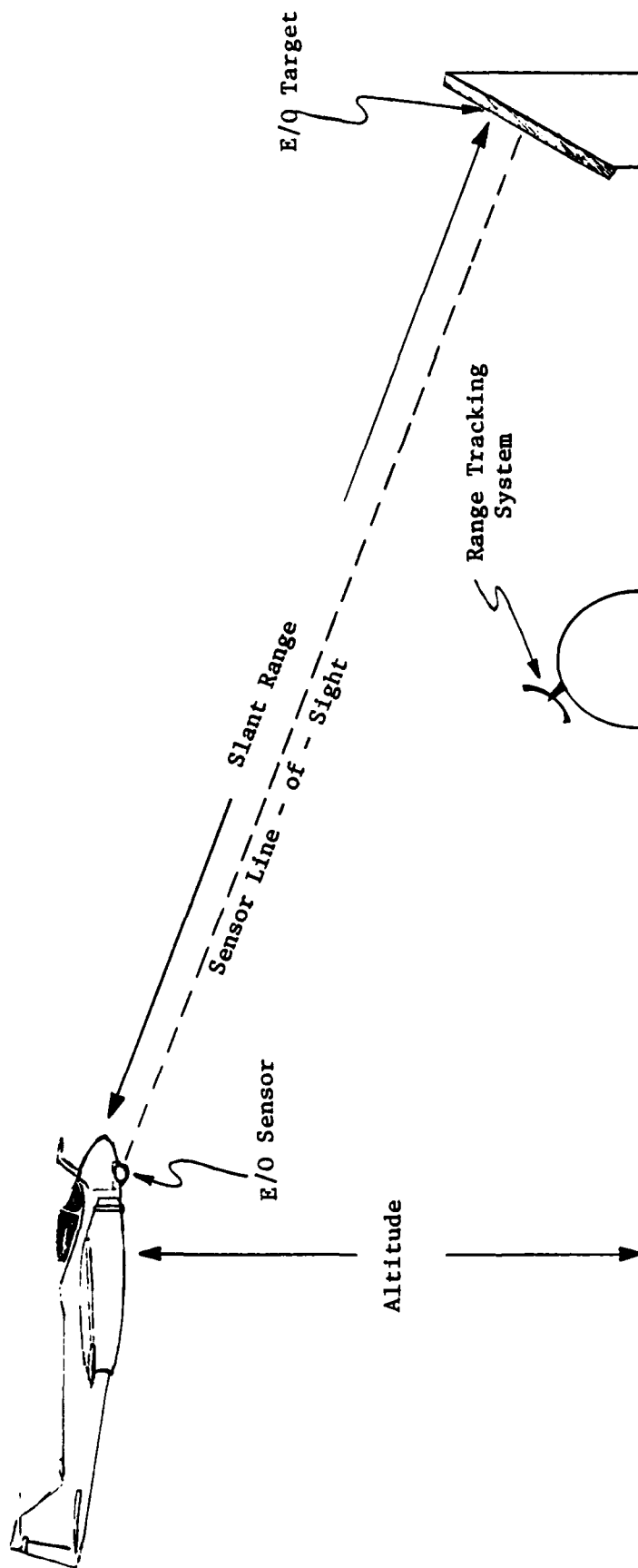
Figure 4.2.13.1 -- Test Setup for Determination of E/O Sensor Maximum Detection and Recognition Ranges

4.18a

4.2.14 Minimum Resolvable Temperature Differential (MRΔT) (Thermal Resolution) -- The minimum target temperature differential resolvable by an imaging thermal detector is best determined by the combined angular resolution/ thermal resolution test described in Section 4.2.20 of this text. A simpler procedure for determining MRΔT also employs a bar target as described in Sections 4.6.1 and 4.6.2 of this text and is presented below.

(a) Set the spatial frequency of the bar target to a value well below one-half of the sensor cut-off frequency.

(b) Adjust the bar target temperature differential to a value well above the expected MRΔT of the sensor under test.

(c) Focus the sensor on the bar target and optimize the sensor control settings.

(d) Gradually reduce the bar target temperature differential, allowing sufficient time for stabilization between changes, until the variations in radiant intensity due to the individual bars are no longer discernible on the sensor display.

(e) Gradually increase the bar target temperature differential until the variations in radiant intensity due to the individual bars are just discernible.

(f) Record the bar target temperature differential attained in Step (e) as the MRΔT for the sensor.

4.2.15 Noise Equivalent Temperature Differential (NEΔT) -- The noise-

equivalent input temperature differential for a thermal detector can be de-

termined by the following procedure.

   (a) Set the spatial frequency of a thermal bar target to a value well
       below one-half of the sensor cut-off frequency.

   (b) Adjust the bar target temperature differential to a value well above
       MRΔT for the sensor under test.

   (c) Focus the sensor on the target and optimize the sensor control settings.

   (d) Adjust the bar target temperature differential to a value that produces
       a target signal just large enough to be measured accurately in the
       presence of the noise.

   (e) Record the target temperature differential and resulting sensor video
       output voltage response attained in step d.

   (f) Block the target input to the sensor and measure the rms noise on the
       sensor video output voltage.

   (g) Calculate the sensor NEΔT according to the equation:

       $$NE\Delta T = \frac{N}{S} \Delta T \qquad \text{(Degrees, Kelvin)}$$

where: N = RMS Noise Voltage on Sensor Video Output Signal. (Volts)

              S = Peak-to-Peak Variation in Sensor Video Output Voltage due to
                  Bar Target   (Volts)

              ΔT = Bar Target Temperature Differential producing the Output
                   Signal S (Kelvin, Degrees).

4.2.16 Pointing Accuracy -- The maximum error within which an E/O sensor line-of-sight reference can be aligned with a given direction (azimuth and elevation) can be determined utilizing a target of known orientation with respect to the aircraft datum line. Such a target is best provided by a collimating fixture similar to that employed for boresight accuracy measurements, (see Section 4.2.5 of this text), but with the capability of providing off-boresight targets.

4.2.17 Ranging Accuracy -- Ranging is performed by a passive E/O sensor by computing range from measurements of the aircraft (sensor) altitude and the sensor line-of-sight depression angle, according to the equation:

$$SR = \frac{h}{\sin(\delta)}$$

where: h = Aircraft (Sensor) Altitude (Meters)

       SR = Sensor-to-Target slant range (Meters)

       δ = E/O Sensor LOS Depression Angle (Angle between sensor-to-target LOS and the horizontal).

Ranging accuracy can be measured directly by ranging on a target of known position relative to the sensor or it can be inferred from sensor LOS pointing accuracy. (See Section 4.2.16 of this text).

4.2.18 Range Resolution -- The range resolution of a passive E/O sensor depends upon its angular resolution (in elevation) and can be inferred from that sensor characteristic.

4.2.19 Spatial Frequency Response -- The spatial frequency response of an E/O sensor can be determined directly by viewing a target the radiance of which varies sinusoidally with position on the target. However, such a target is very difficult to construct and control. For that reason, spatial frequency response generally is determined uti'izing a bar target (a target the radiance of which varies as a square wave with position on the target). Such a target can be an air-to-ground target such as the one described in Section 4.6.1 of this text or it can be a scaled-down target and collimator such as the one described in Section 4.6.2 of this text. Of course, the bar target yields not the response of the system to a sinusoidal variation in radiance but the response to a square wave. The results, however, can be considered an approximation of the response to a sinusoidal variation with spatial frequency equal to that of the fundamental Fourier component of the square wave.

A generalized procedure for determining the spatial response of an E/O sensor to a bar target is as follows.

(a) Adjust the differential radiance of the bar target (temperature difference between hot and cold bars for a thermal sensor) to a value well above the minimum resolvable differential for the sensor under test.

(b) Adjust the spatial frequency of the target as seen by the sensor to a value well below one-half of the expected sensor cut-off frequency.

(As indicated in Section 4.6.1 of this text, the (angular) spatial frequency of a bar target, (such as the one described in Section 4.6.1), at an actual range R_T, is given by the equation:

$$SF_T = \frac{R_T}{W_{/C}}$$

where:

R_T = Sensor-to-Target Range (Meters)

W_{1c} = Width of one cycle of Target (one Bar and Space) (Meters)

The spatial frequency in tests utilizing such targets is usually adjusted by varying sensor-to-target range rather than target bar and space width. As indicated in Section 4.6.2 of this text, the spatial frequency of the collimated image of a bar target, (such as the one described in Section 4.6.2), is independent of the actual sensor-to-target range and is given by:

$$SF_T = \frac{FL_c}{W_{1c}}$$

where:

FL_c = Focal Length of Collimator (Meters)

W_{1c} = Width of one Cycle of Target (One Bar and Space) (Meters)

The spatial frequency in tests utilizing collimated-image targets is usually adjusted by varying the actual target bar and space width.)

(c) Acquire the bar target on the sensor and focus the sensor on the target.

(d) Observe the sensor video output signal and determine the maximum and minimum values of the output signal, as indicated in Figure 4.2.19.1.

(e) Repeat steps (b) through (d), substituting increasingly greater target spatial frequencies in step (b), until the sensor response (Vmax-Vmin) is too small to measure.

(As indicated in Section 2.3.2 of this text, the output of a scanning E/O sensor vanishes at the cut-off spatial frequency. At frequencies above the cut-off value, a "false" response occurs. Care must be taken to avoid mistaking "false" response for true response.)

4.24
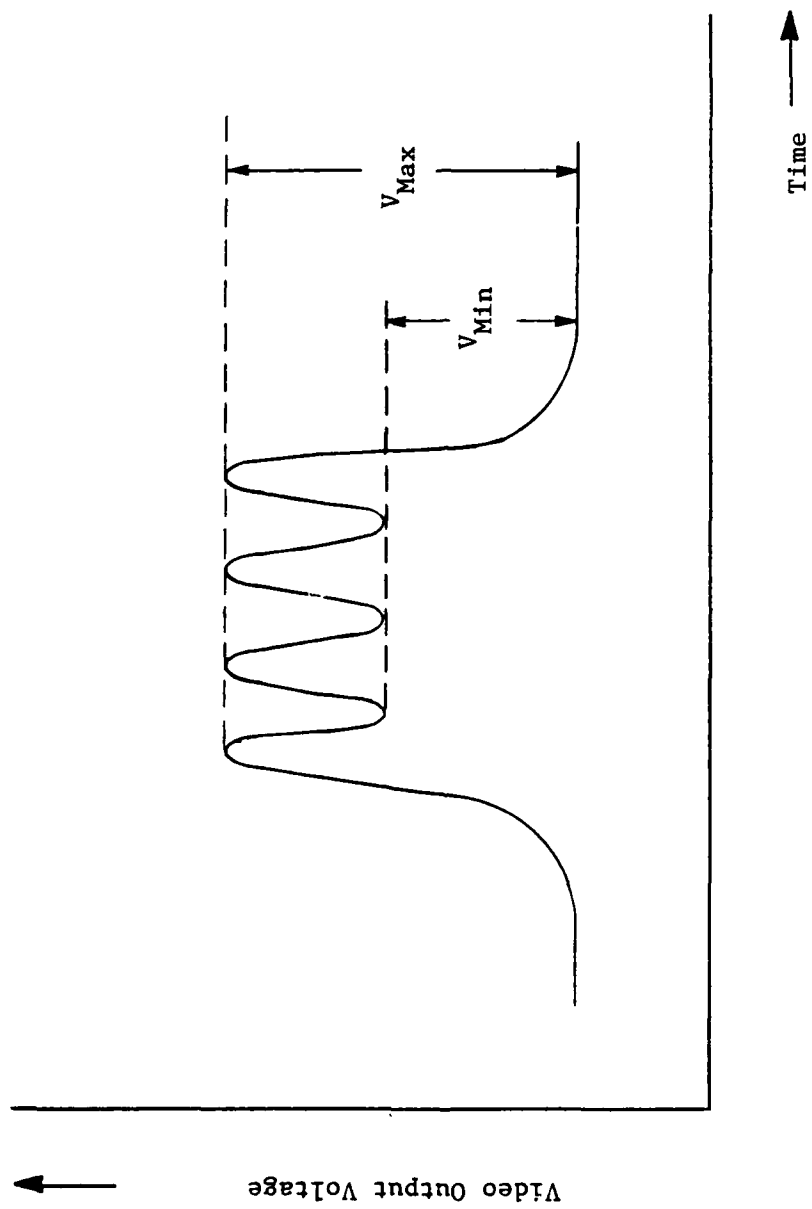
Figure 4.2.19.1 -- E/O Sensor Video Output Response to a 4-Bar Target

4.24a

The spatial response of an E/O sensor to a bar target may be defined as the ratio given by the following equation.

$$SR = \frac{V_{Max} - V_{Min}}{V_{Max} + V_{Min}}$$

Plotted versus the apparent spatial frequency of the target, the spatial response of an E/O sensor to a bar target is similar to those shown in Figures 2.3.2.2 and 3.3.6.4 in Sections 2.3.2 and 3.3.6 of this text, respectively.

4.2.20 Combined Angular Resolution and Thermal Resolution -- The angular resolution and thermal resolution of an E/O sensor are best determined by the integrated test procedure presented below. In order to determine the effect of the in-flight environment on the sensor, the procedure consists of two parts. The ground test is performed first, followed by the in-flight test.

Ground Test Procedure

(a) Adjust the spatial frequency of a collimated bar target, (as described in Section 4.6.2 of this text), to a value well below one-half the expected cutoff frequency for the sensor under test.
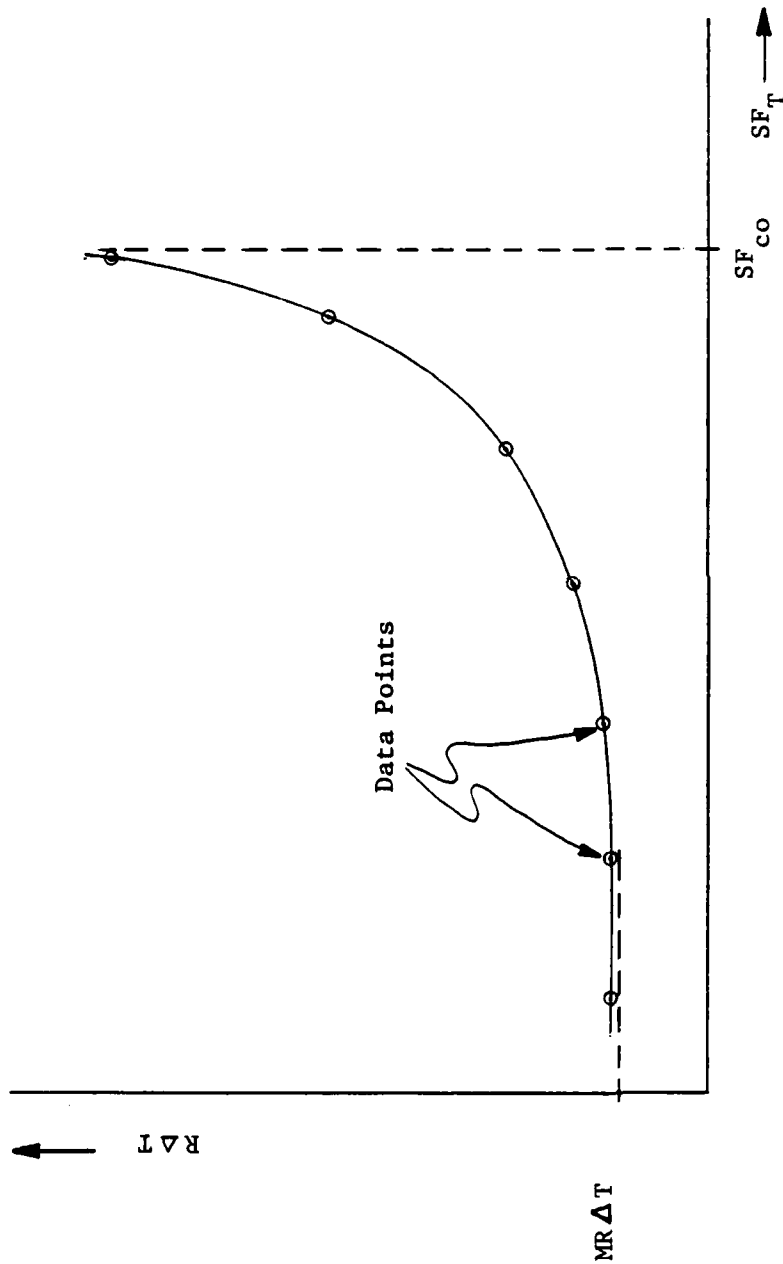
(b) Adjust the bar target temperature differential to a value well above the expected MRΔT of the sensor under test.

(c) Focus the sensor on the target and optimize the sensor control settings.

(d) Reduce the bar target temperature differential to a value below the MRΔT of the sensor under test.

(e) Gradually raise the target temperature differential, while monitoring the sensor display, until the variations in radiant intensity due to the individual bars in the target just become discernible.

(f) Measure the temperature differential attained in step (e).

(g) Record the bar target temperature differential and spatial frequency attained in step (e).

(h) Increase the spatial frequency of the bar target by a suitable increment.

(i) Repeat steps (d) through (h) until the individual bars of the target can no longer be discerned even for the maximum target temperature differentials utilized in the test.

The data acquired in the preceding procedure provide measurements of the resolvable temperature differential, for the sensor, as a function of bar target spatial frequency. The results, when plotted as shown in Figure 4.2.20.1, yield the minimum resolvable temperature differential (MRΔT) and the spatial cutoff frequency (SF$_{co}$), of the sensor under test. As indicated in the figure, the

Data Points

SF_{co}

$SF_T \longrightarrow$

$R\Delta T$

$MR\Delta T$

$R\Delta T$ = Resolvable Temperature Differential (C°)

SF_T = Spatial Frequency of Bar Target (Cycles/Radian)

$MR\Delta T$ = Minimum Resolvable Temperature Differential (C°)

SF_{co} = Cut-off Spatial Frequency (Cycles/Radian)

Figure 4.2.20.1 -- Results of Combined Angular Resolution and Thermal Resolution Test for an E/O Sensor

asymptotic value of RΔT at low spatial frequencies represents the MRΔT for the sensor under test. The asymptotic value of SF_T at high resolvable temperature differentials represents the spatial cutoff frequency for the sensor under test.

In-Flight Test Procedures

(a) Set the bar/space width of a bar target, (as described in Section 4.6.1 of this text), to a value calculated to provide suitable spatial frequencies, at the planned test ranges, for the system under test.

(b) Adjust the effective temperature differential of the bar target to the maximum value planned for the test.

(c) Fly a prescribed flight path, at constant altitude and airspeed, on a heading designed to pass directly over the E/O target, and normal to the face of the target.

(d) Determine the sensor/aircraft position (and, hence, sensor-to-target range) with suitable range instrumentation or an on-board ranging device.

(e) Acquire the E/O target on the sensor under test.

(f) Continue to observe the target on the sensor until the variations in radiant intensity due to the individual bars are just discernible.

(g) Measure and record the resolvable temperature differential and the range (spatial frequency) attained in step (f).

(h) Repeat steps (b) through (g), substituting, in step (b), increasingly small target temperature differentials, until the variations due to individual bars are no longer discernible even at the minimum sensor-to-target ranges planned for the test.

When the resolvable temperatures determined by the in-flight test are plotted versus the spatial frequency of the target, the results are very similar to those, shown in Figure 4.2.20.1, determined by the ground test. The only significant difference should be that the in-flight spatial cut-off frequency of the sensor should be somewhat lower than that attained in ground test. A

4.27

plot showing both in-flight and ground test results is presented in Figure
4.2.20.2. For a properly-functioning sensor, the degradation of angular
resolution in flight is due primarily to sensor line-of-sight jitter. For
given values of stable-line-of-sight sensor cut-off frequency (ground test)
and jittered-line-of-sight sensor cut-off frequency (flight test), the sensor
angular line-of-sight jitter can be determined by the curve presented in
Figure 3.3.5.1 in Section 3.3.5 of this text and reproduced in Figure 4.2.20.3.
The relationship between sensor cut-off spatial frequency, SF_{co}, and sensor
angular resolution, θ_R, is given by the equation:

$$\theta_R = \frac{1}{(SF)_{co}} \qquad \text{(Radians)}$$

The axes of the graph in Figure 4.2.20.3 are labeled in terms of cut-off spatial
frequency.
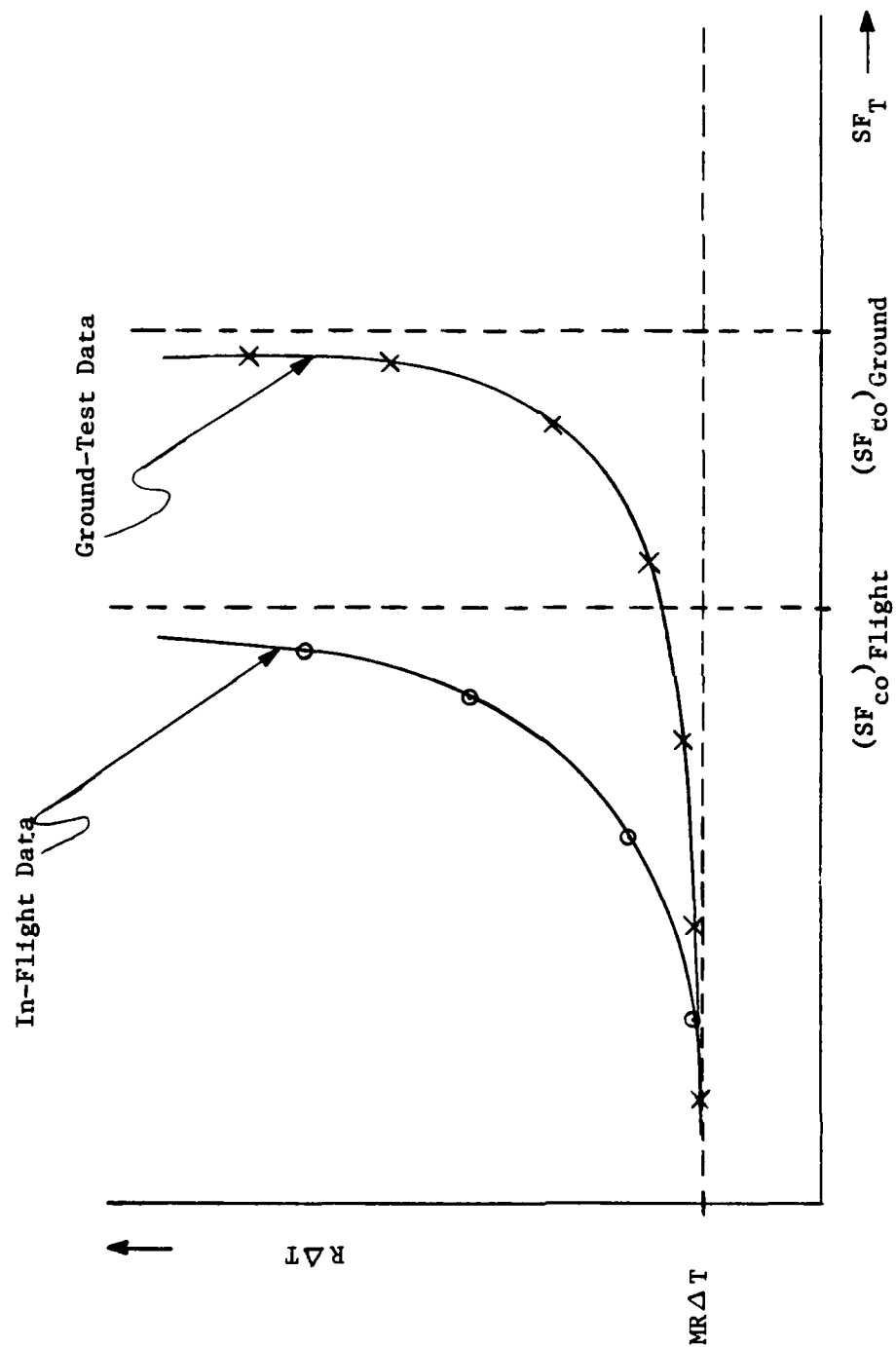
Figure 4.2.20.2 -- Comparison of Ground-Test and In-Flight Data for the Angular and Thermal Resolution of an E/O Sensor

4.28a
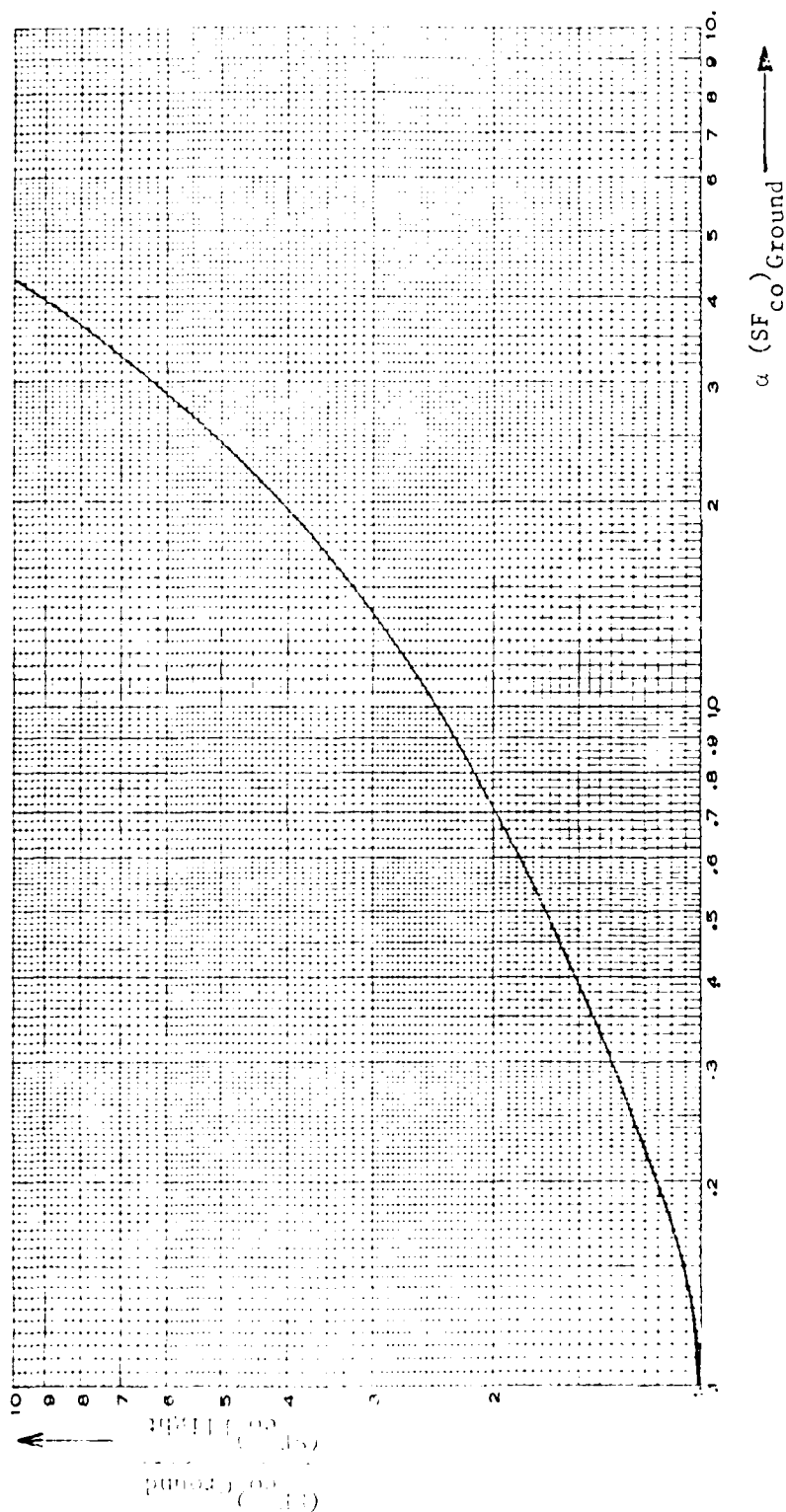
$(SF_{co})_{Flight}$ = Cut-off spatial frequency of sensor with LOS jitter (Cycles/Radian)

$(SF_{co})_{Ground}$ = Cut-off spatial frequency of sensor without LOS jitter (Cycles/Radian)

α = RMS value of sensor LOS jitter (Radians)

α $(SF_{co})_{Ground}$ ⟶

Figure 4.2.20.3 -- Effect of Line-of-Sight Jitter on Sensor Angular Resolution

4.2.21 Sensor Time Response -- The response of an E/O sensor to time-related
variations in target radiant intensity can be determined as steady-state
(sinusoidal) time-frequency response or transient (impulse or step-function)
response. The time-frequency response can be determined by subjecting the
sensor to a sinusoidal intensity modulated source and measuring the amplitude
and phase variations in the video output signal from the sensor. The transient
response can be determined by subjecting the sensor to a pulsed intensity
modulated source and recording the sensor video output signal response as a
function of time.

4.2.22 Tracking Performance -- Three fundamentally different methods of "position tracking" are employed with E/O sensors. True image tracking utilizes the video signal produced by the target and tracks some feature of the target image as seen by the tracker (the centroid of the image, edge of the image, etc.). Inertial position tracking utilizes information from an inertial navigation system and tracks a fixed location on the surface of the earth. Target designator tracking tracks illumination from a laser target designator. In any case, the tracking error can be determined by the following procedure.

(a) Fly a prescribed flight path toward a prominent E/O target of known location.

(b) Determine the sensor/aircraft position and velocity with suitable range or on-board instrumentation.

(c) Acquire the E/O target on the sensor.

(d) Initiate target track at the earliest practicable instant. (Record corresponding range as maximum track acquisition range.)

(e) Alter flight path and attitude of aircraft in order to subject E/O sensor tracking line-of-sight to specified LOS rates.

(f) Measure and record E/O sensor video signal and tracking error signal as a function of time. (The E/O sensor display also can be recorded utilizing a cockpit camera.)

(g) Correlate derived tracking errors with LOS slew rates by time correlating data obtained in steps (b) and (f).

4.3 Low-Light-Level Television Performance Testing

The performance testing methods outlined in Section 4.2 of this text, for scanning infrared sensors, are applicable to the performance testing of low-light level television sensors, with the comments, modifications, and exceptions noted below.

4.3.1 Tests Applicable Without Modification

The following test procedures, outlined in Section 4.2, are applicable without exception to the testing of low-light-level television sensors.

Test	Section
Angular Resolution	4.2.1
Bandwidth	4.2.2
Bearing Accuracy	4.2.3
Blind Ranges	4.2.4
Boresight Accuracy	4.2.5
Field-of-View	4.2.6
Image Definition	4.2.7
Instantaneous FOV	4.2.8
LOS Slew Limits	4.2.9
Max. LOS Slew Rate	4.2.10
LOS Drift Rate	4.2.11
LOS Jitter	4.2.12
Max. Range for Detection and Recognition	4.2.13
Pointing Accuracy	4.2.16
Ranging Accuracy	4.2.17
Range Resolution	4.2.18
Spatial Frequency Response	4.2.19
Time Response	4.2.21
Tracking Performance	4.2.22

4.3.2 Tests Applicable With Modification -- The procedures outlined in Section
4.2.14 (Minimum Resolvable Temperature Differential), Section 4.2.15 (Noise
Equivalent Temperature Differential), and Section 4.2.20 (Combined Angular
Resolution and Thermal Resolution) are applicable to the testing of low-light-
level television sensors with the substitution of the following photometric
terms for radiometric terms.

Radiometric Term	Photometric Term
Radiant Flux (Watts)	Luminous Flux (Lumens)
Radiant Intensity (W/Sr)	Luminous Intensity (Lm/Sr)
Radiance (W/Sr-M^2)	Luminance (Lm/Sr-M^2)
Radiant Exitance (W/M^2)	Luminous Exitance (Lm/M^2)
Irradiance (W/M^2)	Illuminance (Lm/M^2)
Differential Temperature (C°)	Differential Luminous Exitance (Lm/M^2)
Thermal Resolution (C°)	Luminosity Resolution (Lm/M^2)

MICROCOPY RESOLUTION TEST CHART
NATIONAL BUREAU OF STANDARDS-1963-A

4.4 Laser Ranger/Designator Performance Testing

The performance testing methods outlined in Section 4.2 of this text, for
scanning infrared sensors, are applicable to the performance testing of laser
ranger/designators, with the comments, modifications, and exceptions noted
below.

4.4.1 Tests Applicable Without Modification -- The following test procedures,
outlined in Section 4.2, are applicable without exception to the testing of
laser/designators.

Test	Section
Line-of-Sight Slew Limits	4.2.9
LOS Slew Rates	4.2.10

4.4.2 Bandwidth -- The spectral characteristics of the radiation emitted by a laser/designator can be determined utilizing the test setup depicted in Figure 4.6.1.4 in Section 4.6.1 of this text. As indicated in that figure, the laser beam is locked onto a diffuse, uniformly reflecting target and the spectral radiant intensity is determined using a spectral radiometer. Although the figure indicates an in-flight test, the spectral characteristics of a laser beam are more conveniently and accurately determined on the ground and at short range to avoid atmospheric absorption.

4.4.3 Boresight Accuracy -- The boresight alignment of a laser/designator is best determined by ground test, utilizing a collimated-target test fixture similar to the one described in Section 4.6.2 of this text. The test procedure is listed below.

   (a) Acquire and focus E/O sensor on point-source target aligned with aircraft armament datum line.

   (b) Place a paper shield over target and mark ADL reference position on paper. (Materials other than paper can be used.)

   (c) Fire laser, burning small spot on paper shield.

   (d) Measure displacement of laser burn spot from ADL reference mark.

   (e) Convert linear laser boresight error (D_e) to angular laser boresight error (δ_e) according to the equation:

$$\delta_e = Tan^{-1}\left[\frac{D_e}{FL_c}\right] \qquad \text{(Radians)}$$

   where:

   D_e = Linear Laser Boresight Error (Meters)

   FL_c = Focal Length of Collimator (Meters)

The pointing accuracy of a laser/designator can be determined utilizing the above test procedure to check laser alignment with points off boresight (displaced from the aircraft armament datum line).

4.4.4 Line-of-Sight Drift Rate -- The long-term line-of-sight instability (drift rate) of a laser/designator is best determined using the collimated target test setup employed in the boresight test described in Section 4.4.3 of this text. The procedure is as follows.

(a) Conduct steps (a) through (d) of the boresight test, obtaining a laser burn spot on the paper target.

(b) After a suitable designated time, fire the laser again, obtaining a second burn spot on the target.

(c) Measure the relative displacement between the two laser burn spots.

(d) Calculate the laser/designator LOS drift rate, $\dot{\theta}_d$, according to the equation:

$$\dot{\theta}_d = \left(\frac{1}{t_d} \right) Tan^{-1} \left[\frac{D_d}{FL_c} \right] \qquad \text{(Radians/Sec)}$$

where:

D_d = Relative Linear Displacement between Two Burn Spots (Meters

FL_c = Focal Length of Collimator (Meters)

t_d = Time Interval between Two Laser Firings (Secs.)

4.4.5 Line-of-Sight Jitter -- The short-term LOS instability (jitter) of a laser/designator must be determined by flight test since in-flight vibration is a major contributor to LOS jitter. The test procedure employs the test setup depicted in Figure 4.6.1.4 in Section 4.6.1 of this text and consists of the following steps.

(a) Fly prescribed flight path, at constant altitude and airspeed, on a heading designed to pass directly over the E/O target and normal to the face of the target.

(b) Acquire the E/O target on an on-board sensor.

(c) Designate the target (fire the designator laser).

(d) Observe the (designated) target using the ground-based TV camera shown in Figure 4.6.1.4 and record the resulting video as a function of time.

(e) Determine the airborne designator-to-target range using suitable on-board or range instrumentation.

(f) Determine the laser designator LOS angular jitter by time correlating the jitter-induced movement of the laser spot on the target with the designator-to-target range data.

4.37

4.4.6 Laser Ranging Accuracy -- The ranging accuracy of a laser/designator is best determined by flight test employing an E/O target similar to the one described in Section 4.6.1 of this text. The procedure is as follows.

(a) Fly prescribed flight path, at constant altitude and airspeed, on a heading designed to pass directly over the E/O target and normal to the face of the target.

(b) Acquire the E/O target on an on-board sensor.

(c) Designate the target and laser range on the target. Record the resulting data as a function of time.

(d) Independently determine and record aircraft-to-target range using onboard or range instrumentation. (The highly accurate ranging provided by laser ranging makes it extremely difficult to obtain "truth" data of sufficient accuracy.)

(e) Time correlate the laser range data with the "truth" data to determine ranging error.

The static ranging accuracy of a laser ranger can be determined by ground tests utilizing optical retro-reflectors positioned at known ranges from the test aircraft position.

4.4.7 Laser Beam Divergence -- The divergence of a laser beam is best de-
termined by ground test employing the collimating apparatus described in
Section 4.6.2 of this text. The laser is fired into the collimator as shown
in Figure 4.4.7.1. Templates with various circular apertures are placed at
the focal point of the collimator mirror as also shown in the figure. The
size of the circular aperture is varied until the aperture just begins to
occlude the beam as indicated by a reduction in the radiant flux received by
the radiometer. (A reduction to 90% of the no-aperture value is taken as the
reference point.) The angular beam width (divergence) of the laser beam is
then equal to the diameter of the (90% flux) aperture divided by the focal
length of the collimator.

The geometry of the test is illustrated in Figure 4.4.7.2. If all of the rays
in the laser beam were parallel ($\alpha = 0$), they would all be focused to a point
at the focal point of the mirror. If the most divergent rays (edge of the
beam) make an angle α with the beam axis, they will just graze the edge of
the hole in an aperture plate of radius r as shown. Thus, the half-angle of
the beam is equal to:

$$\alpha = \frac{r}{FL_c} \qquad \text{(Radians)}$$

where:

FL_c = Focal Length of Collimator (Meters)

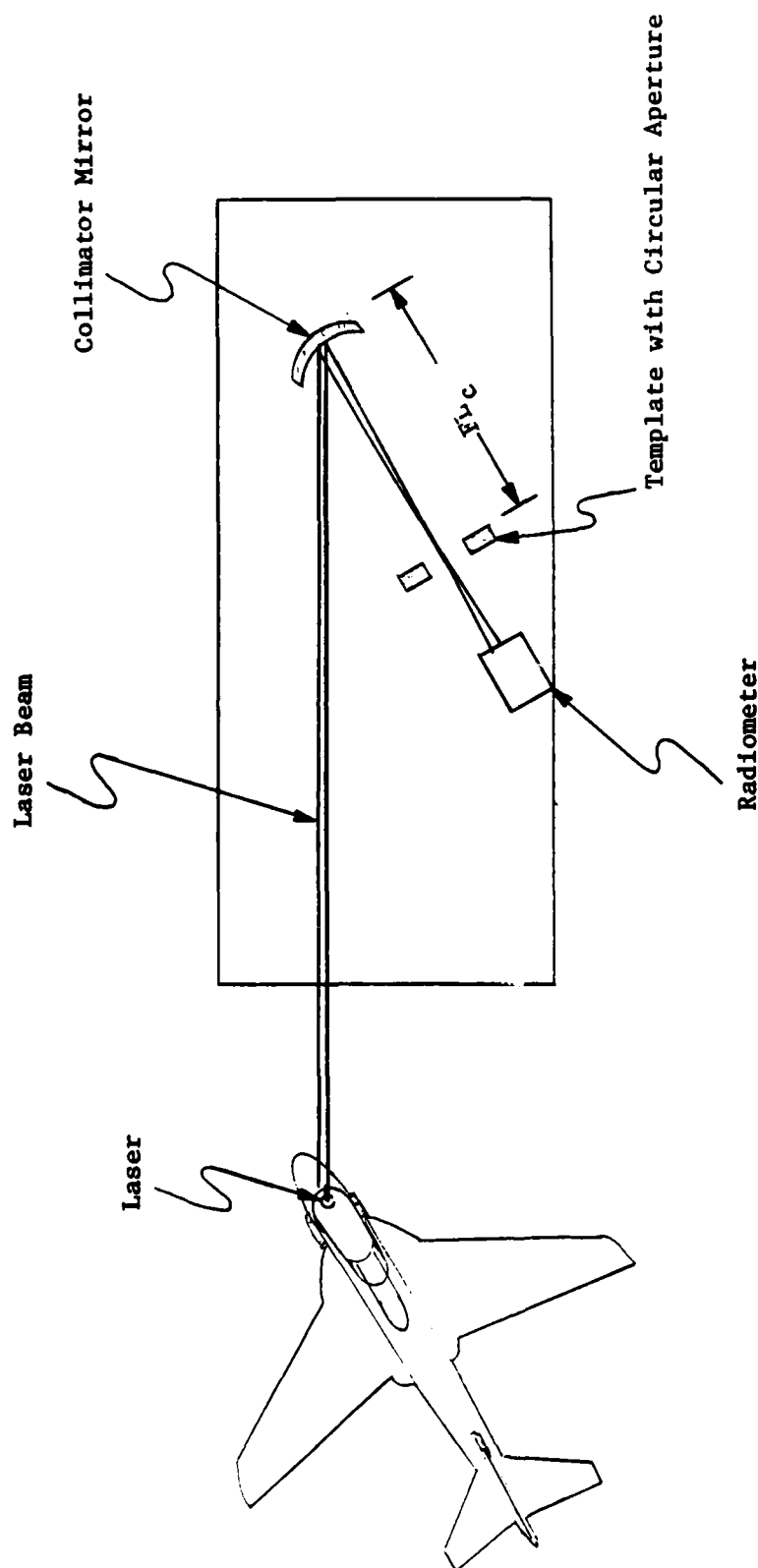r = Radius of aperture that just grazes the beam (Meters)
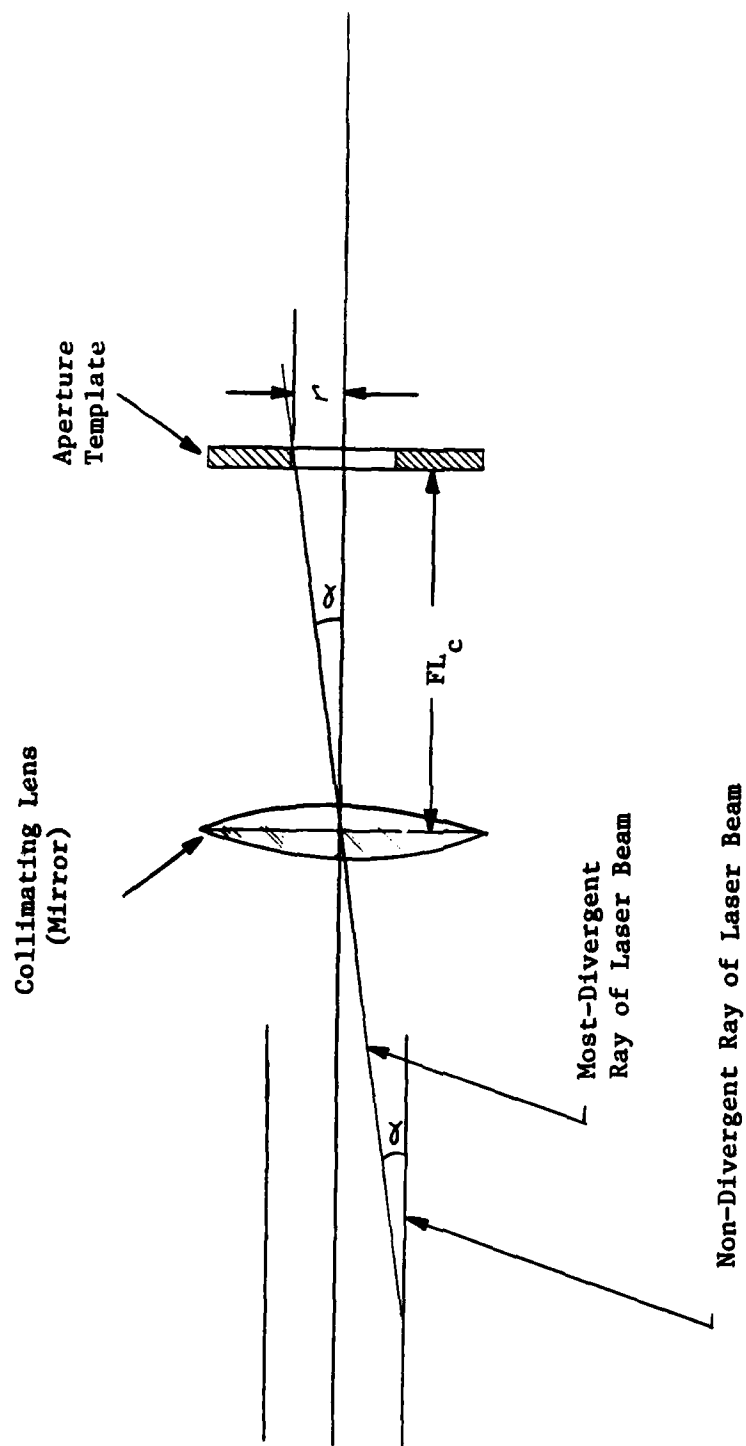
Figure 4.4.7.1 -- Laser Beam Divergence Test Setup

Collimator Mirror

Template with Circular Aperture

F_c

Laser Beam

Radiometer

Laser

4.39a

Figure 4.4.7.2 -- Laser Beam Divergence Test Geometry

4.39b

4.4.8 Laser Output Power -- The average output power of a laser ranger/ designator is best determined by ground test employing the test setup depicted in Figure 4.4.8.1. The test procedure is as follows.

    (a) Align laser output beam with center of calorimeter.

    (b) Fire laser.

    (c) Record calorimeter output reading (laser average output power).

The pulse peak power and pulse energy of a pulsed laser can be calculated from the average power by means of the equations:

$$P_{Peak} = \frac{P_{average}}{DC}$$

$$DC = \frac{\tau_p}{PRI}$$

$$E_{Pulse} = P_{peak} \cdot \tau_p$$

where:

        DC = Duty Cycle (N.D.)

        E_{pulse} = Energy in Single Pulse (Watt-Sec.)

        $P_{average}$ = Laser Average Power (Watts)

        P_{peak} = Laser Pulse Peak Power (Watts)

        PRI = Laser Pulse Repetition Interval (Secs)
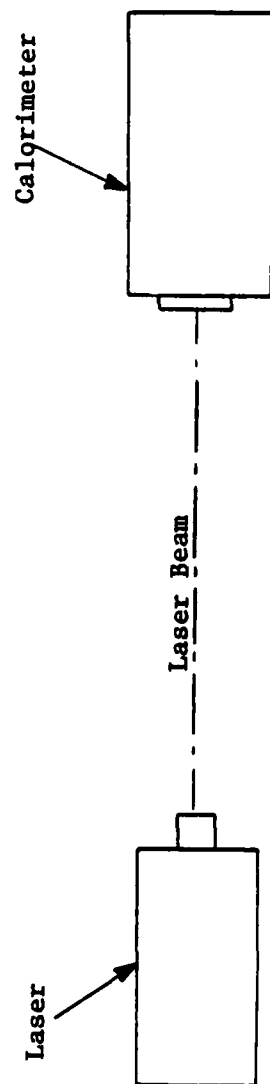
        τ_p = Laser Pulse Width (Secs)

Figure 4.4.8.1 -- Laser Output Power Measurement

4.4.9 Laser Pulse Amplitude -- The pulse amplitude and pulse amplitude stability of a pulsed laser ranger/designator is best determined by ground test employing the test setup depicted in Figure 4.4.9.1. The laser is fired into the radiometer and the output of the radiometer is recorded on the high-speed recorder as shown in the figure. Pulse amplitude stability can be determined by comparing the output recording over a specified time interval. Laser misfire rate (missing pulse rate) also can be determined by examination of the recorded radiometer output.
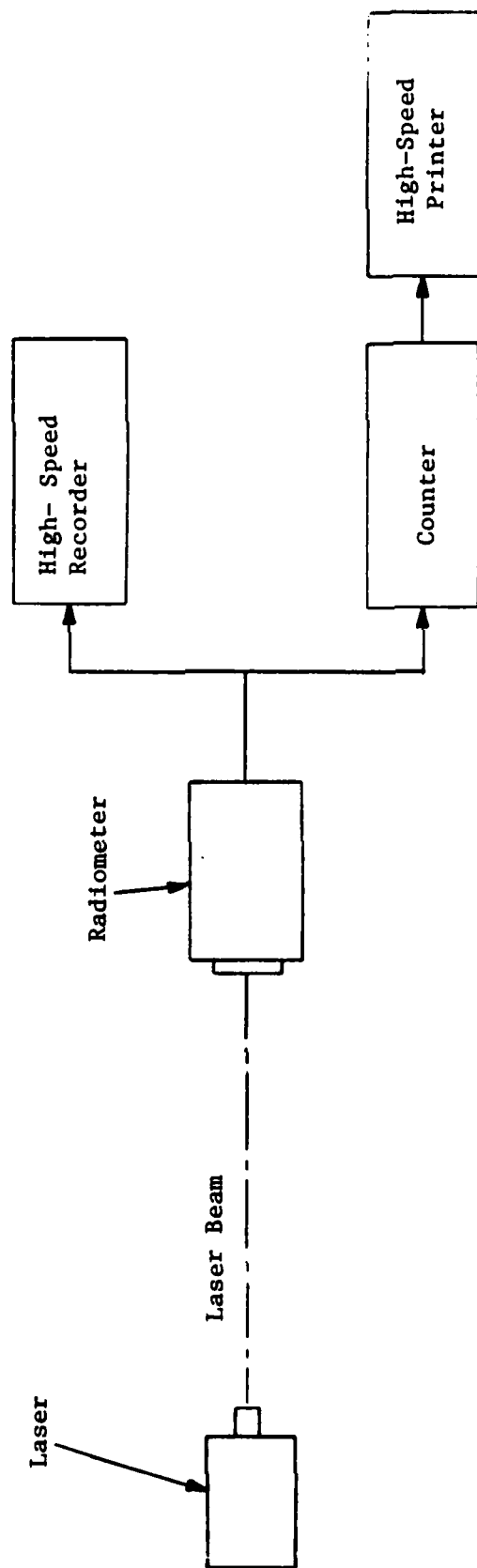
High-Speed Printer

High- Speed Recorder

Counter

Radiometer

Laser Beam

Laser

Figure 4.4.9.1--Laser Pulse Parameter Test Setup

4.41a

4.4.10 Laser Pulse Width -- Tne pulse width of a pulsed laser/designator is best determined by ground test employing the test setup depicted in Figure 4.4.9.1. The laser is fired into the radiometer and the output of the radiometer is recorded as shown. Because of the small pulse widths and the extremely fast rise and fall times associated with a laser pulse, an accurate determination of pulse width requires the use of special, fast-response detectors and recorders. In addition, corrections are generally made for the response times associated with the detector and recorder.

4.4.11 Laser Pulse Repetition Interval -- The pulse repetition interval (or frequency) of a laser ranger/designator is best determined by ground test employing the test setup depicted in Figure 4.4.9.1 The laser is fired into the radiometer and the output pulses are counted and timed by the counter as shown. The output of the counter (pulse count and pulse rate) is recorded by the high-speed printer. Analysis of the high speed printout yields pulse repetition frequency (interval) and PRF stability.

4.5 Photographic Camera Performance Testing

4.5.1 General E/O Sensor Tests -- Many of the E/O sensor performance testing

techniques discussed in Sections 4.2 and 4.3 of this text apply, with only

slight modification, to the evaluation of the photographic camera. The

following tests, described in the sections indicated, are essentially applicable

to photographic camera systems.

Test	Section
Bearing Accuracy	4.2.3
Boresight Accuracy	4.2.5
Field-of-View	4.2.6
LOS Slew Limits	4.2.9
LOS Slew Rates	4.2.10
LOS Drift	4.2.11
LOS Jitter	4.2.12
Pointing Accuracy	4.2.16

Some photographic system performance characteristics are highly dependent upon

the photographic film employed. The results of testing for those characteristics

are, thus, significant only for the specific films used in testing. Film-

dependent characteristics include the following.

Angular Resolution
Bandwidth
Image Definition
Maximum Range
Minimum Resolvable Luminosity Differential

4.5.2 Angular Resolution -- The angular resolution of a photographic system should be evaluated in both static (ground) tests and flight tests. A comparison of ground and flight test results provides an evaluation of line-of-sight stabilization and motion compensation. A ground test of angular resolution can best be made using a collimated target such as that described in Section 4.6.2 of this text. A slight modification of the test procedure outlined in Section 4.2.20 of this text determines both the angular resolution and the luminosity resolution of the camera/film combination. The flight test for the determination of the angular resolution of a photographic system utilizes a photogrammetric E/O target, such as that described in Section 4.6.3 of this text, and consists of the following procedure.

    (a) Fly prescribed flight path, at constant (specified) altitude and air-speed, on a heading designed to pass directly over the E/O target.

    (b) As aircraft overflys target, expose film.

    (c) Determine target luminance using ground instrumentation.

    (d) Calculate camera system angular resolution from the known bar size of the smallest resolvable bar-space group and the altitude.

4.6   Electro-Optical Test Apparatus

4.6.1   The Electro-Optical Test Target -- The Electro-Optical Target shown in
Figures 4.6.1.1 and 4.6.1.2, consists of 60 rotatable, three-sided bars in an
array 30 feet wide and 20 feet high. The three sides of the bars are painted
white, grey, and black, with a special paint designed to provide three values
of diffuse reflectance for illumination by an external source. In addition,
the white faces are provided with electric heaters, as shown in Figure 4.6.1.2,
to provide temperature differentials from about 0.5 centigrade degrees to about
10 centigrade degrees, for the testing of thermal sensors. By rotating the
individual bars, various target patterns can be created as shown in Figure
4.6.1.3. The target array is oriented 15 degrees off the vertical so as to
provide a more-nearly normal line-of-sight for an airborne sensor. A composite
pictorial representation of a test in progress is si.own in Figure 4.6.1.4.
Shown in that figure are:

   (a) The E/O target.

   (b) The test aircraft with E/O sensor/laser designator.

   (c) A radiometer for measuring the radiant intensity of the target to a
       tolerance of about $\pm 0.05 C^\circ$.

   (d) A closed-circuit television camera for detecting illumination of the
       target by the laser/designator.

   (e) A laser designator for the testing of an airborne laser designation
       receiver.

   (f) A radar for determining target-to-sensor range.

   (g) The Master Time Code System that provides time correlation for all
       data recording.

The radiant intensity of the E/O target must be corrected for the effects of
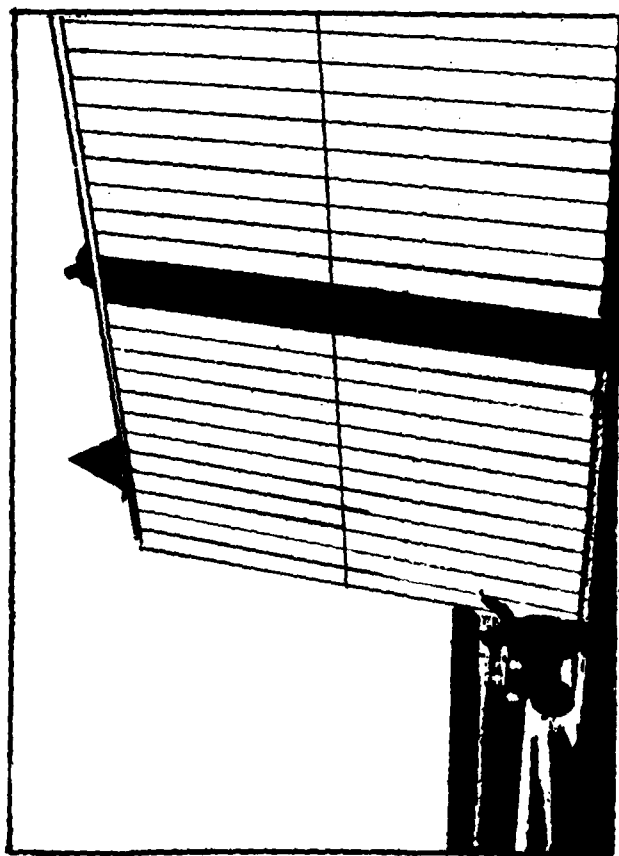range and atmospheric absorption. To effect the correction, sensor-to-target

4.46

Figure 4.6.1.1 -- The Electro-Optical Test Target
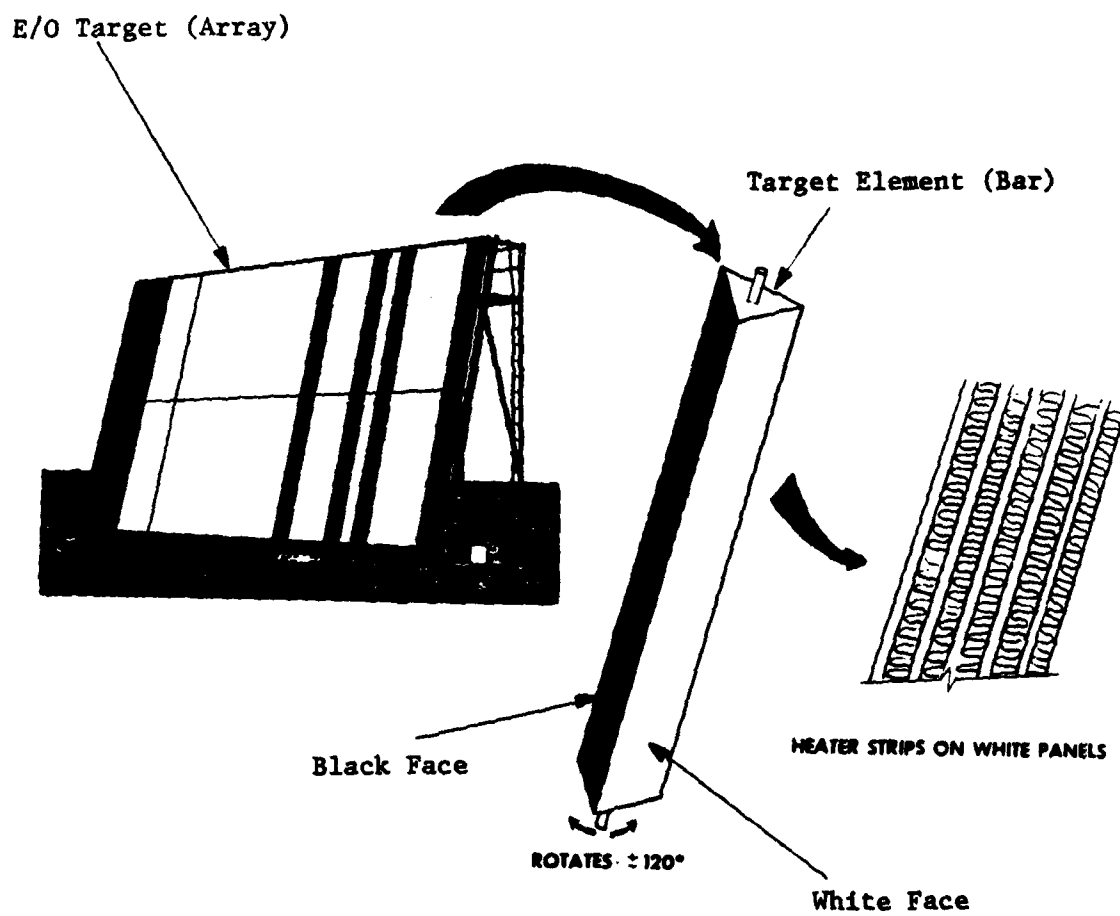
E/O Target (Array)

Target Element (Bar)

Black Face

HEATER STRIPS ON WHITE PANELS

ROTATES ± 120°

White Face

Figure 4.6.1.2--Detail of the E/O Test Target

4.46b
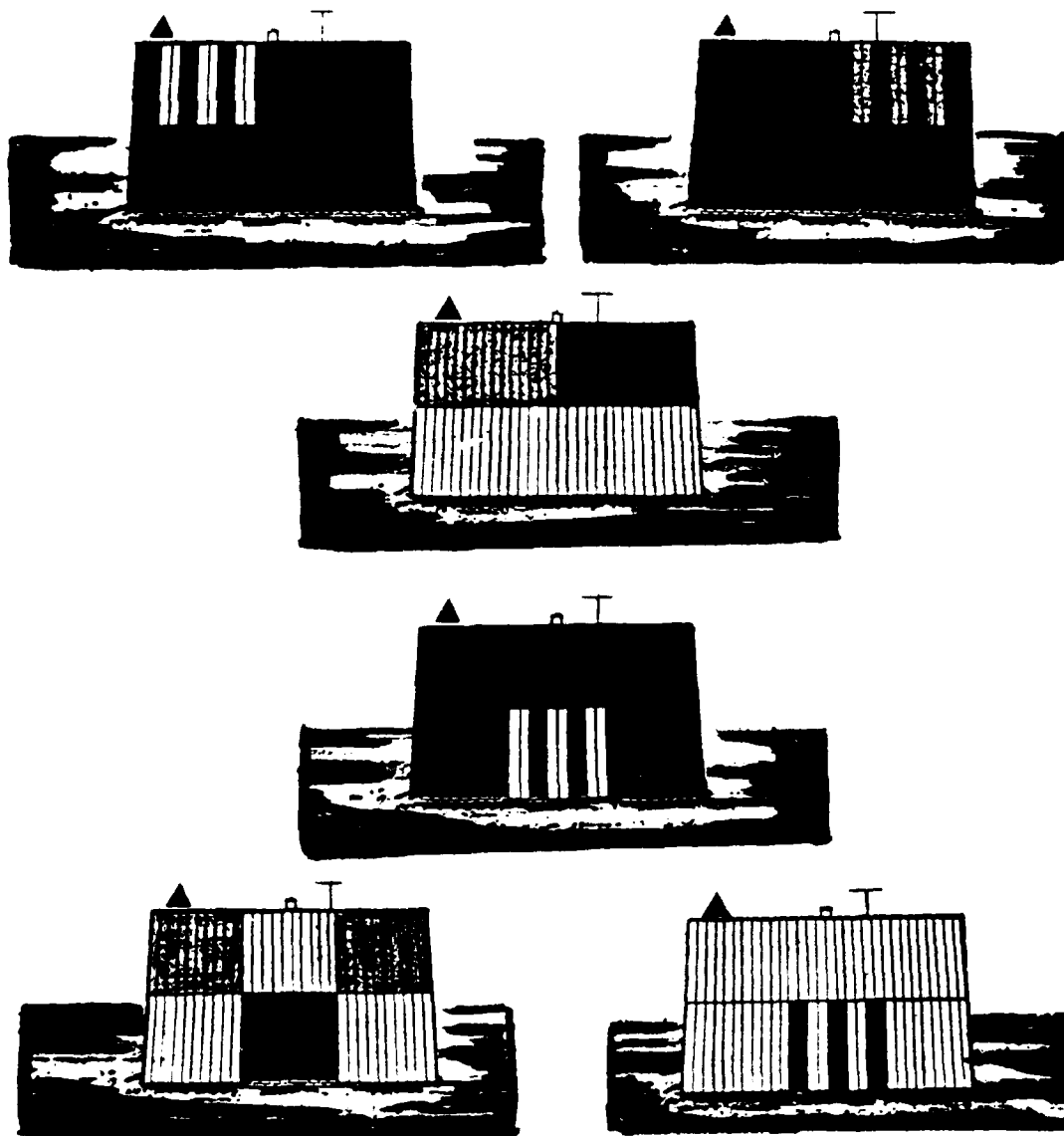
Figure 4.6.1.3 -- Various E/O Target Test Patterns

MASTER TIME
CODE SYSTEM

Line-of-Sight

E/O Sensor/Designator System

Electro Optical
Target

Ranging
Radar

Spectral Radiometer

Closed Circuit Television Camera
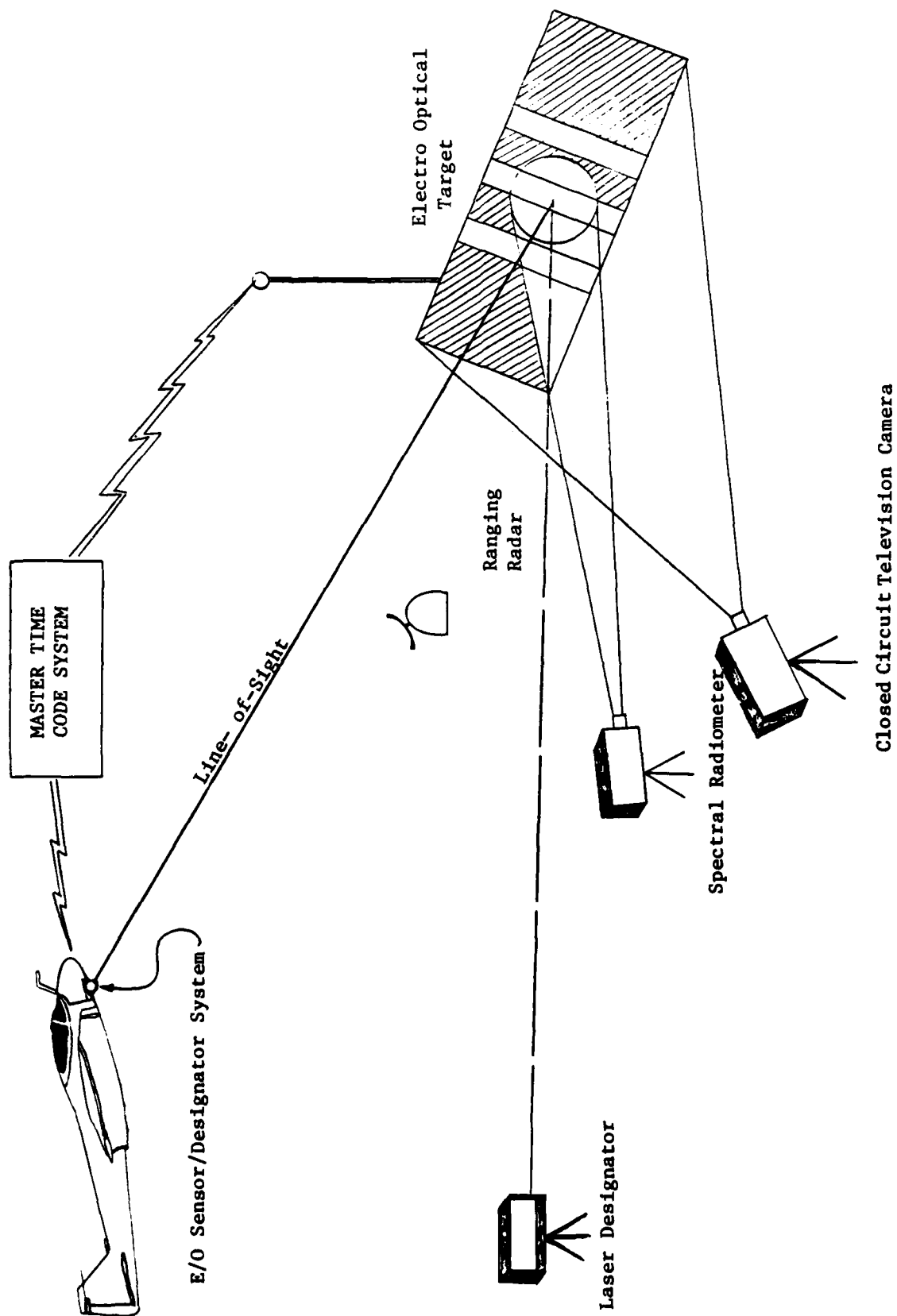
Laser Designator

Figure 4.6.1.4--E/O Sensor Airborne Test Employing E/O Target

4.46d

range and atmospheric moisture content are measured and used to calculate atmospheric transmittance. The atmospheric transmittance is then used to calculate an effective value for target radiant intensity (temperature differential for a thermal sensor). As indicated in Section 3.3.6 of this text, the spatial frequency of a bar target at range R_T is given by:

$$SF_T = \frac{R_T}{W_{1c}} \qquad \text{(Cycles/Radian)}$$

where:

R_T = Sensor-to-Target Range (Meters)

W_{1c} = Width of one cycle of Target (one bar and space) (Meters)

4.6.2 The Optically-Collimated E/O Test Target -- The E/O collimator shown in Figure 4.6.2.1 is mounted on a flat-bed trailer and consists of a spherical collimating mirror and a planar path-folding mirror mounted on an optical bench. Also mounted on the trailer is an electro-optical target. The target can consist of a radiation source such as a laser or other illuminator, a reflective target to be illuminated by an external source, or a thermal bar target for I/R sensor testing. The arrangement of the collimated-target components is as shown in Figure 4.6.2.2. The E/O target is positioned at the focal point of the collimating mirror. The radiation from a single point on the target is thus reflected from the collimating mirror with all rays parallel to the line-of-sight from the E/O sensor under test to the point on the target. The image of the target therefore appears to the sensor as if it were at an infinite range. The purpose of the collimated source is to provide calibrated targets for long-range sensors without the difficulties associated with actually providing targets at large ranges. As indicated in Figure 4.6.2.3, the spatial frequency of a collimated bar target image as seen by the sensor is given by the equation:

$$SF_T = \frac{i}{\theta_{1c}} \cong \frac{FL_c}{W_{1c}}$$ (Cycles/Radian)

where:

FL_c = Focal Length of Collimator (Meters)

W_{1c} = Width of one bar and space of Actual Target (Meters)

The thermal bar target consists of a temperature-controlled surface (I/R source) with a slotted template mounted in such a way as to block part of the radiation from the source. The temperature of the template is held constant at ambient
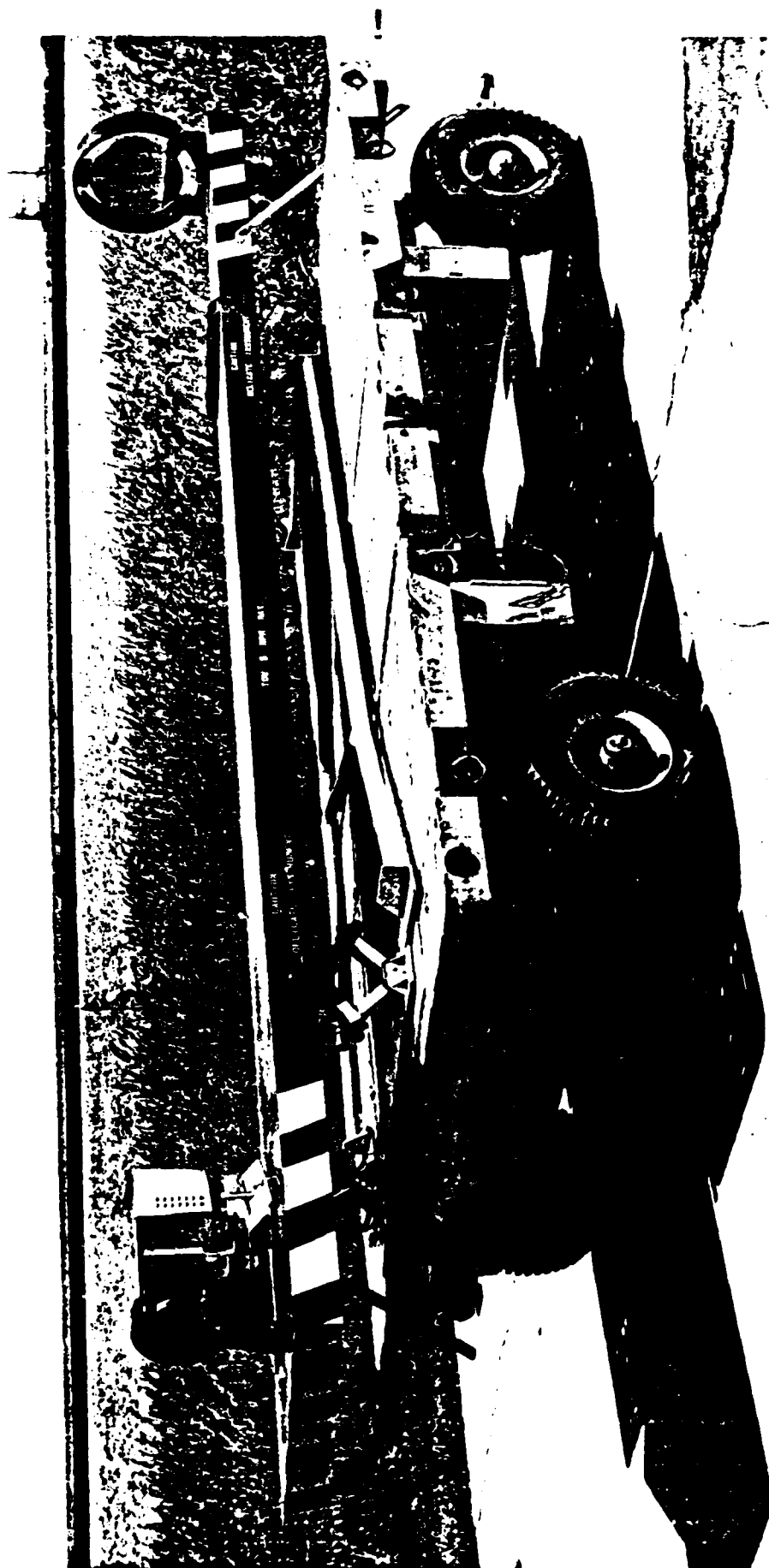
4.48

Figure 4.6.2.1--The Opitcally-Collimated E/O Sensor Test Target

Parabolic
Focusing
Mirror

Sensor Line-of-sight

E/O Target
(Placed at focal
point of mirror)

Planar
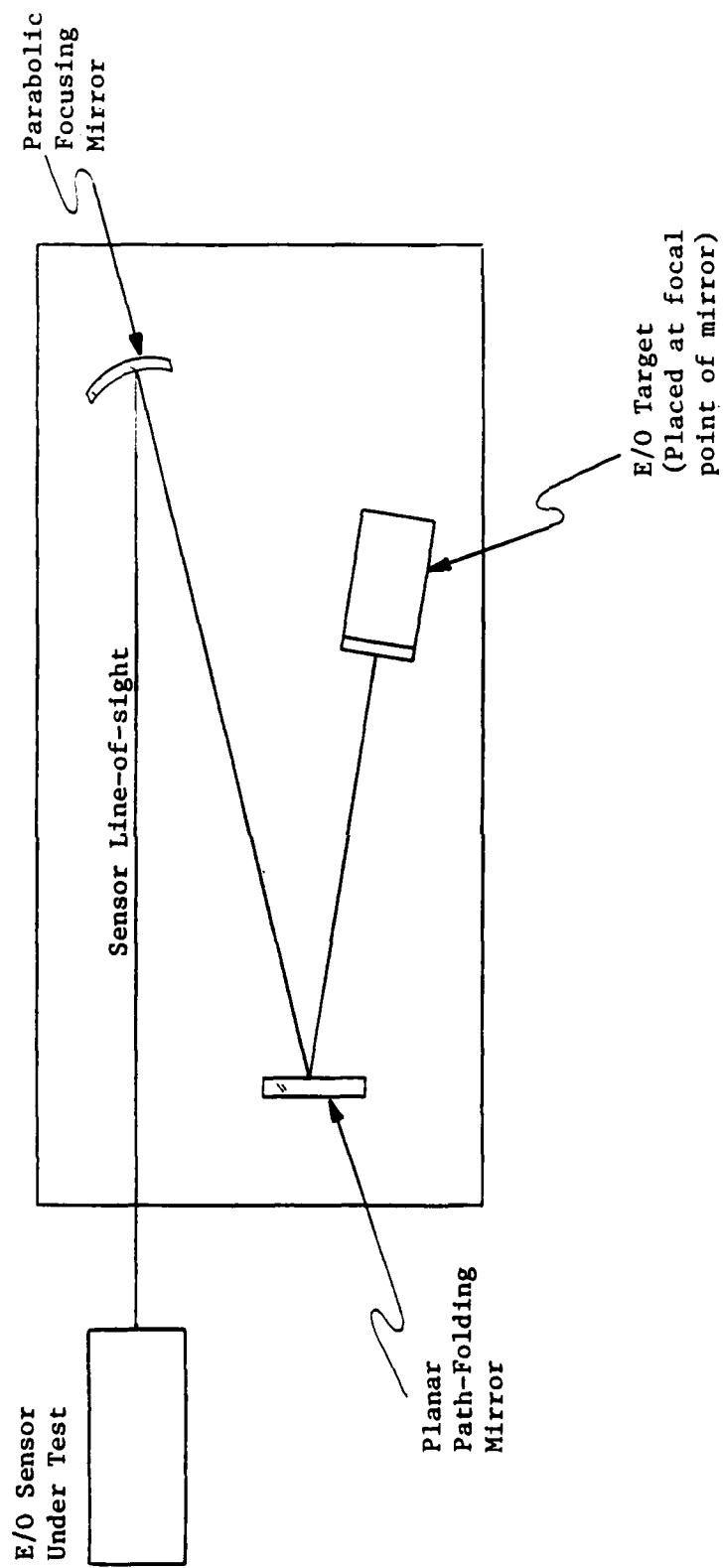Path-Folding
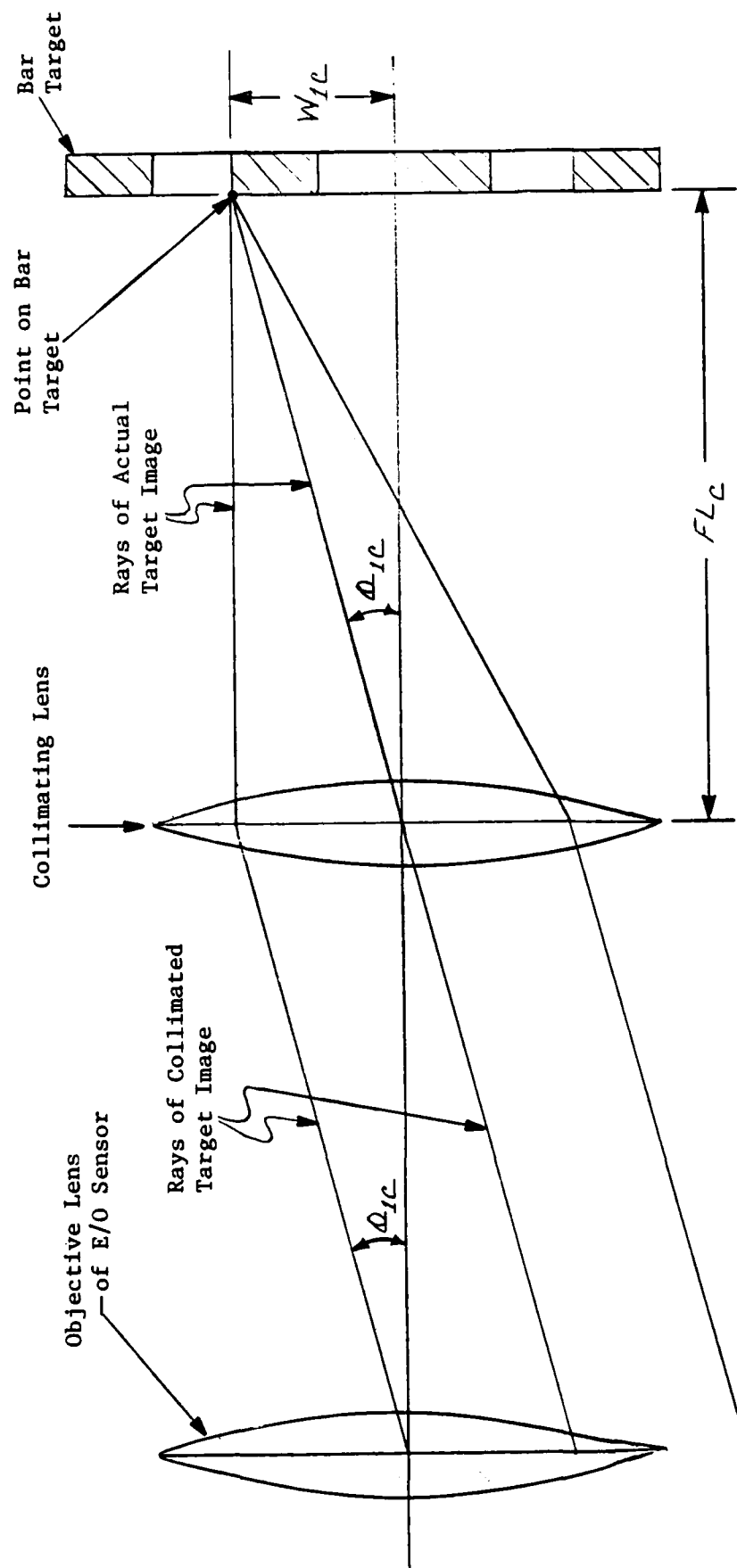Mirror

E/O Sensor
Under Test

Figure 4.6.2.2--Opitcally Collimated E/O Test Target

FL_C = Focal Length of Collimator (Meters)

W_{IC} = Width of Target Cycle (one Bar and Space) (Meters)

α_{IC} = Angular Width of Target Cycle as seen by Sensor (Radians)

Figure 4.6.2.3--Target Image Collimator

temperature by virtue of its being mounted in a large block of aluminum (heat sink). A "bar" of the target is thus formed where a slot in the template allows the sensor under test to view the temperature-controlled source through the template. The "spaces" of the target are formed where the spaces between the slots in the template block the radiation from the temperature-controlled source. The spatial frequency of the collimated bar target image is adjusted by interchanging bar target templates with differing bar/space widths. The temperature-controlled source is electrically heated and thermoelectrically cooled to produce a bar-space temperature differential of -20 to +20 centigrade degrees. The temperature differential can be set to about 0.2 centigrade degrees and measured, by a radiometer, to about 0.05 centigrade degrees. A pictorial representation of an I/R sensor under test is shown in Figure 4.6.2.4.

I/R Sensor

Parabolic Mirror

Optical Collimator
Cart

Planar
Mirror
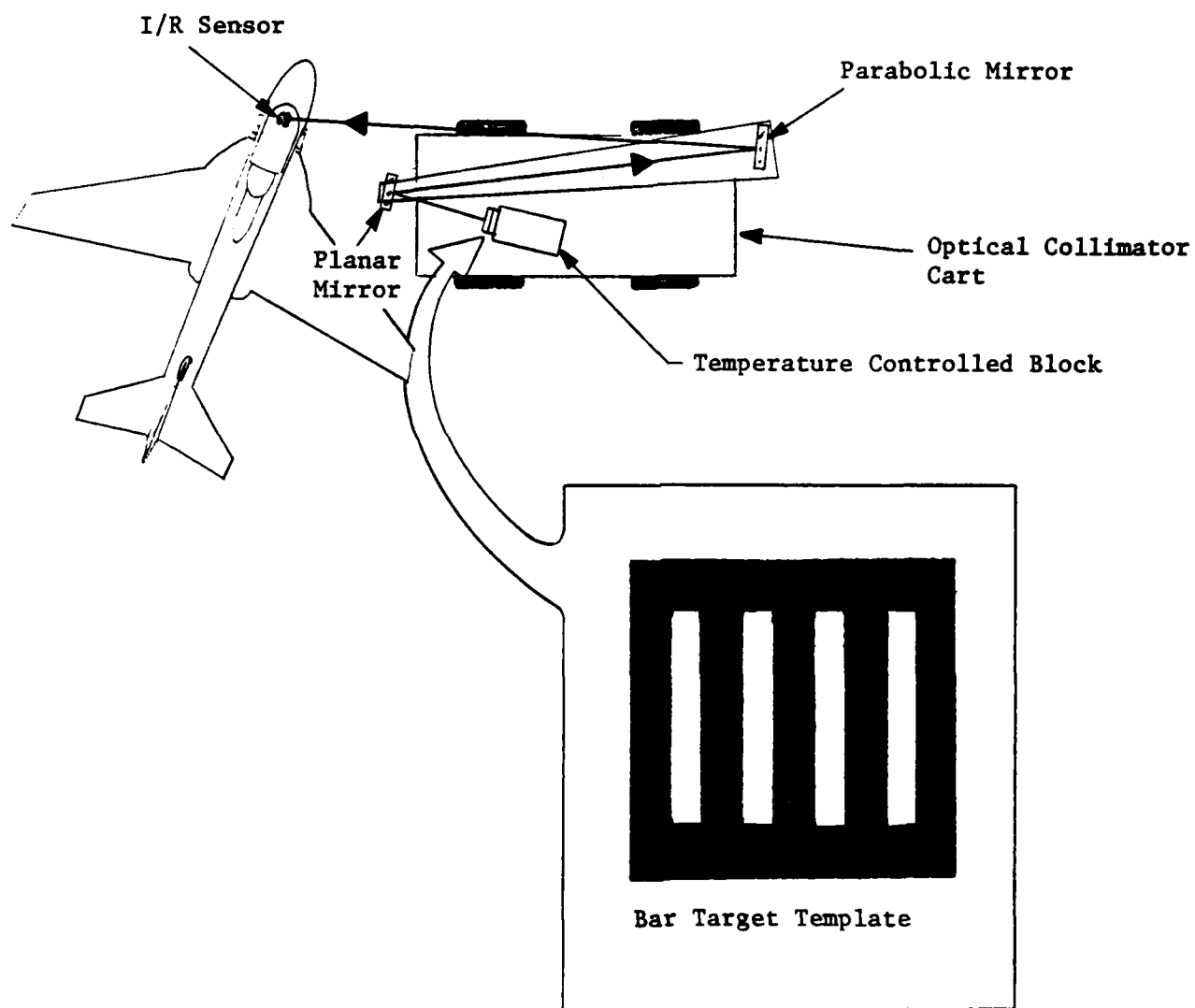
Temperature Controlled Block

Bar Target Template

Figure 4.6.2.4 -- I/R Sensor Under Test Using Collimated Thermal Bar
Target

4.6.3 The Photogrammetric E/O Test Target -- An E/O test target used for the evaluation of photographic systems at NAVAIRTESTCEN is the Type A Photogrammetric Target shown in Figure 4.6.3.1. The target is oriented parallel to the ground and consists of painted strips with the characteristics listed in Tables 4.6.3.1 and 4.6.3.2. In use, the target is overflown and photographed from various altitudes.
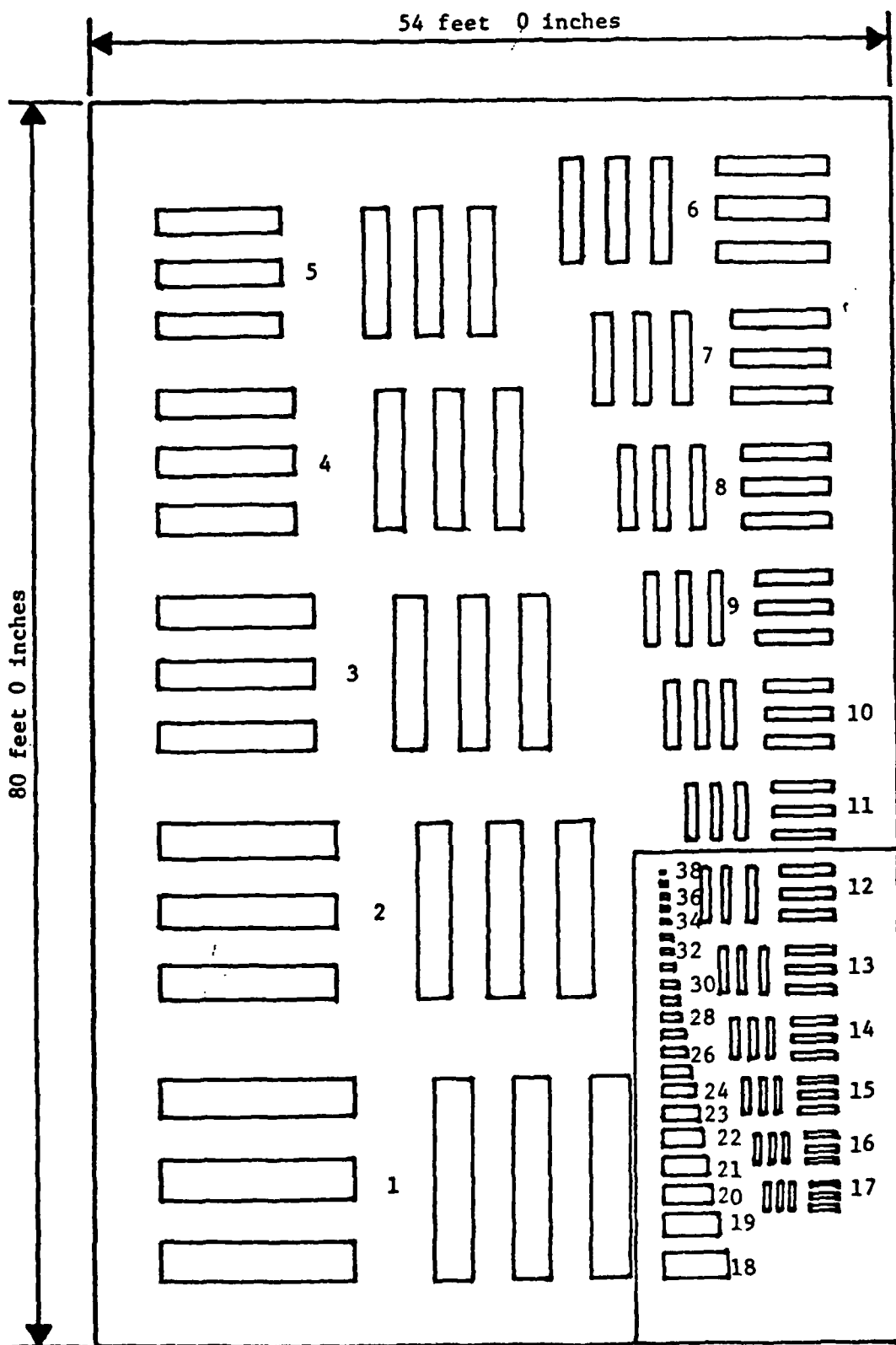
54 feet 0 inches

80 feet 0 inches

5

6

7

8

9

10

11

4

3

2

1

38
36
34
32
30
28
26
24
23
22
21
20
19
18

12

13

14

15

16

17

Figure 4.6.3.1--Type A Photogrammetric Target

Table 4.6.3.1

Type "A" Photogrammetric Target Bar Widths

Bar/Group Number	Feet	Inches	Bar/Group Number	Feet	Inches
1	2	6.250	20	0	3.375
2	2	2.937	21	0	3.000
3	2	0.000	22	0	2.687
4	1	9.375	23	0	2.375
5	1	7.062	24	0	2.125
6	1	5.000	25	0	1.875
7	1	3.125	26	0	1.687
8	1	1.500	27	0	1.500
9	1	0.000	28	0	1.343
10	0	10.687	29	0	1.187
11	0	9.500	30	0	1.062
12	0	8.500	31	0	0.937
13	0	7.562	32	0	0.843
14	0	6.750	33	0	0.750
15	0	6.000	34	0	0.671
16	0	5.312	35	0	0.593
17	0	4.750	36	0	0.531
18	0	4.250	37	0	0.468
19	0	3.812	38	0	0.421

The lengths of the bars conform to MIL. STD. 150-A, that is, each has a length-to-width aspect ratio of 5-to-1.

The listed measurements are for the bar size only. For example using bar/group number 20:   Bar = 3.375 inches; Bar + Space = 6.750 inches

Table 4.6.3.2

Type "A" Photogrammetric Target Characteristics

Target Characteristic	Values/Description
Designation	Type "A" Photogrammetric Target
Type	Photo Resolution Targets
Construction	Painted metal panels bolted to concrete
Reflectance	8% Black / 82% White (Vary with age)
Tone	Black and White

END

FILMED

8-83

DTIC